Investigating and optimizing strategies for quantitative point-of-care diagnostics through chemiluminescence probes and liposomes

Dissertation zur Erlangung des Doktorgrades der Naturwissenschaften (Dr. rer nat.)

an der Fakultät Chemie und Pharmazie
der Universität Regensburg
Deutschland

vorgelegt von

Simone Rink

aus Saal an der Saale

im Jahr 2022

“Once you eliminate the impossible whatever remains, however improbable, must be the truth”

- Sir Arthur Conan Doyle -

… to my fantastic family and friends …

Die vorliegende Dissertation entstand in der Zeit von Dezember 2018 bis April 2022 am Institut für Analytische Chemie, Chemo- und Biosensorik der Universität Regensburg.

Die Arbeit wurde angeleitet von Prof. Dr. Antje J. Baeumner.

Promotionsgesuch eingereicht am: 21.12.2022
Kolloquiumstermin: 10.03.2023

Prüfungsausschuss

Vorsitzender:	Prof. Dr. Oliver Tepner
Erstgutachterin:	Prof. Dr. Antje J. Baeumner
Zweitgutachter:	Prof. Dr. Axel Duerkop
Drittprüferin:	Prof. Dr. Miriam Breunig

Acknowledgement

First, I would like to express my gratitude to **Prof. Dr. Antje Baeumner** and **Prof. Dr. Axel Duerkop** for their great support and for providing proficient guidance along the way. Without their knowledge, experience and commitment, the projects would lack in quality of outcomes. Thank you for encouraging me to choose this path. Special thanks go to **Prof. Dr. Antje Baeumner** for allowing me to work on such innovative projects, for introducing me to great collaboration partners, for challenging and inspiring me and for her continuous motivation and confidence in me and my abilities.

Thanks to **Prof. Dr. Miriam Breunig** and **Prof. Dr. Oliver Tepner** for accepting to be part of the examination board.

I would also like to direct some words of gratitude and appreciation to all my collaboration partners. Thanks to **Barbara Kaiser**, **Dr. Mark-Steven Steiner**, **Anna Go** and **Prof. Min-Ho Lee**, for the scientific discussions, their full support in case of project related troubleshooting and the good cooperation and excellent scientific exchange. Thanks to **PD Dr. Michael Seidel** and **Prof. Jacobi von Wangelin** for their expert advice and the ongoing rewarding collaboration. Thanks to the entire **COVID project team** for relevant scientific discussions and thanks to **all students** for their assistance in the many different projects, I was fortunate to be a part of.

Thanks to **Vanessa Tomanek** for her assistance and support with creating graphics and with many liposome syntheses and thanks to **Joachim Rewitzer** for practical and moral support, fun lab courses and endless coffee supply.

Thanks to the **mechanical** and **electronic workshop** for all the technical advice and emergency assistance.

Thanks to **all colleagues** of the Institute of Analytical Chemistry, Chemo- and Biosensors for the group-wide collaboration.

A big thank you goes to **Christian Griesche**, **Meike Bauer** and **Franziska Beck** for treading this path together with me. Thanks to you, the fun in the lab never missed out. A huge thank you goes to **Christine Unger** for her scientific support and all the encouraging words!

Thanks to **Prof. Dr. Zdeněk Farka** for the nice discussions, for sharing his experiences and encouraging me to pursue this path.

Acknowledgement

I am deeply grateful to my **mum and dad** for helping me make my dreams and wishes come true. Thank you for your unwavering support in any way possible. I am equally thankful to my **sister** for understanding me, listening to me and motivating me. Thank you, guys, for being there, whenever I need you and for supporting and encouraging me with all my decisions.

Last but not least, I am deeply grateful to the **friendships and collaborations** which originated along the way. Thank you for the assistance, support and advice in any kind of situation. I feel honored to have such incredible friends and colleagues!

Table of Contents

DECLARATION OF COLLABORATIONS **8**

RELEVANCE AND STRUCTURE OF THE THESIS **11**

SUMMARY **16**

ZUSAMMENFASSUNG **19**

1. PROGRESSION OF PAPER-BASED POINT-OF-CARE TESTING TOWARD BEING AN INDISPENSABLE DIAGNOSTIC TOOL IN FUTURE HEALTHCARE **22**

Graphical Abstract 22
Abstract 23
1.1. Introduction 23
1.2. Progression from qualitative to quantitative solutions 25
1.2.1. Improvements towards sensitivity 26
1.2.1.1. by optimized material, procedure, and strip architecture 26
1.2.1.2. by advanced detection strategies 29
1.2.2. Improvements towards objective detection 29
1.2.3. Improvements towards public applicability 32
1.3. Progression towards multianalyte detection 33
1.4. Conclusion 35
1.5. References 37
1.6. Supporting Information 42
1.6.1. Overview of selected paper-based analytical devices using advanced nanomaterials 42
1.6.2. References 46

2. NEXT GENERATION LUMINOL DERIVATIVE AS POWERFUL BENCHMARK PROBE FOR CHEMILUMINESCENCE ASSAYS **47**

Graphical Abstract 47
Abstract 48
2.1. Introduction 48
2.2. Material & Methods 50
2.2.1. Determination of absorbance characteristics. 50
2.2.2. Chemiluminescence characterization. 51
2.2.3. Competitive diclofenac assay. 51
2.2.4. L-lactate Assay. 52
2.3. Results & Discussion 52
2.4. Conclusion 58
2.5. References 59
2.6. Supporting Information 61
2.6.1. Experimental Procedures 61
2.6.1.1. Determination of absorbance characteristics. 61
2.6.1.2. Characterization of chemiluminescence properties 62
2.6.1.3. Determination of relative chemiluminescence quantum yield 62

2.6.1.4. Stability measurements. 63
2.6.1.5. Chemiluminescence measurement of hydrogen peroxide. 63
2.6.1.6. Chemiluminescence measurement of luminophore. 63
2.6.1.7. Preparation of BSA-diclofenac conjugate. 63
2.6.1.8. Preparation of LOx conjugate. 64
2.6.1.9. Competitive diclofenac assay. 64
2.6.1.10. Spectral scanning of enhanced and non-enhanced chemiluminescence with HRP 65
2.6.1.11. Preparation of BSA-HRP conjugate. 65
2.6.1.12. Endpoint measurement of enhanced chemiluminescence with HRP 65
2.6.1.13. L-lactate Assay 66
2.6.2. Results and Discussion 66
2.6.2.1. Supplement to introduction of the main article 66
2.6.2.2. Spectral characterization of *m*-carboxy luminol 68
2.6.2.3. Stability of luminophores in water and carbonate buffer 73
2.6.2.4. Mechanistic insights into enhanced chemiluminescence HRP oxidation mechanism 74
2.6.2.5. L-lactate determination 79
2.6.3. References 82

3. ENHANCED CHEMILUMINESCENCE OF A SUPERIOR LUMINOL DERIVATIVE PROVIDES SENSITIVE SMARTPHONE-BASED POINT-OF-CARE TESTING WITH ENZYMATIC µPADS 84

Graphical Abstract 84
Abstract 85
3.1. Introduction 85
3.2. Experimental Section 87
3.2.1. Chemicals and consumables 87
3.2.2. Fabrication of paper substrate 87
3.2.3. Measurement on paper substrate 88
3.3. Results and Discussion 89
3.3.1. Establishing chemiluminescence reaction on simple µPAD for H_2O_2 detection 90
3.3.2. Advanced µPAD design enables enzymatic reaction and detection optimization 91
3.3.3. Benchmarking analytical performance of advanced µPAD towards L-lactate with a standard smartphone camera against a scientific CCD camera 92
3.3.4. Application to real samples 94
3.3.5. Stability of developed µPAD for L-lactate 95
3.4. Conclusion 96
3.5. References 97
3.6. Supporting Information 99
3.6.1. Reproducibility of developed µPAD 99
3.6.2. Hydrogen peroxide detection on original µPAD 100
3.6.3. Advanced µPAD design enables enzymatic reaction and detection optimization 100
3.6.4. Benchmarking analytical performance of advanced µPAD towards L-lactate with a standard smartphone camera against a scientific CCD camera 103
3.6.5. Flexibility of µPAD design by changing assay strategy 104
3.6.6. Application to real samples 106
3.6.7. Stability of developed µPAD for L-lactate 106
3.6.8. Refenences 107

4. LIPOSOMES AS ALTERNATE DETECTION PARTICLES FOR PAPER-BASED POINT-OF-CARE TESTING 108

4.1. Highly Sensitive Interleukin 6 Detection by Employing Commercially Ready Liposomes in an LFA Format 108

Graphical Abstract 108
Abstract 109
4.1.1. Introduction 109
4.1.2. Experimental Section 111
4.1.2.1. Chemicals and consumables 111
4.1.2.2. Synthesis of sulforhodamine B liposomes 112
4.1.2.3. Dynamic light scattering (DLS) and ζ-potential measurements 112
4.1.2.4. Phospholipid concentration 113
4.1.2.5. Protein coupling to liposomes 113
4.1.2.6. Lateral flow assay procedure. 114
4.1.2.7. Apparatus 114
4.1.3. Results and Discussion 114
4.1.3.1. Development of photometric and fluorescent liposomes 114
4.1.3.2. Inherently fluorescent liposomes 115
4.1.3.3. Optimization of photometric liposome detection 117
4.1.3.4. Photometric and fluorescence lateral flow immunoassay 118
4.1.3.5. Stability study and liposome dehydration 122
4.1.4. Conclusion 124
4.1.5. Declarations 125
4.1.6. References 126
4.1.7. Supporting Information 128
4.1.7.1. Experimental Section 128
4.1.7.2. Results 129
4.1.7.3. References 134

4.2. Changing from Standard Photometric and Fluorescence Detection to Chemiluminescence in Lateral Flow Assays 135

Graphical Abstract 135
Abstract 136
4.2.1. Introduction 136
4.2.2. Experimental Section 138
4.2.2.1. Chemicals and consumables: 138
4.2.2.2. Dynamic light scattering and zeta potential 139
4.2.2.3. Determination of phospholipid concentration through ICP-OES 139
4.2.2.4. Synthesis of *m*-carboxy luminol liposomes 139
4.2.2.5. Surface modification of liposomes 142
4.2.2.6. Lateral flow assay procedure 142
4.2.2.7. Competitive biotin assay 144
4.2.2.8. Performance and stability test 144
4.2.2.9. Apparatus 145
4.2.3. Results and Discussion 145
4.2.3.1. Development of functionalized, stable and highly loaded reporter liposomes 145

4.2.3.2. Optimization of surface functionalization through protein coupling and performance on LFA ... 151
4.2.3.3. IL-6 assay ... 153
4.2.3.4. Comparison of high and low encapsulant chemiluminescence liposomes in a lateral flow assay ... 156
4.2.3.5. Evaluation of CAU detector prototype first and second generation ... 158
4.2.4. Conclusion ... 161
4.2.5. References ... 163

5. INVESTIGATION OF ARCHITECTURAL FEATURES OF LIPOSOMES IN TERMS OF THEIR INTERACTION WITH THE HUMAN COMPLEMENT SYSTEM TO ESTABLISH A STRAIGHTFORWARD NEUTRALIZATION ASSAY FOR SARS-COV-2 ... 164

Graphical Abstract ... 164
Abstract ... 165
5.1. Introduction ... 165
5.2. Experimental Section ... 169
5.2.1. Chemicals and consumables: ... 169
5.2.2. Synthesis of *m*-carboxy luminol liposomes ... 170
5.2.3. Dynamic light scattering and zeta potential ... 172
5.2.4. Determination of phospholipid concentration through ICP-OES ... 172
5.2.5. Surface modification of liposomes ... 173
5.2.6. Binding assay ... 173
5.2.6.1. for streptavidin liposomes ... 173
5.2.6.2. for ARMS liposomes ... 174
5.2.6.3. for ACE2 liposomes ... 174
5.2.7. Competitive assay ... 174
5.2.7.1. with biotinylated liposomes ... 174
5.2.7.2. with ARMS-modified liposomes ... 175
5.2.7.3. with streptavidin-modified liposomes ... 175
5.2.8. Heterogenous complement assay ... 176
5.2.9. Heterogenous complement assay with trigger ... 176
5.2.9.1. simple antibody trigger ... 176
5.2.9.2. LPS-modified liposomes as trigger ... 177
5.2.9.3. Bystander assay with antibody ... 177
5.2.9.4. Bystander assay with LPS-modified liposomes ... 178
5.2.10. Performance and stability test ... 178
5.3. Results and Discussion ... *179*
5.3.1. Development of stealth liposomes through variation of the lipid composition ... 179
5.3.1.1. Liposome characteristics ... 179
5.3.1.2. Complement Assay with biotin-modified anionic and cationic CL-liposomes ... 182
5.3.2. Development of liposome trigger ... 184
5.3.2.1. through an internal trigger - anionic LPS liposomes ... 184
5.3.2.2. through an external trigger - antibodies ... 188
5.3.3. Innocent bystander assay – localized and targeted lysis of liposomes ... 193
5.3.3.1. Key characteristics of the tested liposomes ... 193
5.3.3.2. Bystander Assay ... 194
5.3.4. Surface functionalization of liposomes ... 199
5.3.4.1. ARMS coupling Results ... 200

5.3.4.2. Streptavidin functionalization 203
5.3.4.3. ACE2 coupling 205
5.4. Conclusion 211
5.5. References 214

6. CONCLUSION AND PERSPECTIVE 216

CURRICULUM VITAE 222

PUBLICATIONS 223

PRESENTATIONS 224

EIDESSTATTLICHE ERKLÄRUNG 225

Declaration of Collaborations

Most of the theoretical and experimental work presented in this thesis was conducted solely by the author. However, parts of the results were gained in collaboration with other researchers. In accordance with §8 Abs. 1 Satz 2 Punkt 7 of the "Ordnung zum Erwerb des akademischen Grades eines Doktors der Naturwissenschaften (Dr. rer. Nat.) an der Universität Regensburg vom 18. Juni 2009", the following paragraphs specifies the work that was done by the author and the contributions by third parties.

Chapter 1: A perspective on the progression of paper-based POCT towards being an indispensable diagnostic tool in future health-care

This chapter has been submitted for publication in the American Chemical Society journal *Analytical Chemistry* (accepted December 2022). The literature search and writing of the review was done by Antje J. Baeumner and the author. The author wrote the first draft of the manuscript. Antje J. Baeumner revised the manuscript. Antje J. Baeumner is corresponding author.

Chapter 2: Next Generation Luminol Derivative as Powerful Benchmark Probe for Chemiluminescence Assays

This chapter has been submitted for publication to the Elsevier journal *Analytica Chimica Acta* (accepted October 2021). The concept for this research article, on which this chapter is based on, was developed by Antje J. Baeumner, Axel Duerkop and the author. Conceptualization, experimental design, investigation, formal analysis, data curation and writing of the first draft of the manuscript was done by the author. Supervision, project administration, conceptualization and experimental design was done by Antje J. Baeumner as project lead and Axel Duerkop in a supporting role. Michael Seidel supported this work by providing materials. The author wrote the first draft of this chapter. Antje J. Baeumner, Axel Duerkop, Michael Seidel and Axel Jacobi von Wangelin revised the manuscript. Antje J. Baeumner is corresponding author. This chapter is a continuation of the author's master's thesis.

Chapter 3: Enhanced chemiluminescence of a superior luminol derivative provides sensitive smartphone based POCT with enzymatic µPADs

This chapter has been submitted for publication to the Wiley journal *Analysis and Sensing* and is currently under review. The concept for this research article, on which this chapter is

based on, was developed by Antje J. Baeumner, Axel Duerkop and the author. Conceptualization, experimental design, investigation, formal analysis, data curation and writing of the first draft of the manuscript was done by the author. Supervision, project administration and conceptualization was done by Antje J. Baeumner as project lead and Axel Duerkop in a supporting role. Roland Boneder and Florian Blaser were part of preliminary tests of this study. The author wrote the first draft of this chapter. Antje J. Baeumner and Axel Duerkop revised the manuscript. Antje J. Baeumner is corresponding author. This chapter is a continuation of the author's master's thesis.

Chapter 4.1: Highly Sensitive Interleukin 6 Detection by Employing Commercially Ready Liposomes in an LFA Format

This chapter has been submitted for publication to the Springer journal *Analytical and Bioanalytical Chemistry* (accepted October 2021). Antje J. Baeumner, Barbara Kaiser, Mark-Steven Steiner and the author developed the concept for this work. Barbara Kaiser and the author did most of the experimental design and work. Vanessa Tomanek and Anna Go assisted in the liposome synthesis. Roland Rist, Carolin Schrötel, Nora Schulte assisted in the experimental execution. The author wrote the first draft of this chapter. Antje J. Baeumner, Mark-Steven Steiner, Barbara Kaiser and Axel Duerkop, revised the manuscript. Antje J. Baeumner is corresponding author.

Chapter 4.2: Changing from Standard Photometric and Fluorescence Detection to Chemiluminescence in Lateral Flow Assays

This chapter originated in collaboration with Microcoat Biotechnologie GmbH and the Chung Ang University, South Korea. The experimental work was mainly done by the author. Microcoat Biotechnologie GmbH provided reagents and materials and optimized the protein coupling to the liposomes surface. Anna Go and Minho Lee provided the point-of-care detector for chemiluminescence detection and the accompanied expertise. Peter Fuchs helped with programming the software for the detector.

Chapter 5: 5. Investigation of Architectural Features of Liposomes in Terms of Their Interaction with the Human Complement System to Establish a Straightforward Neutralization Assay for SARS CoV 2

The research project described in this chapter was a collaboration with Microcoat Biotechnologie GmbH, Mikrogen GmbH, Diana Pauly and Ralf Wagner. Mikrogen GmbH and Ralf Wagner from the University Hospital of Regensburg kindly provided the purified

angiotensin-converting enzyme 2 receptor and the receptor binding domain protein and the associated expertise. Diana Pauly from the University of Marburg provided the applied ARMS peptides and antibodies and the associated expertise with the human complement system. Microcoat Biotechnologie GmbH kindly provided materials. Christian Griesche, Kilian Höcherl assisted with the liposome synthesis. Antonia Gruber assisted with the experimental execution of the bystander assay.

Relevance and Structure of the Thesis

On November 15th 2022, the global human population reached 8 billion people and is expected to grow to over 10 billion until 2100.[1] To ensure the well-being of every single one in the future, access to proper healthcare with diagnostic is essential. However, diagnostic capacities and healthcare in general are already today a scarce commodity especially in remote region and developing countries.[2] Nevertheless, timely and accessible diagnostic is one of the cornerstones of successful healthcare to determine deficiencies, diseases, or infections. Without correct diagnostic, appropriate and effective treatment and prevention of emerging epi- and pandemics is hard to realize. Yet, even in industrial countries testing capacities are limited and standard *in vitro* diagnostic tests are albeit their high sensitivity often time consuming, elaborate, and expensive and not always publicly accessible. In consequence, low and low-to-middle income countries often struggle with providing this essential part of healthcare to their citizens due to the costs. In high income countries long analysis times and capacity issues often limit efficient diagnosis.[3] Hence, one of today's trends in bioanalysis is to evolve current analysis techniques to function in simple self-test kits and wearable devices.[4] Ideally, these kits and devices are compatible with digitalized and telemedicine-based systems to provide location-independent access to adequate healthcare and reduce the burden to the globally exhausted healthcare systems in the foreseeable future.[5] Thus, in the 1990s the field of point-of-care (POC) diagnostic emerged, that focuses on timely and low-cost diagnosis close to the patients' need. Despite the great achievements in this field with *e.g.,* lateral flow assays (LFA), that can provide test results within minutes, such tests are often constrained to analytes that are present at high concentrations due to their limited sensitivity and provide mostly only "yes" or "no" answers. Especially, quantitative monitoring through point-of-care testing (POCT) of biomarkers such as the cardiac markers N-terminal pro-B-type natriuretic peptide (NT-proBNP)[6] and cardiac troponin (cT)[7] or the inflammation markers such as interleukin-6 (IL-6) and C-reactive protein (CRP)[8], can assist in emergency medical care and the clinical routine to make adequate and in-time treatment decision.[9] Yet, these biomarkers are also present in healthy subjects and show often only low ng/L circulating concentrations. Indication for cardiac distress or an evolving inflammation is then often diagnosed by small increases of these base line levels.[10,11] Despite being very promising, most current POCT solutions only partially fulfil such requirements and address the demand for rapid, accurate, sensitive, reliable and quantitative analysis only to some extent.[11] Integration of signal amplification strategies and more sensitive detection methods in POCT together with suitable readout

systems are key to more sensitive and quantitative POCT applications and hence, open the field to monitor low concentration analytes away from central laboratory testing. This would help to free up testing capacities and reduce the turnaround time on the one side with quantitative and in-time analysis results. On the other side it would offers the possibility of sensitive diagnosis in remote regions where often only temporary healthcare solutions are available.

In this thesis the feasibility of chemiluminescence (CL) as detection technique in various *in vitro* diagnostic systems with focus on point-of-care (POC) applications were studied. Especially, the potential of signal enhancement solely through the inherent stronger CL signal of a new luminol derivative together with an amplification strategy through label enrichment using liposomal nanocontainers were investigated in various analysis platforms. The individual chapters are presented as (published) manuscript drafts.

Diagnosis together with frequent and accurate testing is the cornerstone of efficient disease management. Point of care testing (POCT) is by now indispensable in clinical diagnostics as it provides in-time test results and offers the possibility of layman use, freeing up capacities in clinical laboratories. Yet, POCT is a relatively young discipline which still endures pioneering advances. **Chapter 1** provides a perspective on current trends in paper-based POCT with regard to improving the sensitivity, measurability, multiplexing, sample throughput and overall public applicability. Here, the development of more efficient labelling strategies, which are ideally qualified for multiplexing approaches and increase the overall signal response together with improved readout strategies, are current major trends. Changing the detection technique from colorimetric to more sensitive optical detection such as chemiluminescence or developing equipment-free quantification with multiple labels are intensively studied.

Using chemiluminescence over other optical detection techniques such as fluorescence or absorbance, benefits from its minimal technical requirements on the detection device, while maintaining its superior sensitivity due to its naturally low background.[12] However, common luminol and its many derivatives often struggle with low quantum yields or limited water solubility impeding certain bioanalytical applications.[13] Hence, the advantage of a more water soluble luminol derivative and a higher quantum yield is appealing to expand the current chemiluminescence product portfolio in (bio)analysis. Initially, the higher water soluble luminophore, *m*-carboxy luminol, was investigated in direct comparison to standard luminol to evaluate its photophysical properties and analytical performance (**chapter 2**).

Here, inorganic, organic and enzymatic catalyst systems were studied to verify a catalyst-independent stronger chemiluminescence of *m*-carboxy luminol over luminol. A striking enhancement of the chemiluminescence quantum yield of 5 % for *m*-carboxy luminol compared to 1 % for standard luminol was determined. Furthermore, the power of a stronger emitting chemiluminescence probe in typical assay systems, where hydrogen peroxide is either detected or consumed was evaluated. Specifically, an enzymatic assay for the detection of L-lactate in synthetic sweat was developed and benchmarked to a commercial colorimetric system. Here, *m*-carboxy luminol excelled with higher resolution over luminol while posing a valid alternative to the colorimetric approach. Furthermore, the superiority of chemiluminescence and especially *m*-carboxy luminol was confirmed in a competitive diclofenac assay. The change from colorimetric detection to chemiluminescence detection with *m*-carboxy luminol showed a significant sensitivity improvement with a lower limit of detection compared to luminol and the colorimetric approach.

The verified improvement of the photophysical properties together with the successful transfer of the enhanced chemiluminescence to superior analytical performance laid the foundation to investigate this luminophore further towards its applicability and benefit in novel POC systems based on paper-based microfluidics (µPAD) and lateral flow assays (LFA). Developing a chemiluminescence enzymatic µPAD for the detection of L-lactate together with the stronger emitting *m*-carboxy luminol unveils the significance of such a probe, especially when intended for POC applications with POC detectors as simple as standard mobile phones (**chapter 3**). Here, the sensitivity of the built-in camera unit is typically lower compared to high-end cooled CCD camera or photomultiplier tubes, which are the gold standard for the detection of poor photoemitter systems such as chemiluminescence. A stronger emitting probe hence compensates for this drop in sensitivity while maintaining excellent assay sensitivity and makes chemiluminescence accessable to POC applications.

In a second approach, sensitivity enhancement by increasing the analyte to label ratio was investigated by taking advantage of lipid nanoparticles as nanocontainers. Here, *m*-carboxy luminol impresses in contrast to luminol due to its increased water solubility and thus ability to be encapsulated with high efficiency within the hydrophilic interior of liposomes. The high flexibility in the surface design of liposomes together with their stability and the label enrichment possibility renders these particles, beside their drug delivery properties, a promising diagnostic tool.[14] Within this work, liposomes were investigated in twofold assay strategies. In a first instance, liposome were tested as POC label to present an alternative

to colloidal gold in a standard LFA by investigating the performance of colorimetric and fluorescent, readout strategies. To replace colloidal gold as first-choice label, the developed liposomes were tested towards their stability, dehydration properties and performance in an interleukin-6 LFA test. To evolve the LFA from a mainly qualitative tool to a sensitive quantitative approach, we expanded on the applied liposome portfolio and transferred the findings to a fully chemiluminescence approach. In the presented work, we focused on refining the reporter probe itself and simultaneously developed a self-contained platform including a POCT detection device (**chapter 4**).

Concomitantly, chemiluminescence liposomes were tested as detection label for the development of a novel microtiter plate-based heterogenous binding assay for the detection of neutralizing antibodies against SARS-CoV 2. Here, the main goal aimed to replace the elaborate benchmark neutralization assay. The human complement system was utilized to destabilize the lipid bilayer specifically in the presence of a trigger molecule by the formation of pores through the membrane attack complex (MAC). This complex is able to form pores in the lipid bilayer membrane[15] which consequently leads to the release of the encapsulated label molecules as analytical signal. In **chapter 5** the preparation, characterization, and surface modification of liposomes together with the effect of varying surface charges and architecture of these liposomes on the human complement system are described as proof-of-concept study for the subsequent assay development.

Chapter 6 puts the findings and achievements of this study into context with current challenges in (bio)analysis and highlights the main advantages and limitations of the reported innovations. Furthermore, a perspective into future investigative avenues of these findings in the field of bioanalysis is given.

References

[1] "Population", can be found under https://www.un.org/en/global-issues/population.

[2] T. Y. Akintunde, O. D. Akintunde, T. H. Musa, M. Sayibu, A. E. Tassang, L. M. Reed, S. Chen, *Global health journal (Amsterdam, Netherlands)* **2021**, *5*, 128.

[3] P. Luppa, R. Junker (Eds.) *Point-of-care testing*. *Principles and Clinical Applications*, Springer Berlin Heidelberg, Berlin, Heidelberg, **2018**.

[4] P. B. Deroco, D. Wachholz Junior, L. T. Kubota in *Tools and Trends in Bioanalytical Chemistry* (Eds.: L. T. Kubota, J. A. F. da Silva, M. M. Sena, W. A. Alves), Springer International Publishing, Cham, **2022**, pp. 543–558.

[5] D. C. Christodouleas, B. Kaur, P. Chorti, *ACS central science* **2018**, *4*, 1600.

[6] a) J. Chami, S. Fleming, C. J. Taylor, C. R. Bankhead, T. James, B. Shine, J. McLellan, F. R. Hobbs, R. Perera, *BJGP open* **2022**, *6*; b) M. Richards, R. W. Troughton, *European journal of heart failure* **2004**, *6*, 351.

[7] I. Yan, C. S. Börschel, J. T. Neumann, N. A. Sprünker, N. Makarova, J. Kontto, K. Kuulasmaa, V. Salomaa, C. Magnussen, L. Iacoviello et al., *JACC. Heart failure* **2020**, *8*, 401.

[8] G. Lippi, *Clinical Chemistry and Laboratory Medicine* **2019**, *57*, 1281.

[9] P. Collinson, *Journal of Laboratory Medicine* **2020**, *44*, 89.

[10] A. Clerico, A. Padoan, M. Zaninotto, C. Passino, M. Plebani, *Clinical Chemistry and Laboratory Medicine* **2021**, *59*, 641.

[11] A. Pfäfflin, E. Schleicher, *Analytical and bioanalytical chemistry* **2009**, *393*, 1473.

[12] A. Roda, M. Mirasoli, E. Michelini, M. Di Fusco, M. Zangheri, L. Cevenini, B. Roda, P. Simoni, *Biosens. Bioelectron.* **2016**, *76*, 164.

[13] a) A. G. Griesbeck, Y. Díaz-Miara, R. Fichtler, A. Jacobi von Wangelin, R. Pérez-Ruiz, D. Sampedro, *Chem. - Eur. J.* **2015**, *21*, 9975; b) M. Mayer, S. Takegami, M. Neumeier, S. Rink, A. Jacobi von Wangelin, S. Schulte, M. Vollmer, A. G. Griesbeck, A. Duerkop, A. J. Baeumner, *Angew. Chem., Int. Ed. Engl.* **2018**, *57*, 408.

[14] K. A. Edwards, O. R. Bolduc, A. J. Baeumner, *Curr. Opin. Chem. Biol.* **2012**, *16*, 444.

[15] a) S. M. Moghimi, I. Hamad, *Journal of liposome research* **2008**, *18*, 195; b) A. Menny, M. Serna, C. M. Boyd, S. Gardner, A. P. Joseph, B. P. Morgan, M. Topf, N. J. Brooks, D. Bubeck, *Nature communications* **2018**, *9*, 5316.

Summary

In the following, different strategies were investigated to improve current POCT concepts to a quantitative diagnostic tool using chemiluminescence for detection. Chemiluminescence (CL) provides outstanding analytical performance due to its independence from external light sources, uniquely suiting quantitative POCT due to minimal instrumental requirements. Furthermore, it is exceptionally sensitive due to its background-free nature. The initial photophysical characterization of a new luminol derivative, *m*-carboxy luminol, revealed a 5-time higher quantum yield towards standard luminol and improved water solubility. Changing to this stronger emitting luminophore favored already standard microtiter plate-based assays by improving their sensitivity and limit of detection (LOD). Transferring these findings to a paper-based POCT setup demonstrated the benefit of a simply stronger emitting luminophore in the POCT field as signal recording becomes accessible to ubiquitous available detection devices such as simple smartphones. Specifically, a universal enzymatic microfluidic paper-based analytical device (µPAD) using L-lactate as model analyte was developed. Despite the involvement of the enzyme, lactate oxidase, a simple to perform µPAD platform that is stable for at least three months at room temperature was the result of this study. Introducing *m*-carboxy luminol as signaling molecule resulted in extraordinary signal-to-noise ratios in the final POCT setup, leading to µmolar detection limits for L-lactate and a dynamic range covering up to three orders of magnitude.

The increased hydrophilicity further allows encapsulation of this new luminophore into nanocontainer such as liposomes, to further amplify the signal intensity. In a second line of research, the previously reported *m*-carboxy luminol loaded liposomes were refined and investigated in standard lateral flow assay to be integrated in the current portfolio of suitable POCT labels. Initial experiments with fluorescent sulforhodamine B (SRB) liposomes, revealed the power of signal amplification already for photometric detection in direct comparison to gold nanoparticles (AuNP). Specifically, liposomes with 350 nm in diameter yield a 10-times lower LOD, in direct comparison to commercial AuNP, even in complex matrices such as human serum. Exploiting the liposomes' fluorescence by releasing the SRB through liposome lysis, yielded in an extraordinary gain in signal intensity. Yet, taking advantage of fluorescence did not directly translate into lower limits of detection in its current state due to the necessity of liposomes lysis on the test strip introducing heterogeneity in the signal location and thus negatively influences the detection. Inherently fluorescent liposomes were investigated as well, to maintain the signal position but were not feasible

due to the comparably low overall signal intensity. Based on these results, a new chemiluminescent liposome, with the highly water-soluble *m*-carboxy luminol, was developed to generate an exceptionally sensitive label. In a direct comparison of these liposomes in an interleukin-6 LFA, changing from photometric detection to fluorescence and chemiluminescence detection increased the sensitivity. Specifically, the CL approach yielded a significantly higher signal-to-noise (S/N) ratio of over 20. With fluorescence a S/N ratio of only 3.5 and surprisingly 12.8 for the colorimetric approach, was achieved which already rivals the commercial AuNP approach. Yet, changing to CL detection could so far not considerably reduce the LOD compared to fluorescence detection. This is currently attributed to non-specifically bound liposomes that interfere with the actual signal and has to be addressed in the future before CL liposomes can reveal their true potential.

In a third line of research, chemiluminescence liposomes were used as sensitive marker in an advanced assay system that is based on the principle of the standard neutralization assay. Here, specific interaction between the human complement system and liposomes is utilized. In a defined environment, the human complement system is able to release the dye molecules from the liposomes by directed lysis through a trigger molecule. The liposomes are designed to bind the analyte of interest, depicting the virus in this scenario. The trigger molecule on the other hand, is designed to bind the analyte. Hence, the trigger molecule is only present in close proximity to the liposomes surface if a binding event takes place and thus only triggers liposomes lysis through the complement system upon binding. Within this work, initial proof-of-concept studies were conducted to first of develop liposomes with lipid compositions that are stable in human serum, so-called stealth liposomes. Subsequent to this, specific lysis through different types of trigger molecules was demonstrated. Here, antibodies or lipopolysaccharide were tested for their ability to function as complement trigger. Both molecules were able to efficiently trigger the complement system and thus initiate directed lysis. Furthermore, a bystander assay confirmed that the complement system only attacks liposomes with a trigger molecule attached to the surface. Liposomes without a trigger in close proximity to the surface remain unaffected. This further supports the possibility of directed lysis through the complement system with adequate trigger molecules. Finally, successful surface modification of liposomes with relevant proteins and peptides was demonstrated and the suitability of side-directed versus random coupling evaluated. Although, side-directed coupling through streptavidin and biotin offers advantages such as oriented attachment of the biomolecule to the liposomes surface, the random coupling approach yielded in a more efficient attachment of the respective

biomolecules. In summary, proof-of-concept was achieved for the individual components and the basis for the combination of the single parts to a functioning assay was generated.

Zusammenfassung

Im Folgenden wurden verschiedene Strategien untersucht, um aktuelle POCT-Konzepte zu einem quantitativen diagnostischen Instrument weiterzuentwickeln. Hierfür wurden Chemilumineszenz als Detektionsmethode und Liposome als Signalverstärker untersucht. Die Chemilumineszenz (CL) bietet aufgrund ihrer Unabhängigkeit von externen Lichtquellen hervorragende analytische Performance und eignet sich aufgrund minimaler instrumenteller Anforderungen in einzigartiger Weise für quantitatives POCT. Darüber hinaus ist sie aufgrund der Abwesenheit von Hintergrundsignalen außergewöhnlich empfindlich. Die anfängliche photophysikalische Charakterisierung eines neuen Luminol Derivats, *m*-Carboxyluminol, zeigte eine 5-fach höhere Quantenausbeute und eine verbesserte Wasserlöslichkeit gegenüber Luminol. Der Wechsel zu diesem stärker emittierenden Luminophor begünstigt bereits standardmäßige Mikrotiterplatten basierte Assays, indem deren Empfindlichkeit und Nachweisgrenze (LOD) verbessert wurden. Die Übertragung dieser Erkenntnisse auf einen papierbasierten POCT-Aufbau zeigte den Vorteil eines stärker emittierenden Luminophors im POCT-Bereich, da die Signalerfassung für allgegenwärtig verfügbare Detektionsgeräte wie einfache Smartphones zugänglich wird. Insbesondere wurde ein universelles enzymatisches mikrofluidisches papierbasiertes System (µPAD) entwickelt unter Verwendung von L-Laktat als Modell Analyt. Trotz der Beteiligung des Enzyms Laktatoxidase war das Ergebnis dieser Studie eine einfach zu handhabende µPAD-Plattform, die mindestens drei Monate bei Raumtemperatur stabil ist. Die Nutzung von *m*-Carboxyluminol als Signalmolekül führte zu außergewöhnlichen Signal-zu-Rausch-Verhältnissen im finalen POCT-Aufbau, was zu µmolaren Nachweisgrenzen für L-Lactat und einem dynamischen Bereich von über drei Größenordnungen führte.

Die erhöhte Hydrophilie ermöglicht außerdem das Einschließen dieses neuen Luminophors in Nanocontainer wie Liposome, um die Signalintensität weiter zu verstärken. In einem zweiten Forschungsschwerpunkt wurden die zuvor beschriebenen *m*-Carboxyluminol beladenen Liposome optimiert und in einem standardmäßigen LFA untersucht, um sie in das aktuelle Portfolio geeigneter POCT Labels zu integrieren. Erste Experimente mit fluoreszierenden Sulforhodamin B (SRB)-Liposomen zeigten die Stärke der Signalverstärkung bereits für die photometrische Detektion im direkten Vergleich zu Goldnanopartikeln (AuNP). Insbesondere Liposomen mit 350 nm Durchmesser ergeben selbst in komplexen Matrizes wie Humanserum einen 10-fach niedrigeren LOD im direkten Vergleich zu kommerziellem AuNP. Die Ausnutzung der Fluoreszenz der Liposome durch

Freisetzung des SRB Farbstoffs durch Lyse der Liposome führte zu einem außergewöhnlichen Gewinn an Signalintensität. Die Nutzung der Fluoreszenz führte jedoch nicht direkt zu niedrigeren Nachweisgrenzen in ihrem derzeitigen Zustand, da die Lyse der Liposomen auf dem Teststreifen eine Heterogenität in der Signalposition bewirkt und somit die Detektion fehleranfälliger wird. Inhärent fluoreszierende Liposomen wurden ebenfalls untersucht, um die Signalposition nicht zu verändern, waren jedoch aufgrund der vergleichsweise geringen Gesamtsignalintensität nicht durchführbar.

Basierend auf diesen Ergebnissen wurde eine neue Klasse Liposome mit dem hochgradig wasserlöslichen *m*-Carboxyluminol weiterentwickelt, um ein außergewöhnlich empfindliches chemilumineszentes Label zu generieren. Im direkten Vergleich dieser Liposome in einem Interleukin-6 LFA erhöhte die Umstellung von photometrischer Detektion auf Fluoreszenz und Chemilumineszenz die Sensitivität. Insbesondere der CL Ansatz ergab ein deutlich höheres Signal-zu-Rausch-Verhältnis (S/N) von über 20. Mit Fluoreszenz wurde ein S/N-Verhältnis von nur 3,5 und überraschenderweise 12,8 für den kolorimetrischen Ansatz erreicht, was bereits mit dem kommerziellen AuNP-Ansatz konkurriert. Allerdings konnte der Wechsel zur CL Detektion den LOD im Vergleich zur Fluoreszenzdetektion bisher nicht wesentlich reduzieren. Dies wird derzeit als Folge von unspezifisch gebundener Liposomen vermutet, die das eigentliche Signal stören, und muss in Zukunft optimiert werden, bevor CL Liposome ihr wahres Potenzial entfalten können.

In einem dritten Forschungsschwerpunkt wurden CL Liposome als empfindliche Marker in einem fortschrittlichen Assay System verwendet, das auf dem Prinzip des standardmäßigen Neutralisationsassays basiert. Hier wird eine spezifische Wechselwirkung zwischen dem menschlichen Komplementsystem und Liposome ausgenutzt. In einer definierten Umgebung ist das menschliche Komplementsystem in der Lage, die Farbstoffmoleküle durch gerichtete Lyse durch ein Triggermolekül von den Liposomen freizusetzen. Die Liposome sind so konzipiert, dass sie den relevanten Analyten binden, welcher in diesem Szenario den Virus darstellt. Das Triggermolekül hingegen ist dazu bestimmt, an den Analyten zu binden. Daher ist das Triggermolekül nur dann in unmittelbarer Nähe der Liposomoberfläche, wenn ein Bindungsereignis stattfindet, und löst somit nur nach erfolgreicher Bindung die Lyse der Liposome durch das Komplementsystem aus. Im Rahmen dieser Arbeit wurden erste Proof-of-Concept Studien durchgeführt, um zunächst Liposome mit humanserumstabilen Lipidzusammensetzungen, sogenannte Stealth Liposome, zu entwickeln. Anschließend wurde die spezifische Lyse durch verschiedene Arten von Triggermolekülen demonstriert. Hier wurden Antikörper oder Lipopolysaccharide

auf ihre Fähigkeit getestet, als kompetenter Komplementauslöser zu fungieren. Beide Moleküle waren in der Lage, das Komplementsystem effizient zu aktivieren und so eine gerichtete Lyse einzuleiten. Darüber hinaus bestätigte ein Bystander-Assay, dass das Komplementsystem nur Liposome mit einem an der Oberfläche angebrachten Triggermolekül angreift. Liposome ohne Auslöser in unmittelbarer Nähe zur Oberfläche bleiben unbeeinflusst. Dies unterstützt weiter das Konzept einer gerichteten Lyse durch das Komplementsystem mit geeigneten Triggermolekülen. Schließlich wurde die erfolgreiche Oberflächenmodifikation von Liposomen mit relevanten Proteinen und Peptiden demonstriert und die Eignung von gerichteter versus zufälliger Kopplung bewertet. Obwohl die gerichtete Kopplung durch Streptavidin und Biotin Vorteile bietet, wie z. B. eine orientierte Bindung des Biomoleküls an die Liposomeoberfläche, führte in dieser Arbeit der zufällige Kopplungsansatz zu einer effizienteren Fixierung der jeweiligen Biomoleküle. Zusammenfassend wurde für die einzelnen Komponenten des Gesamtassays ein Proof-of-Concept erreicht und die Grundlage für die Kombination der einzelnen Teile zu einem funktionierenden Assay geschaffen.

1. Progression of Paper-Based Point-of-Care Testing toward Being an Indispensable Diagnostic Tool in Future Healthcare

Graphical Abstract

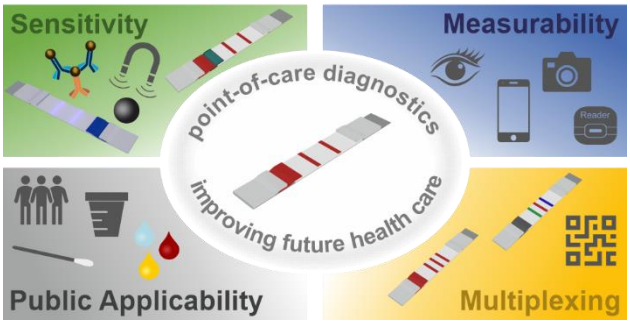

This chapter has been published in the American Chemical Society journal Analytical Chemistry.

reprinted with permission from Rink, S., Baeumner, A.J. Progression of Paper-Based Point-of-Care Testing toward Being an Indispensable Diagnostic Tool in Future Healthcare. *Anal. Chem.* 2023, 95, 3, 1785–1793 (**2023**). https://doi.org/10.1021/acs.analchem.2c04442.

Authors' contributions

Simone Rink: Conceptualization, visualization, literature review, writing: original draft – lead contribution

Antje J. Baeumner: Conceptualization, supervision, writing: review & editing – lead contribution

Abstract

Point-of-care (POC) diagnostics in particular focuses on the timely identification of harmful conditions close to the patients' needs. For future healthcare these diagnostics could be an invaluable tool especially in a digitalized or telemedicine-based system. However, while especially paper-based POC tests, with its most prominent example the lateral flow assay (LFA), have been successful due to their simplicity and timely response, the COVID-19 pandemic highlighted their limitations such as low sensitivity and ambiguous responses. This perspective discusses strategies that are currently pursued to evolve such paper-based POC tests towards a superior diagnostic tool that provides high sensitivities, objective result interpretation and multiplexing options. Here, we pinpoint the challenges with respect to (i) measurability and (ii) public applicability exemplified with select cases. Furthermore, we highlight those promising endeavors focused on (iii) increasing the sensitivity, (iv) multiplexing capability and (v) objective evaluation to also ready the technology for integration with machine learning into digital diagnostics and telemedicine. The status quo in academic research and industry is outlined and the likely highly relevant role of paper-based POC tests in future healthcare is suggested

1.1. Introduction

Pandemics, food safety recalls, diabetes, surging chronic diseases and more demonstrate in today's world the importance of point-of-care testing (POCT) and on-site diagnostics in general. It allows to timely identify pathogens, biomarkers, drugs or metabolites to ensure in time treatment and precautions and thus prevention of disease spreading or progression. POCT has been one of the continuing major trends in analytical chemistry over the last decades and great advances have been made since the term evolved in the early 1990s. Several rapid diagnostic tests are listed on the "WHO Model List of Essential *In Vitro* Diagnostics (IVD)" which serves as guide for countries to establish a national testing system.[1] Historically, POCT emerged as one of four major innovative driving forces in the *in vitro* diagnostic field along with automation, personalized healthcare, and digitalization.[2] It is defined in the international standard for Point-of-care testing (ISO 22870) as "testing that is performed near or at the site of a patient with the result leading to possible change in the care of the patient",[3] but is undoubtedly still undergoing very dynamic progression in various directions.[4] Today, POCTs should be subdivided into laboratory, near-patient and true POCT. With special focus on POCT for resource-limited settings, the Word Health Organization (WHO) defined characteristics that these systems should meet to be true POCT and thus coincides with disease control needs. They are known as the ASSURED criteria (affordable, sensitive, specific, user-friendly, rapid and robust, equipment-free and deliverable). These

ASSURED criteria for an ideal POC test are currently under debate to be refined to the REASSURED criteria where R stands for real-time connectivity and E for ease of specimen collection to leverage today's global networks in this digital age.[5] However, only a small portion of the commercially available POCT tests meet even the ASSURED criteria. Most of the emerging tests are often only near-patient or laboratory POCT.[6] In addition, most of the POCT systems reported in literature typically concentrate on the ASSR but often lack the UED criteria.[7] Nevertheless, advances in POCT research focus mostly on either reducing costs, increasing sensitivity, or reduced analysis time or steps. Yet, they often neglect the needs such as appropriate quality control as well as usability and adaption of these procedures in the clinical and hospital daily routine, as one of the largest end-users for POCT. This is also true for practicality of in-field and home-use tests.

One the one hand, reducing time and cost and increasing sensitivity is indeed highly relevant, especially if POCT is intended to be used in resources limited areas. Here, it is often intended for analysis of low biomarker concentrations to replaces laboratory tests. However, it is a fallacy that POCT in general is cheaper compared to advanced laboratory testing, even when innovations can reduce the per test costs. Currently established POCT systems in *e.g.,* hospitals, lack the testing capacities which high-throughput systems normally offer. In fact, in the clinical environment POCT is more expensive in general and the crucial benefit is rather the in-time response than the costs. This applies particularly if the test results are only qualitative and must be confirmed additionally through conventional laboratory testing. The cost aspect, instead, is crucial for home testing purposes and in critical infrastructure settings. Luppa and Junker reported in detail about the divergent demands, which are required and addressed by developers and users.[4] They concluded that in its current state POCT in hospitals and clinics is rather an asset for clinical diagnostics than a replacement. Furthermore, the ongoing pandemic revealed the problematic nature that is accompanied with self-testing.[4] Yet, the original POCT concept has expanded by now far beyond solely clinical and laboratory use, and current academic research is nevertheless driven by the vision of the development of fully stand-alone devices for the application (i) at any possible location (ii) by everyone ideally with (iii) the possibility of detecting multiple analytes, (iv) continuously at its best, (v) with a capability to be seamlessly integrated into a digital diagnostic approach – simply speaking a "Swiss army knife" system.

Thus, POCT covers an immense field of various analytical approaches and platforms, ranging from handheld and benchtop devices, single-use and reusable tests and continuous and end-point processes. Among all these systems, paper-based analytical devised (PAD) comply the ASSURED criteria the best.[6] The potential of lateral flow assays (LFA) and paper-based

microfluidics (µPADs) beyond the clinical and laboratory use is undeniable. Together with their professional use, especially LFAs for self-tests have a key role in managing the ongoing pandemic and expectantly in the near future the ever-increasing demand in *in vitro* diagnostics in general. This perspective will hence focus mainly on the (bio)analytical advances and progression of these paper-based POCTs by reviewing selected works on innovation of LFAs in general. Many of these strategies can also be found in the further advancements of µPADs, with the caveat that many of these 2D and 3D paper-based systems still lack in performance needed for commercial viability. Links to further improvement strategies for LFAs and µPADs in recent years are given with special focus on the hurdles and limits, that paper-based POCT still struggle with. This is exemplified by *e.g.,* the SARS-CoV-2 rapid antigen test, which has been relentlessly disclosed by the global endurance test 2020-2022 already.

1.2. Progression from qualitative to quantitative solutions

In 2022, The Guardian published an article with the exaggerated headline “The rise of lateral flow tests: are these ‘heroes’ of the pandemic here to stay?”.[8] It is the authors opinion that it is not the question whether these test will stay, but rather how far can we go with these test. What has long been limited to the knowledge and existence of solely pregnancy tests in the broader public, prior to the COVID-19 pandemic, has now evolved to a basic understanding, acceptance, and experience in handling LFAs in society. However, in this large-scale stress test of strategic integration of LFAs in disease control, the need for progression of this technology to be an even better asset was highlighted and will be addressed in the following. Almost parallel to the market entry of the first SARS-CoV-2 rapid tests, voices of criticism questioned the sensitivity of these tests and hence their reliability, especially when performed by lay people. Lateral flow assays are commonly known as POCT with low sensitivity, which were initially designed to only give quick yes/no responses.[7] However, when carried out by unexperienced users especially faint signals are challenging to interpret correctly. The progression to objective quantitative POCT also in the self-testing segment is hence inevitable. Furthermore, with proper quantification, access to monitoring relevant biomarkers through POCT would be conceivable which consequently allows more efficient disease control. LFAs in their originally design consist of a test and control line which contain either a capture probe against the analyte of interest (test line) or which is directed towards the reporter particles (control line). Upon binding of the reporter particle to the membrane they generate, in its easiest form, a color signal allowing visual readout. Paper-based microfluidic devices (µPAD) tap into a similar strategy by utilizing the inherent properties of paper. Likewise, the biomolecules adsorb to the paper substrate and passive fluid transport takes place through capillary forces. Despite the similarities, µPAD can convince with the cost advantage as well as spatial and design flexibility over standard LFAs. The full potential of these tests, however,

has not yet been uncovered and researchers currently focus on bringing paper-based POCT towards quantitative rather than a semi-quantitative/qualitative technique. Here, research focuses on (i) sensitivity improvement to allow the detection of low abundant biomarkers, (ii) POCT-qualified detection devices or strategies to be able to quantify the results and (iii) public applicability focusing on controlled sample application as well as controlled and transparent quantification to obtain user independent results.

1.2.1. Improvements towards sensitivity

With the constant exploration of new materials and reagents whether it be paper materials[7,9], recognition elements[10] or labeling systems[11,12], in addition with rethinking the spatial arrangement of these parts[13], limitations with regard to low sensitivity could already be partially addressed. Increasing the sensitivity of paper-based systems means increasing the contrast between test and background signal. This requires understanding and optimizing the interaction between the employed nanomaterials and involved biomolecules.[14] Current strategies to amplify the signal are either by changing the architecture of the test strip, using enzymes, hybrid nanoparticles or nanocontainers as label, chemical post-staining of the membrane or harnessing more sensitive detection methods such as fluorescence, chemiluminescence, surface enhanced Raman scattering (SERS), magnetism or photothermal illumination.[15] In the following we focus on recent promising innovations showing sensitivity enhancement through (i) new materials, (ii) changing the procedure itself, (iii) alteration of the strip architecture, or (iv) by merely advancing existing detection approaches. There are recent reviews published that discuss this topic in more detail. Interested readers are forwarded to the review of Shirshahi *et al.* in which various strategies for sensitivity enhancement are discussed in depth.[16] A comprehensive review on recent advances and trends in paper-based immunoassays for POCT in general is given by Li *et al.*[17] Recently, Sena-Torralba *et al.* published a thorough review article with focus on trends and advances in LFA. [18]

1.2.1.1. by optimized material, procedure, and strip architecture

From the advancing field of nanomaterial research, interesting and highly relevant designs have made an impact as labels in POCTs (**Table S 1**).[19,20] Extraordinary sensitivity enhancements of up to three orders of magnitudes towards standard gold nanoparticles (AuNP) were achieved by using palladium-based nanozyme labels catalyzing a dye formation on the strip for signal enhancement. Quite promising are also strategies that use embedding methods or nanocontainers. These methods can maximize the density of signal molecule per reporter probe with sensitivity enhancement of over one order of magnitude[21] up to an about 250-fold sensitivity increase[22]. Multifunctional nanocomposite probes are of interest as they

typically combine features *e.g.,* magnetic enrichment and separation, paired with their detection properties[23] or allow detection with low and high sensitivity modes[24] (see next paragraph). However, this is typically accompanied with multiple steps and the need of sophisticated detectors which may limit the use of these probes in true POCT. Advances through the recognition elements are accomplished *e.g.,* through bioengineering of antibodies increasing binding capacity and specificity toward the target analyte. Also, artificial reporter molecules such as short peptides, nanobodies and aptamers prove highly advantages, as these demonstrate greater stability than antibodies and can be manufactured in a more cost-effective manner.[25] Site-directed immobilization and strategies that do not negatively affect their binding strength are currently under evaluation. Of most recent impact have been specific binding domains that can be bioengineered into the recognition element itself. Most relevant for the paper-based POCT field are the cellulose binding domains which enable strong, oriented attachment to the test strip.[26]

POCT demands by definition the utmost simple assay protocols. Yet, more complicated assay steps, longer assay times and a bit of sophistication in sample preparation would render all POCTs more sensitive. Hence, much effort should be put toward the assay procedure itself to maximize assay performance. Sample preconcentration techniques are very efficient in improving the sensitivity. However, they are typically accompanied by increased user intervention. Hence, to take advantage of such techniques self-contained systems which do not require external action, are of great need. Promising examples include isothermal nucleic acid amplification such as the loop-mediated isothermal amplification for the detection of malaria[27] or protein preconcentration.[28] Yet, simplification of these processes or automation has not been addressed by the authors. Sequential delivery of the reagents was found by Liang *et al.* to improve the sensitivity.[29] Changing the sequence of reagent delivery from premixing of analyte and detection particle to allowing the analyte to bind first to the test line before the detection particle is introduced, resulted in a nonuniform binding profile with an 4- to 10-times lower limit of detection (LOD). Bradbury *et al.* developed a clever self-regulated system based on liquid-liquid extraction with sequential reagent delivery that includes preconcentration and signal enhancement. This ACE-system (**A**queous two-phase system-automated **C**oncentration and **E**nhancement) allows automated and timed addition of reagents to concentrate, capture, and enhance the test signal. The herewith achieved 30-fold improvement towards standard LFA protocols demonstrates the great potential of such strategies.[30] The ability to control flow rates themselves in a POCT also leads to better assay performance, *e.g.,* slower flow rates increase the interaction time which often benefits the sensitivity but simultaneously may also increase non-specific interactions. Capillary driven flows can only be controlled through the materials chosen or smart buffer additions that alter

the solutions viscosity. A temporary stop is generally not possible but often beneficial for certain reactions to maximize their output or to design automated sequential reagent delivery. Various materials have thus been investigated to manipulate the fluidic flow such as cotton threads[31], hydrogels[32], aerogels[33], wax barriers[18] or pillars[34], delaminating ink[35] and stacking pads[36]. All of them have in common that with increased interaction time the signal output increases and thus a lower limit of detection was achieved.

The findings with regard to procedural steps and time dependency of horizontal paper-based tests led researchers to reflect on the geometry and architecture of traditional strips.[37] Increasing the size of the sample and conjugate pad is a simple architectural change which can improve the sensitivity.[38] However, it comes at the expense of larger sample volumes, which may sometimes be difficult to obtain such as from finger pricks. Evolving the horizontal 2D layout into the 3D space expands the field to vertical flow assays (VFA). The main advantage of these VFAs for POCT is the independency of timed results, improved multiplexing capabilities and short assay times.[39] This supremacy of VFA over LFA has great relevance for true POCT. Hence it is not surprising that this technology has reached the market already (https://www.insti.com/hiv-test/, https://www.medmira.com/contact/). One of the first laymen approved paper-based POCT for the human immunodeficiency virus (HIV) is based on a VFA. This laymen test for the HIV is commercialized by biolytical laboratories (https://www.insti.com/hiv-test/) and provides fast and sensitive responses with a small drop of blood and a minimum of procedural steps. Further VFAs for the detection of syphilis or hepatitis B and C currently seek FDA approval together with their multiplexed systems. Especially, the simple integration of a multiplexed analysis and the rapidness allows VFA to compete with LFAs. Furthermore, VFAs are considered to be more sensitive than LFAs due to the absence of a Hook effect at high analyte concentrations. This avoids false-negative results and allows a higher sample loading capacity.[40] Devadhasan *et al.* improved the sensitivity of an active flow-through VFA by a factor of 10 simply by using a four times smaller reaction membrane. Additionally, they compared the VFA with a traditional LFA and showed an up to 80-times improved sensitivity when switching to a mini VFA.[40] However, so far, the reported VFAs are mostly qualitative with visual readout and lack quantitative evaluation solutions with POCT suited devices.[39] An intensive field of studies is the expansion of the LFA concept to 2D and 3D paper-based systems, *i.e.*, µPADs. These remain constrained by limited sensitivities and stabilities and are predominantly an academic technology especially in the field of diagnostics. The improvement strategies exemplified for LFAs here, would also be valid for µPADs. In addition though, µPADs enable easier adaptation to other detection strategies such as ePADs.[41]

1.2.1.2. by advanced detection strategies

Another approach to improve the sensitivity is to expand visual readouts with more sensitive detection methods such as chemiluminescence. Roda *et al.* reported on a dual lateral flow test for IgA in saliva and serum of COVID-19 patients.[42] Here, they developed a system which can either be run with visual or with chemiluminescence readout. Chemiluminescence detection was especially useful with low serological IgA responses. However, it requires additional user intervention for initiation of the CL reaction and a separate LFA strip to perform this assay along with the colorimetric detection. In contrast, Chen *et al.* reported a true dual readout system combining visual and chemiluminescence detection in one strip. Here, various biomarkers were tested in a single and multiplex LFA. In addition, the performance of the CL in the dual system for a low abundance biomarker in human serum was studied. In all scenarios, switching from visual detection of gold nanoparticles to chemiluminescence detection a sensitivity improvement by up to three orders of magnitude was demonstrated.[43] Wang *et al.* combined fluorescence with visual readouts by developing magnetic quantum dot hybrid nanoparticle. These particles hold separation and concentration properties in addition to the dual readout feature.[24] Furthermore, catalytic and chemical reactions which increase the signal output are under evaluation. These reactions, however, often require timed reagent addition which requires smart strip design to maintain the simplicity of traditional LFAs. Mulvaney *et al.* introduced a chemistry release fiber that contains the relevant dried reagents and integrated the fiber in the LFA to self-time the catalytic reaction.[44] Another smart design utilizes a water swelling polymer that is connected to the sample pad. This stamp-like principle initiates, *e.g.,* a chemiluminescence reaction, in a sequential manner by releasing reagents to the nitrocellulose (NC) membrane. The swollen polymer eventually connects the reagent pad with the NC membrane.[45] Furthermore, understanding the non-uniform color development in µPADs leads to design improvements. Here, anchoring of chromogenic agents can help to avoid uncontrolled movement and color gradient formation which typically hampers quantification.[46] A true sensitivity improvement in µPADs, can be achieved when switching from colorimetric to electrochemical detection (ePAD).[41,47] Despite several improvements with regard to the electrode fabrication, biorecognition elements and paper designs itself to reach clinically relevant detection limits[48], amplification strategies are often vital which can interfere with the POCT requirements.

1.2.2. Improvements towards objective detection

To provide a true quantitative system, an affordable readout system that plainly presents the test result to the end-user is indispensable. Three strategies reached the market by now for LFAs. The first strategy uses an on-strip disposable digital readout as integrated in the

Clearblue Digital Pregnancy Test (SPD Swiss Precision Diagnostics GmbH).[49] This all-in-one system already yields semi-quantitative test results. In view of sustainability and limited resources, however, it is questionable if small disposable devices will continue to be used without an eligible recycling plan. Mira (https://www.miracare.com/) and Bloom diagnostics GmbH (https://www.bloomdiagnostics.com/en_DE/how-it-works) on the contrary, count on portable handheld readers, together with the test strips for varying analytes of interest and app-based expert advice. Bloom diagnostics offers such POCTs already for ferritin, anti-mueller hormone and thyroid stimulating hormone. Mira provides a panel of tests for fertility hormones. The initial purchase price of such technologies, however, lies in the three-digit range. Hence, economical use only sets in with repeated testing and is focused rather on continuous measurements and the wealthier clientele. The third route of enhancing LFAs and µPAD to be truly POCT ready is the development of equipment-free readout strategies due to smart design alterations or the use of universal and ubiquitous available detection devices. Here, the most prominent example are mobile phones. This third route of enhancing LFA results is currently pursued among others by Abingdon Health with the AppDx® Smartphone Reader (https://www.abingdonhealth.com/de/lateral-flow-services/appdx-smartphone-reader/). They provide software solutions to make smartphones an independent reader to improve home test reliability.

Overall, mobile POCT remains to be a topic of utmost interest in academic research and several attempts have been made to successfully use smartphones as POCT detector.[20,50] Especially in the field of paper-based microfluidic devices, smartphones are extensively studied, even though diagnostic µPADs enter the market only very slowly. Also, for example, two start-up companies are currently working on the commercialization of a paper-based system for the detection of Zika virus, a liver function test and a comprehensive metabolic panel test by GroupK Diagnostics (https://groupkdiagnostics.com/) and a kidney function test card by Molecular Robotics (http://www.molecularrobotics.io/) with near future market readiness. In parallel, the non-profit organization, Diagnostics For All, developed a liver function test that is currently in the process of obtaining regulatory approval.[51] All these systems rely on image processing to get quantitative results. However, a big constrain for mobile POCT is the non-uniform nature of the built-in components such as the camera or batteries, the alternating junctions and sizes when looking at different smartphone manufacturers or product series and the need of user-friendly apps with qualified result interpretation.[52] Hence, calibration of the respective device is mandatory for accurate results[53], often accessories such as lenses or adapters are needed and sophisticated algorithms and artificial intelligence (AI)[54] that can run on a mobile phone are required. Recent studies show already promising examples on the integration of AI in POCT.[55] Especially,

post-image analysis of colored images needs special attention. Manufacturer-specific correction algorithms, which are applied in the image taking process with cameras or benchtop scanners, can distort the linear relation between color intensity and concentration.[56] Bermejo Peláez *et al.* conducted an in-field study, that digitalized the test result via an app. These results were processed through AI to evaluate various real SARS-CoV2 rapid tests and showed high performance of the AI interpretation in contrast to the visual readout.[57] No significant difference was obtained with different smartphones or recording conditions. Another strategy to bypass the accompanied issues with image analysis, especially for µPADs, are true equipment-free quantification strategies. These strategies are based on smart designs and have recently raised attention (**Figure 1**). Here, the user quantifies the result either by distance measurement (**Figure 1 A**), counting the number of colored bars or spots (**Figure 1 B**), measuring the time until a specific event takes place (**Figure 1 C**) or the display of interpreting text in dependency of the analyte concentration (**Figure 1 D**). Li *et al.* give a comprehensive overview of the most recent innovations in this field.[58]

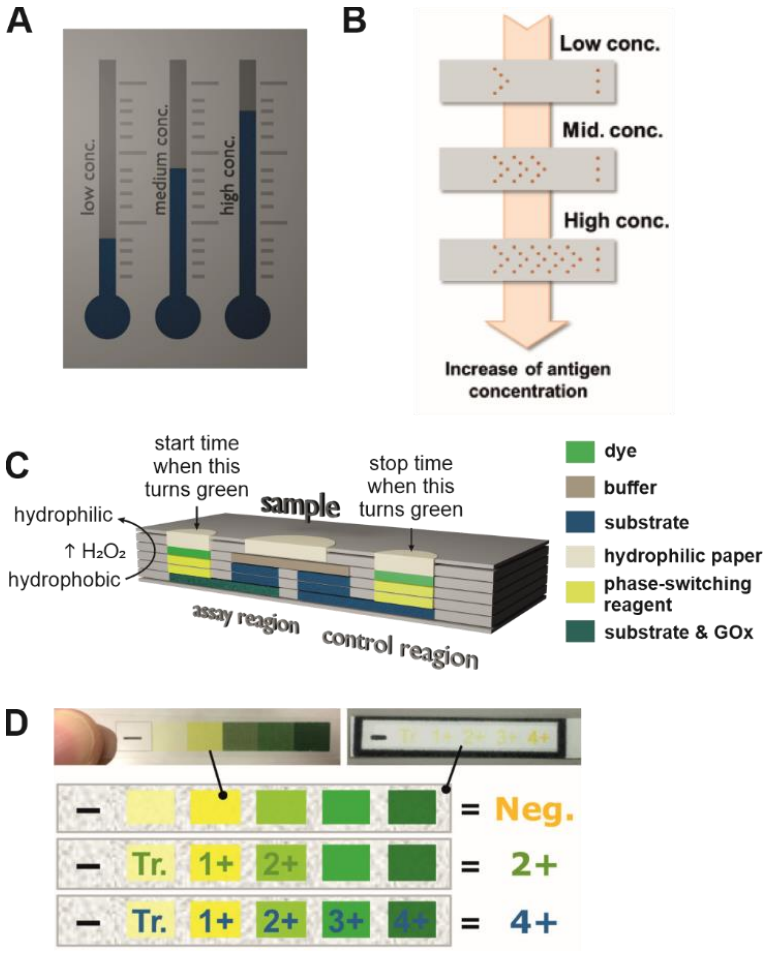

Figure 1 Strategies for equipment-free detection in paper-based analysis, quantification by A) distance after preconditioning of the µPAD[59], B) counting spots, reproduced from reference [60] Lee, K.W.; Yu, Y.C.; Chun, H.J.; Jang, Y.H.; Han, Y.D.; Yoon, H.C. Biosensors, 10, 87. Copyright © 2020 MDPI, C) time measurement [61] and D) text display, adapted in part with permission from[62], Copyright © 2017 American Chemical Society

1.2.3. Improvements towards public applicability

Besides the effort towards strategies for valid quantitative measurements in paper-based POCT, unequivocal result-to-patient assignment as well as transparent performance of the test are of essence. Here, steps which require user intervention are most critical and refer to correct sampling together with correct execution of the test as well as correct interpretation of the result. Whereas qualitative tests are more forgiving to deviations of the test protocol, quantitative analysis is strictly dependent on accurate performance. Current studies, however, pay only minor attention to sample processing such as uniform sample collection, preparation, application and especially to the integration of these processes into the final test. Yet, the accuracy of diagnostic results depends on the quality of the sample, the correct sampling time, area and matrix, and the correct execution of such tests along with the chosen method as demonstrated by the SARS-CoV2 antigen tests.[63] Here, general awareness and training of the executer is of essence, together with smart designs minimizing the human-induced error. Most importantly, for actual POCT systems, minimal to non-invasive sampling is required. Matrices such as saliva, sweat, urine, nasal mucosa or capillary blood qualify as such. Yet, these matrices differ by their biomarker composition, excreted volumes, and viscosity.[11] Urine for example is typically present in excess and with low viscosity, allowing direct application. However, its composition is very time-dependent. In contrast, in nasal mucosa the biomarker concentration is less dependent of the patients' action, but it is of high viscosity and only limited amount is available. This necessitates further processing before application to PADs is possible. Here, homogenous, and consistent uptake and efficient recovery from the nasal swab are critical. When taking the step toward quantitative tests, a control over the applied sample amount is vital. Yet, increasing manual steps in the sample preparation by the operator, especially when not trained, is challenging to control. Besides various fluid control mechanisms[64] that have been integrated into paper-based analytics to mostly increase the sensitivity, the issue of controlled sample application is often only of secondary importance. In the laboratory, volumetric instruments such as pipettes are frequently available for the addition of defined amount of sample. However, for quantitative measurements in-field this poses a critical issue. Here, engineers, analytical chemists and material scientists are in demand to design automatic sample preparation and controllable sampling mechanisms. Zangheri *et al.*, for example, developed a hybrid LFA cassette with an upstream microfluidic-based sample metering chamber for the quantitative detection of cortisol.[65] This is one option to ensure user-independent and consistent sample application. Komatsu *et al.* developed a dip-type µPAD that is independent of precise sample introduction. Here, the sample was applied by simply dipping the µPAD into the sample for at least 3 s. The recorded calibration curves for simultaneous detection of pH and ascorbic acid showed no significant difference when

changing the dipping time.[66] This allows for a pipette-free and user-friendly sample application. However, for both approaches a sample volume of at least 35 µl to several milliliter is needed.

In the end, the user must be able to make a valid quantitative statement enabled through the POCT system. This requires besides an controlled sample application also controlled and transparent quantification to avoid result mix-up and guarantees the validity of the result when performed by non-professionals. This is not only desirable in the professional use, where several tests are performed in parallel, but also in the private POCT field to be a practical help to the health system in the end. Here, digitalization of the result through barcoding provides a solution. As it is common in many settings already, platforms that are integrated in[67] or combined with[68] a QR code or barcode benefit from automatic readout. With QR codes, easy analysis that is independent from size and orientation is possible. Relevant manufacturing details can be embedded in the code, such as test type, expiration date and lot number allowing better quality assurance of these test.[69] In general, the technical integration of POCTs into a digital diagnostic health care system is theoretically not complicated, as long as readout devices like smartphones, POC analyzer, potentiostats, etc. with automated evaluation software have access to a secure cloud system.[70] Here, difficulties often derive from design ideas which do not fit the criteria of regulatory authorities stalling digital diagnostic's progress. Numerous examples suggest that focus on app development and the use of smartphone cameras for optical LFAs and µPADs will be essential to drive eHealth even further.[71] Yet, also here, it is obvious that such strategies should always be part of research and development to ensure the progression of individual POC testing to be a true relief for the health system.

1.3. Progression towards multianalyte detection

Aside from increasing the POCT performance with respect to its sensitivity and precision, a major additional improvement from the current state-of-the-art is the adaptation of POCTs for multianalyte detection. This has been addressed already extensively[72], yet remains a hot topic. Most strategies included, achieve multiplexing in paper-based systems through a spatial separation of the signals. Here, additional test lines are included upstream on the NC membrane, allowing for simultaneous detection of two or more biomarkers (**Figure 2 A**).[73] The multiplex capacity, however, is limited by the available detection area and has not been exceeded to eight parallel test lines in one strip.[74] Changing from lines to dots as detection areas enables microarray like structures which can be either used to detect a variety of biomarkers or integrate replicates or standards as additional quality control.[75]

It reduces the amount of sample needed and allows simultaneous detection of several analytes within the time frame of one test. This would be especially interesting in the clinical environment

as here, diagnostic and therapeutic decisions are typically based on a panel of biomarkers.[76] However, with increasing detection areas higher chance of cross reactivity unfolds and hence, a certain degree of ambivalence towards the results may remain. This is circumvented by changing the strip architecture for example by separating the NC membrane by laser cutting (**Figure 2 B**). Here, the strip still shares the sample, conjugate and waste pad, but the applied sample is split onto differently functionalized NC membrans.[77] Similarly to this, a disc-like arrangement of several LFAs was introduced by Zhao *et al.* allowing the simultaneous detection of ten pathogens (**Figure 2 D**).[78]

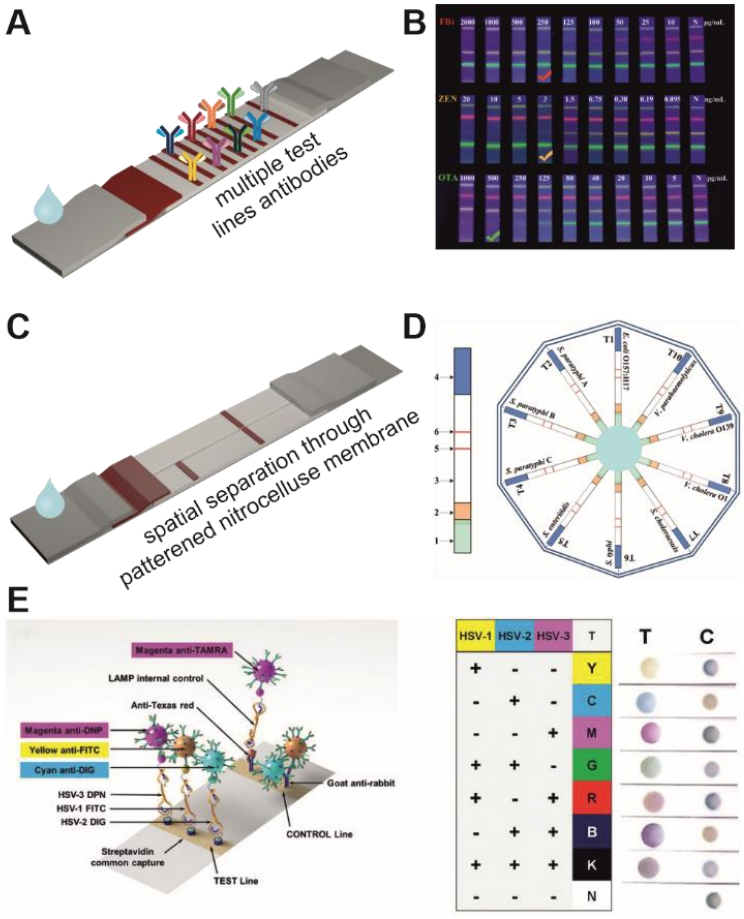

Figure 2 Multiplexing strategies in paper-based test systems A) by multiple test lines, each consisting of an different analyte specific antibody[74], B) by multiple test lines and differently colored labels, reprinted with permission from[79], Copyright © 2020 American Chemical Society, C) by spatial separation through splitting the nitrocellulose membrane[77], D) by aligning several monofunctional lateral flow assays with-in the testing cassette sharing the sample pad, reproduced from reference [78] Zhao, Y.; Wang, H.; Zhang, P.; Sun, C.; Wang, X.; Wang, X.; Yang, R.; Wang, C.; Zhou, L. Scientific Reports, 6, 21342. Copyright © 2016 Springer Nature, E) using differently colored labels within one test line, reproduced from reference [80] Zhang, Y.; Yu, Y.; Ying, J. Y. Advanced Functional Materials, 32, 2109553. Copyright © 2021 Wiley-VCH GmbH

Here, the sample pads of each LFA are located toward the center where the sample is added and upon addition, the sample migrates homogenously along each strip. Any of these strategies make quantification through a read-out device challenging. Alternatively, to the spatial separation the utilization of different detection probes has been studied. It allows to

maintain the original structure of the LFA with one test and control line but may requires several signal acquisition steps. Instead, unraveling of a mixed signal or detection techniques that allow single signal acquisition with distinct outputs for each analyte can be employed (**Figure 2 B,E**). Zhang *et al. e.g.*, utilized metallic nanotags modified with different Raman dyes for the detection of three cardiac biomarkers in a single test line via SERS. The results were obtained in 9 min and with good sensitivity matching the clinical relevant range.[81] In another study, multicolor Au/Ag nanoparticles were developed which yield up to seven distinct colors upon mixing (**Figure 2 E**).[80] With the applied spatial and color separation five target analytes were visually identified by three nanoparticle types using tags with distinct properties. However, this often requires multiple signal acquisition steps or spectral scanning to elucidate each individual signal. Hence, accurate evaluation of such tests require sophisticated algorithms so that they can be used as true POCT. Machine learning or simple chemometric approaches embedded into apps, on cell phones or located on a central server in digital diagnostic health care systems, will enhance such capabilities in the future.

Commercially only few multiplex LFA are available. Here, the dominating strategies to measure several analytes simultaneously are by spatial separation of the test lines on a single strip or a combination of test strips with single analyte specificity and shared sample pads. Becton Dickinson *e.g.,* launched a multiplexed rapid antigen test for influenza A + B and SARS-CoV-2 integrated in a single test strip (https://bdveritor.bd.com/en-us/main/rapid-antigen-testing/covid19-flu). Similarly, Quidel offers a dipstick test for influenza A + B (https://www.quidel.com/immunoassays/rapid-influenza-tests/quickvue-influenza-test) with distinct colors for the test and control line. Sensing.self developed a multiple detection kit which contains two test strips, with one being sensitive for influence A + B and the other strip being sensitive to SARS-CoV2 and MERS-CoV (https://sensingself.me/antigen_s4.php).

1.4. Conclusion

Paper-based POCT has proven its value and became rightly one of the cornerstones of modern diagnostics. However, the stress test during the COVID-19 pandemic has demonstrated its limitations such as false interpretation of ambiguous results, unsatisfying limits of detection, incorrect performance due to unskilled users, missing quality controls and the necessity of professional knowledge of disease progression for correct result interpretation and timely reasonable application. Although many innovations regarding this technology have been introduced, paper-based POCT is still in an early stage and has not yet unraveled its full potential. Sensitivity issues have been extensively addressed in recent years with the development of more sensitive materials and procedures. Here, especially the ongoing advances in nanotechnology introduces materials with hybrid properties. New nanoparticles

for example offer high and low sensitivity modes or additional separation properties. Advanced recognition elements on the contrary can specifically detect the target analyte while having an increased affinity to their substrate with the benefit of side-directed immobilization. Furthermore, switching to highly sensitive detection techniques such as fluorescence, chemiluminescence or SERS allow the detection of low concentration biomarkers already with POCT. The ongoing trend of miniaturization either for the analysis platform itself or for electronic parts allows to progress paper-based POCT from an originally only qualitative format to being quantitative, instead. This is mainly due to affordable but still highly sensitive detection possibilities that are available by now. Although they are not fit to fully replace standard laboratory tests in their current state, they are a priceless tool not only to free-up capacities for laboratory tests but also to ensure the necessity of such laborious tests, already. Fully automated PADs (especially ePADs and standalone µPADs) will challenge the market of paper-based POCT in the future due to their design adaptability and thus increased multiplexing capability once they are fit for commercialization. POCT and especially rapid diagnostic tests such as LFAs or µPADs can help meet the current and future needs of *in vitro* diagnostic. They can help with the exploding demands due to the ever-growing population and emerging pan- and epidemics, the increasing health awareness of each individual and the appreciation of preventative medical check-ups. A foreseeable digitalization of our healthcare system including telemedicine, central data servers that are available for the interpretation of test results, and the overall internet-of-things strategy in health care is a unique opportunity for POCTs. Thus, we can expect further boosts in innovative developments in the next 5 – 10 years. Furthermore, looking beyond the current driving force of health care, all of the solutions offered for on-site testing will find additional markets in veterinary care, environmental monitoring, forensics, and food analysis.

1.5. References

[1] Geneva: World Health Organization, *The selection and use of essential in vitro diagnostics*. *Report of the third meeting of the WHO Strategic Advisory Group of Experts on In Vitro Diagnostics, 2020 (including the third WHO model list of essential in vitro diagnostics)*, WHO Press, World Health Organization, Geneva, **2021**.

[2] B. BIOCOM AG, *Company Directory: In Vitro Diagnostics*.

[3] *ISO 22870:2016-11, Point-of-care testing (POCT) - Requirements for quality and competence*, Beuth Verlag GmbH, Berlin.

[4] P. Luppa, R. Junker (Eds.) *Point-of-care testing*. *Principles and Clinical Applications*, Springer Berlin Heidelberg, Berlin, Heidelberg, **2018**.

[5] K. J. Land, D. I. Boeras, X.-S. Chen, A. R. Ramsay, R. W. Peeling, *Nat. Microbiol.* **2019**, *4*, 46.

[6] M. Naseri, Z. M. Ziora, G. P. Simon, W. Batchelor, *Reviews in Medical Virology* **2022**, *32*.

[7] A. Nilghaz, L. Guan, W. Tan, W. Shen, *ACS Sens.* **2016**, *1*, 1382.

[8] Hannah Devlin, "The rise of lateral flow tests: are these 'heroes' of the pandemic here to stay?", can be found under https://www.theguardian.com/world/2022/jan/07/the-rise-of-lateral-flow-tests-are-these-heroes-of-the-pandemic-here-to-stay, **2022**.

[9] R. H. Tang, L. N. Liu, S. F. Zhang, X. C. He, X. J. Li, F. Xu, Y. H. Ni, F. Li, *Mikrochimica acta* **2019**, *186*, 521.

[10] a) W. Li, X. Zhang, T. Li, Y. Ji, R. Li, *Analytica chimica acta* **2021**, *1148*, 238196; b) M. M. Ali, R. Silva, D. White, S. Mohammadi, Y. Li, A. Capretta, J. D. Brennan, *Angewandte Chemie* **2022**, *134*.

[11] C. Parolo, A. Sena-Torralba, J. F. Bergua, E. Calucho, C. Fuentes-Chust, L. Hu, L. Rivas, R. Álvarez-Diduk, E. P. Nguyen, S. Cinti et al., *Nature protocols* **2020**, *15*, 3788.

[12] Y. Zhong, Y. Chen, L. Yao, D. Zhao, L. Zheng, G. Liu, Y. Ye, W. Chen, *Microchim Acta* **2016**, *183*, 1989.

[13] J. C. Cunningham, P. R. DeGregory, R. M. Crooks, *Annual review of analytical chemistry (Palo Alto, Calif.)* **2016**, *9*, 183.

[14] H. de Puig, I. Bosch, L. Gehrke, K. Hamad-Schifferli, *Trends in biotechnology* **2017**, *35*, 1169.

[15] J. D. Bishop, H. V. Hsieh, D. J. Gasperino, B. H. Weigl, *Lab on a chip* **2019**, *19*, 2486.

[16] V. Shirshahi, G. Liu, *TrAC, Trends Anal. Chem.* **2021**, *136*, 116200.

[17] F. Li, M. You, S. Li, J. Hu, C. Liu, Y. Gong, H. Yang, F. Xu, *Biotechnology advances* **2020**, *39*, 107442.

[18] A. Sena-Torralba, D. B. Ngo, C. Parolo, L. Hu, R. Álvarez-Diduk, J. F. Bergua, G. Rosati, W. Surareungchai, A. Merkoçi, *Biosensors & bioelectronics* **2020**, *168*, 112559.

[19] a) S. Ge, L. Zhang, Y. Zhang, F. Lan, M. Yan, J. Yu, *Nanoscale* **2017**, *9*, 4366; b) Z. Wang, J. Zhao, X. Xu, L. Guo, L. Xu, M. Sun, S. Hu, H. Kuang, C. Xu, A. Li, *Small Methods* **2022**, *6*, e2101143.

[20] S. Shrivastava, T. Q. Trung, N.-E. Lee, *Chemical Society reviews* **2020**, *49*, 1812.

[21] S. Rink, B. Kaiser, M.-S. Steiner, A. Duerkop, A. J. Baeumner, *Analytical and bioanalytical chemistry* **2022**, *414*, 3231.

[22] J. Hu, Z.-L. Zhang, C.-Y. Wen, M. Tang, L.-L. Wu, C. Liu, L. Zhu, D.-W. Pang, *Analytical chemistry* **2016**, *88*, 6577.

[23] T. S. Le, S. He, M. Takahashi, Y. Enomoto, Y. Matsumura, S. Maenosono, *Langmuir : the ACS journal of surfaces and colloids* **2021**, *37*, 6566.

[24] C. Wang, W. Shen, Z. Rong, X. Liu, B. Gu, R. Xiao, S. Wang, *Nanoscale* **2020**, *12*, 795.

[25] J. H. Soh, H.-M. Chan, J. Y. Ying, *Nano Today* **2020**, *30*, 100831.

[26] A. Elter, T. Bock, D. Spiehl, G. Russo, S. C. Hinz, S. Bitsch, E. Baum, M. Langhans, T. Meckel, E. Dörsam et al., *Scientific reports* **2021**, *11*, 7880.

[27] J. Reboud, G. Xu, A. Garrett, M. Adriko, Z. Yang, E. M. Tukahebwa, C. Rowell, J. M. Cooper, *Proc. Natl. Acad. Sci. U. S. A.* **2019**, *116*, 4834.

[28] Y. Deng, H. Jiang, X. Li, X. Lv, *Microchim Acta* **2021**, *188*, 379.

[29] T. Liang, R. Robinson, J. Houghtaling, G. Fridley, S. A. Ramsey, E. Fu, *Analytical chemistry* **2016**, *88*, 2311.

[30] D. W. Bradbury, M. Azimi, A. J. Diaz, A. A. Pan, C. H. Falktoft, B. M. Wu, D. T. Kamei, *Analytical chemistry* **2019**, *91*, 12046.

[31] S.-F. Zhang, L.-N. Liu, R.-H. Tang, Z. Liu, X.-C. He, Z.-G. Qu, F. Li, *Cellulose* **2019**, *26*, 8087.

[32] J. R. Choi, K. W. Yong, R. Tang, Y. Gong, T. Wen, H. Yang, A. Li, Y. C. Chia, B. Pingguan-Murphy, F. Xu, *Advanced healthcare materials* **2017**, *6*.

[33] Y. Tang, H. Gao, F. Kurth, L. Burr, K. Petropoulos, D. Migliorelli, O. T. Guenat, S. Generelli, *Biosensors & bioelectronics* **2021**, *192*, 113491.

[34] L. Rivas, M. Medina-Sánchez, A. de La Escosura-Muñiz, A. Merkoçi, *Lab on a chip* **2014**, *14*, 4406.

[35] D. Lee, T. Ozkaya-Ahmadov, C.-H. Chu, M. Boya, R. Liu, A. F. Sarioglu, *Science advances* **2021**, *7*, eabf9833.

[36] T.-T. Tsai, T.-H. Huang, C.-A. Chen, N. Y.-J. Ho, Y.-J. Chou, C.-F. Chen, *Scientific reports* **2018**, *8*, 17319.

[37] M. Díaz-González, A. de La Escosura-Muñiz, *Analytical and bioanalytical chemistry* **2021**, *413*, 4111.

[38] C. Parolo, M. Medina-Sánchez, A. de La Escosura-Muñiz, A. Merkoçi, *Lab on a chip* **2013**, *13*, 386.

[39] N. Jiang, R. Ahmed, M. Damayantharan, B. Ünal, H. Butt, A. K. Yetisen, *Advanced healthcare materials* **2019**, *8*, e1900244.

[40] J. P. Devadhasan, J. Gu, P. Chen, S. Smith, B. Thomas, M. Gates-Hollingsworth, D. Hau, S. Pandit, D. AuCoin, F. Zenhausern, *Analytical chemistry* **2021**, *93*, 9337.

[41] C. Carrell, A. Kava, M. Nguyen, R. Menger, Z. Munshi, Z. Call, M. Nussbaum, C. Henry, *Microelectron. Eng.* **2019**, *206*, 45.

[42] A. Roda, S. Cavalera, F. Di Nardo, D. Calabria, S. Rosati, P. Simoni, B. Colitti, C. Baggiani, M. Roda, L. Anfossi, *Biosensors & bioelectronics* **2021**, *172*, 112765.

[43] Y. Chen, J. Sun, Y. Xianyu, B. Yin, Y. Niu, S. Wang, F. Cao, X. Zhang, Y. Wang, X. Jiang, *Nanoscale* **2016**, *8*, 15205.

[44] S. P. Mulvaney, D. A. Kidwell, J. N. Lanese, R. P. Lopez, M. E. Sumera, E. Wei, *Sensing and Bio-Sensing Research* **2020**, *30*, 100390.

[45] K. Kim, H.-A. Joung, G.-R. Han, M.-G. Kim, *Biosensors & bioelectronics* **2016**, *85*, 422.

[46] S. V. de Freitas, F. R. de Souza, J. C. Rodrigues Neto, G. A. Vasconcelos, P. V. Abdelnur, B. G. Vaz, C. S. Henry, W. K. T. Coltro, *Analytical chemistry* **2018**, *90*, 11949.

[47] E. Noviana, C. P. McCord, K. M. Clark, I. Jang, C. S. Henry, *Lab Chip* **2020**, *20*, 9.

[48] X. Sun, H. Wang, Y. Jian, F. Lan, L. Zhang, H. Liu, S. Ge, J. Yu, *Biosensors & bioelectronics* **2018**, *105*, 218.

[49] "Pregnancy Test with Weeks Indicator", can be found under https://uk.clearblue.com/pregnancy-tests/digital-with-weeks-indicator.

[50] J. Liu, Z. Geng, Z. Fan, J. Liu, H. Chen, *Biosensors & bioelectronics* **2019**, *132*, 17.

[51] N. R. Pollock, J. P. Rolland, S. Kumar, P. D. Beattie, S. Jain, F. Noubary, V. L. Wong, R. A. Pohlmann, U. S. Ryan, G. M. Whitesides, *Science translational medicine* **2012**, *4*, 152ra129.

[52] a) T. Kong, J. B. You, B. Zhang, B. Nguyen, F. Tarlan, K. Jarvi, D. Sinton, *Lab on a chip* **2019**, *19*, 1991; b) A. Roda, E. Michelini, M. Zangheri, M. Di Fusco, D. Calabria, P. Simoni, *TrAC, Trends Anal. Chem.* **2016**, *79*, 317.

[53] J. Choi, A. J. Bandodkar, J. T. Reeder, T. R. Ray, A. Turnquist, S. B. Kim, N. Nyberg, A. Hourlier-Fargette, J. B. Model, A. J. Aranyosi et al., *ACS Sens.* **2019**, *4*, 379.

[54] Ö. B. Mercan, V. Kılıç, M. Şen, *Sensors and Actuators B: Chemical* **2021**, *329*, 129037.

[55] a) W. Wang, K. Chen, X. Ma, J. Guo, *Fundamental Research* **2022**; b) H. Tong, C. Cao, M. You, S. Han, Z. Liu, Y. Xiao, W. He, C. Liu, P. Peng, Z. Xue et al., *Biosensors and Bioelectronics* **2022**, *213*, 114449.

[56] Y. Soda, E. Bakker, *ACS Sens.* **2019**, *4*, 3093.

[57] D. Bermejo-Peláez, D. Marcos-Mencía, E. Álamo, N. Pérez-Panizo, A. Mousa, E. Dacal, L. Lin, A. Vladimirov, D. Cuadrado, J. Mateos-Nozal et al., *JMIR public health and surveillance* **2022**.

[58] Z. Li, M. You, Y. Bai, Y. Gong, F. Xu, *Small Methods* **2020**, *4*, 1900459.

[59] C. T. Gerold, E. Bakker, C. S. Henry, *Analytical chemistry* **2018**, *90*, 4894.

[60] K. W. Lee, Y. C. Yu, H. J. Chun, Y. H. Jang, Y. D. Han, H. C. Yoon, *Biosensors* **2020**, *10*.

[61] G. G. Lewis, J. S. Robbins, S. T. Phillips, *Analytical chemistry* **2013**, *85*, 10432.

[62] K. Yamada, K. Suzuki, D. Citterio, *ACS Sens.* **2017**, *2*, 1247.

[63] a) W. Wang, Y. Xu, R. Gao, R. Lu, K. Han, G. Wu, W. Tan, *JAMA* **2020**, *323*, 1843; b) O. Vandenberg, D. Martiny, O. Rochas, A. van Belkum, Z. Kozlakidis, *Nature reviews. Microbiology* **2021**, *19*, 171; c) B. Baro, P. Rodo, D. Ouchi, A. E. Bordoy, E. N. Saya Amaro, S. V. Salsench, S. Molinos, A. Alemany, M. Ubals, M. Corbacho-Monné et al., *The Journal of infection* **2021**, *82*, 269.

[64] T. H. Kim, Y. K. Hahn, M. S. Kim, *Micromachines* **2020**, *11*.

[65] M. Zangheri, M. Mirasoli, M. Guardigli, F. Di Nardo, L. Anfossi, C. Baggiani, P. Simoni, M. Benassai, A. Roda, *Biosensors & bioelectronics* **2019**, *129*, 260.

[66] T. Komatsu, R. Maeda, M. Maeki, A. Ishida, H. Tani, M. Tokeshi, *ACS Sens.* **2021**, *6*, 1094.

[67] a) A. Burklund, H. K. Saturley-Hall, F. A. Franchina, J. E. Hill, J. X. J. Zhang, *Biosensors & bioelectronics* **2019**, *128*, 97; b) T. F. Scherr, S. Gupta, D. W. Wright, F. R. Haselton, *Lab on a chip* **2017**, *17*, 1314.

[68] M. Yang, W. Zhang, W. Zheng, F. Cao, X. Jiang, *Lab on a chip* **2017**, *17*, 3874.

[69] M. Yang, Y. Liu, X. Jiang, *Chemical Society reviews* **2019**, *48*, 850.

[70] D. C. Christodouleas, B. Kaur, P. Chorti, *ACS central science* **2018**, *4*, 1600.

[71] B. Purohit, A. Kumar, K. Mahato, P. Chandra, *Current Opinion in Biomedical Engineering* **2020**, *13*, 42.

[72] a) C. Dincer, R. Bruch, A. Kling, P. S. Dittrich, G. A. Urban, *Trends in biotechnology* **2017**, *35*, 728; b) B. Gil Rosa, O. E. Akingbade, X. Guo, L. Gonzalez-Macia, M. A. Crone, L. P. Cameron, P. Freemont, K.-L. Choy, F. Güder, E. Yeatman et al., *Biosensors & bioelectronics* **2022**, *203*, 114050; c) J. Li, J. Macdonald, *Biosensors & bioelectronics* **2016**, *83*, 177; d) Y. Wu, Y. Zhou, Y. Leng, W. Lai, X. Huang, Y. Xiong, *Biosensors & bioelectronics* **2020**, *157*, 112168.

[73] K. Xiao, K. Wang, W. Qin, Y. Hou, W. Lu, H. Xu, Y. Wo, D. Cui, *Talanta* **2017**, *164*, 463.

[74] M. Han, L. Gong, J. Wang, X. Zhang, Y. Jin, R. Zhao, C. Yang, L. He, X. Feng, Y. Chen, *Sensors and Actuators B: Chemical* **2019**, *292*, 94.

[75] a) N. A. Taranova, N. A. Byzova, V. V. Zaiko, T. A. Starovoitova, Y. Y. Vengerov, A. V. Zherdev, B. B. Dzantiev, *Microchim Acta* **2013**, *180*, 1165; b) R. Charlermroj, S. Phuengwas, M. Makornwattana, T. Sooksimuang, S. Sahasithiwat, W. Panchan, W. Sukbangnop, C. T. Elliott, N. Karoonuthaisiri, *Talanta* **2021**, *233*, 122540.

[76] A. Poschenrieder, M. Thaler, R. Junker, P. B. Luppa, *Analytical and bioanalytical chemistry* **2019**, *411*, 7607.

[77] P. J. W. He, I. N. Katis, R. W. Eason, C. L. Sones, *Biosensors* **2018**, *8*.

[78] Y. Zhao, H. Wang, P. Zhang, C. Sun, X. Wang, X. Wang, R. Yang, C. Wang, L. Zhou, *Scientific reports* **2016**, *6*, 21342.

[79] J.-X. Yan, W.-J. Hu, K.-H. You, Z.-E. Ma, Y. Xu, Y.-P. Li, Q.-H. He, *Journal of agricultural and food chemistry* **2020**, *68*, 2193.

[80] Y. Zhang, Y. Yu, J. Y. Ying, *Adv Funct Materials* **2022**, *32*, 2109553.

[81] D. Zhang, L. Huang, B. Liu, E. Su, H.-Y. Chen, Z. Gu, X. Zhao, *Sensors and Actuators B: Chemical* **2018**, *277*, 502.

1.6. Supporting Information

1.6.1. Overview of selected paper-based analytical devices using advanced nanomaterials

Several nanomaterials have already been employed in paper-based analytical devices. An overview of recently applied nanomaterials in paper-based systems is given in **Table S 1**.

Table S 1 Selected advanced nanomaterials employed in paper-based analytical devices

Nanomaterial type	Target	Limit of Detection	Sensitivity Enhancement	Detection	Special Notes	Ref.
Metallic Nanoparticles						
Au nanospheres	procalci-tonin	0.5 ng mL^{-1} (20 nm)	-	color intensity (image analysis)	silver staining improves sensitivity by a factor of 10	[1]
Au nanopopcorn	procalci-tonin	0.1 ng mL^{-1}	5-times compared to Au nanospheres	color intensity (image analysis)	-	[1]
Au nanostars	procalci-tonin	comparable to 50 nm Au nanospheres	-	color intensity (image analysis)	-	[1]
Au nanoflowers (GNF)	fatty acid-binding protein (FABP) cardiac troponins (cTnT, cTnI)	0.03 ng mL^{-1} GNF1 (FABP) 0.06 ng mL^{-1} GNF1 and 0.01 ng mL^{-1} GNF2 (cTnT) 1.2 ng mL^{-1} GNF2 (cTnI)	3- to 10-fold decrease (visual) up to 100-times (instrumental)	visual and color intensity (image analysis)	low nonspecific binding	[2]
Au nanorod	DNA	2 pM	250-fold lower compared to AuNP	strip reader	-	[3]
Carbon Based Nanoparticles						
carbon nanotubes	rabbit IgG	1.3 pg mL^{-1}	3-times compared to AuNP	strip reader	-	[4]
carbon nanostring	influenza A	3.5×10^2 $TCID_{50}mL^{-1}$	-	image intensity	no cross reactivity to proteins	[5]

Table S 1 Selected advanced nanomaterials employed in paper-based analytical devices (continued)

Nanomaterial type	Target	Limit of Detection	Sensitivity Enhancement	Detection	Special Notes	Ref.
Magnetic Nanoparticles (MNP)						
MNP	morphine fentanyl metham-phetamine	0.20 ng·mL^{-1} 0.36 ng·mL^{-1} 1.30 ng·mL^{-1}	-	MPQ reader	multiplexing possible	[6]
MNP	prostate-specific antigen	25 pg mL^{-1}	-	MPQ reader	quantitative MP mapping	[7]
Luminescence Nanoparticles						
Upconverting nanoparticles	brain natriuretic peptide, suppression of tumori-genicity 2	5 pg mL^{-1} (BNP) and 1 ng mL^{-1} (ST2)	-	smartphone-based reader	multiplexing possible	[8]
quantum dots	S. pneu-moniae detection	10^4 cells mL^{-1}	-	fluorescence	-	[9]
near-infrared lanthanide-doped nanoparticles	alpha fetoprotein	0.742 ng mL^{-1}	-	fluorescence (EMCCD camera)	better stability than NIR organic dyes	[10]
Vesicles						
sulforhodamine B liposomes	inter-leukin 6	7 pg mL^{-1}	11-times lower compared to commercial AuNP	strip reader	-	[11]
polydiacetylene vesicles	hepatitis B surface antigen	0.1 ng mL^{-1} (fluorescence) 1 ng mL^{-1} (visual)	10-times lower compared to PS beads	visual, fluorescent microscopy image	red color and red fluorescence emission.	[12]
CdSe/ZnS QD containing fluorescent nanospheres	C-reactive protein	27.8 pM in buffer, 34.8 pM in serum	257-fold towards AuNP	fluorescence	EMCCD single photon detector/micro scope	[13]

Table S 1 Selected advanced nanomaterials employed in paper-based analytical devices (continued)

Nanomaterial type	Target	Limit of Detection	Sensitivity Enhancement	Detection	Special Notes	Ref.
Enzymatic Labels						
nano luciferase	human chorionic gonado-tropin	11.04 ng mL^{-1}	3-times higher compared to commercial AuNP	biolumi-nescence	uncontrolled diffusion of signal-generating products may hamper sensitivity improvement	[14]
horseradish peroxidase	cortisol	0.4 ng mL^{-1}	-	chemilumi-nescence	operated in space	[15]
Nanozymes						
PdNP	human chorionic gonado-tropin	100 nIU	10^3-times towards AuNP	color intensity (image analysis)	total chemistry for color development stored on chemistry release fibers	[16]
Au@Pt4L NPs	prostate-specific antigen	2 ng mL^{-1} low intensity mode (similar to pure AuNP) 20 pg mL^{-1} high intensity mode	100-fold towards AuNP	color intensity (image analysis)	plasmonic and catalytic activity	[17]

Table S 1 Selected advanced nanomaterials employed in paper-based analytical devices (continued)

Nanomaterial type	Target	Limit of Detection	Sensitivity Enhancement	Detection	Special Notes	Ref.
Multifunctional Nanocomposite Probes						
Pt/Au nanoparticle-latex nanocomposite (Pt/Au-P2VP)	influenza A (H1N1)	6.25×10^{-3} HAU mL^{-1} (Au-P2VPs) 2.5×10^{-2} HAU mL^{-1} (Pt-P2VPs)	64-fold for Au-P2VPs 16-fold for Pt-P2VPs compared to AuNP	visual or strip reader	surface functiona-lization through biotin	[18]
Pt-2VP@ superparamagnetic iron oxide nanoparticles (SPION)	C-reactive protein	0.08 ng mL^{-1} Pt-P2VP@ SPION	26-fold lower	visual	antigen–antibody binding and magnetic separation will increase with magnetic enrichment factor	[19]
Polyelectrolyte-coated Au magnetic nanoparticles	anti-Treponema pallidum	1 NCU mL^{-1}	absence of false positive result compared to bare Au magnetic nanoparticles	visual	prevents aggregation in conjugate pad	[20]
magnetic core @dual quantum dot-shell nanoparticles	Strepto-coccus pneu-moniae	8 pfu mL^{-1}	-	visual and fluorescent	high specificity & selectivity for biological samples	[9]

AuNP: gold nanoparticles, PdNP: palladium nanoparticles, QD: quantum dot, HAU: hemagglutinating unit, IU: international units, NCU: National Health Laboratory Center units, $TCID_{50}$: 50 % tissue culture infectious dose, pfu: plate forming

1.6.2. References

[1] K. Serebrennikova, J. Samsonova, A. Osipov, *Nano-micro letters* **2018**, *10*, 24.

[2] N. A. Taranova, N. A. Byzova, S. M. Pridvorova, A. V. Zherdev, B. B. Dzantiev, *Sensors (Basel, Switzerland)* **2021**, *21*.

[3] Q. Yu, J. Zhang, W. Qiu, K. Li, L. Qian, X. Zhang, G. Liu, *Microchim Acta* **2021**, *188*, 133.

[4] W. Qiu, K. Baryeh, S. Takalkar, W. Chen, G. Liu, *Microchim Acta* **2019**, *186*, 436.

[5] N. Wiriyachaiporn, H. Sirikett, W. Maneeprakorn, T. Dharakul, *Microchim Acta* **2017**, *184*, 1827.

[6] N. V. Guteneva, S. L. Znoyko, A. V. Orlov, M. P. Nikitin, P. I. Nikitin, *Microchim Acta* **2019**, *186*, 621.

[7] A. V. Orlov, V. A. Bragina, M. P. Nikitin, P. I. Nikitin, *Biosens. Bioelectron.* **2016**, *79*, 423.

[8] M. You, M. Lin, Y. Gong, S. Wang, A. Li, L. Ji, H. Zhao, K. Ling, T. Wen, Y. Huang et al., *ACS nano* **2017**, *11*, 6261.

[9] C. Wang, W. Shen, Z. Rong, X. Liu, B. Gu, R. Xiao, S. Wang, *Nanoscale* **2020**, *12*, 795.

[10] Q. Liu, S. Cheng, R. Chen, J. Ke, Y. Liu, Y. Li, W. Feng, F. Li, *ACS applied materials & interfaces* **2020**, *12*, 4358.

[11] S. Rink, B. Kaiser, M.-S. Steiner, A. Duerkop, A. J. Baeumner, *Analytical and bioanalytical chemistry* **2022**, *414*, 3231.

[12] J. Roh, S. Y. Lee, S. Park, D. J. Ahn, *Chemistry, an Asian journal* **2017**, *12*, 2033.

[13] J. Hu, Z.-L. Zhang, C.-Y. Wen, M. Tang, L.-L. Wu, C. Liu, L. Zhu, D.-W. Pang, *Analytical chemistry* **2016**, *88*, 6577.

[14] a) S. Eom, Y. Bae, S. Kim, H. Choi, J. Park, S. Kang, *Anal. Chem.* **2020**, *92*, 5473; b) Y. Ding, X. Hua, H. Chen, F. Liu, G. González-Sapien, M. Wang, *Anal. Chem.* **2018**, *90*, 2230.

[15] M. Zangheri, M. Mirasoli, M. Guardigli, F. Di Nardo, L. Anfossi, C. Baggiani, P. Simoni, M. Benassai, A. Roda, *Biosensors & bioelectronics* **2019**, *129*, 260.

[16] S. P. Mulvaney, D. A. Kidwell, J. N. Lanese, R. P. Lopez, M. E. Sumera, E. Wei, *Sensing and Bio-Sensing Research* **2020**, *30*, 100390.

[17] Z. Gao, H. Ye, D. Tang, J. Tao, S. Habibi, A. Minerick, D. Tang, X. Xia, *Nano letters* **2017**, *17*, 5572.

[18] Y. Matsumura, Y. Enomoto, M. Takahashi, S. Maenosono, *ACS applied materials & interfaces* **2018**, *10*, 31977.

[19] T. S. Le, S. He, M. Takahashi, Y. Enomoto, Y. Matsumura, S. Maenosono, *Langmuir : the ACS journal of surfaces and colloids* **2021**, *37*, 6566.

[20] D. Yang, J. Ma, Q. Zhang, N. Li, J. Yang, P. A. Raju, M. Peng, Y. Luo, W. Hui, C. Chen et al., *Analytical chemistry* **2013**, *85*, 6688.

2. Next Generation Luminol Derivative as Powerful Benchmark Probe for Chemiluminescence Assays

Graphical Abstract

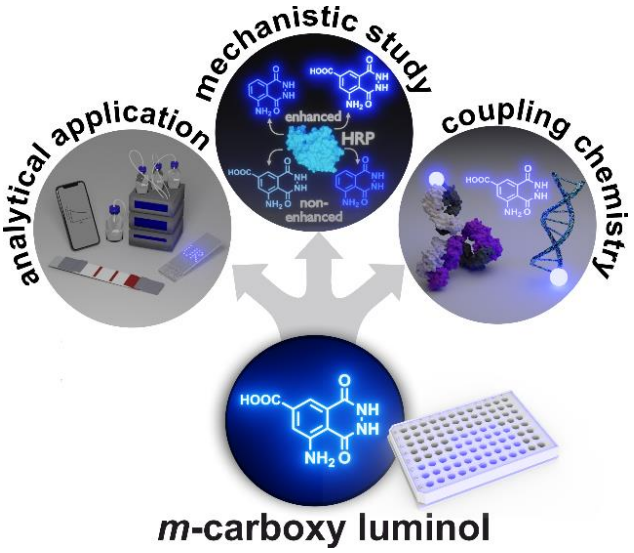

This chapter has been published in the Elsevier Journal Analytica Chimica Acta.

reprinted with permission from Rink, S., Duerkop, A., Jacobi von Wangelin, A., Seidel, M., Baeumner, AJ. Next Generation Luminol Derivative as Powerful Benchmark Probe for Chemiluminescence Assays. *Anal. Chim. Acta* 1188, 339161 (**2021**). https://doi.org/10.1016/j.aca.2021.339161.

Authors' contributions

Simone Rink: Conceptualization, visualization, investigation, formal analysis, data curation, writing: original draft – lead contribution

Antje J. Baeumner: Conceptualization, supervision, project administration, experimental design, writing: original draft – lead contribution

Axel Duerkop: Conceptualization, supervision, project administration, experimental design, writing: original draft – supporting contribution.

Michael Seidel: Resources, writing: review & editing - supporting contribution

Axel Jacobi von Wangelin: writing: review & editing - supporting contribution

Abstract

Chemiluminescence (CL) provides outstanding analytical performance due to its independence from external light sources, background-free nature and exceptional sensitivity and selectivity. Yet, ultra-sensitive (bio)analysis is impeded by low hydrophilicity, poor quantum yields, fast kinetics or instability of most CL reagents such as luminol, acridinium esters, dioxetanes or peroxyoxalic derivatives. Photophysical studies show that *m*-carboxy luminol overcomes these limitations as its hydrophilic design provides a 5-fold increase in relative quantum yield resulting in superior performance in H_2O_2-dependent bioassays with 18-fold higher sensitivity for the quantification of its co-reactant H_2O_2, and 5-times lower detection limits for the luminophore. Studies with CL enhancers suggest its significance for mechanistic investigations in tandem with peroxidases. Finally, its integration into enzymatic and immunoassay applications demonstrates that *m*-carboxy luminol will provide signal enhancement, lower detection limits, and increased dynamic ranges for any other luminol-based CL assay, thus comprising the potential to replace luminol as benchmark probe.

Keywords

analytical methods, luminescence, enzymatic lactate detection, immunoassay, luminol derivative

2.1. Introduction

Chemiluminescence (CL) has proven its superiority as detection strategy as it affords high sensitivity down to the attomolar level [1] due to its background-free nature [2]. CL is already a standard tool in clinical diagnostic, pharmaceutical and biomedical research, environmental control and several other areas [3], where it is favored for the detection of low-concentration analytes, such as metabolites and pharmaceuticals as well as heavy metal water pollutants [4] and biomarkers[5]. It provides rapidness, simplicity and flexible integration into (bio)analytical strategies.[6] The feature of quantitative detection with inexpensive instrumentation makes CL especially attractive for miniaturization and low-cost point-of-care (POC) devices as no additional light source or electrode material is required for light generation.[7] Luminol (**1**) is the most common CL reagent, albeit it suffers from very low water solubility and low CL quantum yield (Φ) [2] of about 1.2 % [8] along with reduced CL when measured in aqueous solution in contrast to aprotic solvents. Extensive research has been performed over the last three decades to primarily elucidate the underlying mechanism of the luminol CL reaction with the benefit of identifying the most efficient

alteration of the luminol core to ascertain its entire CL potential and improve the CL outcome (see ESI). For most of the reported structural alterations, stronger CL emission was typically obtained at the expense of reduced hydrophilicity grading these derivatives even less applicable to bioanalytical challenges and water-based analysis (ESI, **Figure A.1** B). The easily accessible, water-soluble, yet hitherto under-utilized derivative *m*-carboxy luminol (**2**, see **Figure 1**) has been demonstrated to display four-fold signal enhancement over the parent luminol (**1**) in electro-chemiluminescence (ECL) while maintaining the electrochemical characteristics of luminol.[9] Still, not much is known about its photophysical properties and the related CL enhancement mechanisms. Thus, we herein specify for the first time *m*-carboxy luminol's (**2**) photophysical and chemiluminescence characteristics and focus not only on its analytical profit but also on its potential as probe for mechanistic studies in tandem with horseradish peroxidase.

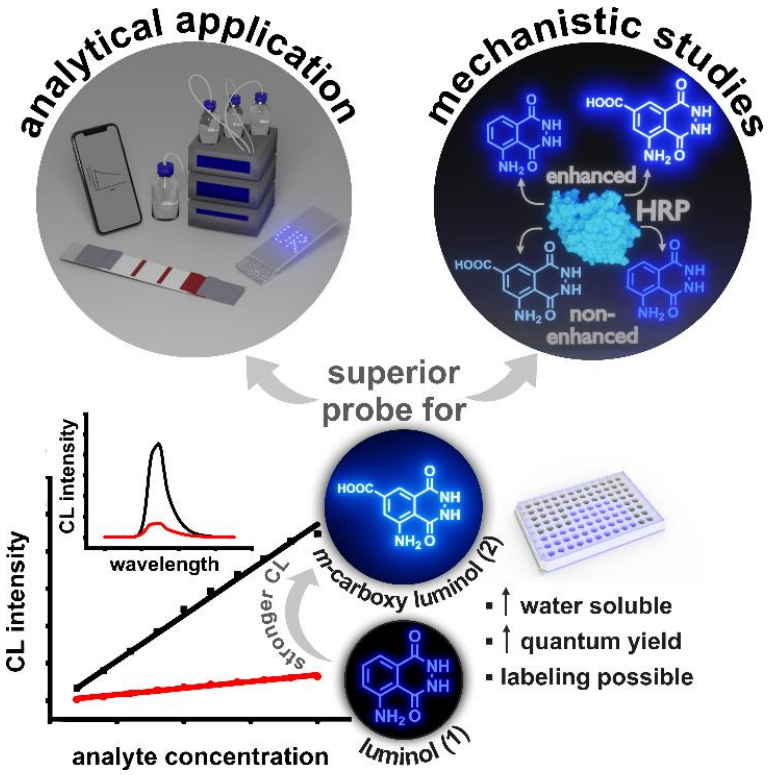

Figure 1 Evolution of a multitude of potential applications of *m*-carboxy luminol (**2**) to (bio)analytical studies with enhanced performance over the benchmark probe luminol (**1**)

Chemiluminescence (CL) reactions are powerful analytical tools with utmost importance and broad utility as they are applicable throughout the entire analytical spectrum of methods as demonstrated by their routine use in commercial chromatography, flow injection analysis, and immunoassays. These methods are applied in all chemistry disciplines to study structure-activity relationships, elucidate reaction mechanisms, or for ultrasensitive

monitoring of low-concentration analytes.[10] CL probes that show enhanced photophysical properties over the common benchmark luminol are highly desired. With its high water solubility and strong luminescence, *m*-carboxy luminol (**2**) could thus be of high applicability in CL assays.

2.2. Material & Methods

Chemicals and consumables. All chemicals were of commercial HPLC grade or higher and were used without purification. Sodium hydroxide solution, potassium dihydrogen phosphate and potassium chloride were purchased from Merck (Darmstadt, Germany). Tris(hydroxymethyl)aminomethane (Tris) was purchased from Affymetrix, Thermo Fisher Scientific Inc. (Waltham, Massachusetts). Sodium chloride was purchased from neoFroxx GmbH (Einhausen, Germany). Luminol, hydrochloric acid, disodium hydrogen phosphate dihydrate, hydrogen peroxide (HP) solution, hemin, 3,3´,5,5´-Tetramethylbenzidine (TMB) liquid substrate (T8665), *p*-coumaric acid, cobalt chloride, diclofenac sodium salt (D6899), anti-mouse IgG peroxidase antibody (A9044) and sodium L-lactate were ordered from Sigma Aldrich Chemie GmbH (Munich, Germany) and BSA (T844.2), potassium hydrogen carbonate and sulfuric acid were purchased from Carl Roth (Karlsruhe, Germany). Horseradish peroxidase (HRP) was purchased from Sigma Aldrich Chemie GmbH (Munich, Germany) and a 300 U mL^{-1} stock solution in 10X PBS buffer, pH 7.4 was prepared. Lactate Oxidase (LOx) was obtained from AG Scientific (San Diego, USA) and a 100 U mL^{-1} in 1X PBS buffer, pH 7.4 was prepared. Both enzymes were aliquoted and stored at 4 °C and respective working solutions were prepared freshly before each measurement. *m*-Carboxy luminol was initially synthesized by the group of Professor Jacobi von Wangelin according to [9] and in course of the study custom-made by Taros Chemicals GmbH & Co (Germany) to maintain consistent quality and supply of the luminophore. However, **2** is hitherto not commercially available. Mouse anti-DCF, 12G5 was kindly provided by the research group of Dr. Seidel (Technical University of Munich, Germany). For luminescence measurements, standard white 96-well microtiter plates (MTP) from Porvair were used if not stated differently. All of the experiments were performed at 25 °C.

CL measurements were performed with a Synergy Neo 2 microplate reader from BioTek (Bad Friedrichshall, Germany) either in the chemiluminescence spectral or endpoint mode.

2.2.1. Determination of absorbance characteristics.

Absorbance spectra of *m*-carboxy luminol and luminol were recorded with a Varian Cary 50 Bio photometer from 230 nm to 700 nm in 0.5 nm steps with slow reading speed. The

luminophore stock solutions were diluted to 100 µmol L^{-1} luminophore in 0.1 mol L^{-1} carbonate buffer (pH 10.5). The determination of the extinction coefficient was performed by measuring the absorbance of both luminophores at the λ_{max} determined previously.

2.2.2. Chemiluminescence characterization.

Emission spectra, quantum yield determination, H_2O_2 and luminophore calibration were all performed according to the following procedure. First the luminescence solution (LS) consisting of the luminophore and either hydrogen peroxide or the catalyst (hemin, cobalt or HRP) was measured before adding the initiation solution (IS) consisting either of hydrogen peroxide or catalyst. A machine-controlled luminescence reading procedure was applied which started an automated protocol directly after initiation of the CL reaction in a in a sequential measurement, one well after the other. The automated program included an initial 5 s shaking step to homogenously mix IS and LS. Experimental details to each individual measurement are given in the ESI.

2.2.3. Competitive diclofenac assay.

The competitive diclofenac (DCF) assay was performed in a 96-well high binding microtiter plate from (655074, Greiner BioOne, Germany) according to an already published procedure.[11] First, the MTP was coated with 200 µL of 5 µg mL^{-1} BSA-DCF in coating buffer (80 mmol L^{-1} Na_2CO_3/100 mmol L^{-1} H_3BO_3, pH 9.4) overnight at 4 °C. The subsequent assay steps were carried out at RT. After coating, the plate was washed three times with 200 µL of washing buffer (1X PBS pH 7.4, 0.05% (w/v) TWEEN®20; WB) for 5 min. 200 µL of blocking buffer (1% (w/v) BSA in WB) were added for 1 h under constant shaking for saturation of free bindings sites. The plate was washed again three times with 200 µL of WB. DCF standard dilutions were prepared in ultrapure water and 50 µL double concentrated DCF dilution were premixed with 50 µL double concentrated mouse anti DCF (12G5, final concentration: 0.25 µg mL^{-1} in 100 µL) in 1X PBS buffer, pH 7.4. 100 µL of the premix was added and incubated for 1 h under constant shaking. After three washing steps, each 5 min, 100 µL of secondary anti-mouse IgG LOx conjugate was added (5 µg mL^{-1} in WB) and incubated for 1 h under constant shaking. After the final washing with three times 200 µL of WB, 100 µL of L-lactate (10 mmol L^{-1} in ultrapure water) was added and incubated for 15 min. CL measurement was done by adding 100 µL of CL substrate (200 µmol L^{-1} luminophore, 2 µmol L^{-1} hemin in 0.1 mol L^{-1} carbonate buffer pH 10.5) followed by direct measurement. The colorimetric DCF assay was performed similar to the chemiluminescence DCF assay. After the incubation of the DCF premix and three washing

steps, 200 µL of secondary anti-mouse IgG horseradish peroxidase antibody (A9044, Sigma Aldrich) was added (0.25 µg mL^{-1} in WB) and incubated for 1 h while shaking. After three times washing with 200 µL of WB, 100 µL of ready to use TMB liquid substrate (T8665, Sigma Aldrich) was added and incubated for 5 min before 100 µL of 1 N sulphuric acid were added to stop the enzymatic reaction and absorbance was measured at 450 nm. In accordance with recommended TMB detection strategies in ELISAs, the detection of the single absorbance peak for the diimine at 450 nm upon acid addition was chosen in order to take advantage of the higher extinction coefficient of this peak and avoid any transient signal changes that would result in larger standard deviations across measurements.

The BSA-DCF loading study and the anti-mouse IgG-LOx dilution experiment were performed accordingly with slight adjustments (see ESI).

2.2.4. L-lactate Assay.

In the CL-based L-lactate assay an endpoint measurement was conducted. Therefore, L-lactate in the respective concentration and 2 µL of LOx (100 U mL^{-1}) were preincubated at 25 °C in a total volume of 100 µL for 20 min in 1X PBS pH 7.4 during constant agitation. Subsequently, a background luminescence reading was carried out. After the incubation, 100 µL of detection solution containing 200 µmol L^{-1} luminophore and 20 µmol L^{-1} hemin in 0.1 mol L^{-1} carbonate buffer (pH 10.5) were simultaneously added to a triplicate of one concentration. The measurement was started instantaneously after shaking for 5 s. The luminescence intensity was recorded for 2 s at a reading height of 1 mm and a gain of 70 at 25 °C. The synthetic sweat samples were diluted one to 40. It consists of a mixture of sodium chloride, urea and lactic acid with pH 6.53 (according to DIN 53160-2).

2.3. Results & Discussion

Filling the knowledge gap, we studied the photophysical characteristics and inherent efficiency of *m*-carboxy luminol (**2**) as CL probe in direct comparison to the current benchmark luminol (**1**). A broad scope of organic, inorganic and enzymatic catalyst systems were evaluated to ascertain structure-activity relationships of both luminol derivatives.[9] Photophysical studies demonstrated that the carboxy-substituted luminol retains typical luminol characteristics (**Figure 2**) but exhibits a five-fold higher CL quantum yield (**Table 1**).

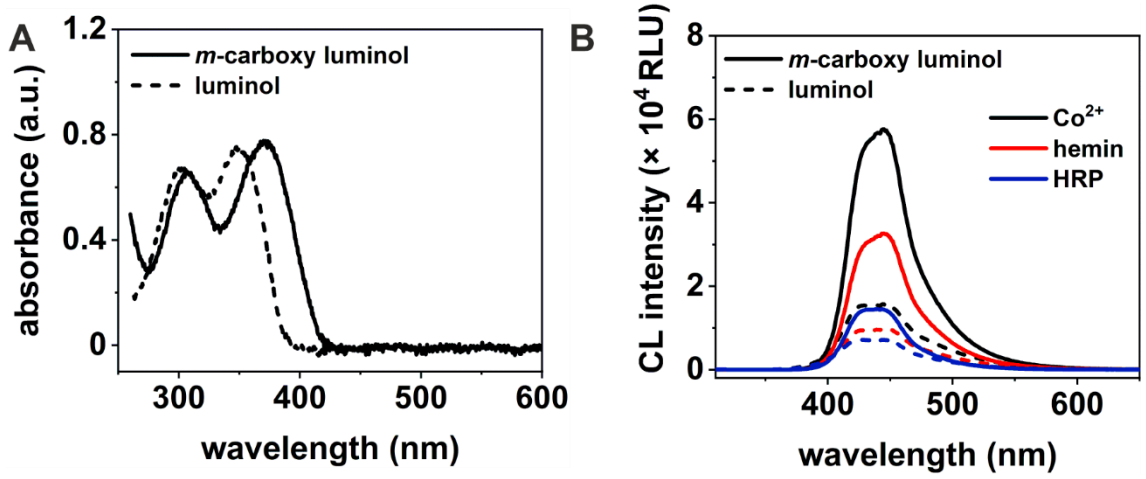

Figure 2 Photophysical characteristics and enhanced chemiluminescence (CL) of *m*-carboxy luminol. Absorbance spectra (A) and chemiluminescence (CL) spectra (B) of *m*-carboxy luminol (solid line) and luminol (dashed line) of a solution containing 100 µmol L^{-1} luminophore in 0.1 mol L^{-1} carbonate buffer (pH 10.5). Absorbance spectra (A) were recorded from 230 nm to 700 nm in 0.5 nm steps, with normal read speed, spectra were background-corrected. CL reaction (B) was initiated with 30 mmol L^{-1} H_2O_2 and 1 µmol L^{-1} Co(II) or hemin in 0.1 mol L^{-1} carbonate buffer (pH 10.5) or 30 mmol L^{-1} H_2O_2 in 0.033 mol L^{-1} Tris-HCl (pH 8.5) and 1.5 U mL^{-1} horseradish peroxidase and 50 µmol L^{-1} *p*-coumaric acid, recorded with gain 90, reading height 4.5 mm, integration time 20 ms (uncorrected spectra), recorded from 300 to 650 nm in 1 nm steps, data are presented as mean ± SD (error bar) with n = 3

Three standard catalysts, Co(II), hemin and horseradish peroxidase (HRP), were evaluated that all gave comparably stable CL signals with analogous spectral characteristics to luminol (**1**) but significantly enhanced CL for **2**, independent of the applied catalyst (**Figure 2 B**).

Table 1 Chemiluminescence of *m*-carboxy luminol with different catalysts and derived quantum yields

Catalyst	Luminol 2 I (× 10^4) (RLU)[a]	Luminol 1 I0 (× 10^4) (RLU)[b]	I/I_0	Luminol 2 ΦCL (%)[c]
Co(II)	6.5 ± 0.1	2.34 ± 0.05	2.79 ± 0.08	3.4 ± 0.1
hemin	37 ± 3	8.7 ± 0.1	4.2 ± 0.3	5.1 ± 0.4
horseradish peroxidase[d]	13 ± 2	3.7 ± 0.3	3.6 ± 0.6	4.3 ± 0.7

[a]CL intensity of *m*-carboxy luminol, [b]CL intensity of luminol, [c]relative CL quantum yield determination adapted from Griesbeck *et al.* [12], [d]through enhanced pathway with *p*-coumaric acid, data are presented as mean ± SD (error bar) with n = 4

The exact nature of the CL signal improvement is not clear yet as it can derive from either an accelerated reaction due to initially higher available amount of peroxide species or overall improved kinetic of the excited aminophthalate formation. Further theoretical and basic studies are needed to fully elucidate the new mechanism.

Furthermore, stability studies revealed that *m*-carboxy luminol is similarly stable as luminol in carbonate buffer pH 10.5 (**ESI**, **Figure A.6 A**) and even more stable in water (**ESI, Figure A.6 B**). We probed the applicability of luminol **2** to the detection of trace amounts of hydrogen peroxide (HP) which is typically notorious due to the lack of sensitivity of spectrophotometry, fluorimetry or amperometry.[13] HP can initiate CL reactions with luminol and is involved in various physiological processes in the human body. It is not only a common product of enzyme reactions, but trace amount analysis of HP is especially crucial for a better understanding of cell signaling pathways and immune activation.[14] Wide-range screening of HP concentrations with all three catalysts (Co(II), hemin, HRP) showed a non-linear relationship as described by Burdo *et al.* [15] for both luminophores, but with much stronger signals for the new luminol derivative **2** (**ESI, Figure A.3**). Here, a similar trend regarding the CL enhancement by *m*-carboxy luminol was obtained at ideal CL reaction conditions with hemin showing the strongest enhancement followed by HRP and Co(II). The observed decrease of the CL signal at high HP concentrations suggests radical self-reaction rather than a reaction with the luminophore.[15] Also, despite an overall known non-linear correlation, low HP concentrations are expected to provide proportionality between CL emission and HP concentration as long as the catalyst-peroxide complex concentration is lower than the concentration of the catalyst.[15] The superior performance of *m*-carboxy luminol (**2**) was confirmed in quantitative HP measurements (**Figure 3 A and ESI**) especially in the (bio)analytically relevant nanomolar to low micromolar range.[16,17]

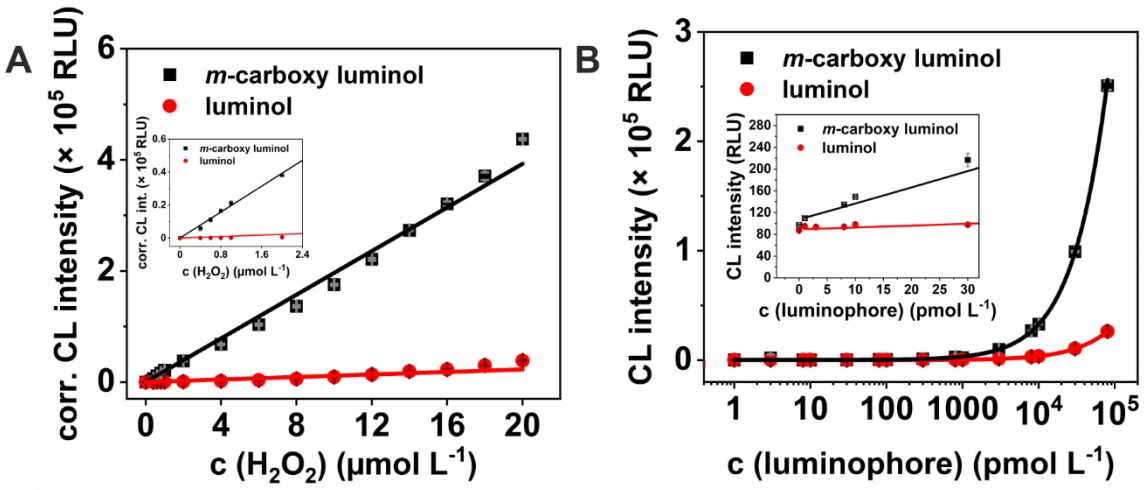

Figure 3 CL enhancement with *m*-carboxy luminol for H_2O_2 and luminophore detection. Dose-response curve of H_2O_2 (A) and luminophore detection (B) with *m*-carboxy luminol (black) and luminol (red). For (A) 100 µmol L^{-1} luminophore and 10 µmol L^{-1} hemin and for (B) 10 mmol L^{-1} H_2O_2 and 10 µmol L^{-1} hemin in 0.1 mol L^{-1} carbonate buffer (pH 10.5) were used, CL signals were recorded with gain 100, reading height 1 mm, integration time 2 s, data are presented as mean ± SD (error bar) with n = 3; figure insets show enlargements of the low concentration region

The high water solubility of the new benchmark luminophore **2** enables analytical performance in more biocompatible environments as no organic solvents or strong bases are needed. Here, the different catalysts provided varying limits of detection (LOD) (ESI, **Table A.2**), which is due to the various numbers of active peroxide species involved in the different catalytic reaction mechanisms. In case of HRP, CL enhancement with *m*-carboxy luminol (**2**) was only obtained for the enhanced pathway (**ESI, Figure A.8 B**), possibly due to the direct interaction of the enhancer, *p*-coumaric acid, with the enzyme which decouples the formation of the luminophore radical from the enzymatic reaction (**ESI, Figure A.7 B**). Aside from this, **2** probably possesses a different redox potential than **1** and altered reaction kinetics when reacting with HRP-I and HRP-II which likely accounts for the adverse effect observed (**ESI, Figure A.8 A**) in the non-enhanced pathway (**ESI, Figure A.7 A**). The linkage between redox potential and reaction rate and their effect on the enhanced system are discussed in-depth by Díaz and colleagues.[18] However, we also found that the increased polarity of **2** may actually hinder direct enzymatic oxidation in the non-enhanced pathway resulting in a decreased CL signal towards standard luminol (**ESI, Figure A.8 A**). Thus, for the quantification of HP with HRP a more complex HP reaction was observed, which is strongly dependent on the optimal concentrations of HP, *p*-coumaric acid and HRP, respectively.[19] A more detailed study on the HRP mediated CL reaction is given in the ESI. Surprisingly, the significant sensitivity enhancement (SE) of an up to 18-times steeper slope (**ESI, Table A.2**) for hemin showed only minor improvement of the LODs due to a significantly stronger background CL signal for **2**. We assume that this is due to trace amounts of HP present in natural water and ultrapure water which can be overcome by simply subtracting any background signal in real-world bioassays.[16,20]

As a second approach, we detected the luminophore itself in a preliminary study elucidating its potential for highly sensitive non-enzymatic immunoassays that will offer experimental set-ups independent of external light sources. We conclude that its superior aqueous solubility and its additional functional group for coupling reactions make it of substantial bioanalytical interest. Specifically, labeling with standard luminol (**Figure A.1, (1)**) or its derivatives ABEI or AHEI (**Figure A.1, (3)**) typically result in reduced CL signals as it is typically achieved through the amine group of the benzene ring for **1** or modification of the benzene ring as in **3** which itself is a substantial contributor for the CL mechanism. The freely available carboxyl group of **2** suggests that it has the potential to become a routine CL label of biomolecules.[21] Furthermore, its higher water solubility allows *e.g.,* encapsulation into liposomes, porous silica nanoparticles and other labeling nanomaterials

to a much higher degree than standard luminol or its derivatives. Enzyme-free signal amplification strategies can hence be significantly improved. This is an important step towards highly sensitive non-enzymatic immunoassays.[5,22] Here, the new luminol derivative **2** outperformed the standard luminol **1** by a great margin. Specifically, detection down to picomolar levels were easily possible and extraordinary signal-to-noise ratios of 2.6×10^3 were achieved with *m*-carboxy luminol (**ESI, Table A.3**). A sensitivity enhancement was obtained for all three catalyst systems (**ESI, Table A.3, Figure A.5**). The LODs, especially for hemin (**Figure 3 B**), were improved up to 5.2-times and a dynamic range over five orders of magnitude was observed. We therefore suggest hemin as most efficient catalyst which in addition benefits from its non-toxic nature and thermal stability in contrast to Co(II) and HRP.

In most current diagnostic CL assays, two main strategies are employed, either the detection of HP, generated through an inherent biological reaction, or the detection of HP released by an enzyme label attached to the analyte of interest.[23] We investigated the adaptation of *m*-carboxy luminol to both strategies through an enzymatic detection of L-lactate in synthetic sweat and a competitive chemiluminescence ELISA for the detection of diclofenac. First, HP detection using hemin with the strongest SE was successfully applied to a simple enzymatic L-lactate bioassay. L-lactate is a relevant biomarker in clinical diagnostics as well as for monitoring fitness levels with a wide concentration range (0.1 to 115.8 mmol L^{-1}) [24] depending on the matrix. Lactate oxidase (LOx) transforms L-lactate to pyruvate and HP.[25] When combining this assay with either of the two luminol derivatives **1** and **2**, *m*-carboxy luminol outperformed luminol for HP detection already at low µM concentrations by an over 6-fold steeper slope resulting in a significantly higher resolution (**Figure 4 B**). This is of great importance for point-of-care (POC) applications incl. sweat, blood and tear-fluid analysis, where increased resolution and signal intensities are key for successful transfer to low-cost POC solutions. The accuracy of the CL assay was confirmed by a commercial L-lactate assay providing similar results within the error (ESI 3.5).

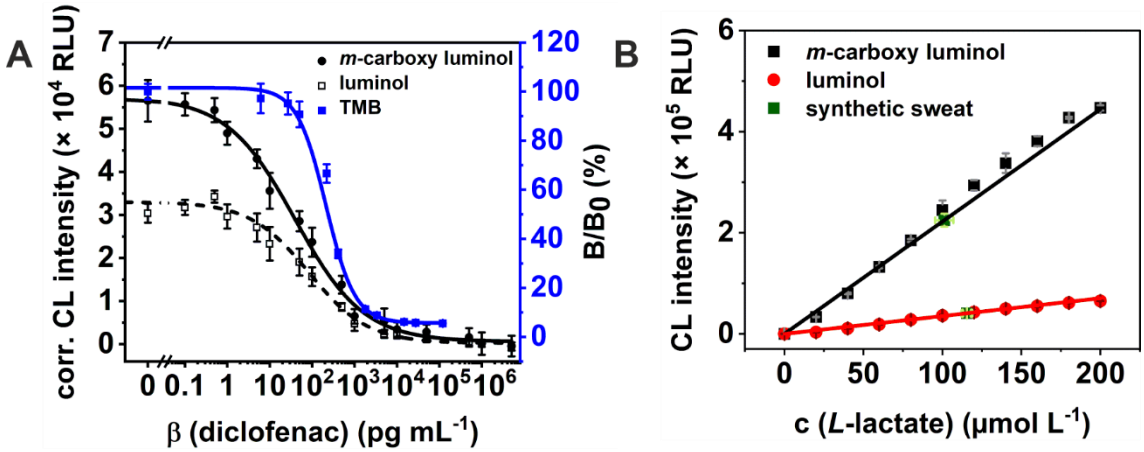

Figure 4 Analytical application of *m*-carboxy luminol in enzyme assays. Dose-response curve of (A) a competitive diclofenac ELISA with anti-mouse IgG-LOx for chemiluminescence (CL) detection of produced H_2O_2 and an anti-mouse IgG-HRP for photometric detection. Hemin catalyzed CL measurement, gain 100, reading height 1 mm, integration time 2 ms, data was background-corrected. Absorbance was measured at 450 nm, logistic fitting by Origin2020 with R^2 = 0.9908 (●), R^2 = 0.9935 (□) R^2 = 0.9889 (■), $y_{LOD} = A_1 - 3 \times \sigma_{blank}$. (B) CL determination of L-lactate, CL measurement with hemin, gain 70, reading height 1 mm, integration time 2 s, linear fitting by Origin2020 with R^2 = 0.9860 (black) and R^2 = 0.9964 (red), $x_{LOD} = 3 \times \sigma_{blank}/slope$; data are presented as mean ± SD (error bar) with n = 3

Secondly, *m*-carboxy luminol was compared to luminol and tetramethylbenzidine (TMB) as chemiluminescent and photometric standards, respectively, in a competitive ELISA for diclofenac. Diclofenac contamination of freshwater is of major concern due to its increased use in medicine as analgesic and thus rising global consumption rate, accompanied by its poor environmental degradation. This leads to typical diclofenac concentrations in the aquatic environment between pg mL^{-1} up to ng mL^{-1}.[26] The ELISA was adapted from an already established protocol [11] and uses LOx-modified secondary antibodies with luminol and *m*-carboxy luminol, respectively, for signal generation to allow direct comparison of both luminophores. Initially, an optimal coating of the microtiter plate with BSA-DCF with 5 µg mL^{-1} conjugate (**ESI, Figure A.12 A**) and a working dilution of 1:100 of the IgG-LOx was identified (**ESI, Figure A.12 B**). *m*-Carboxy luminol outperformed standard luminol (**Figure 4 A**) with an up to 2.6-times higher signal (**ESI, Figure A.13**). This is favorable for the obtained LODs with 5 pg mL^{-1} for *m*-carboxy luminol and 9 pg mL^{-1} for luminol which is almost 15-times lower compared to the colorimetric approach (TMB: LOD = 0.07 ng mL^{-1}, **Figure 4 A**) and 10-times lower than obtained with photon upconversion nanoparticles (0.05 ng mL^{-1}) [11], another class of labels emphasized in recent years due to a negligible background luminescence signal. A combination of a wider working range (four orders of magnitude *vs.* three) and a much higher change of signal intensity (four orders of magnitude *vs.* three) resulted in an over 10^4-times steeper slope for the linear region of the assay with *m*-carboxy luminol (**2**) in comparison to the fully optimized TMB detection system and a >1.5-times SE over standard luminol (**1**).

2.4. Conclusion

Overall, our results demonstrate in a wide selection of bioanalytical assays a consistent enhancement of *m*-carboxy luminol´s performance over luminol for all three CL catalysts of this study. While previously reported luminol derivatives (**mainly Figure A.1, (6)**) show higher CL intensities, they lack of easy assessable functional groups for labeling and have a reduced water solubility which limits their application in bioanalysis significantly. We herein, showed the impact of the enhancement on real bioanalytical approaches and achieved higher resolution and lower LODs along with increased dynamic ranges. Mechanistically, *m*-carboxy luminol can assist in further elucidating the underlying mechanism of the HRP-mediated CL reaction due to its irregular CL enhancement within the HRP system towards standard luminol. With optimized parameters for the detection of either HP or the luminophore itself, an advantageous toolset is provided for new applications of luminol-based CL detection. The universal approaches tested herein demonstrate the superior characteristics of this new luminophore which opens further investigative avenues: Direct labeling of biomolecules becomes accessible due to the additional carboxyl group and its increased water solubility allows better bioassay compatibility and insertion into various nanovesicles and particles, permitting to approach the signal amplification properties of enzymes. Including its overall structure-related stronger CL, this qualifies *m*-carboxy luminol as a new benchmark CL probe in analytical and bioanalytical approaches.

2.5. References

[1] D. Hong, H.-A. Joung, D. Y. Lee, S. Kim, M.-G. Kim, *Sens. Actuators, B* **2015**, *221*, 1248.

[2] A. Roda, M. Mirasoli, E. Michelini, M. Di Fusco, M. Zangheri, L. Cevenini, B. Roda, P. Simoni, *Biosens. Bioelectron.* **2016**, *76*, 164.

[3] L. Gámiz-Gracia, A. M. García-Campaña, J. F. Huertas-Pérez, F. J. Lara, *Anal. Chim. Acta* **2009**, *640*, 7.

[4] a) X. Wang, J.-M. Lin, M.-L. Liu, X.-L. Cheng, *TrAC, Trends Anal. Chem.* **2009**, *28*, 75; b) T. Li, E. Wang, S. Dong, *Anal. Chem.* **2010**, *82*, 1515.

[5] A. J. Steckl, P. Ray, *ACS Sens.* **2018**, *3*, 2025.

[6] C. Dodeigne, *Talanta* **2000**, *51*, 415.

[7] M. Zangheri, F. Di Nardo, D. Calabria, E. Marchegiani, L. Anfossi, M. Guardigli, M. Mirasoli, C. Baggiani, A. Roda, *Anal. Chim. Acta* **2021**, *1163*, 338515.

[8] Y. Ando, K. Niwa, N. Yamada, T. Irie, T. Enomoto, H. Kubota, Y. Ohmiya, H. Akiyama, *Photochem. Photobiol.* **2007**, *83*, 1205.

[9] M. Mayer, S. Takegami, M. Neumeier, S. Rink, A. Jacobi von Wangelin, S. Schulte, M. Vollmer, A. G. Griesbeck, A. Duerkop, A. J. Baeumner, *Angew. Chem., Int. Ed. Engl.* **2018**, *57*, 408.

[10] M. Vacher, I. Fdez Galván, B.-W. Ding, S. Schramm, R. Berraud-Pache, P. Naumov, N. Ferré, Y.-J. Liu, I. Navizet, D. Roca-Sanjuán et al., *Chem. Rev. (Washington, DC, U. S.)* **2018**, *118*, 6927.

[11] A. Hlaváček, Z. Farka, M. Hübner, V. Horňáková, D. Němeček, R. Niessner, P. Skládal, D. Knopp, H. H. Gorris, *Anal. Chem.* **2016**, *88*, 6011.

[12] A. G. Griesbeck, Y. Díaz-Miara, R. Fichtler, A. Jacobi von Wangelin, R. Pérez-Ruiz, D. Sampedro, *Chem. - Eur. J.* **2015**, *21*, 9975.

[13] a) C. Lu, G. Song, J.-M. Lin, *TrAC, Trends Anal. Chem.* **2006**, *25*, 985; b) A. Roda, F. Arduini, M. Mirasoli, M. Zangheri, L. Fabiani, N. Colozza, E. Marchegiani, P. Simoni, D. Moscone, *Biosens. Bioelectron.* **2020**, *155*, 112093.

[14] a) E. W. Miller, O. Tulyathan, O. Tulyanthan, E. Y. Isacoff, C. J. Chang, *Nat. Chem. Biol.* **2007**, *3*, 263; b) D. Lee, S. Khaja, J. C. Velasquez-Castano, M. Dasari, C. Sun, J. Petros, W. R. Taylor, N. Murthy, *Nat. Mater.* **2007**, *6*, 765.

[15] T. G. Burdo, W. R. Seitz, *Anal. Chem.* **1975**, *47*, 1639.

[16] European Centre for Ecotoxicology and Toxicology of Chemicals, *Hydrogen Peroxide OEL Criteria Document: CAS No. 7722-84-1*, ECETOC, **1996**.

[17] J. R. Stone, S. Yang, *Antioxid. Redox Signaling* **2006**, *8*, 243.

[18] A. N. Díaz, F. G. Sánchez, J. A. González Garcia, *J. Biolumin. Chemilumin.* **1998**, *13*, 75.

[19] L. Li, M. A. Arnold, J. S. Dordick, *Biotechnol. Bioeng.* **1993**, *41*, 1112.

[20] A. Lorber, Z. Goldbart, A. Harel, *Anal. Chem.* **1985**, *57*, 2537.

[21] X. Yang, Y. Guo, A. Wang, *Anal. Chim. Acta* **2010**, *666*, 91.

[22] C. Hofmann, A. Duerkop, A. J. Baeumner, *Angew. Chem., Int. Ed. Engl.* **2019**, *58*, 12840.

[23] Z. Zhang, S. Zhang, X. Zhang, *Anal. Chim. Acta* **2005**, *541*, 37.

[24] a) L. Rassaei, W. Olthuis, S. Tsujimura, E. J. R. Sudhölter, A. van den Berg, *Anal. Bioanal. Chem.* **2014**, *406*, 123; b) P. J. Derbyshire, H. Barr, F. Davis, S. P. J. Higson, *J. Physiol. Sci.* **2012**, *62*, 429.

[25] I. S. Kucherenko, Y.V. Topolnikova, O. O. Soldatkin, *TrAC, Trends Anal. Chem.* **2019**, *110*, 160.

[26] L. Lonappan, S. K. Brar, R. K. Das, M. Verma, R. Y. Surampalli, *Environ. Int.* **2016**, *96*, 127.

2.6. Supporting Information

2.6.1. Experimental Procedures

Chemicals and consumables. All chemicals were of commercial HPLC grade or higher and were used without purification. Sodium hydroxide solution, potassium dihydrogen phosphate and potassium chloride were purchased from Merck (Darmstadt, Germany). Tris(hydroxymethyl)aminomethane (Tris) was purchased from Affymetrix, Thermo Fisher Scientific Inc. (Waltham, Massachusetts). Sodium chloride was purchased from neoFroxx GmbH (Einhausen, Germany). Luminol, hydrochloric acid, disodium hydrogen phosphate dihydrate, hydrogen peroxide (HP) solution, hemin, 3,3´,5,5´-Tetramethylbenzidine (TMB) liquid substrate (T8665), *p*-coumaric acid, cobalt chloride, diclofenac sodium salt (D6899), anti-mouse IgG peroxidase antibody (A9044) and sodium L-lactate were ordered from Sigma Aldrich Chemie GmbH (Munich, Germany) and BSA (T844.2), potassium hydrogen carbonate and sulfuric acid were purchased from Carl Roth (Karlsruhe, Germany). Horseradish peroxidase (HRP) was purchased from Sigma Aldrich Chemie GmbH (Munich, Germany) and a 300 U mL^{-1} stock solution in 10X PBS buffer, pH 7.4 was prepared. Lactate Oxidase (LOx) was obtained from AG Scientific (San Diego, USA) and a 100 U mL^{-1} in 1X PBS buffer, pH 7.4 was prepared. Both enzymes were aliquoted and stored at 4 °C and respective working solutions were prepared freshly before each measurement. *m*-Carboxy luminol was custom-made by Taros Chemicals GmbH & Co. KG (Germany). Mouse anti-DCF, 12G5 was kindly provided by the research group of Dr. Seidel (Technical University of Munich, Germany). For all experiments, ultrapure water was used and stock solutions were prepared for luminol (1 mmol L^{-1} in 0.1 mol L^{-1} carbonate buffer, pH 10.5), *m*-carboxy luminol (1 mmol L^{-1} in 0.1 mol L^{-1} carbonate buffer, pH 10.5), hemin (1 mmol L^{-1} in 0.1 mol L^{-1} carbonate buffer, pH 10.5), Co(II) (1 mmol L^{-1} in ultrapure water), *p*-coumaric acid (1 mmol L^{-1} in ethanol, 96%) and L-lactate (10 mmol L^{-1} in ultrapure water). For H_2O_2, the stock solution (100 mmol L^{-1}) was prepared freshly before each measurement. For luminescence measurements, standard white 96-well microtiter plates (MTP) from Porvair were used if not stated differently. All of the experiments were performed at 25 °C.

CL measurements were performed with a Synergy Neo 2 microplate reader from BioTek (Bad Friedrichshall, Germany) either in the chemiluminescence spectral or endpoint mode.

2.6.1.1. Determination of absorbance characteristics.

Absorbance spectra of *m*-carboxy luminol and luminol were recorded with a Varian Cary 50 Bio photometer from 230 nm to 700 nm in 0.5 nm steps with slow reading speed. The

luminophore stock solutions were diluted to 100 µmol L^{-1} luminophore in 0.1 mol L^{-1} carbonate buffer (pH 10.5). The determination of the extinction coefficient was performed by measuring the absorbance of both luminophores at the λ_{max} determined previously. Absorbance of the 100 µmol L^{-1} luminophore in 0.1 mol L^{-1} carbonate buffer (pH 10.5) was used to calculate the extinction coefficient.

2.6.1.2. Characterization of chemiluminescence properties.

Emission spectra of the investigated chemiluminescent systems were recorded from 300 nm to 650 nm in 1 nm steps. For determining the kinetics, several spectra over a defined period of time were recorded and the intensity integrals at λ_{max} utilized for illustrating the CL decay at $\lambda_{max.}$ After adding the initiation solution (IS) to luminescence solution (LS) and 5 s shaking, the luminescence read-out was started. For the Co(II)- and hemin-catalyzed system, 100 µL of LS, containing 200 µmol L^{-1} luminophore, 2 µmol L^{-1} catalyst in 0.1 mmol L^{-1} carbonate buffer pH 10.5, was added to a MTP and CL was initiated by adding 100 µL of double concentrated hydrogen peroxide solution (60 mmol L^{-1}). For HRP, LS contained luminophore (100 µmol L^{-1} in 200 µL), hydrogen peroxide (2 mmol L^{-1} in 200 µL), and for enhanced CL reactions *p*-coumaric acid (6.67 µmol L^{-1} in 200 µL) in Tris-HCl buffer, pH 8.5 (33 mmol L^{-1} in 200 µL) in the respective final concentration in 199 µL. The final volume of 200 µL was obtained by adding 1 µL of IS containing HRP (300 U mL^{-1}). The luminescence reading procedure was identical to the previous described procedure for Co(II) and hemin. CL was recorded with gain 90, reading height 4.5 mm, integration time 20 ms (uncorrected spectra).

2.6.1.3. Determination of relative chemiluminescence quantum yield.

Total emitted photons over 2 s and relative chemiluminescence quantum yield for Co(II), hemin and horseradish peroxidase catalyzed chemiluminescence of *m*-carboxy luminol were performed with the BioTek microtiter plate reader for all three catalyst systems by combining 100 µL of luminescence solution (LS) (20 µmol L^{-1} luminophore, 20 µmol L^{-1} catalyst in 0.1 mol L^{-1} carbonate buffer pH 10.5) and 100 µL of initiation solution (IS) (20 mmol L^{-1} H_2O_2) for both luminophores and Co(II) and hemin as catalysts. For HRP, 199 µL of LS containing 100 µmol L^{-1} luminophore, 50 µmol L^{-1} *p*-coumaric acid and 10 mmol L^{-1} H_2O_2 in 0.033 mol L^{-1} Tris-HCl, pH 8.5 (final concentration in 200 µL) and 1 µL of HRP (300 U mL^{-1}) were combined directly before the CL measurement was performed. The CL intensity was measured for 2 s, gain 50 and with a reading height of 1 mm. The Φ_{CL} was subsequently calculated according to equation (Eq.(A.1)).[1]

2.6.1.4. Stability measurements.

For the detection of the stability of the luminophores, the respective intensity integral of the CL reaction was recorded with the endpoint mode of the microplate reader and the CL measurement was corrected by an initial background luminescence reading of LS as described previously. Chemiluminescence was detected by using the hemin system. The same pipetting scheme, with 100 µL of LS (200 µmol L^{-1} luminophore, 20 µmol L^{-1} catalyst in 0.1 mol L^{-1} carbonate buffer pH 10.5) and 100 µL of IS (5 mmol L^{-1} H_2O_2) was applied. 100 µL of LS were added to an MTP, the background was recorded and subsequently, 100 µL of IS were added.

2.6.1.5. Chemiluminescence measurement of hydrogen peroxide.

The respective intensity integral of the CL reaction was recorded in endpoint mode of the microplate reader. The CL measurement was corrected by an initial background reading of luminescence solution (LS). HP was detected by using all three catalysts. 100 µL of LS (200 µmol L^{-1} luminophore, 20 µmol L^{-1} hemin or Co(II) in 0.1 mol L^{-1} carbonate buffer pH 10.5) and 100 µL of IS (varying H_2O_2 dilution in 0.1 mol L^{-1} carbonate buffer pH 10.5) were combined. For HRP, 199 µL of LS containing 100 µmol L^{-1} luminophore, 50 µmol L^{-1} *p*-coumaric acid and varying H_2O_2 concentrations in 0.033 mol L^{-1} Tris-HCl, pH 8.5 (final concentration in 200 µL) and 1 µL of HRP (300 U mL^{-1}) were combined directly before the CL measurement was performed. CL signals were recorded with gain 100, reading height 1 mm and integration time 2 s.

2.6.1.6. Chemiluminescence measurement of luminophore.

The CL signal was similarly recorded to the HP measurement. All three catalysts were studied by either combining 100 µL of LS (varying luminophore concentration, 20 µmol L^{-1} hemin or Co(II) in 0.1 mol L^{-1} carbonate buffer pH 10.5) and 100 µL of IS (20 mmol L^{-1} H_2O_2) or for HRP, using 199 µL of LS containing varying concentration of luminophore, 50 µmol L^{-1} *p*-coumaric acid and 10 mmol L^{-1} H_2O_2 in 0.033 mol L^{-1} Tris-HCl, pH 8.5 (final concentration in 200 µL) with 1 µL of HRP (300 U mL^{-1}) directly before the CL measurement was performed.

2.6.1.7. Preparation of BSA-diclofenac conjugate.

The conjugation process was adapted from an already published procedure which is briefly described in the following.[2] First, 30 µL of 100 mmol L^{-1} diclofenac (DCF) in DMF (3 µmol) were mixed with 970 µL of MES buffer (100 mmol L^{-1}, pH 6.1), containing 4.42 mg of

sulfo-NHS (19.4 µmol) and 19.1 mg of EDC (94 µmol) and incubated at room temperature (RT) for 30 min. 1 mL BSA (20 mg mL^{-1}) and 500 µL of 80 mmol L^{-1} Na_2CO_3 and 100 mmol L^{-1} H_3BO_3, pH 9.4 were added and incubated for 4 h in the dark at RT while stirring. The conjugate was dialyzed (cellulose membrane: 12 kDa –14 kDa MWCO, Spectra/Por® 4, 2718.1, Carl Roth, Germany) against five times 800 mL 80 mmol L^{-1} Na_2CO_3/100 mmol L^{-1} H_3BO_3, pH 9.4 at 4 °C. BSA-DCF was adjusted to 1.5 mg mL^{-1} by adding 80 mmol L^{-1} Na_2CO_3/100 mmol L^{-1} H_3BO_3, pH 9.4 and stored at 4 °C in presence of 0.05% (w/v) NaN_3. The conjugate was tested by performing the diclofenac assay without free DCF (**Figure A.12**).

2.6.1.8. Preparation of LOx conjugate.

Similar conjugation process was applied as for the BSA-DCF conjugate. First, 0.84 mg (5.4 µmol) EDC, 1.47 mg (6.8 µmol) sulfo-NHS and 2.43 mg (0.03 µmol) lactate oxidase (LOx) were diluted in 1 mL MES buffer (100 mmol L^{-1}, pH 6.1), and incubated at RT for 30 min. 500 µL of activated LOx (15 nmol) were added to 500 µL of rabbit anti-mouse IgG (315-005-0031, Jackson ImmunoResearch Inc., diluted to 1 mg mL^{-1} in 80 mmol L^{-1} Na_2CO_3/ 100 mmol L^{-1} H_3BO_3, pH 9.4, equaling 3.3 nmol) and incubated for 4 h in the dark at RT while stirring. The conjugate was dialyzed (cellulose membrane: 12 kDa –14 kDa MWCO, Spectra/Por® 4, 2718.1, Carl Roth, Germany) against six-times 600 mL 1X PBS buffer, pH 7.4 at 4 °C to remove excess of EDC and sulfo-NHS. A final antibody concentration of 0.5 mg mL^{-1} was obtained, and the conjugate was stored at 4 °C.

2.6.1.9. Competitive diclofenac assay.

The BSA-DCF loading study and the anti-mouse IgG-LOx dilution experiment were performed according to the described protocol for the competitive DCF assay in the main manuscript with the following adjustments. The BSA-DCF loading study was done with varying BSA-DCF concentrations for coating of the MTP and by incubating the coated BSA-DCF with 100 µL of anti-DCF antibody (12G5, 0.5 µg mL^{-1}) without free DCF. The anti-mouse IgG-LOx dilution experiment was done with varying anti-mouse IgG-LOx dilution, respectively, on a BSA-DCF (5 µg mL^{-1}) coated MTP which was incubated with 100 µL of anti-DCF antibody (12G5, 0.25 µg mL^{-1}) without free DCF. 100 µL of L-lactate (2 mmol L^{-1}, 1X PBS buffer, pH 7.4) was incubated for 5 min before 100 µL of 200 µmol L^{-1} luminophore and 2 µmol L^{-1} hemin in 0.1 mol L^{-1} carbonate buffer pH 10.5 was added.

2.6.1.10. Spectral scanning of enhanced and non-enhanced chemiluminescence with HRP

Emission spectra were recorded from 300 nm to 700 nm in 1 nm steps. After adding the initiation solution (IS) to luminescence solution (LS) and 5 s shaking, the luminescence reading was started. The LS contained luminophore (100 µmol L^{-1} in 200 µL), hydrogen peroxide (10 mmol L^{-1} in 200 µL), and for enhanced CL reactions coumaric acid (50 µmol L^{-1} in 200 µL) in Tris-HCl buffer, pH 8.5 (33 mmol L^{-1} in 200 µL) in the respective final concentration in 199 µL. The final volume of 200 µL was obtained by adding 1 µL of IS containing HRP (300 U mL^{-1}).

2.6.1.11. Preparation of BSA-HRP conjugate.

Similar conjugation process was applied as for the BSA-DCF conjugate. First, 0.7 mg (4.5 µmol) EDC and 1.42 mg (6.5 µmol) sulfo-NHS were added to 1 mL of 1 mg mL^{-1} horseradish peroxidase (HRP) (equaling 22.7 nmol) in MES buffer (100 mmol L^{-1}, pH 6.1), and incubated at room temperature for 30 min. 1 mL of 1 mg mL^{-1} BSA in 80 mmol L^{-1} Na_2CO_3/100 mmol L^{-1} H_3BO_3, pH 9.4, (equaling 16.4 nmol) were added and incubated for 3.5 h in the dark at room temperature while stirring. The conjugate was dialyzed (D-Tube Dialyzer Maxi (cellulose membrane), MWCO 12-14 kDa, 71505, Merck Millipore, Germany) against four-times 600 mL 80 mmol L^{-1} Na_2CO_3/100 mmol L^{-1} H_3BO_3, pH 9.4 at 4 °C to remove excess of EDC and sulfo-NHS and a final conjugate concentration of 0.2 mg mL^{-1} was adjusted. The conjugate was stored at 4 °C.

2.6.1.12. Endpoint measurement of enhanced chemiluminescence with HRP

Enhancer calibration with *p*-coumaric acid was performed by recording the respective intensity integral of the CL reaction with the endpoint mode of the microplate reader and the CL measurement was corrected by an initial background luminescence reading of LS as described previously. 100 µL of LS containing 200 µmol L^{-1} luminophore, varying *p*-coumaric acid concentration and 20 mmol L^{-1} H_2O_2 in 0.033 mol L^{-1} Tris-HCl, pH 8.5 were added to a MTP and 100 µL of HRP (10 µg mL^{-1} HRP (P8375, Sigma Aldrich), 0.250 µg mL^{-1} rabbit anti-mouse IgG-HRP (A9044, Sigma Aldrich) or 0.16 µg mL^{-1} goat anti-mouse IgG-HRP (115-035-003, Jackson ImmunoResearch Laboratories, Inc., UK) were added. For the HRP concentration dependency with BSA-HRP, a high binding MTP (655074, Greiner BioOne, Germany) was coated with 200 µL of BSA-HRP dilution in 80 mM Na_2CO_3 and 100 mM H_3BO_3, pH 9.4 and incubated overnight at 4°C, the MTP was washed 3-times for 5 min with 300 µL of WB (1X PBS, 0.05% Tween20, pH 7.4) and for absorbance, 100 µL

of ready-to-use TMB liquid substrate (T8665, Sigma Aldrich) was added to MTP and incubated for 5 min. before it was stopped with 100 µL of 1 N H_2SO_4, 50 µL of the reaction mix were added to 150 µL of ultrapure water and absorbance measurement was performed at 450 nm and 21 °C in a transparent MTP (655101, Greiner BioOne, Germany). For chemiluminescence, 200 µL of chemiluminescence substrate (100 µmol L^{-1} luminophore, 50 µmol L^{-1} *p*-coumaric acid concentration and 10 mmol L^{-1} H_2O_2 in 0.033 mol L^{-1} Tris-HCl, pH 8.5) was added direct before measurement, either containing luminol or *m*-carboxy luminol. Reading was performed with gain 100, reading height 1mm and integration time 2 s at 25 °C. For the HRP concentration dependency with varying HRP conjugates, 100 µL of HRP dilution in 1X PBS pH 7.4 (HRP (P8375, Sigma Aldrich) with and without free BSA (T844.2, Carl Roth, equal BSA concentration to HRP), rabbit anti-mouse IgG-HRP (A9044, Sigma Aldrich,) and BSA-HRP conjugate) was added to a MTP. 100 µL of chemiluminescence substrate containing 200 µmol L^{-1} luminophore, 100 µmol L^{-1} *p*-coumaric acid and 20 mmol L^{-1} H_2O_2 in 0.066 mol L^{-1} Tris-HCl buffer (pH 8.5) was added direct before measurement, either containing luminol or *m*-carboxy luminol and CL intensity was recorded at 25 °C in endpoint mode with gain 45, reading height 1 mm, integration time 2 s.

2.6.1.13. L-lactate Assay.

The CL-based L-lactate assay was performed according to the describe procedure in the main manuscript. The commercially colorimetric L-lactate assay kit from Sigma Aldrich (MAK064) was used as quality control and the assay was performed according to the manual provided by the supplier. In contrary to the CL-based L-lactate measurements the synthetic sweat sample was used in a one to 50 dilution.

2.6.2. Results and Discussion

2.6.2.1. Supplement to introduction of the main article

Besides various structural variations, the most attractive way to increase the CL of luminol (**1**) was either an amplification strategy via metal-nanoparticles [3], application of chemical enhancers such as *p*-substituted phenols or *p*-coumaric acid mostly for the horseradish peroxidase system [4] or rather complex and sophisticated procedures like G-quadruplex DNAzymes mimicking hemin[5] or nanoencapsulation of isoluminol derivatives with cyclodextrins[6] yielding up to 15-fold enhancement. Furthermore, tuning of CL intensity via catalyst concentration and pH value is possible.[7] Especially the strategies using primary chemical enhancers, such as *p*-iodophenol[8], or the interplay of a secondary with a primary

enhancer molecule, like the combination of 3-(10′-phenothiazinyl)-propane-1-sulfonate (SPTZ) with 4-morpholinopyridine (MORP)[9], have led to an up to 2500-fold enhancement[8] over the most simple designed HRP-luminol-based CL reaction and in addition stabilizes the chemiluminescence signal.[10] Combining the above-mentioned enhancement strategies with improvement of the inherent CL properties of luminol (**1**) (**Figure A.1 B**) would yield in an exceptionally sensitive and stable chemiluminescent reagent. Thus, much research has been reported on the structural modulation of luminol, since its extraordinary chemiluminescence properties were reported in 1928 by Albrecht.[11] Initially, researchers were interested in understanding the luminol-based chemiluminescence mechanism (**Figure A.1 A**). Studies focused on relevant structural elements and reaction products of 3-aminophthalhydrazid´s chemiluminescence reaction leading to some generalized trends[12,13]

- modification of the heterocyclic ring erases the chemiluminescence properties completely
- electron-donating substituents on the carbocyclic ring enhance the chemiluminescence efficiency whereas electron-withdrawing substituents on the benzene ring diminish the CL efficiency
- favorable substituents in 5- and 8-position have a greater effect than in 6- and 7-position; and multiple substitutions in 5- and 8-position are more efficient as mono-substitution in these positions (**Figure A.1 B, (7)**)

However, only a small amount of the studied derivatives were found to produce more light than luminol itself.[13] **Figure A.1 B** shows the most efficient derivatives that were synthesized so far. Whereas the synthesis of isoluminol derivatives (**3**) lead to chemiluminescence compounds that are almost as efficient as luminol [14] and were later used for chemiluminescence labeling of proteins, nucleotides or small molecules [15], the aminonaphthal-hydrazide derivatives (**4**) exhibited up to 4.2-times enhanced chemiluminescence [14,16] and the L012 derivative (**5**) even 6-fold enhancement.[17] In fact, the most efficient derivative with 20-fold enhancement was obtained by introducing dialkyl substituents as in (**6**).[1] These structural variations with alkyl groups, however, lead to lower hydrophilicity.[13] The very poor solubility in water and the requirement of alkaline pH ≥ 8.6 conditions if not organic solvents for sufficient dissolution of the compounds (as for the parent molecule luminol) are a major drawback in bioanalytical studies.[18]

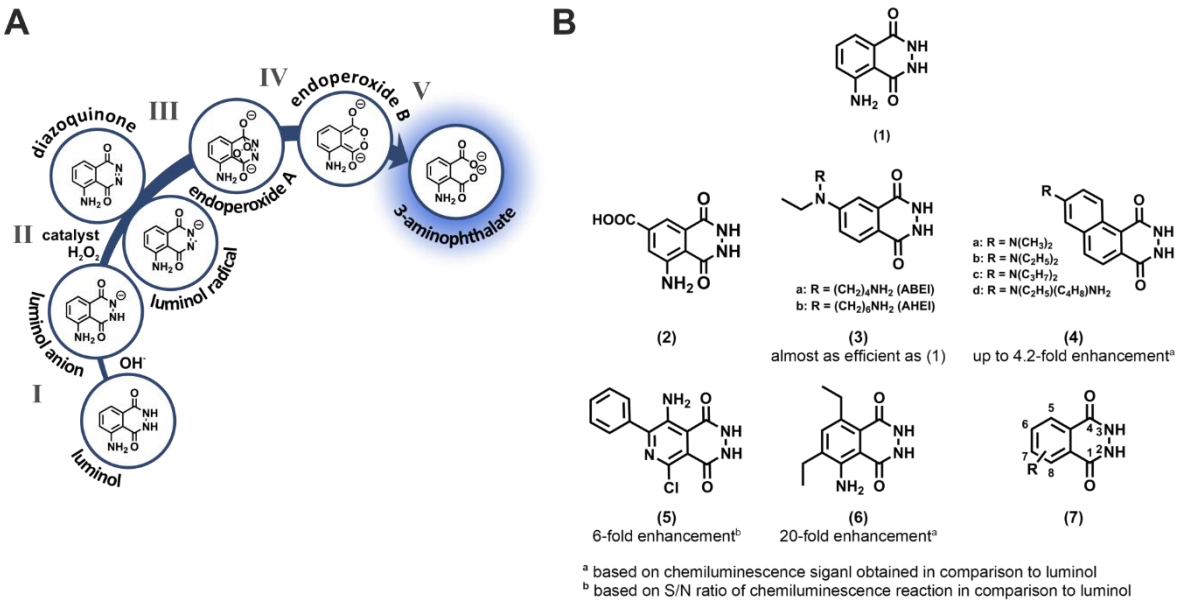

Figure A.1 Chemiluminescence mechanism of the luminol (1)/hydrogen peroxide (HP) system in aqueous solution in (A), (I) the deprotonation of luminol to form the luminol anion (LH^-), (II) oxidation of LH^- by HP in presence of a catalyst to form the luminol radical anion ($L^{\bullet -}$) or diazoquinone (L), (III) oxidation of $L^{\bullet -}$ or L by HP or superoxide, respectively, (IV) generating an endoperoxide which forms 3-APA* through release of N_2, (V) 3-APA* emits the photon responsible for CL [19,20] and Phthalhydrazide derivatives in (B) luminol (1) and its most efficient derivatives, *m*-carboxy luminol (2), isoluminol derivatives (3) [14], aminonaphthal-hydrazides (4) [14,16], L-012 (5) [17], diethyl luminol (6) [1], generalized phthalhydrazide structure (7)

2.6.2.2. Spectral characterization of *m*-carboxy luminol

2.6.2.2.1. Absorbance measurements

Photophysical studies showed that the absorbance spectra of *m*-carboxy luminol also exhibit a characteristic double peak (**Figure1 A, main article**) that is typical for luminol as well. The absorbance maximum (λ_{max}) at 300 nm results from the cyclic hydrazide unit is identical to the first λ_{max} of luminol. The second maximum at 370 nm is red-shifted compared to the second λ_{max} of luminol.[21] This maximum originates from the benzene ring which exhibits a larger conjugated π-system due to the additional carboxy group in meta-position. The extinction coefficients found for both luminophores are in good correlation with literature values for luminol (**Table A.1**).[21]

Absorbance measurements of *m*-carboxy luminol are summarized in **Table A.1**.

Table A.1 Spectrophotometric characteristics for luminol and *m*-carboxy luminol

Absorbance parameter	***m*-carboxy luminol (experimental)**	**luminol (experimental)**	**luminol (literature [21])**
λ_{max} (1)	300 nm	300 nm	300 nm
λ_{max} (2)	370 nm	350 nm	350 nm
ε_{300}	(6218 ± 1) L mol^{-1} cm^{-1}	(6782 ± 1) L mol^{-1} cm^{-1}	6800 L mol^{-1} cm^{-1}
ε_{350}	-	(7582 ± 2) L mol^{-1} cm^{-1}	7200 L mol^{-1} cm^{-1}
ε_{370}	(7843 ± 2) L mol^{-1} cm^{-1}	-	-

2.6.2.2.2. Quantum Yield

The relative quantum yield of *m*-carboxy luminol was determined by direct comparison of obtained chemiluminescence signal of *m*-carboxy luminol to luminol for all three catalyst systems and calculated according to equation (Eq. (A.1)). The CL intensity was measured for 2 s and with a reading height of 1 mm with a Synergy Neo 2 microplate reader from BioTek (Bad Friedrichshall, Germany) after starting the CL reaction.

$$\Phi_{CL} = (I/I_0)\ \Phi_{CL}^{0} \qquad \text{(Eq. (A.1))}$$

Φ_{CL}^{0} = absolute quantum yield of luminol (0.012) [22]

I = number of photons emitted by *m*-carboxy luminol

I_0 = number of photons emitted by luminol

The results for all three catalyst systems are listed in **Table 1**, main article. In case of the relative chemiluminescence quantum yield (Φ_{CL}) of *m*-carboxy luminol, a value of up to 0.05 was determined in the protic luminophore-hydrogen peroxide system. This Φ_{CL} was independent on the applied catalyst (**Table 1, main article**) and is a 5-times higher value than the reported absolute quantum yield of luminol (0.012).[22]

2.6.2.2.3. Characterization of chemiluminescence properties.

The chemiluminescence spectral behavior was studied for the luminophore-hydrogen peroxide system with Co(II), hemin and horseradish peroxidase (HRP) as catalysts. The Co(II)-catalyzed CL represents the most sensitive inorganic catalyst system due to low abundance of Co(II) in natural water samples, thus resulting in a minimized background luminescence.[23] Hemin, in contrast to Co(II), is a less toxic inorganic alternative with similar sensitivity levels.[23] To achieve biocompatibility, HRP was studied, which is already

integrated into a multitude of immunoassays and shows a higher selectivity compared to its inorganic alternatives.[24] Comparison of *m*-carboxy luminol with standard luminol revealed chemiluminescent emission maxima at 425 nm and 445 nm for luminol and 445 nm for *m*-carboxy luminol (**Figure A.2**). The CL decay within one catalyst system was similar for both luminol derivatives. A clearly enhanced chemiluminescence (up to 3.3-times) across the entire spectrum for *m*-carboxy luminol towards luminol was observed (**Figure A.2**).

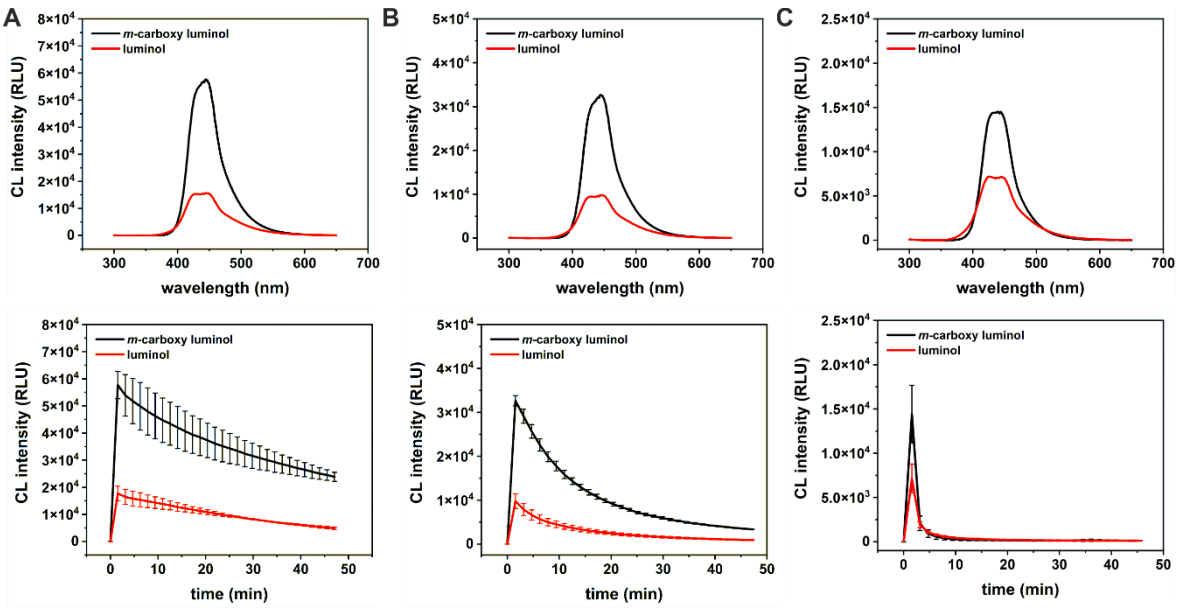

Figure A.2 Chemiluminescence spectra of *m*-carboxy luminol (black) and luminol (red) of a solution containing 100 µmol L^{-1} luminophore, and 30 mmol L^{-1} H_2O_2 in 0.1 mol L^{-1} carbonate buffer (pH 10.5) and in (A) 1 µmol L^{-1} Co(II), in (B) 1 µmol L^{-1} hemin or 30 mmol L^{-1} H_2O_2 in 0.033 mol L^{-1} Tris-HCl (pH 8.5) and in (C) 1.5 U mL^{-1} horseradish peroxidase and 50 µmol L^{-1} *p*-coumaric acid, recorded with gain 90, reading height 4.5 mm, integration time 20 ms (uncorrected spectra) with upper row equals chemiluminescence spectrum recorded from 300 to 650 nm in 1 nm steps with λ_{max} at 445 nm and lower row equals chemiluminescence decay at 445 nm for 45 min, data are presented as mean ± SD (error bar) with n = 3

The differences in intensity decay are a result of different reaction kinetics and can be influenced by variation of catalyst concentration, considering the luminophore concentration remains constant. A low radical concentration results in slow reaction rates and thus prolonged CL.[4,20] The Co(II) system showed the most stable signal compared to the enhanced HRP and hemin system. This correlates well with the fact that two active peroxide species are involved in the oxidation of the luminophore in the HRP [4] and hemin [25] system, whereas in the Co(II) system [26] only one active peroxide species is formed.

Figure A.3 shows the chemiluminescence signal dependency on varying hydrogen peroxide concentrations.

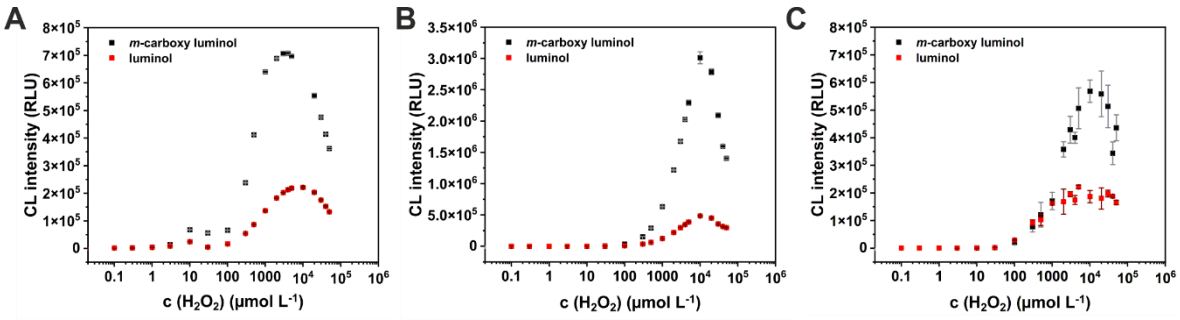

Figure A.3 Chemiluminescence dependency on hydrogen peroxide concentration of *m*-carboxy luminol (black) and luminol (red) using in (A) Co(II), in (B) hemin and in (C) horseradish peroxidase as catalyst. The reaction mixture contained 100 µmol L^{-1} luminophore, 10 µmol L^{-1} Co(II) or hemin in 0.1 mol L^{-1} carbonate buffer (pH 10.5) and 1.5 U mL^{-1} horseradish peroxidase, 50 µmol L^{-1} *p*-coumaric acid in 0.033 mol L^{-1} Tris-HCl (pH 8.5), recorded in endpoint mode with gain 45, reading height 4.5 mm, integration time 20 ms, data are presented as mean ± SD (error bar) with n = 3

Figure A.4 shows the respective dose-response curves for the hydrogen peroxide detection with all three catalysts. Whereas in **Figure A.4 C**, the chosen H_2O_2 concentration range exhibits a linear correlation for *m*-carboxy luminol, for luminol this linear range starts at higher H_2O_2 concentrations. This correlates with the overall non-linear H_2O_2 concentration dependency shown in **Figure A.3 C** depicting that at higher H_2O_2 concentrations saturation will be reached following an S-curve. In **Figure A.4 C** – luminol, the lower part of the overall non-linear dependency is depicted in higher resolution necessitating a logistic fit for this dataset. **Table A.2** summarizes the determined parameters for the hydrogen peroxide detection in **Figure A.4**. The obtained CL enhancement values from **Figure A.2** and **Figure A.3** cannot be directly compared to the sensitivity enhancement values obtained in **Figure A.4** and **Table A.2**, respectively.

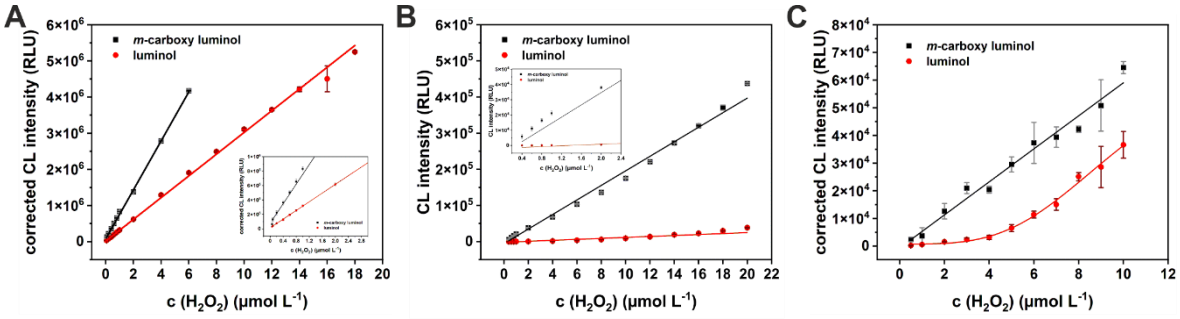

Figure A.4 Calibration curve of H_2O_2 detection with (A) Co(II), (B) hemin and (C) horseradish peroxidase in a microtiter plate for *m*-carboxy luminol (black) and luminol (red) with 100 µmol L^{-1} luminophore and 10 µmol L^{-1} Co(II) or hemin in 0.1 mol L^{-1} in carbonate buffer (pH 10.5) and 1.5 U mL^{-1} horseradish peroxidase, 50 µmol L^{-1} *p*-coumaric acid in 0.033 mol L^{-1} Tris-HCl (pH 8.5), recorded in endpoint mode with gain 100, reading height 1 mm, integration time 2 s, linear fitting was performed by Origin2020 with R^2 = 0.9983 (black) and R^2 = 0.9989 (red) for Co(II), R^2 = 0.9897 (black) and R^2 = 0.8680 (red) for hemin and R^2 = 0.9732 (black) for *m*-carboxy luminol- horseradish peroxidase and four-parameter logistic fitting was performed by Origin2020 with R^2 = 0.9917 (red) for luminol-horseradish peroxidase, data are presented as mean ± SD (error bar) with n = 3, figure insets show zoom of low concentration region

Furthermore, different recording settings were applied due to the limitations of the detection device. However, despite these experimental limitations, similar trends in sensitivity enhancements in **Figure A.3** and **Figure A.4** were obtained, although different concentration ranges are considered, with hemin having the highest sensitivity enhancement followed by cobalt and finally HRP with the lowest increase in the slope towards luminol (**Figure A.3 and Figure A.4**).

Table A.2 Hydrogen peroxide detection with Co(II), hemin and horseradish peroxidase

Luminophore	**Catalyst**	**LOD[a] [µmol L^{-1}]**	**Slope[b] [L µmol $^{-1}$]**	**R^2 [c]**	**SE[d]**
m-carboxy luminol	Co(II)	0.112	(7.02 ± 0.12) × 10^5	0.9969	2.3
luminol	Co(II)	0.004	(3.07 ± 0.07) × 10^5	0.9913	
m-carboxy luminol	hemin	0.076	(1.96 ±0.04) × 10^4	0.9938	17.8
luminol	hemin	0.14	(0.11 ± 0.01) × 10^4	0.8527	
m-carboxy luminol	HRP	0.3	(5.6 ± 0.2) × 10^3	0.9894	-
luminol	HRP	1.4[d]	(5.2 ± 0.4) × 10^3[e]	0.9635[f]	

[a]limit of detection (x_{LOD} = 3 × σ_{blank}/slope), [b]slope derived from fitting of linear region, [c]correlation coefficient, [d]sensitivity enhancement by slope

In addition, it should be noted that for HRP we did not obtain a linear relationship for luminol in the chosen concentration range (**Figure A.4**). Hence, no conclusive statement of the sensitivity enhancement in the chosen concentration range is possible. **Figure A.5** shows the respective dose-response curves for the luminophore detection with all three catalysts.

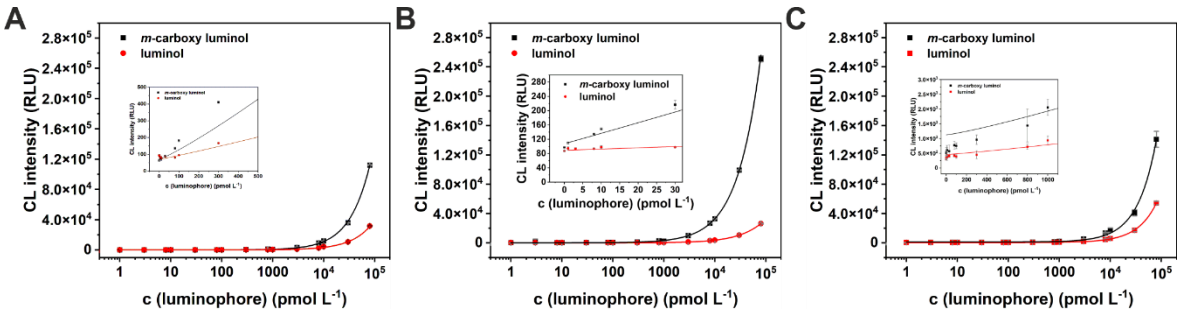

Figure A.5 Calibration curve for luminophore detection with (A) Co(II), (B) hemin and (C) horseradish peroxidase in a microtiter plate for *m*-carboxy luminol (black) and luminol (red) with 10 µmol L^{-1} Co(II) or hemin in 0.1 mol L^{-1} in carbonate buffer (pH 10.5) and 1.5 U mL^{-1} horseradish peroxidase and 50 µmol L^{-1} *p*-coumaric acid in 0.033 mol L^{-1} Tris-HCl buffer (pH 8.5) and 10 mmol L^{-1} H_2O_2, recorded in endpoint mode with gain 100, reading height 1 mm, integration time 2 s, four-parameter logistic fitting was performed by Origin2020 with R^2 = 0.9847 (black) and R^2 = 0.9848 (red) for Co(II), R^2 = 0.9958 (black) and R^2 = 0.9992 (red) for hemin and R^2 = 0.9968 (black) and R^2 = 0.9995 (red) for horseradish peroxidase, data are presented as mean ± SD (error bar) with n = 3, figure insets show zoom of low concentration region

Table A.3 summarizes the relevant parameters for the luminophore detection.

Table A.3 Luminophore detection with Co(II), hemin and horseradish peroxidase

Luminophore	Catalyst	LOD[a] [pmol L^{-1}]	LOQ[b] [pmol L^{-1}]	S/N [@ 80 nmol L^{-1}]	R^{2c}	SE[d]	EF[e]
m-carboxy luminol	Co(II)	26	73.9	(18 ± 1.2) × 10^2	0.9847	5.5	2.5
luminol	Co(II)	67	206	(3.3 ± 0.19) × 10^2	0.9848		
m-carboxy luminol	hemin	2.5	8.05	(26 ± 0.73) × 10^2	0.9958	8.7	5.2
luminol	hemin	13	43.2	(3.0 ± 0.074) × 10^2	0.9992		
m-carboxy luminol	HRP	125	349	(4.6 ± 0.50) × 10^2	0.9968	2.7	0.7
luminol	HRP	82	231	(1.7 ± 0.079) × 10^2	0.9995		

[a]limit of detection ($y_{LOD} = A_1 + 3 \times \sigma_{blank}$), [b]limit of quantification ($y_{LOQ} = A_1 + 10 \times \sigma_{blank}$), [c]correlation coefficient, [d]sensitivity enhancement by signal-to-noise ratio, [e]enhancement factor (obtained for LOD with standard luminol over *m*-carboxy luminol)

2.6.2.3. Stability of luminophores in water and carbonate buffer

Stability of *m*-carboxy luminol was studied in direct comparison to luminol and similar stability in carbonate buffer for both luminophores was obtained (**Figure A.6**). The CL signal decreases significantly for both luminophores after 5 days in carbonate buffer. In water,

m-carboxy luminol is stable for at least 3 weeks. Luminol was not fully soluble in water as 1 mmol L^{-1} stock solution, thus cannot be compared to *m*-carboxy luminol in ultrapure water.

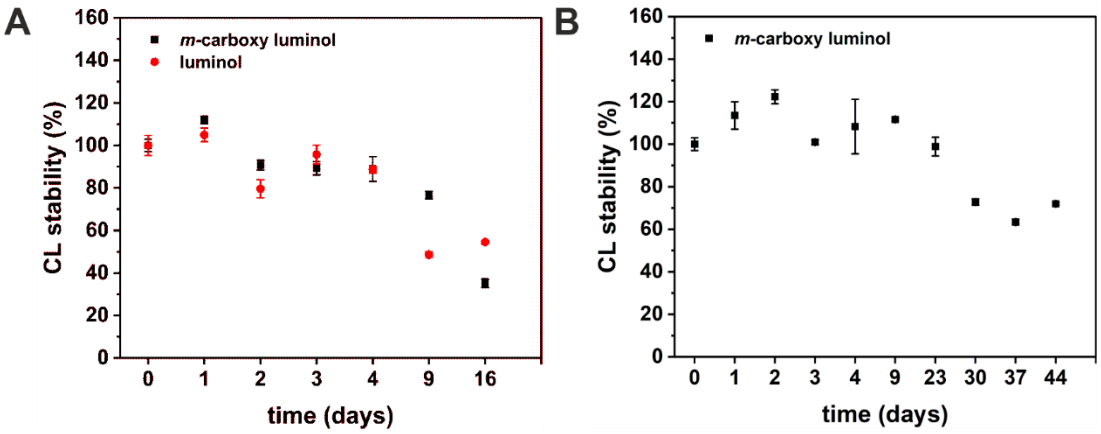

Figure A.6 Stability of *m*-carboxy luminol (black) in solution in comparison to luminol (red) (A) in 0.1 mol L^{-1} carbonate buffer (pH 10.5) and (B) in ultrapure water, reaction mix with 100 µmol L^{-1} luminophore, 1 µmol L^{-1} hemin and 5 mmol L^{-1} H_2O_2 in 0.05 mol L^{-1} carbonate buffer (pH 10.5), recorded in endpoint mode with (A) gain 45 and (B) gain 70, reading height 1 mm, integration time 2 s, n = 4

2.6.2.4. Mechanistic insights into enhanced chemiluminescence HRP oxidation mechanism

2.6.2.4.1. Schematic mechanistic steps for enhanced and non-enhanced HRP mechanism

Figure A.7 shows the proposed oxidation mechanism of horseradish peroxidase with and without enhancer with (3) and (5) being the rate limiting steps of the reaction, respectively. The following studies demonstrate that still much is unknown about this reaction both for luminol and *m*-carboxy luminol. For a better understanding of the following phenomena, a deeper study into the not yet fully resolved underlying catalytic mechanism of HRP is needed.[4,27] The interaction between the luminophore in combination with enhancer molecules and the enzyme appears more complex than proposed so far (**Figure A.7 B**). A precise balancing of enhancer, catalyst and hydrogen peroxide is needed to obtain signal enhancement with *m*-carboxy luminol.

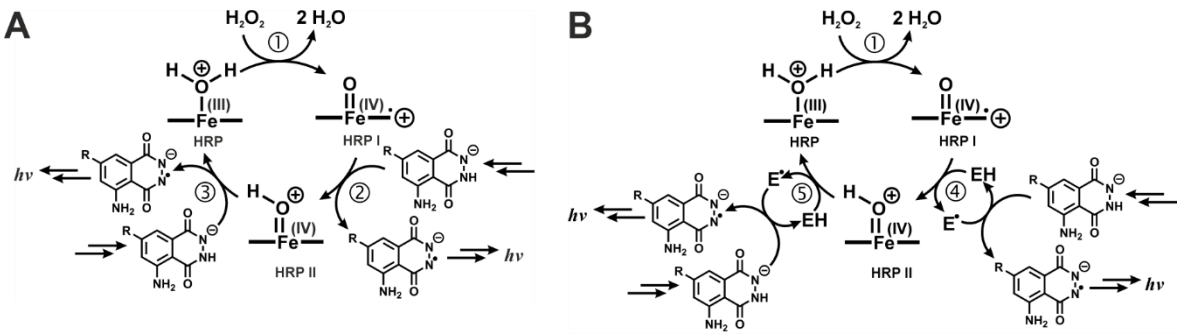

Figure A.7 Schematic mechanism of horseradish peroxidase induced chemiluminescence (A) with direct oxidation of the luminophore in three steps (1) two-electron oxidation of the ferric group to HRP I, (2) reduction of porphyrin π cation by single electron transfer of luminophore anion to HRP II, (3) single electron transfer of luminol anion to reduce HRP II back to the ground state and (B) with an enhancer to oxidize the luminophore in four steps with (1) being similar as in (A), (4) single electron transfer of an enhancer molecule followed by the oxidation of the luminophore anion by the enhancer radical and (5) single electron transfer of HRP II to an enhancer molecule regenerating HRP [4,27]

The current enhanced mechanism postulates that the luminophore oxidation is detached from the enzyme reaction and the light production is solely dependent on the reduction potential of the enhancer molecule, which needs to be balanced to be easily oxidized by the enzyme and simultaneously easily reduced by the luminophore. A similar or greater reduction potential of the enhancer in contrast to the luminophore favors the generation of luminophore radicals and thus promotes the steps for light emission.[4] The HP, however, works on the one hand as substrate of HRP, but at high concentration on the other hand it converts HRP II to an oxyperoxidase which is inactive.[27] This, in turn, can be regenerated to HRP which can again participate in the peroxidase catalytic cycle.[27] In addition it is stated, that no long lived ternary complexes are observed during the oxidation procedure of the HRP and thus no intermediate complex is observed, containing bound luminol.[28] The reaction between luminol and enhancer is assumed to proceed via outer sphere electron transfer, in other words, no bond formation will occur during electron transfer.[19] Under ideal conditions, luminol is considered a pure radical acceptor rather than a substrate of horseradish peroxidase, which is supported by its protective abilities towards the HRP within the enhanced system by accepting free radicals which otherwise would react with the HRP and partially inactivate it. [29] This makes competition between luminol and enhancer in the active center of the enzyme very unlikely. This and the fact that typical enhancer molecules exhibit a log P value equal or higher than that of luminol has led us to the conclusion that the reason of the different behavior of *m*-carboxy luminol and luminol in the enhanced and non-enhanced pathway is probably caused by *m*-carboxy luminol´s increased water

solubility and thus rather limited access to the hydrophobic active center of the enzyme and thus increased electron transfer distance.

2.6.2.4.2. Comparison between enhanced and non-enhanced chemiluminescence behavior

Increase of the CL signal with *m*-carboxy luminol in the horseradish peroxidase (HRP) system was only obtained for the enhanced pathway with optimized conditions (**Figure A.8**).

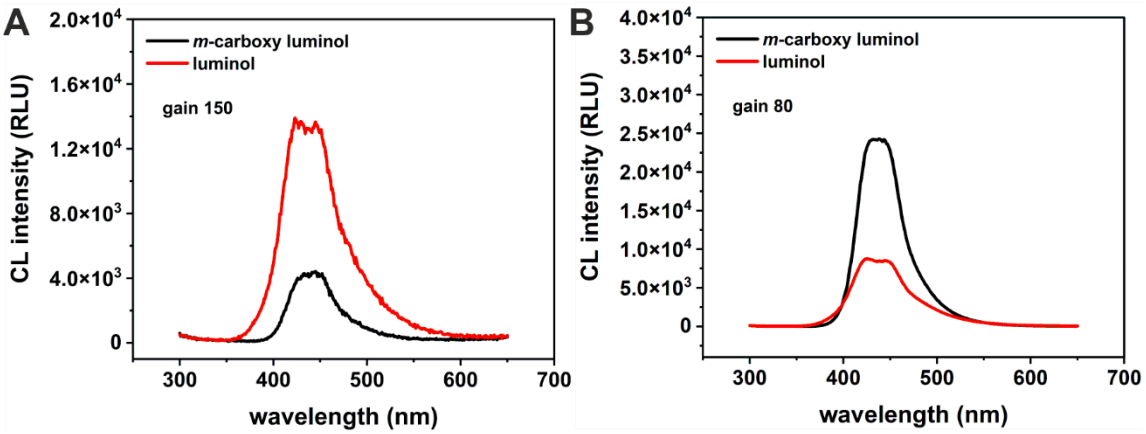

Figure A.8 Chemiluminescence spectra of *m*-carboxy luminol (black) and luminol (red) for the horseradish peroxidase system (A) without 50 µmol L^{-1} *p*-coumaric acid and (B) with 50 µmol L^{-1} *p*-coumaric acid of a solution containing 100 µmol L^{-1} luminophore, and 10 mmol L^{-1} H_2O_2 in 0.033 mol L^{-1} Tris-HCl (pH 8.5) and 1.5 U mL^{-1} horseradish peroxide, data are presented as mean with n = 3 (error bars not shown)

In the process of optimizing the enhancer concentration (*p*-coumaric acid), three HRP enzymes were compared, *i.e.,* high concentrations of free HRP (5 µg mL^{-1}) and comparably low concentrations of HRP bound to IgG (0.125 µg mL^{-1}, and 0.08 µg mL^{-1}). In all cases, the optimal *p*-coumaric acid concentration was 50 µmol L^{-1} (**Figure A.9**).

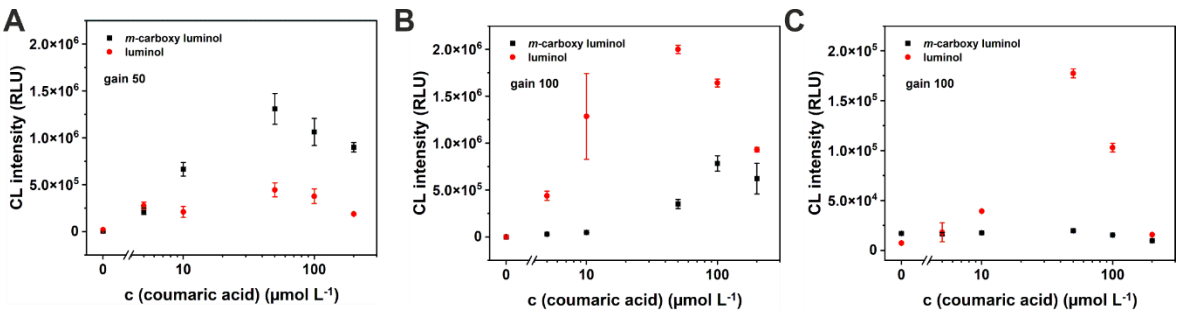

Figure A.9 Horseradish peroxidase (HRP) mediated chemiluminescence dependency on *p*-coumaric acid concentration for *m*-carboxy luminol (black) and luminol (red) of a solution containing 100 µmol L^{-1} luminophore and 10 mmol L^{-1} H_2O_2 in 0.033 mol L^{-1} Tris-HCl buffer (pH 8.5) and in (A) 5 µg mL^{-1} HRP, in (B) 0.125 µg mL^{-1} anti-mouse IgG-HRP (A9044, Sigma Aldrich,) and in (C) 0.08 µg mL^{-1} anti-mouse IgG-HRP (115-035-003, Jackson ImmunoResearch Laboratories, Inc.), recorded with reading height 1 mm, integration time 2 s, data are presented as mean ± SD (error bar) with n = 3

The decrease of CL intensity with higher enhancer concentration can be attributed to radical destruction by radical self-reaction.[4] Surprisingly, luminol and *m*-carboxy luminol behaved differently for the free (**Figure A.9 A**) and bound HRP (**Figure A.9 B and C**) studies. To further investigate this, a broad range of bound HRP concentrations was studied by creating BSA-HRP conjugates as a less expensive substitute for HRP-IgG (**Figure A.10**). Successful coupling of HRP to BSA via EDC/NHS chemistry was demonstrated by adsorbing BSA-HRP to a MTP and performing a colorimetric TMB assay (**Figure A.10 A**) and confirmed also in the enhanced CL format (**Figure A.10 B**).

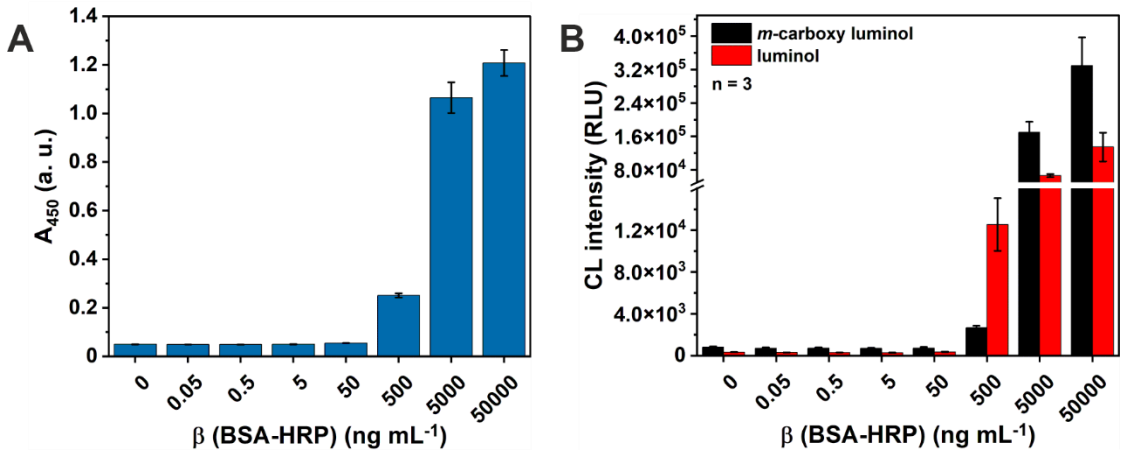

Figure A.10 Horseradish peroxidase calibration developed with in (A) a ready-to-use TMB liquid substrate showing maintained enzyme functionality after EDC/NHS coupling to BSA and in (B) with CL substrate containing either luminol (red) or m carboxy luminol (black). A high binding microtiter plate was coated with 200 µL of the respective BSA-HRP dilution in 80 mmol L^{-1} Na_2CO_3/100 mmol L^{-1} H_3BO_3, pH 9.4 overnight at 4 °C. After coating the MTP was washed three times for 5 min with 300 µL of 1X PBS, 0.05% TWEEN®20 before in (A) 100 µL of ready-to-use TMB liquid substrate was added and the enzymatic reaction was stopped after 5 min with 100 µL of 1 N H_2SO_4 and in (B) 200 µL of chemiluminescence substrate (100 µmol L^{-1} luminophore, 50 µmol L^{-1} *p*-coumaric acid and 10 mmol L^{-1} H_2O_2 in 0.066 mol L^{-1} Tris-HCl buffer, pH 8.5) was added before the measurement. Absorbance was measured at 450 nm and chemiluminescence with gain 100, integration time 2 s and reading height 1 mm, data are presented as mean ± SD (error bar) with n = 3

This study was furthermore expanded to ensure that BSA or IgG molecules would not influence the catalytic reactions (**Figure A.11**). In all instances, it can be observed that at HRP concentrations at or below 0.5 µg mL^{-1}, luminol outperforms *m*-carboxy luminol, whereas this reverses at higher HRP concentrations dramatically. It should be noted that the decrease of signals starting from 50 µg mL^{-1} HRP concentrations is due to the very strong chemiluminescence signal which decays very fast and cannot be properly recorded.

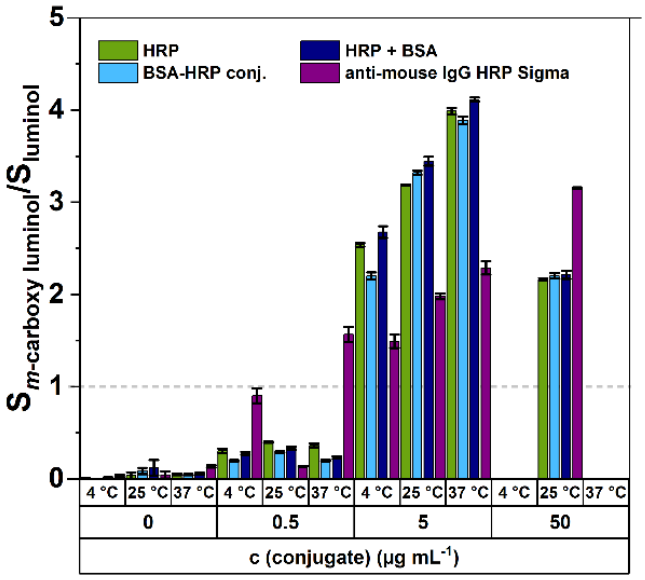

Figure A.11 Evaluation of different horseradish peroxidase conjugates with regard to their concentration dependent enhanced chemiluminescence behaviour towards *m*-carboxy luminol, measurement was performed with 100 µL of HRP dilution in 1X PBS pH 7.4 and 100 µL of 200 µmol L^{-1} luminophore, 100 µmol L^{-1} *p*-coumaric acid and 20 mmol L^{-1} H_2O_2 in 0.066 mol L^{-1} Tris-HCl buffer (pH 8.5), recorded in endpoint mode with gain 45, reading height 1 mm, integration time 2 s, the grey reference line indicates equivalent CL intensity of both luminophores, data are presented as mean ± SD (error bar) with n = 3

2.6.2.4.3. Optimization of the competitive DCF Assay

Before the competitive DCF assay was studied, optimization towards BSA-DCF coating concentration and anti-mouse IgG-LOx conjugate dilution was conducted. A loading concentration of 5 µg mL^{-1} BSA-DCF and a 1:100 dilution of the anti-mouse IgG-LOx was determined (**Figure A.12**).

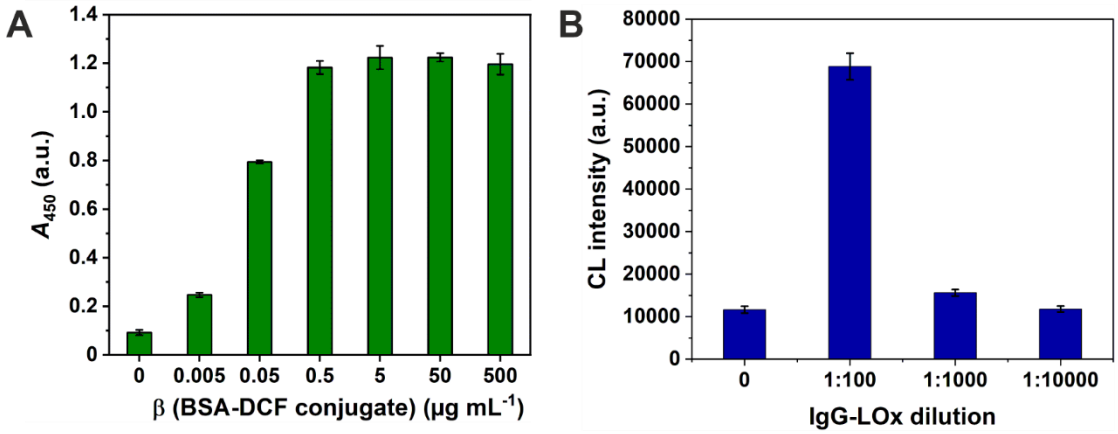

Figure A.12 Optimization experiments of competitive diclofenac assay showing in (A) the loading study of BSA-DCF on a high binding MTP with a ready-to-use TMB liquid substrate for colorimetric readout and in (B) the determination of the applicable dilution of the anti-mouse IgG-LOx conjugate via chemiluminescence measurements, n = 3

Figure A.13 shows the effect of the variation in the instrument settings. With increasing the sensitivity of the detector an overall increased signal range and thus a higher resolution can be obtained.

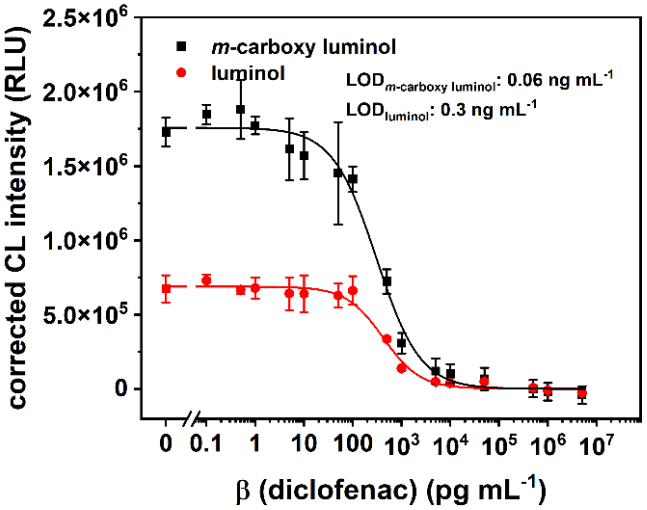

Figure A.13 Dose-response curve of competitive diclofenac assay employing an anti-mouse IgG secondary antibody coupled to lactate oxidase and L-lactate for chemiluminescence detection of produced H_2O_2. Chemiluminescence measurement was performed with 100 µmol L^{-1} *m*-carboxy luminol (black) or luminol (red) as luminophore and 1 µmol L^{-1} hemin in a final volume of 200 µL in endpoint mode with gain 150, reading height 1 mm, integration time 2 ms, displayed data was background corrected, the LOD was calculated according to $y_{LOD} = A1 - 3 \times \sigma_{blank}$, n = 3

2.6.2.5. L-lactate determination

A straightforward chemiluminescence-based enzymatic L-lactate assay using lactate oxidase was developed to point out the benefit of *m*-carboxy luminol in bioanalytical assays (**Figure A.14**). To confirm the correctness of the herein developed assay the L-lactate concentration of synthetic sweat was also determined using a commercial assay kit.

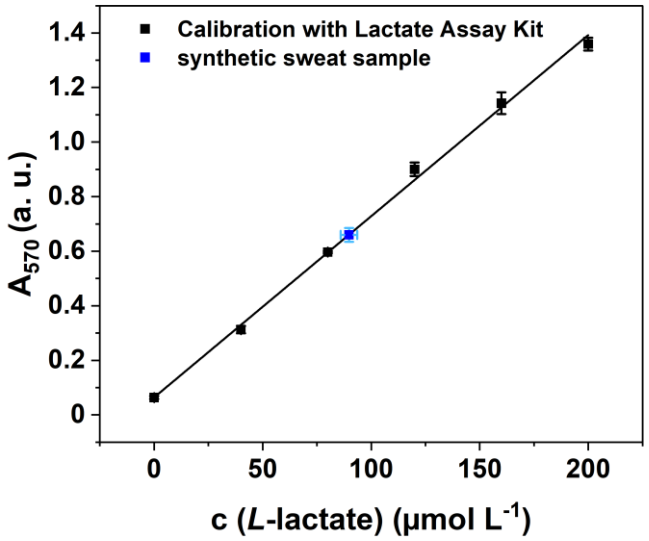

Figure A.14 Determination of L-lactate in synthetic sweat using a photometric detection at 570 nm, using a commercially available L-lactate assay kit from Sigma Aldrich, dilution factor of synthetic sweat sample 0.02, n = 3

Significant signal enhancement (6.3-times) was obtained by exchanging luminol with *m*-carboxy luminol (**Table A.4**).

Table A.4 Overview over limits of detection of L-lactate Assay in MTP

Luminophore	LOD[a] [µmol L^{-1}]	LOQ[b] [µmol L^{-1}]	Slope [L µmol $^{-1}$]	R^2 [c]	SE[d]
m-carboxy luminol	0.4	1.3	(2.2 ± 0.025) × 10^3	0.9861	6.3
luminol	0.04	0.12	(0.35 ± 0.010) × 10^3	0.9964	

[a]limit of detection (x_{LOD} = 3 × σ_{blank}/slope), [b]limit of quantification (x_{LOQ} = 10 × σ_{blank}/slope), [c]correlation coefficient, [d]sensitivity enhancement by slope

Comparison between the herein developed chemiluminescence L-lactate assay with a commercially available assay showed that within the error similar L-lactate concentration for synthetic sweat according to DIN 53160-2 were obtained (**Table A.5**). Synthetic sweat according to DIN 53160-2 contains 1.002 g L^{-1} lactic acid (90%) equaling 10 mmol L^{-1} lactic acid.

Table A.5 Determination of L-lactate in synthetic sweat (DIN 53160-2)

Lactate assay kit	Detection method	Luminophore	L-lactate in synthetic sweat (DIN 53160-2) [mmol L^{-1}][a]
custom-made (within this study)	chemiluminescence	*m*-carboxy luminol	4.0 ± 0.2 (CV: 5.7%)
custom-made (within this study)	chemiluminescence	luminol	4.6 ± 0.1 (CV: 2.5%)
commercial (Sigma Aldrich)	photometric	-	4.5 ± 0.2 (CV: 4.2%)

[a]A Tukey-test at the 0.05 significance level was performed and no significant difference of the mean of the commercially available assay to both custom-made assays was obtained

2.6.3. References

[1] A. G. Griesbeck, Y. Díaz-Miara, R. Fichtler, A. Jacobi von Wangelin, R. Pérez-Ruiz, D. Sampedro, *Chem. - Eur. J.* **2015**, *21*, 9975.

[2] A. Hlaváček, Z. Farka, M. Hübner, V. Horňáková, D. Němeček, R. Niessner, P. Skládal, D. Knopp, H. H. Gorris, *Anal. Chem.* **2016**, *88*, 6011.

[3] a) A. Fan, C. Lau, J. Lu, *Anal. Chem.* **2005**, *77*, 3238; b) D. Hu, H. Han, R. Zhou, F. Dong, W. Bei, F. Jia, H. Chen, *Analyst* **2008**, *133*, 768; c) N. Li, D. Liu, H. Cui, *Anal. Bioanal. Chem.* **2014**, *406*, 5561.

[4] A. N. Díaz, F. G. Sánchez, J. A. González Garcia, *J. Biolumin. Chemilumin.* **1998**, *13*, 75.

[5] Y. Xiao, V. Pavlov, R. Gill, T. Bourenko, I. Willner, *ChemBioChem* **2004**, *5*, 374.

[6] R. Maeztu, G. González-Gaitano, G. Tardajos, *J. Phys. Chem. B* **2010**, *114*, 10541.

[7] H. Cui, M.-J. Shi, R. Meng, J. Zhou, C.-Z. Lai, X.-Q. Lin, *Photochem. Photobiol.* **2004**, *79*, 233.

[8] G. H. Thorpe, L. J. Kricka, S. B. Moseley, T. P. Whitehead, *Clin. Chem. (Washington, DC, U. S.)* **1985**, *31*, 1335.

[9] a) E. Marzocchi, S. Grilli, L. Della Ciana, L. Prodi, M. Mirasoli, A. Roda, *Anal. Biochem.* **2008**, *377*, 189; b) M. M. Vdovenko, V. Papper, R. S. Marks, I. Y. Sakharov, *Anal. Methods* **2014**, *6*, 8654.

[10] G. Chen, M. Jin, P. Du, C. Zhang, X. Cui, Y. Zhang, J. Wang, F. Jin, Y. She, H. Shao et al., *Food Agric. Immunol.* **2017**, *28*, 315.

[11] H. O. Albrecht, *Zeitschrift für Physikalische Chemie* **1928**, *136U*, 321.

[12] H. D. K. Drew, F. H. Pearman, *J. Chem. Soc.* **1937**, 586.

[13] E. H. White, D. F. Roswell, *Acc. Chem. Res.* **1970**, *3*, 54.

[14] H. R. Schroeder, F. M. Yeager, *Anal. Chem.* **1978**, *50*, 1114.

[15] a) H.A.H. Rongen, R.M.W. Hoetelmans, A. Bult, W. P. van Bennekom, *J. Pharm. Biomed. Anal.* **1994**, *12*, 433; b) M. Yang, C. Liu, K. Qian, P. He, Y. Fang, *Analyst* **2002**, *127*, 1267.

[16] Y. Nishinaka, Y. Aramaki, H. Yoshida, H. Masuya, T. Sugawara, Y. Ichimori, *Biochem. Biophys. Res. Commun.* **1993**, *193*, 554.

[17] K.-D. Gundermann, W. Horstmann, G. Bergmann, *Chem. - Eur. J.* **1965**, *684*, 127.

[18] A. Mayer, S. Neuenhofer, *Angew. Chem., Int. Ed. Engl.* **1994**, *33*, 1044.

[19] G. Merényi, J. Lind, T. E. Eriksen, *J. Biolumin. Chemilumin.* **1990**, *5*, 53.

[20] A. L. Rose, T. D. Waite, *Anal. Chem.* **2001**, *73*, 5909.

[21] R. Radi, T. P. Cosgrove, J. S. Beckman, B. A. Freeman, *Biochem. J.* **1993**, *290 (Pt 1)*, 51.

[22] Y. Ando, K. Niwa, N. Yamada, T. Irie, T. Enomoto, H. Kubota, Y. Ohmiya, H. Akiyama, *Photochem. Photobiol.* **2007**, *83*, 1205.

[23] G. M. Greenway, T. Leelasattarathkul, S. Liawruangrath, R. A. Wheatley, N. Youngvises, *Analyst* **2006**, *131*, 501.

[24] C. A. Marquette, L. J. Blum, *Anal. Bioanal. Chem.* **2006**, *385*, 546.

[25] E. L. Bastos, P. Romoff, C. R. Eckert, W. J. Baader, *J. Agric. Food Chem.* **2003**, *51*, 7481.

[26] T. G. Burdo, W. R. Seitz, *Anal. Chem.* **1975**, *47*, 1639.

[27] H. H. Gorris, D. R. Walt, *J. Am. Chem. Soc.* **2009**, *131*, 6277.

[28] a) M. J. Cormier, P. M. Prichard, *J. Biol. Chem.* **1968**, *243*, 4706; b) P. M. Prichard, M. J. Cormier, *Biochem. Biophys. Res. Commun.* **1968**, *31*, 131.

[29] Y. L. Kapeluich, M. Y. Rubtsova, A. M. Egorov, *J. Biolumin. Chemilumin.* **1997**, *12*, 299.

3. Enhanced Chemiluminescence of a Superior Luminol Derivative Provides Sensitive Smartphone-based Point-of-Care Testing with Enzymatic µPADs

Graphical Abstract

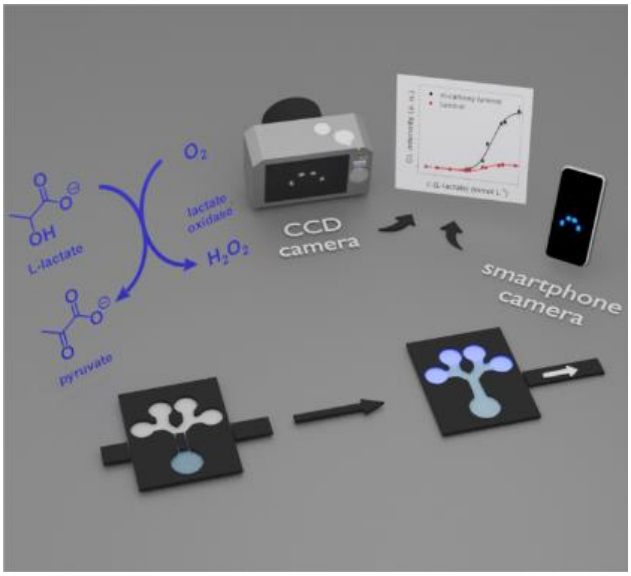

This chapter has been published in the Wiley-VCH GmbH journal Analysis and Sensing.

Authors' contributions

Simone Rink: Conceptualization, visualization, investigation, formal analysis, data curation, writing: original draft– lead contribution

Antje J. Baeumner: Conceptualization, supervision, project administration, experimental design, writing: review & editing – lead contribution

Axel Duerkop: Conceptualization, supervision, project administration, experimental design, writing: review & editing – supporting contribution

Abstract

Chemiluminescence (CL) provides ideal conditions for point-of-care testing (POCT) with wide dynamic ranges, superior sensitivities, and detection simplicity. It has not arrived routinely in the POCT field due to naturally low quantum yields of typical probes and the lack of sensitive low-cost detection devices. Here, we developed a universal microfluidic paper-based analytical device (µPAD) using L-lactate as model analyte. We demonstrate that a smartphone camera can compete with a scientific CCD camera as performance benchmark when using the strong CL emitter, *m*-carboxy luminol, resulting in extraordinary signal-to-noise ratios of 67. The µPAD provides CV <10 %, stability at room temperature for ≥ 3 months and simple processing. Furthermore, the µPAD enables the detection of picomoles of the luminophore providing additional design flexibility. Thus, this new CL-µPAD is available for translating the many CL standard analytical assays performed in microtiter plates, microarrays or other more complex detection strategies to the POC.

3.1. Introduction

One of today's challenges in analytical research is the development of highly sensitive and selective analysis platforms, which can easily be carried out in-field by trained and non-trained personnel. For this, sensitive and low-cost assay principles are required, which are easy to operate.[1] Chemiluminescence (CL) provides simple, portable and cost-efficient detection due to its independency of external light sources and may use detectors as easy and popular as smartphone cameras.[2] Yet, it competes with regard to detection limits with radioanalytical assays[3] and allows ultrasensitive measurements down to zeptomole detection limits due to its background-free nature[4]. It further convinces with short measuring times, wide dynamic ranges and universal (bio)analytical application, such as in routine clinical laboratories for immunoassays or DNA probe assays, as well as in biochemical research for reporter gene assays, cell viability assays and many more.[3] The Whitesides group on the other hand pioneered in a new class of point-of-care testing (POCT) platforms, the microfluidic paper-based analytical devices (µPADs).[5] Combining CL detection with this new class of POCT, which shows already promising prospects for mobile POCT with broad diagnostic applications[6], allows for ultrasensitive but still affordable point-of-care (POC) platforms. µPADs combine the flexibility of microfluidic total analysis systems (µTAS) with regard to the integration of multiple processes, multiplexing and variability in analytical assays with the simplicity and cost-efficiency of lateral flow assays (LFA).[7] However, the majority of current paper-based microfluidic systems are dominated by colorimetric, fluorescent or electrochemical detection.[8,9] The drawbacks of

these detection techniques, are either their lack in sensitivity, challenging manufacturing or their requirement of costly detection devices.[10] Thus, current µPADs struggle, among others, with reproducibility, modest sensitivity, insufficient specificity[8] and the lack of detection devices with freely available evaluation software.[11] Especially colorimetric µPADs often suffer from inhomogeneous color development[12] *e.g.*, caused by bleaching of colored products over time or their overoxidation due to ongoing enzymatic reactions, ambient light imbalance, and shadow formation while image taking and variation in color generation algorithms of different camera manufacturers[13] hampering commercialization[14]. CL, on the contrary, relies on the generated light intensity which can be captured without external illumination and extracted from the unprocessed raw monochromatic images and is thus independent of the generated color signal, shooting angle and external illumination. Despite CL's great potential as detection technique, it has not yet arrived routinely in the POCT field. This is probably due to the transient signal and in general low quantum yields (1 % for CL reactions) and thus low degrees of emitted light of typical CL reagents[15]. Furthermore, the lack of sensitive low-light sensor chips for non-scientific and affordable cameras limited the progression as well. Thus, ideally, expensive cooled charge-coupled device (CCD) cameras or photomultiplier tubes[15,16] are required for sensitive detection which do not fit the budget nor the application mode of POCT. Together with easier readout strategies, minimal instrumental requirements along with the sensor chip improvement of smartphone cameras towards higher light sensitivity (the ISOCELL image sensor from Samsung, the SuperSpectrum Sensor from Huawei, the ExmorRS from Sony or the OmniVision image sensors), CL poses a powerful and elegant alternative detection principle.[15] In addition, with the enhanced CL signal of the herein studied *m*-carboxy luminol, CL is now ready for inexpensive sensitive POCT solutions.

We show in this study a universal µPAD principle for the detection of typical biomarkers based on enzymatic conversion with the byproduct H_2O_2 such as the reaction of L-lactate into pyruvate through lactate oxidase (LOx). Especially L-lactate has recently raised interest as it is not only promising as POCT solution for clinical practice and emergency care, but relevant as well for the ongoing trend of self-monitoring of fitness levels with easy, portable and economic analytical devices.[17,18] Depending on the biological fluid, lactate concentrations can range from 0.1 mmol L^{-1} to 2.5 mmol L^{-1} in saliva[19] and can also be as high as 115.8 mmol L^{-1} in sweat after exhaustive exercise.[20] Thus, detection over a vast dynamic range is required to cover the complete relevant area with high resolution. This is provided by CL in general, as it shows low background signals and broad linearity and is

furthermore strengthened by the increased CL emission of *m*-carboxy luminol used in this work. Furthermore, we studied the detection of the luminophore itself in a generalized paper-based microfluidic approach and achieved higher signal-to-noise ratios along with lower limits of detection. This highlights our CL probe not only as substrate but also as chemiluminescent label for biomolecules which introduces extra selectivity to CL-µPADs and overall broader application possibilities.

3.2. Experimental Section

3.2.1. Chemicals and consumables

All chemicals were commercial HPLC grade and were used without purification. Standard chemicals were purchased from Merck. Horseradish peroxidase (HRP) was purchased from Merck (Darmstadt, Germany) and a 300 U mL^{-1} stock solution in 1 X PBS buffer, pH 7.4 was prepared. Lactate oxidase (LOx) was obtained from AG Scientific (San Diego, USA) and a 100 U mL^{-1} in 1 X PBS buffer, pH 7.4 was prepared. Both enzymes were aliquoted and stored at 4 °C and respective working solutions were prepared freshly before each measurement. *m*-Carboxy luminol was custom-made by Taros Chemicals GmbH & Co. KG (Germany), according to a standard procedure.[21] Synthetic sweat according to DIN 53160-2 was purchased from Synthetic Urine e. K. company (Nußdorf, Germany). For all experiments ultrapure water was used and stock solutions were prepared for luminol (1 mmol L^{-1} in 0.1 mol L^{-1} carbonate buffer, pH 10.5), *m*-carboxy luminol (1 mmol L^{-1} in 0.1 mol L^{-1} carbonate buffer, pH 10.5), hemin (1 mmol L^{-1} in 0.1 mol L^{-1} carbonate buffer, pH 10.5), Co(II) (1 mmol L^{-1} in ultrapure water), *p*-coumaric acid (1 mmol L^{-1} in ethanol, 96 %) and L-lactate (10 mmol L^{-1}). For H_2O_2 the stock solution (100 mmol L^{-1} in ultrapure water) was freshly prepared before each measurement.

3.2.2. Fabrication of paper substrate

The fluidic layout was designed by using CorelDraw 2017 and printed with a Xerox ColorQube™ 8580 wax printer, on chromatography paper Grade 1 CHR (3001-917, GE Healthcare Life Science, Germany). The paper (**Figure 1 B**) was cut to the respective size and the wax was melted on a heating plate for approximately 30 s at 200 °C. After the melting process the back of the paper substrate was sealed with adhesive tape (927, 3M™). The final paper substrate was produced by drop-coating of each 1 µL luminophore, catalyst and enhancer (only for HRP) on the detection zone.(**Figure 1 A**). The solutions were allowed to dry in between. The paper substrate was ready to use after all reagents were

dried on the filter paper. For lactate determination the paper substrate was adjusted with an additional wax barrier including a bridging strip partially modified with wax (**Figure 1 C,D**).

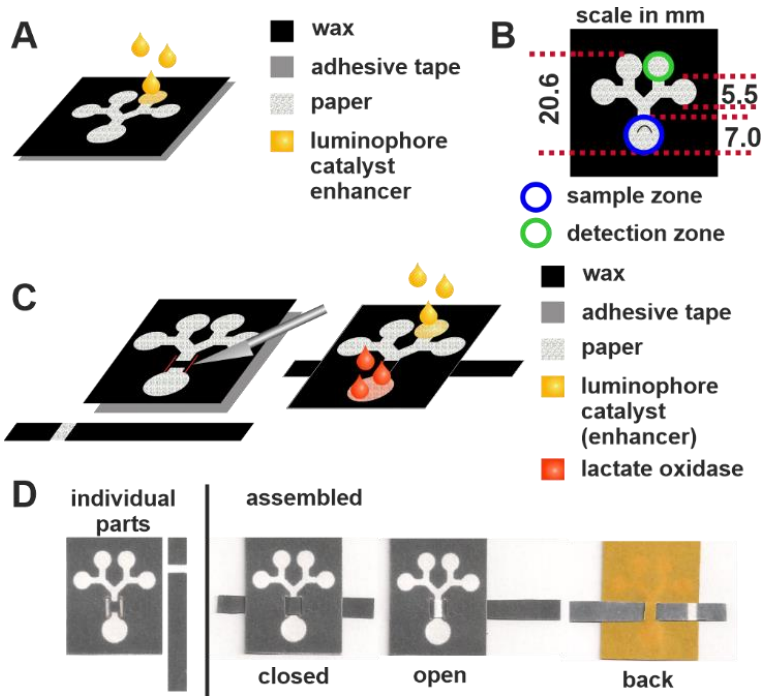

Figure 1 Fabrication of the paper substrate with (A) layout for H_2O_2 detection and luminophore detection, (B) dimensions of the paper substrate, (C) layout for the L-lactate assay and (D) real images of the µPAD.

3.2.3. Measurement on paper substrate

The paper device was placed in a dark box with a Lumenera LW135RM CCD camera and 30 µL of analyte solution were applied to the sample zone. After the analyte solution reached the capturing start point (**Figure 2 A (2)**) the box was closed and 15 images with 2 s exposure time in stacking mode were recorded. For luminophore detection the detection zones were prepared with varying luminophore concentrations. For H_2O_2 detection, varying HP concentrations were applied to the sample zone (**Figure 2 A**). For L-lactate determination, 4 µL of LOx (5 U μL^{-1}) were dried on the sample zone before L-lactate in synthetic sweat matrix was added. L-lactate was incubated for 10 min on the sample zone before the barrier was removed (**Figure 2 B**). For the CCD camera 15 images with 2 s exposure in stacking mode were recorded after the solution reached the capturing start point. For detection with a Samsung S21 5 G smartphone, an image series of 9 images was recorded manually with 30 s exposure time and ISO 800. The images were taken each minute after the solution reached the detection zone and stacked afterwards through ImageJ before post processing. CL intensity was determined with ImageJ from the stacked image. The limit of detection (LOD) and the limit of quantification (LOQ) were determined

according to $y_{LOD} = A1 + 3 \times \sigma_{blank}$ and $y_{LOQ} = A1 + 10 \times \sigma_{blank}$, respectively, if a four-parameter logistic fit was applied. For linear fitting, the LOD and LOQ were calculated according to $x_{LOD} = 3 \times \sigma_{blank}/slope$ and $x_{LOQ} = 10 \times \sigma_{blank}/slope$.

All measurements were conducted at 22 °C and 38 % humidity. A circular region of interest (ROI) was used covering the area of the detection zone and the mean gray value was determined by ImageJ (Fiji, 2.0.0-rc-67/1.52c).[22] The mean gray values were multiplied by the evaluation area to yield the final CL signal response. For the enzymatic µPAD, the S/N ratio was determined as relative measure, using the top asymptote (A2) as signal and bottom asymptote (A1) of the calibration curve as noise.

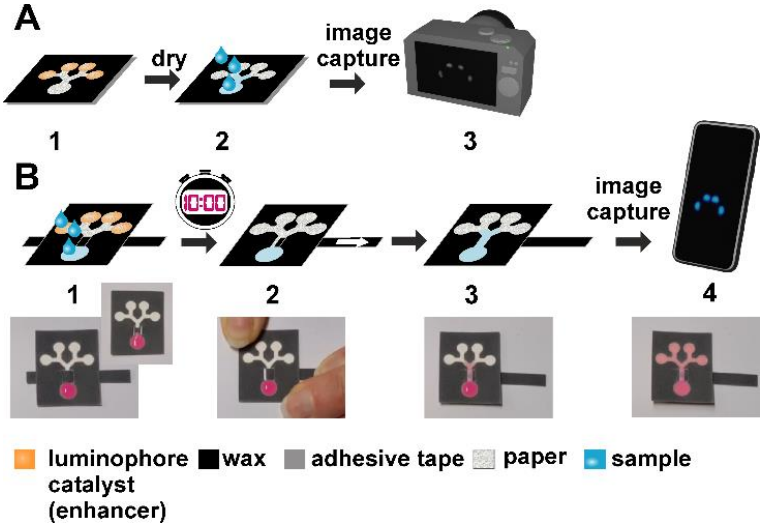

Figure 2 Stepwise illustration of the assay procedure in (A) for H_2O_2 detection and luminophore detection with (1) applying sample to sample zone, (2) signal development and (3) taking images with a CCD camera and in (B) for the L-lactate assay with (1) applying sample to sample zone, incubation for 10 min, (2) opening sample chamber (3) signal development and (4) taking images with either a smartphone or CCD camera, schematic illustration, and real images with sulforhodamine B dye solution for better illustration.

3.3. Results and Discussion

The obtained extraordinary chemiluminescence enhancement of *m*-carboxy luminol over standard luminol in microtiter plate-based bioassays[23] encouraged us to transfer our findings to a microfluidic paper-based analytical device (µPAD) to investigate its feasibility towards a sensitive POCT system. Here, the determined photophysical characteristics of *m*-carboxy luminol in Rink et. al. laid the foundation for this work. The initial design of the µPAD (**Figure 2 A**) consists of two individual zones, one sample and four detection zones which are connected through paper-based channels allowing to record the entire CL reaction. The sample zone was either modified with lactate oxidase (LOx) or simply used as bare application zone. The four detection zones contain drop-coated luminophore and

catalyst and allow multiple determination within one paper substrate with good reproducibility and a coefficient of variation (CV) < 10 %. Similar results were obtained when using three individual paper substrates, independent from the employed analyte. Here the CV is again mainly < 10 % in both designs (**Figure S 1, Figure S 2**) which is remarkable considering the manual fabrication process and the heterogenous nature of the paper. Furthermore, the design allows to extract the entire CL signal due to the designed channel structure and the accompanied reaction delay. The channel structure additionally provides flexibility to introduce structural features such as incubation areas or waste zones if needed. The original design was used for direct analyte detection when no prior conversion of the sample and incubation, respectively, was needed. We investigated three major catalysts, namely cobalt, hemin and horseradish peroxidase (HRP)[23] regarding their catalytic and analytic performance. We first tested our system with the initial design and H_2O_2 as analyte to identify ideal conditions before switching to the enzymatic µPAD for the analysis of L-lactate in synthetic sweat. As a second approach we altered the assay strategy towards the luminophore as analyte which suggests that *m*-carboxy luminol has indeed a great potential as ultrasensitive chemiluminescence label in POC devices.

3.3.1. Establishing chemiluminescence reaction on simple µPAD for H_2O_2 detection

Detection of H_2O_2 has great relevance in bioanalysis. Besides its role as signaling messenger and biomarker for oxidative stress, it functions as substrate for peroxidases and is often a byproduct of oxidase-based enzymatic reactions. The latter can be exploited for the detection of clinically relevant metabolites such as glucose, lactate or uric acid.[24] Thus, we preliminary studied our chemiluminescence µPADs for H_2O_2 detection to design the initial µPAD platform. We observed enhancement in sensitivity (up to three times) over standard luminol and were able to detect H_2O_2 down to low µmolar concentrations (**Table S 1**) which is sufficient for most of these metabolites. All three tested catalyst systems showed an increase in signal response with *m*-carboxy luminol. When using hemin and HRP as catalyst, we obtained a linear relation between 0 to 2 mmol L^{-1} H_2O_2 (**Figure 3**), whereas with cobalt the CL intensity increased non-linearly in the chosen concentration range.

This correlates very well with our observation in the microtiter plate[23], where the CL reaction with cobalt exhibits non-linear behavior already starting at approximately 1 mmol L^{-1} H_2O_2, which makes cobalt a less suitable catalyst for a simple POC application. We decided to use hemin as catalyst due to its similar performance to HRP (**see SI, Table S 2**). Whereas

standard colorimetric µPADs for metabolites such as uric acid, glucose and L-lactate rely on HRP for color generation, the µPAD developed herein has the unique feature to function without the additional peroxidases, simplifying the final preparation, recording and storage conditions. Although slightly lower LODs were obtained when employing *m*-carboxy luminol, the more decisive advantage here is the significant improvement in resolution by an up to three times steeper slope.

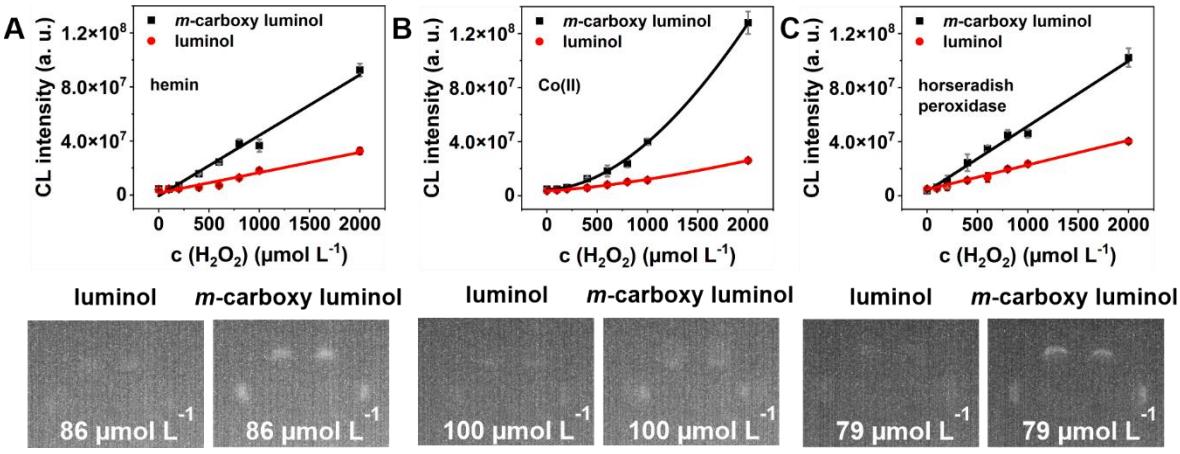

Figure 3 Dose-response curve for H_2O_2 detection with (A) hemin, (B) Co(II) and (C) horseradish peroxidase (HRP) including validation of calculated LOD, with paper substrate for *m*-carboxy luminol (black) and luminol (red) with 1 nmol luminophore, 1 nmol Co(II) or hemin and 0.3 U HRP with 1 nmol *p*-coumaric acid were dried in the detection zone, 30 µL H_2O_2 in 0.1 mol L^{-1} carbonate buffer (pH 10.5) were applied to the sample zone, linear fitting was performed by Origin2020 with $R^2 = 0.978$ (black) and $R^2 = 0.954$ (red) for hemin and $R^2 = 0.984$ (black) and $R^2 = 0.994$ (red) for HRP and four-parameter logistic fit was performed by Origin2020 with $R^2 = 0.978$ (black) and $R^2 = 0.998$ (red) for Co(II), mean ± SD (n = 4), 15 images, 2 s exposure, adjustment of brightness and contrast for each luminophore pair image for better visualization.

Combined with a signal-to-noise ratio of around 20 for *m*-carboxy luminol in contrast to around eight for luminol, this new luminol is an ideal label for highly sensitive but low-cost POCT systems (**Figure 3**). To test our µPAD system for real applications, we transferred these findings towards an enzymatic µPAD using LOx to detect L-lactate through the oxidation-product H_2O_2. The µPAD contains all reagents in a dried state. When L-lactate is added to the sample zone, it is oxidized by LOx to pyruvate generating a stoichiometric amount of H_2O_2 which reacts subsequently with the luminophore to generate light (**Figure 4 A**).

3.3.2. Advanced µPAD design enables enzymatic reaction and detection optimization

To obtain a homogenous signal when employing LOx to oxidize L-lactate, an incubation step prior to the CL reaction is needed to allow for efficient conversion. Hence, refining our original µPAD design for the H_2O_2 detection with a wax barrier upstream of the sample zone

which can be bridged with a functionalized filter paper strip, allowed efficient sample conversion (**Figure 2 B**). We tested different drying times and concentrations of LOx along with different substrate incubation times to determine ideal execution conditions (**Figure S 3**). Incubation for 10 min with 5 U μL^{-1} LOx prior to detection was finally chosen (see SI). In a second line of research, we tested ideal recording conditions to maximize signal collection. Multiple images were taken over a specific time span and subsequently merged before analysis (see SI). To account for time delays and to balance noise generation, 15 images for the CCD camera and nine images for the smartphone camera were recorded (**Figure S 4**). Furthermore, we are currently working on a software-based solution which filters the accumulated noise to improve the overall signal-to-noise ratio especially after merging. Ultimately, we can conclude that using a scientific CCD camera *versus* a simple smartphone camera further demonstrates the benefit of a stronger emitting detection probe when switching from lab to in-field equipment as a strong response allows to use less sensitive detection devices (*e.g.,* cell phones or photodiodes) while maintaining the overall performance.

3.3.3. Benchmarking analytical performance of advanced µPAD towards L-lactate with a standard smartphone camera against a scientific CCD camera

The CL recording was done in a simple dark box with the distance adjusted to the respective front focal distance of both cameras (smartphone camera: 8 cm, CDD: 47.8 cm). Transitioning the assay to smartphone recording the assay remained the same while the recording process was optimized (**see SI, chapter 4**). While the smartphone camera provided lower signal responses, its signal-to-noise ratio (S/N) of 67 was in fact superior to that of the CCD camera (S/N of 38) in the enzymatic µPAD. Whereas full conversion of L-Lactate is anticipated in absolute determinations, only partial, but still quantifiable conversion into H_2O_2 is observed in most biosensors and intended in our µPAD (**Figure S 2**). This enables a dynamic range expansion of our analysis platform while avoiding detector saturation or early substrate inhibition. However, due to the incomplete conversion of L-lactate the generated signal is not as intense as for the equivalent H_2O_2 sample (**Figure S 2**). Our more intense CL probe (**Figure 4 D**, single images of maximum intensity at 480 mmol L^{-1} L-lactate) compensates for this allowing even higher resolution despite lower product concentration in contrast to standard luminol. Despite this, the calculated limits of detection (LOD) for luminol and *m*-carboxy luminol (**Figure 4 B**) are similar ($LOD_{m\text{-carboxy luminol}}$: 0.03 mmol L^{-1}, $LOD_{luminol}$: 0.02 mmol L^{-1}), however, when actually

measuring those, only the *m*-carboxy luminol exhibits a visible CL signal (**Figure 4 C**). In any event, with the obtained LODs the clinically relevant range of 0.5 - 2 mmol L^{-1} as baseline serum concentration is easily covered, similar to values > 2 mmol L^{-1} which are typically associated with hyperlactatemia.[25]

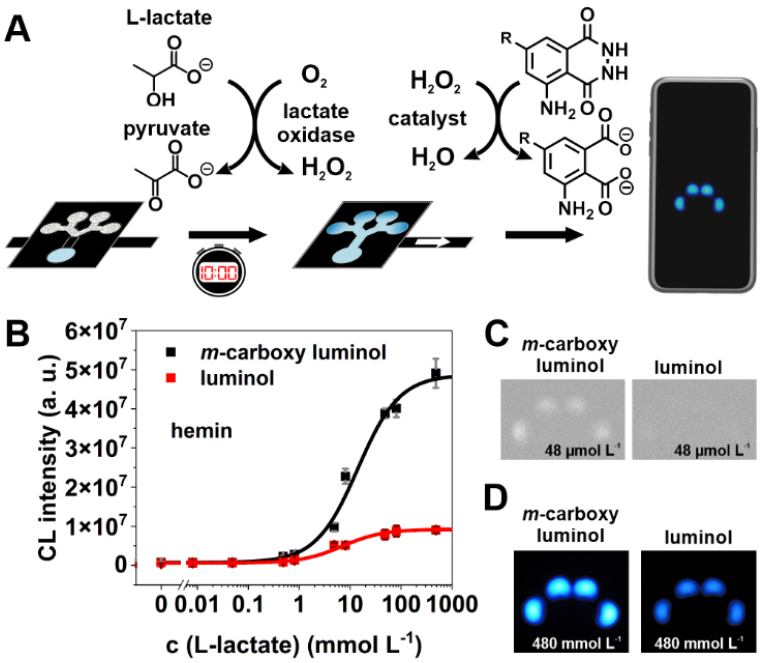

Figure 4 Chemiluminescence L-lactate determination with smartphone (A) illustration of workflow (B) calibration curve of L-lactate in synthetic sweat matrix, using µPADs with stacked 16-bit raw images mean ± SD (n = 4), (C) stacked raw images close to LOD with both luminophores (D) single RGB images for both luminophores at maximum intensity.

Presupposing a correlation between blood and sweat lactate, our µPAD allows for simple non-invasive lactate detection over a fast dynamic range (0.03 – 100 mmol L^{-1}) in a matrix with low potential of interfering species (99 % water, electrolytes, metabolites and micronutrients).[18] However, the positive correlation between blood and sweat lactate is still under vivid debate in the field and non-controversial scientific data have not yet been provided.[18] Even extreme L-lactate levels up to 100 mmol L^{-1} which are possible after exhaustive exercises are quantifiable with a higher resolution when using *m*-carboxy luminol over luminol. Similar results were obtained with the CCD camera (**Figure S 5**). The slightly higher LODs ($LOD_{m\text{-carboxy luminol}}$: 0.09 mmol L^{-1}, $LOD_{luminol}$: 0.3 mmol L^{-1}) are most likely caused by the increased background noise of the CCD camera (**Figure S 5 C, Table S 3**) and hence the decreased S/N ratio.

The unique combination of luminophore, µPADs and smartphone enable a point-of-care lactate detection with highest sensitivity and a broad dynamic range. For example, Li *et al.*

obtained a similar LOD as with our smartphone approach. However, they employed an ultraweak luminescence analyzer to obtain such sensitivity values and report a dynamic range of only 0.02 – 5 mmol L^{-1}.[26] Roda *et al.*, on the other hand, developed a nitrocellulose-based cartridge system being a µPAD in a much broader sense with a LOD of 0.1 mmol L^{-1} for lactate in sweat which further needs special smartphone-dependent detection accessories.[28] Li *et al.*, introduced a colorimetric µPAD with smartphone detection for inter alia lactate with an LOD of 0.03 mmol L^{-1} and a linear range from 0.04 - 24 mmol L^{-1}, but simultaneously show the color alteration with increasing concentrations within their assay when using color reactions.[29] Furthermore, the related electrochemiluminescence (ECL) approach for the enzymatic detection of biomarkers on paper substrate showed promising results toward improving the sensitivity.[27] Yet, despite its advantage of controlled reaction initiation, the ECL approach requires to apply a certain voltage to the paper device. The additional instrumental requirements may diverge from the overall POCT idea in their current state but may compete with paper-based CL in the future using smart device fabrication to avoid manual cable connections. Furthermore, the stability of the drop coated enzyme on the electrode is yet to be determined. A true improvement with our new CL probe regarding the sensitivity was obtained when changing from the detection of H_2O_2 to the luminophore itself with low picomole detection limits (**Figure S 6, Table S 4**). This is especially evident when considering the LOQ which is the diagnostically more relevant value.

3.3.4. Application to real samples

To evaluate the applicability and accuracy of the developed µPAD to real samples, we detected L-lactate in synthetic sweat. The synthetic sweat was prepared according to DIN 53160-2. It contains a defined amount of lactic acid and provides a representative sample matrix which is common in literature.[30,31] As lactic acid consists of d-lactate and L-lactate, the L-lactate level was first determined with a commercial colorimetric microtiter plate assay to be (4.5 ± 0.2) mmol L^{-1}.[23] With both luminophores, the determined concentration correlates very well with the value obtained by the commercial assay (**Table 1**). Considering the intensity values the coefficient of variation (CV) is still around 10 % (**Table S 5**). With error propagation this value rises to ≤ 18 %. We believe that this can be easily reduced by reducing the manual preparation steps, such as the pretreatment of the detection zone.

Table 1 Validation of developed chemiluminescence µPAD for L-lactate by determining L-lactate in synthetic sweat (DIN 53160-2)[30,31] with a commercial assay

Lactate assay kit	**Luminophore**	**L-lactate in synthetic sweat (DIN 53160-2)**
custom-made smartphone (within this study)	*m*-carboxy luminol	5.2 ± 0.9 (CV: 18 %)[a]
	luminol	3.5 ± 0.3 (CV: 10 %)[a]
custom-made CCD (within this study)	*m*-carboxy luminol	4.5 ± 0.5 (CV: 11 %)[a]
	luminol	3.23 ± 0.06 (CV: 2.0 %)[a]
commercial (Sigma Aldrich)	-	4.5 ± 0.2 (CV: 4.2 %)[b]

A Tukey test at the 0.05 significance level was performed and no significant difference of the mean of the commercial assay to the chemiluminescence µPADs with *m*-carboxy luminol was obtained. [a] mean ± SD (n = 4), [b] [23], mean ± SD (n = 3)

No significant difference for *m*-carboxy luminol was obtained between the L-lactate levels with the CCD camera or the smartphone camera towards the commercial assay, making both detectors valuable choices. Although only the CCD approach yields a significant statistical difference between the obtained L-lactate level towards the commercial approach, luminol tends to yield slightly underestimated results in the smartphone approach as well, pointing again towards *m*-carboxy luminol as superior probe. Finally, when diluting the synthetic sweat sample in synthetic sweat matrix, the CL response decreases linearly with an R^2 of 0.996 (**Figure S 7**) excluding matrix interference on the enzymatic and CL reaction. This is also shown in **Figure S 2** where L-lactate was measured in ultrapure water and synthetic sweat without any significant effect on the generated CL signal.

3.3.5. Stability of developed µPAD for L-lactate

In view of a costumer-orientated solution, the stability of the employed reagents is of high relevance and their activity needs to be maintained throughout long-time storage. Especially, enzymes pose a critical reagent as they are pH-sensitive and can be affected by varying environmental conditions such as temperature, humidity or exposure to proteases.[32] However, it was shown that µPADs with physisorbed enzymes can retain their activity for up to 10 weeks when stored in a sealed container at 4 °C.[33] Yet, these storage conditions are not always feasible. The stability of the µPAD developed herein was thus tested toward its robustness against elevated temperature, and enzyme batch-to-batch variation. The developed µPAD was weekly tested with a standardized 20 mmol L^{-1} L-lactate solution and enzyme functionality was maintained for three months when stored at room temperature dried on the µPAD and in solution at 4°C and applied before use without

significant activity loss and no batch-to-batch variation of the applied enzyme (**Figure S 8 B**). Together with the stable response from the dried luminophore on paper which was routinely tested with 1 mmol L^{-1} H_2O_2 (**Figure S 8 A**), a robust µPAD was developed which can be stored at room temperature for at least three months.

3.4. Conclusion

In this proof of principle study, we investigated different strategies for chemiluminescence µPADs to expand the current POCT portfolio. We propose that exchanging the dominant colorimetric, simple readout strategy, with an equally simple approach using chemiluminescence, will address exactly the challenge of limited sensitivity, that µPADs still endure. This enables µPADs to provide simple solutions to analytical challenges, such as the performance of multiplex reactions and the easy expansion of the assay layout into the 3D space. We demonstrated that with a stronger emitting luminol a ubiquitous detector *i.e.*, a normal smartphone camera, can maintain the simplicity of detection strategy while providing superior detection capabilities. Our developed µPAD system for L-lactate further could facilitate non-invasive and fast sample collection due to the inherent material characteristics of the paper-based device, simplifying and speeding up the overall process. Moreover, this enzymatic µPAD can be stored at room temperature for at least three months enabling simple in-field application. This concept can easily be expanded to other enzymatic reactions with H_2O_2 as side product and, together with the incubation barrier, sufficient conversion can be easily accomplished. Furthermore, in contrast to colorimetric µPADs, a wide dynamic range is covered without the alteration of the signal due to overoxidation and thus color change. In comparison to other CL POCT strategies, our approach convinces by its simple procedure already directed toward user-friendliness. In contrary to others, needing sophisticated detectors that are not fit for POCT to reach low limits of detection, here a simple smartphone camera reached similar sensitivity levels due to the strong CL emitter used. Finetuning of the measurement setup is still possible by developing a smartphone adapter integrating macro lenses to correct for the optics[34] which would increase light collection and guarantee the exclusion of ambient light but was not the main focus in this study. Additionally, a tailored software addressing user-friendly evaluation and compression of background signals is currently under evaluation to further simplify the process and the accompanied user-interventions. This would provide a low-cost µPAD system with excellent analytical performance ready for the POC.

3.5. References

[1] N. Jiang, N. D. Tansukawat, L. Gonzalez-Macia, H. C. Ates, C. Dincer, F. Güder, S. Tasoglu, A. K. Yetisen, *ACS Sens.* **2021**, *6*, 2108.

[2] M. Zangheri, L. Cevenini, L. Anfossi, C. Baggiani, P. Simoni, F. Di Nardo, A. Roda, *Biosens. Bioelectron.* **2015**, *64*, 63.

[3] L.J. Kricka, *Anal. Chim. Acta* **2003**, *500*, 279.

[4] W.R.G. Baeyens, S.G. Schulman, A.C. Calokerinos, Y. Zhao, A.M. García Campaña, K. Nakashima, D. de Keukeleire, *J. Pharm. Biomed. Anal.* **1998**, *17*, 941.

[5] A. W. Martinez, S. T. Phillips, G. M. Whitesides, E. Carrilho, *Anal. Chem.* **2010**, *82*, 3.

[6] M. M. Gong, D. Sinton, *Chem. Rev. (Washington, DC, U. S.)* **2017**, *117*, 8447.

[7] a) S. Shrivastava, T. Q. Trung, N.-E. Lee, *Chem. Soc. Rev.* **2020**, *49*, 1812; b) A. M. López-Marzo, A. Merkoçi, *Lab Chip* **2016**, *16*, 3150.

[8] C. Carrell, A. Kava, M. Nguyen, R. Menger, Z. Munshi, Z. Call, M. Nussbaum, C. Henry, *Microelectron. Eng.* **2019**, *206*, 45.

[9] a) L.-M. Fu, Y.-N. Wang, *TrAC, Trends Anal. Chem.* **2018**, *107*, 196; b) A. Nilghaz, L. Guan, W. Tan, W. Shen, *ACS Sens.* **2016**, *1*, 1382.

[10] W. Zheng, K. Wang, H. Xu, C. Zheng, B. Cao, Q. Qin, Q. Jin, D. Cui, *Anal. Bioanal. Chem.* **2021**, *413*, 2429.

[11] B. R. Sun, A. G. Zhou, X. Li, H.-Z. Yu, *ACS Sens.* **2021**, *6*, 1731.

[12] H. Jang, J.-H. Park, J. Oh, K. Kim, M.-G. Kim, *ACS Sens.* **2019**, *4*, 1103.

[13] G. G. Morbioli, T. Mazzu-Nascimento, A. M. Stockton, E. Carrilho, *Anal. Chim. Acta* **2017**, *970*, 1.

[14] P. Wang, L. J. Kricka, *Clin. Chem. (Washington, DC, U. S.)* **2018**, *64*, 1439.

[15] A. Roda, M. Mirasoli, E. Michelini, M. Di Fusco, M. Zangheri, L. Cevenini, B. Roda, P. Simoni, *Biosens. Bioelectron.* **2016**, *76*, 164.

[16] L. Ge, S. Wang, X. Song, S. Ge, J. Yu, *Lab Chip* **2012**, *12*, 3150.

[17] a) S. Imani, A. J. Bandodkar, A. M. V. Mohan, R. Kumar, S. Yu, J. Wang, P. P. Mercier, *Nat. Commun.* **2016**, *7*, 11650; b) C.-C. Tseng, C.-T. Kung, R.-F. Chen, M.-H. Tsai, H.-R. Chao, Y.-N. Wang, L.-M. Fu, *Sens. Actuators, B* **2021**, *342*, 130078.

[18] K. van Hoovels, X. Xuan, M. Cuartero, M. Gijssel, M. Swarén, G. A. Crespo, *ACS Sens.* **2021**, *6*, 3496.

[19] L. Rassaei, W. Olthuis, S. Tsujimura, E. J. R. Sudhölter, A. van den Berg, *Anal. Bioanal. Chem.* **2014**, *406*, 123.

[20] P. J. Derbyshire, H. Barr, F. Davis, S. P. J. Higson, *J. Physiol. Sci.* **2012**, *62*, 429.

[21] M. Mayer, S. Takegami, M. Neumeier, S. Rink, A. Jacobi von Wangelin, S. Schulte, M. Vollmer, A. G. Griesbeck, A. Duerkop, A. J. Baeumner, *Angew. Chem., Int. Ed.* **2018**, *57*, 408.

[22] J. Schindelin, I. Arganda-Carreras, E. Frise, V. Kaynig, M. Longair, T. Pietzsch, S. Preibisch, C. Rueden, S. Saalfeld, B. Schmid et al., *Nat. Methods* **2012**, *9*, 676.

[23] S. Rink, A. Duerkop, A. Jacobi von Wangelin, M. Seidel, A. J. Baeumner, *Anal. Chim. Acta* **2021**, *1188*, 339161.

[24] C. Marquette, *Biosens. Bioelectron.* **2003**, *19*, 433.

[25] R. M. Pino, J. Singh, *Anesthesiology* **2021**, *134*, 637.

[26] F. Li, J. Liu, L. Guo, J. Wang, K. Zhang, J. He, H. Cui, *Biosens. Bioelectron.* **2019**, *141*, 111472.

[27] a) M. L. Bhaiyya, S. Gangrade, P. K. Pattnaik, S. Goel, *IEEE Trans. Instrum. Meas.* **2022**, *71*, 1; b) D. Wang, C. Liu, Y. Liang, Y. Su, Q. Shang, C. Zhang, *J. Electrochem. Soc.* **2018**, *165*, B361-B369.

[28] A. Roda, M. Guardigli, D. Calabria, M. M. Calabretta, L. Cevenini, E. Michelini, *Analyst (Cambridge, U. K.)* **2014**, *139*, 6494.

[29] F. Li, X. Wang, J. Liu, Y. Hu, J. He, *Sens. Actuators, B* **2019**, *288*, 266.

[30] A. L. Suherman, M. Lin, B. Rasche, R. G. Compton, *ACS Sens.* **2020**, *5*, 519.

[31] H. S. Toh, C. Batchelor-McAuley, K. Tschulik, R. G. Compton, *The Analyst* **2013**, *138*, 4292.

[32] J. Hu, S. Wang, L. Wang, F. Li, B. Pingguan-Murphy, T. J. Lu, F. Xu, *Biosens. Bioelectron.* **2014**, *54*, 585.

[33] J. Yu, S. Wang, L. Ge, S. Ge, *Biosens. Bioelectron.* **2011**, *26*, 3284.

[34] S. Kanchi, M. I. Sabela, P. S. Mdluli, Inamuddin, K. Bisetty, *Biosens. Bioelectron.* **2018**, *102*, 136.

3.6. Supporting Information

3.6.1. Reproducibility of developed µPAD

Initially, the developed µPAD design was tested with regard to its analytical performance using cobalt, hemin and horseradish peroxide (HRP) as catalyst on a single paper substrate (**Figure S 1 A**) and on three different paper substrates (**Figure S 1 B**) to evaluate its reproducibility. The residual standard deviations (RSD) are mainly < 10 % for the intra-intensity comparison as well as for the inter-intensity comparison illustrating a good reproducibility of the paper substrates. Only *m*-carboxy luminol with cobalt shows an RSD of 11 % for the intra- and 18 % for the inter-intensity comparison which might be a consequence of the different shape of the accumulated chemiluminescence signal (**Figure S 1 C**). Whereas for hemin and horseradish peroxidase the signal is distributed across the entire detection zone, for cobalt the signal is concentrated in the center as bar-like signal. Being not the primary focus of this study, this was not further investigated.

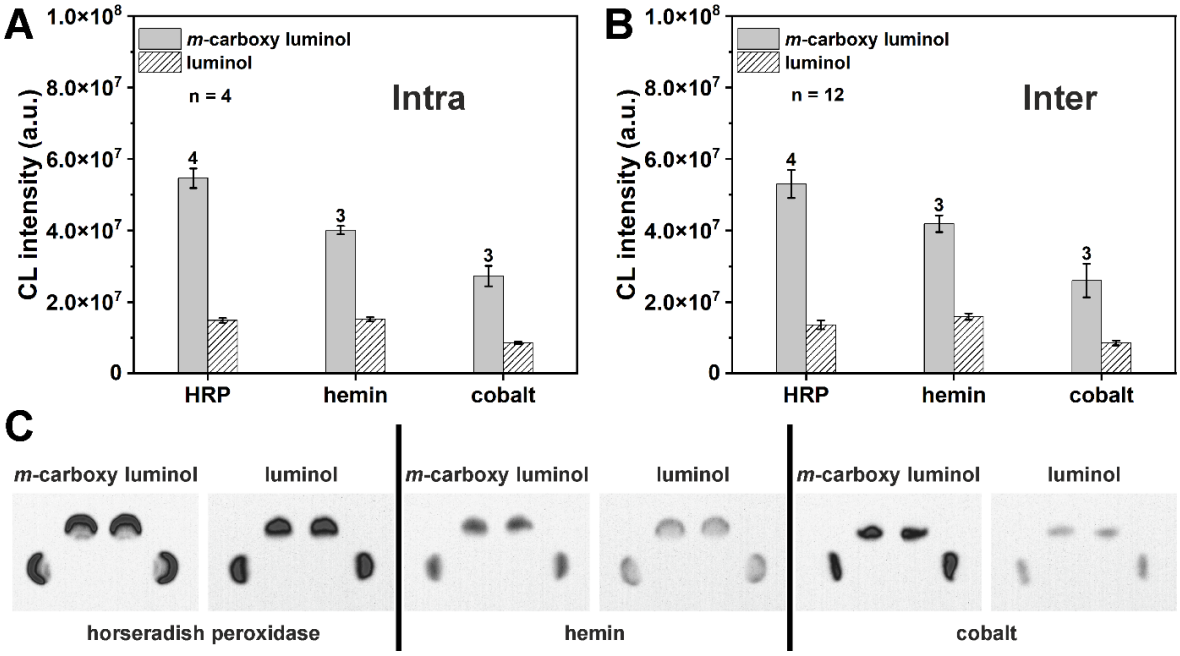

Figure S 1 Performance of different catalysts on paper with *m*-carboxy luminol (grey) and luminol (dashed) with (A) an intra-intensity comparison limiting the measurement on a single paper substrate (mean ± SD, n = 4) and (B) an inter-intensity comparison including measurements on three paper substrates (mean ± SD, n = 12), (C) illustrates the flow profile of the obtained CL signal on a single paper substrate with the different catalysts, the paper substrates were prepared with 1 nmol luminophore and 1 nmol cobalt (Co(II)) or hemin or 0.3 U horseradish peroxidase *(*HRP*)* immobilized on the detection zone, 30 µL of 1 mmol L^{-1} H_2O_2 solution diluted in 0.1 mol L^{-1} carbonate buffer (pH 10.5) for Co(II) and hemin or 0.1 mol L^{-1} Tris-HCl buffer (pH 8.5) for HRP was applied to the sample zone, 15 images with 2 s exposure time were recorded and the intensity values of image 15 were plotted, the measurements were conducted at 22 °C, label of the bars indicate enhancement factor obtained by *m*-carboxy luminol over luminol, recorded with CCD camera

3.6.2. Hydrogen peroxide detection on original µPAD

Challenging the developed µPAD systems with varying hydrogen peroxide concentrations revealed equal performance of hemin and horseradish peroxidase as catalyst, whereas cobalt already exhibits a non-linear relationship within the tested concentration range. The determined key parameters are summarized in **Table S 1**. It is known that enzymes typically increase the complexity and thus also the costs of the final µPAD due to higher sensitivity towards reaction conditions such as pH changes, the need of an additional enhancer molecule and the more expensive enzyme itself.[1] Considering the calculated key parameters (**Table S 1**) with the experimental proof (**Figure 3**, images, main article), we decided to use the hemin catalyzed system due to its similar performance to HRP and could thus avoid a second enzyme in the overall reaction scheme.

Table S 1 Figures of merit obtained for hydrogen peroxide detection using cobalt, hemin and horseradish peroxidase

Catalyst	Luminophore	LOD[a] (µmol L^{-1})	LOQ[b] (µmol L^{-1})	S/N[g] @ 2 mmol L^{-1}	Slope × 10^4 (L µmol^{-1})	R^2 [h]	EF[i]	SE[j]
Co(II)	*m*-carboxy luminol	104[c]	200[d]	27	-	0.978	0.9	-
	luminol	98[c]	230[d]	7.1	-	0.998		
Hemin	*m*-carboxy luminol	13[e]	45[f]	20	4.5 ± 0.3	0.978	2.3	3.0
	luminol	31[e]	104[f]	8.4	1.5 ± 0.1	0.954		
HRP	*m*-carboxy luminol	79[e]	264[f]	28	4.8 ± 0.2	0.984	0.7	2.6
	luminol	59[e]	198[f]	8.3	1.82 ± 0.06	0.994		

[a] limit of detection, [b] limit of quantification, [c] $y_{LOQ} = A1 + 10 \times \sigma_{blank}$, [d] $y_{LOD} = A1 + 3 \times \sigma_{blank}$, [e] $x_{LOD} = 3 \times \sigma_{blank}/slope$, [f] $x_{LOQ} = 10 \times \sigma_{blank}/slope$, [g] S/N: signal-to-noise ratio, [h] R^2: correlation coefficient, [i] EF: enhancement factor of *m*-carboxy luminol over luminol ($LOD_{luminol}/LOD_{m\text{-carboxy luminol}}$), [j] SE: sensitivity enhancement obtained through $slope_{m\text{-carboxy luminol}}/slope_{luminol}$

3.6.3. Advanced µPAD design enables enzymatic reaction and detection optimization

The adjusted enzymatic µPAD was tested with regard to the conversion efficiency of L-lactate into hydrogen peroxide and the susceptibility toward synthetic sweat as matrix. No full conversion was observed (**Figure S 2**) as the L-lactate signal is only 45 % ± 8 % for *m*-carboxy luminol and 55 % ± 9 % for luminol. The decrease of the CL signal in synthetic sweat over the measurement in water, however, lies within the error of the measurement. Thus, a negative effect of the synthetic matrix was not obtained.

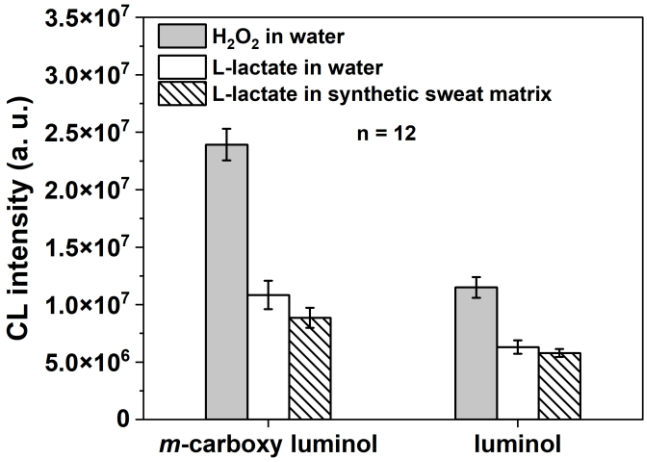

Figure S 2 Conversion efficiency of L-lactate into hydrogen peroxide through lactate oxidase and matrix effect of synthetic sweat on CL signal, mean ± SD (n = 12), three individual paper devices were used, recorded with CCD camera

Prior to using the refined µPAD for the detection of L-lactate the reaction conditions were adjusted. Here, the incubation time of L-lactate with lactate oxidase (LOx) was tested (**Figure S 3 A**) and the effect of the immobilization of 4 µL of high (5 U μL^{-1}) and low (0.1 U μL^{-1}) concentrations of LOx solution was examined (**Figure S 3 B**)**.** We found that the applied amount of LOx has a critical role towards the enzyme stability on paper. With lower LOx concentration, the stability of the enzyme is affected, and the CL response rapidly decreased to less than 30 % of the original response within the first 4 h, whereas the CL signal intensity for the higher concentration of LOx remained stable, even when dried overnight (**Figure S 3 B**). Linked to this, testing different substrate incubation times showed, not surprisingly, a signal decrease with increasing incubation from 5 to 30 min (**Figure S 3 A**). This is most likely attributed to the rather instable nature of the generated H_2O_2, and the accompanied evaporation of the sample at room temperature with increasing incubation time. This likely promotes decomposition of H_2O_2 on paper which consequently leads to a decreasing signal response. Hence, L-lactate was incubated for 10 min with LOx prior to detection as compromise between convenient handling and maximum signal generation.

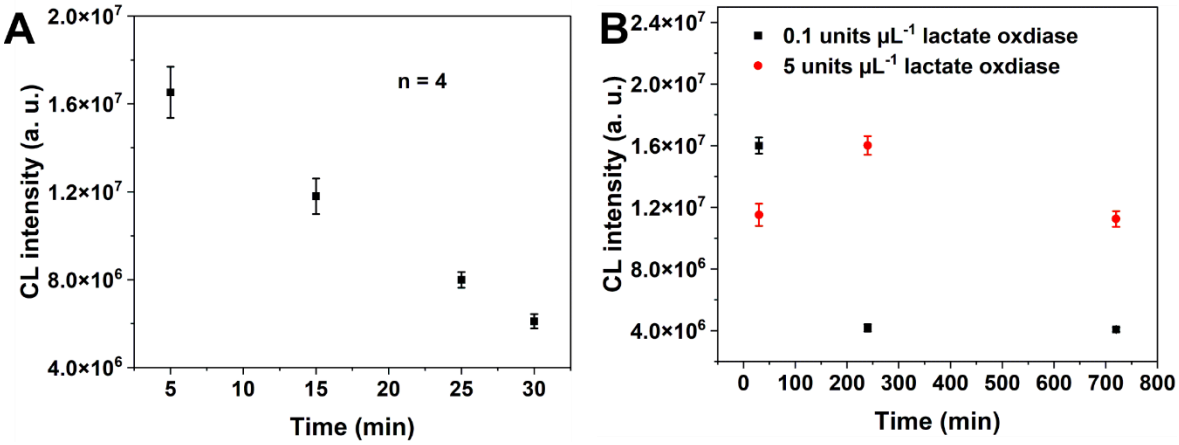

Figure S 3 Adjustment of reaction conditions for enzymatic L-lactate detection with (A) testing different incubation times of L-lactate with lactate oxidase on the µPAD and (B) testing different lactate oxidase concentration dried on paper, mean ± SD (n = 4), 15 images, 2 s exposure, recorded with CCD camera

In a second line of research, we tested ideal recording conditions to maximize signal collection. When the chemiluminescence reaction is started, the signal instantaneously starts to decrease after an initial spike. However, owing to the design and capillary flow on the paper, the intensity profile is not a simple exponential decay of the initiated CL but is rather depicted as peak function across the detection zone with a defined maximum. In order to minimize the errors due to time shifts introduced by the manual procedure and the inhomogeneous structure of the paper itself, multiple images were taken over a specific time span. The individual images of one series were subsequently merged before analysis to combine the single responses. Depending on the recording interval (restricted by the camera settings), an image series of nine images (CCD camera, each 30 s with 2 s exposure) or five images (smartphone camera, each 60 s with 30 s exposure) collects the majority of the CL signal **(Figure S 4**). While this process is simple and efficient, its major drawback is the accompanied amplification also of the camera background noise.

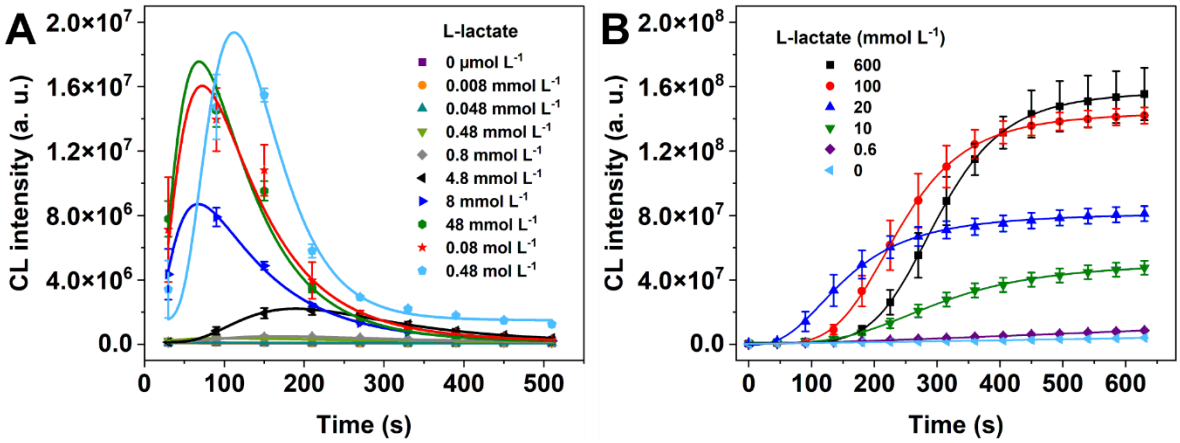

Figure S 4 Exemplary time courses of recorded CL signal in (A) with the smartphone Samsung S21 5G, individual image series with post-stacking, mean ± SD (n = 4), 9 images, 30 s exposure time, ISO 800 and (B) with the CCD camera and simultaneous software guided signal accumulation, mean ± SD (n = 4), 15 images, 2 s exposure time

3.6.4. Benchmarking analytical performance of advanced µPAD towards L-lactate with a standard smartphone camera against a scientific CCD camera

Using the smartphone camera, images with a size of 4032 × 3024 pixels were taken, whereas with the CCD camera the image size was 1392 × 1040 pixel. Thus, the used evaluation area is 44068 square pixels for the smartphone camera versus 10405 square pixels for the CCD camera to cover the entire detection zone. Both cameras operate with 16-bit color depth. Due to software limitations, different exposure times were used. With increased exposure times, the signal intensity should in theory increase, provided that the same camera is used. However, despite the increased exposure time (30 s for the smartphone camera *versus* 2 s for the CCD camera), the increased evaluation area and the reduced focal distance, the smartphone camera still yields less intense images (**Figure S 5 D**) emphasizing the need of stronger emitting probes especially for non-scientific cameras and for in-field conditions.

The developed enzymatic µPAD was initially tested with a scientific CCD camera as detector and the procedure shown in **Figure S 5 A**. Similarly, to the pretests, the stronger CL signal was obtained with *m*-carboxy luminol over luminol (**Figure S 5 B**) which yielded in a lower limit of detection of 0.09 mmol L^{-1} L-lactate (**Figure S 5 C**). However, when changing from the CCD camera to the smartphone camera a slight improvement of the LOD (**Table S 2**) was possible although the overall signal was lower compared to the CCD camera (**Figure S 5 D**). We believe that the increased background noise of the CCD camera is most likely causing this effect.

Table S 2 Fitting parameters obtained for L-lactate determination with the CCD camera and the smartphone camera

Detector	Luminophore	LOD[a] (mmol L^{-1})	S/N[b]	A_1[c] × 10^5	A_2[d] × 10^7	x_0[e]	p[f]	R^2 [g]
CCD camera	*m*-carboxy luminol	0.09	38	43	17	22	1.05	0.983
	luminol	0.3	5.3	43	2.27	5.3	1.2	0.977
Smartphone	*m*-carboxy luminol	0.03	67	7.3	4.9	14	1.06	0.985
	luminol	0.02	16	5.78	0.9	7	1.08	0.960

[a] limit of detection (y_{LOD} = A1 + 3 × σ_{blank}), [b] S/N: signal-to-noise ratio (A_2/A_1), [c] lower asymptote, [d] upper asymptote, [e] center, [f] power, [g] R^2: correlation coefficient, four-parameter logistic fitting was done according to $y = ((A_1-A_2)/ (1+ (x/x_0)^p)) + A_2$

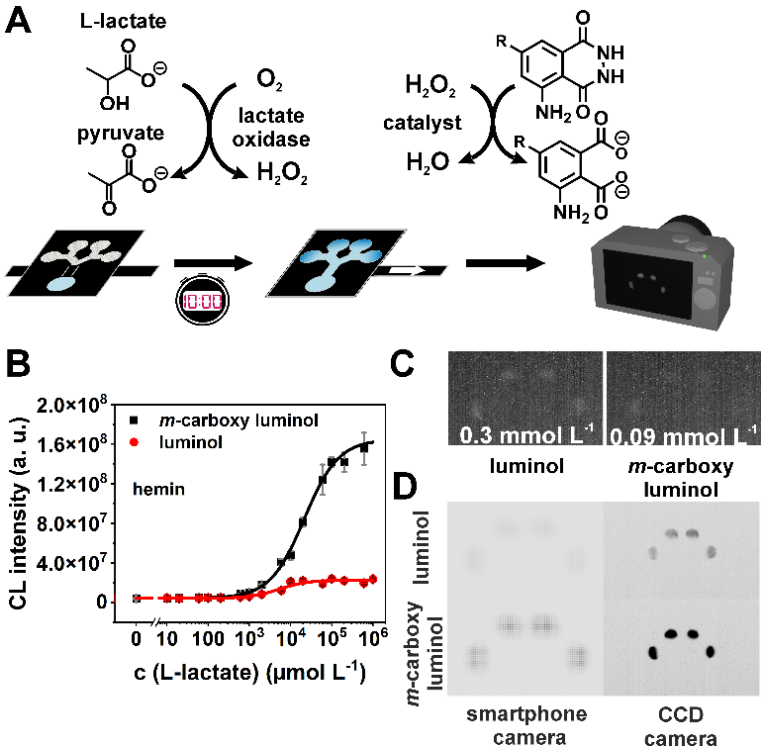

Figure S 5 L-lactate determination with CCD camera (A) illustration of workflow (B) detection of L-lactate in synthetic sweat matrix, using µPADs with 20 U lactate oxidase (LOx) dried on the sample zone and 1 nmol hemin and luminophore dried on the detection zone, 30 µL of L-lactate in synthetic sweat was applied and incubated 10 min with LOx prior to detection. An image series of 15 images in stacking mode was recorded with 2 s exposure time and subsequently evaluated with ImageJ, mean ± SD (n = 4), (C) proof of calculated LODs, (D) comparison of camera performance of smartphone and CCD camera with both luminophores for the measurement of the synthetic sweat sample (brightness and contrast were adjusted uniformly for each image set

3.6.5. Flexibility of µPAD design by changing assay strategy

Although the detection of hydrogen peroxide is of great interest in point-of-care diagnostics, chemiluminescent labeling of biomolecules could give access to typical bioassays on

µPADs with sensitivities approaching those of laboratory test systems. Thus, as universal approach we studied the detection of the luminophore on a µPAD and were able to detect down to picomole levels of luminophore (**Figure S 6**). With *m*-carboxy luminol, we lowered the limits of detection by a factor of up to two over standard luminol but more importantly we achieved exceptional signal-to-noise ratios of over 60 with our *m*-carboxy luminol versus 16 at most for standard luminol (**Table S 3**).

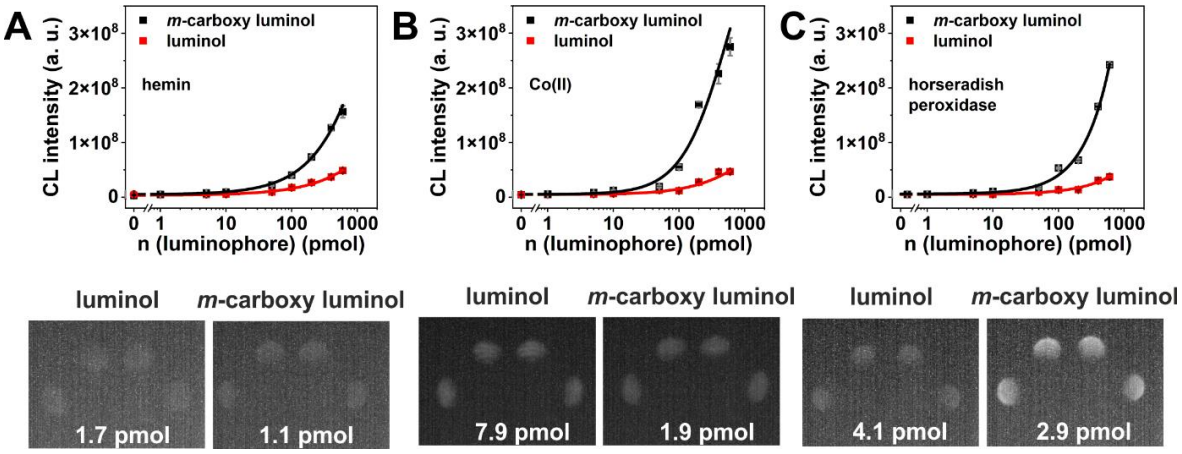

Figure S 6 Calibration curve for luminophore detection with (A) Co(II), (B) hemin and (C) horseradish peroxidase (HRP) including validation of LOD with paper substrate for *m*-carboxy luminol (black) and luminol (red) with 1 nmol Co(II) or hemin and 0.3 U HRP with 1 nmol *p*-coumaric acid were dried with 1 µL luminophore in the detection zone, 30 µL 10 mmol L^{-1} H_2O_2 in 0.1 mol L^{-1} carbonate buffer (pH10.5) were applied to sample zone, D, four-parameter logistic fitting was performed by Origin2020 with R^2 = 0.857 (black) and R^2 = 0.940 (red) for Co(II), R^2 = 0.991 (black) and R^2 = 0.952 (red) for hemin and R^2 = 0.991 (black) and R^2 = 0.971 (red) for HRP, n = 4, 15 images, 2 s exposure, recorded with CCD camera

Table S 3 Figures of merit obtained for luminophore detection with cobalt, hemin and horseradish peroxidase

Catalyst	Luminophore	LOD[a] (pmol)	LOQ[b] (pmol)	S/N [c] @ 600 pmol	R^2 [d]	EF [e]
Co^{2+}	*m*-carboxy luminol	2.6	6.8	62	0.857	2.2
	luminol	5.6	20	10	0.940	
Hemin	*m*-carboxy luminol	1.2	4.5	31	0.991	0.9
	luminol	1.1	5.6	16	0.952	
HRP	*m*-carboxy luminol	3.3	9.8	44	0.991	1.9
	luminol	6.2	24	7.8	0.971	

[a] limit of detection (y_{LOD} = A1 + 3 × σ_{blank}), [b] limit of quantification (y_{LOQ} = A1 + 10 × σ_{blank}), [c] S/N: signal-to-noise ratio, [d] R^2: correlation coefficient, [e] EF: enhancement factor of *m*-carboxy luminol over luminol ($LOD_{luminol}/LOD_{m\text{-carboxy luminol}}$)

3.6.6. Application to real samples

Another potential matrix effect was tested by dilution of the synthetic sweat sample in synthetic sweat matrix. Here, a linear decrease of the response was obtained with $R^2 = 0.996$ (**Figure S 7**) excluding reaction inhibition by the applied matrix.

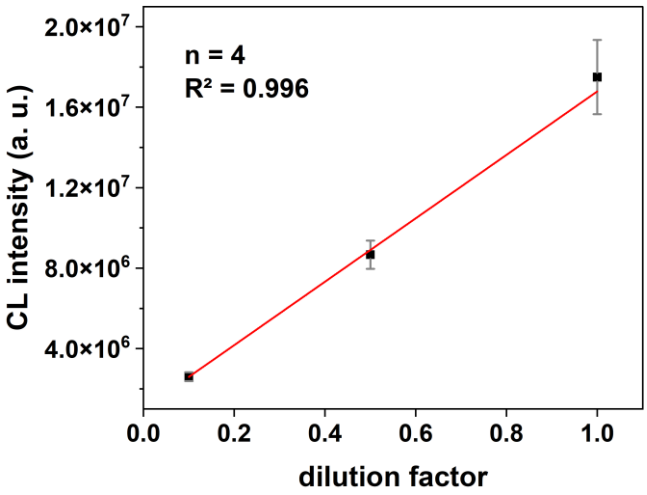

Figure S 7 Matrix effect on CL signal and enzymatic reaction of synthetic sweat sample with *m*-carboxy luminol µPAD, mean ± SD (n = 4)

3.6.7. Stability of developed µPAD for L-lactate

To determine the stability of the developed assay system the prepared µPADs were tested regularly for three months with focus on the luminophore stability (**Figure S 8 A**) and enzyme stability (**Figure S 8 B**). We tested the enzyme stability at different temperatures and evaluated the batch-to-batch variation of the enzyme by using two different enzyme batches. Furthermore, we tested the function of the enzyme when stored solubilized and stored in the fridge with application on the µPAD direct before the measurement in comparison to the on paper dried and stored enzyme (**Figure S 8 B**).

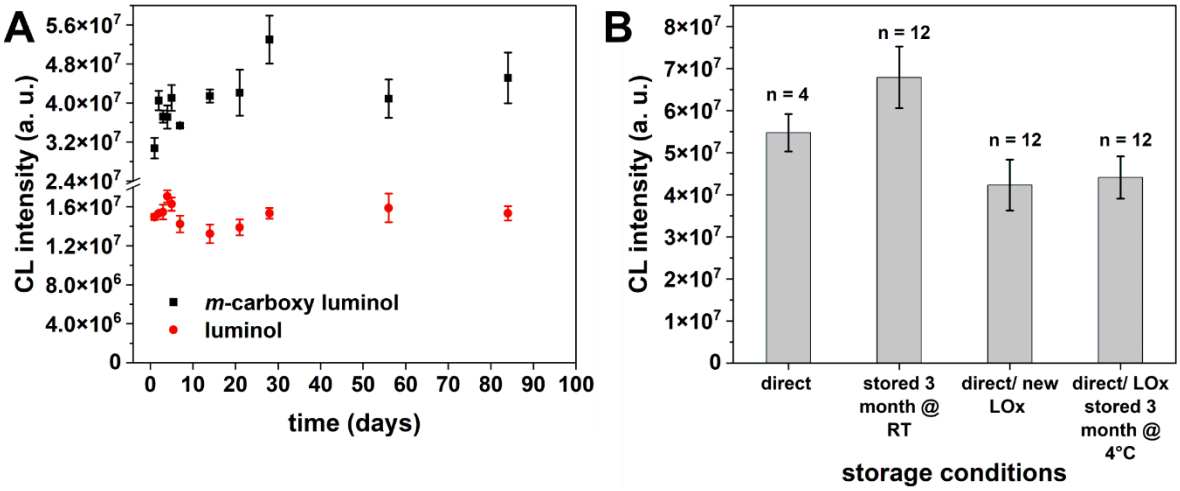

Figure S 8 Stability determination of assay and reagents on paper devices. (A) illustrates the stability of the immobilized luminophore determined with 10 mmol L^{-1} hydrogen peroxide in ultrapure water (mean ± SD, n = 4) and (B) illustrates the stability of immobilized lactate oxidase on the paper device determined with 20 mmol L^{-1} L-lactate in ultrapure water either directly dried on paper before the measurement or when stored in dried form on the paper device, 15 images, 2 s exposure, recorded with CCD camera

Here, no significant difference between the various storage conditions were obtained. This shows that the enzyme is fully functional after three months storage even at room temperature.

3.6.8. Refenences

[1] S. Mross, S. Pierrat, T. Zimmermann, M. Kraft, *Biosens. Bioelectron.* **2015**, *70*, 376.

4. Liposomes as alternate detection particles for paper-based point-of-care testing

4.1. Highly Sensitive Interleukin 6 Detection by Employing Commercially Ready Liposomes in an LFA Format

Graphical Abstract

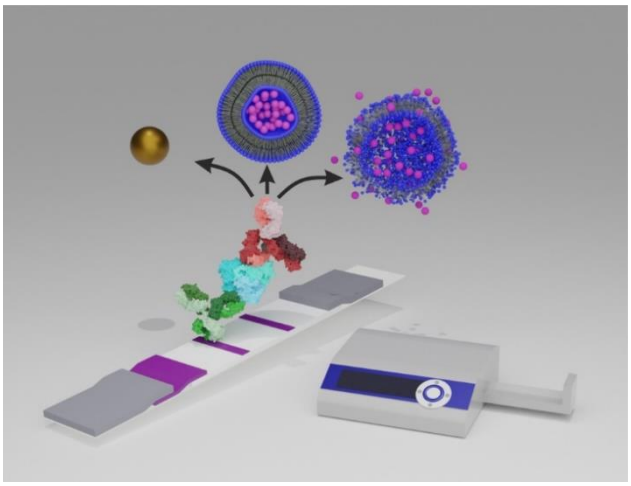

This chapter has been published in the Springer Nature Journal Analytical and Bioanalytical Chemistry.

Authors' contributions

Antje J. Baeumner: Conceptualization, supervision, project administration, experimental design, writing: original draft – lead contribution

Axel Duerkop: Conceptualization, supervision, project administration, experimental design, writing: original draft – supporting contribution.

Barbara Kaiser: Conceptualization, visualization, investigation, formal analysis, data curation, writing: original draft– lead contribution

Simone Rink: Conceptualization, visualization, investigation, formal analysis, data curation, writing: original draft– lead contribution

Mark-Steven Steiner: Conceptualization, supervision, project administration, experimental design, writing: original draft – lead contribution

Abstract

Recent years have confirmed the ubiquitous applicability of lateral flow assays (LFA) in point-of-care testing (POCT). To make this technology available for low abundance analytes, strategies towards lower limits of detections (LOD) while maintaining the LFA's ease-of-use, are still being sought. Here, we demonstrate how liposomes can significantly improve the LOD of traditional gold nanoparticle (AuNP)-based assays while fully supporting a ready-to-use system for commercial application. We fine-tuned liposomes towards photometric and fluorescence performance on the synthesis level and applied them in an established interleukin 6 (IL-6) immunoassay normally using commercial AuNP labels. IL-6's low abundance (<10 pg mL^{-1}) and increasing relevance as prognostic marker for infections make it an ideal model analyte. It was found that liposomes with a high encapsulant load (150 mmol L^{-1} sulforhodamine B (SRB)) easily outperform AuNPs in photometric LFAs. Specifically, liposomes with 350 nm in diameter yield a lower LOD even in complex matrices such as human serum below the clinically relevant range (7 pg mL^{-1}) beating AuNP by over an order of magnitude (81 pg mL^{-1}). When dehydrated on the strip, liposomes maintained their signal performance for over a year even when stored at ambient temperature and indicate extraordinary stability of up to 8 years when stored as liquid. Whereas no LOD improvement was obtained by exploiting the liposomes fluorescence an extraordinary gain in signal intensity was achieved upon lysis which is a promising feature for high resolution and low-cost detection devices. Minimizing the procedural steps by inherently fluorescent liposomes, however, is not feasible. Finally, liposomes are ready for commercial applications as they are easy to mass-produce and can simply be substituted for the ubiquitously used AuNPs in the POCT market.

Keywords

lateral flow assay, point-of-care diagnostics, bioanalysis, fluorescence liposomes, colloidal gold, interleukin 6

4.1.1. Introduction

Not only the global pandemic in 2020 emphasized the need and relevance of simple, fast, sensitive and one-site point-of-care (POC) solution in the medical diagnostic field, but also a market size of USD 29 billion in 2020 (which is estimated to rise to USD 67 billion in 2026, www.reportsanddata.com) [1] depicts its global interest. In this fast-growing market, lateral flow assays (LFA) belong to the major gameplayers, as they are typically very fast, offer low costs and straight forward operation even by non-experts.[2] Aside from the numerous benefits of LFAs, such as amenability to inexpensive mass production, autonomy of

additional external equipment and optical readout, in its simplest form with the human eye, standard LFA platforms still have to face limitations with regard to sensitivity due to their mostly semi-quantitative nature and often provide users only with yes/no answers. A lateral flow assay is typically conducted in either a competitive or sandwich assay format.[3] Here, the test strip consists of a test line typically utilizing a biomolecule directed against the analyte as capture probe and a control line which is directed against the reporter particle. The sample is added to the sample pad and resolubilizes the reporter particles such as gold nanoparticles (AuNP) or colored latex beads from the subsequent conjugate pad along its capillary force driven flow throughout the test strip.[4] Depending on the applied format the analyte-reporter complex binds to the test line yielding an increasing signal with increasing analyte concentration in a sandwich assay format. The test strip consists of various porous materials with each having its unique feature, *i.e.,* assisting in sample transport, containment, and homogenous release of reagents, ensuring homogenous fluid flow, and capturing relevant biomolecules through capture probes via precise test-line manufacturing. This general design of the LFA allows vast room for sensitivity enhancement at several stages of the LFA development. Bishop and colleagues[4] critically assessed the adjusting screws which have recently been studied to push the development and potential of lateral flow assays towards sensitivity levels similar to those of laboratory-based test systems. Especially, the applied reagents and envisioned reactions and their realization on an LFA were thoroughly discussed. Key factors for enhancing the sensitivity of an LFA by several orders of magnitude is the development of high affinity reagents, tweak of transport dynamics for ideal reaction kinetics as well as label and detection optimization of conventional reporter particles or even integration of signal amplification strategies.[4] Ultimately, investigating a combination of these individual strategies is of special interest. In this study we focused on the reporter particles and signal amplification strategies by exchanging conventional AuNP with fluorescent dye-loaded liposomes. Liposomes are mainly known as delivery vehicles in medicine and pharmacology but paved their way into analytical and bioanalytical application as detection particles due to their comparably high surface area, a large internal volume and flexible surface modification with various biorecognition elements.[5,6] IL-6 is an important biomarker for immune response and inflammatory processes in the human body. It belongs to the class of pro-inflammatory cytokines currently under evaluation *inter alia* as potential biomarker to identify COVID-19 positive patients who are at risk of respiratory failure and death due to severe inflammatory response.[7] Its growing diagnostic relevance as prognostic marker for infections, especially due to COVID-19, and its presence in low pg mL^{-1} concentrations in serum.[8] (in healthy subjects <10 pg mL^{-1}) makes it an ideal candidate for this study. We herein study

sulforhodamine B (SRB) loaded liposomes with different sizes in a sandwich-based LFA for the detection of interleukin 6 (IL-6) in direct comparison to conventional AuNP. These liposomes were synthesized entrapping SRB, a highly water-soluble fluorescent dye allowing encapsulation of *e.g.,* up to 1.2 million molecules of a 150 mmol L^{-1} dye solution in a single 300 nm liposome[6] enabling visual and fluorescence readout possibilities when applied to an LFA.[9] The accompanied signal amplification and their double readout feature rise interest in these liposomes for ultrasensitive detection in lateral flow assays. Although these particles have been applied to lateral flow assays previously[9,10], these publications only exploit the colorimetric readout possibility of liposomes focusing on the academic point of view, as the fluorescence of SRB is quenched in intact liposomes. The flexible nature of liposomes with regard to encapsulated dye, size, and surface modification give additional advantages over standard AuNP such as *e.g.,* multiplexing. We herein demonstrate the evolution of these liposomes to commercially ready detection particles and the gain in sensitivity by applying liposomes with optimized size in direct comparison to a commercial standard AuNP approach and designed for colorimetric and fluorescence readout. Sensitivity improvement by one order of magnitude was already obtained for the colorimetric readout with 350 nm sized liposomes whereas fluorescence measurement can significantly enhance the resolution due to an extraordinary gain in signal intensity. In addition, we show that our protein-modified liposomes remain highly stable for long-term storage in solution and also when dehydrated on the conjugate pad for a ready-to-use LFA. This renders the here demonstrated IL-6 liposome-based LFAs as model system for any AuNP-based LFA that requires significantly lower LODs to become relevant as POCTs.

4.1.2. Experimental Section

4.1.2.1. Chemicals and consumables

All chemicals were commercial analytical reagent grade and were used without purification. Phospholipids, 1,2-dipalmitoyl-sn-glycero-3-phosphocholine (DPPC), 1,2-dipalmitoyl-sn-glycero-3-phospho-(1′-rac-glycerol) (sodium salt) (DPPG), and 1,2-dipalmitoyl-sn-glycero-3-phosphoethanolamine-N-(glutaryl) (sodium salt) (N-glutaryl-DPPE), 1,2-dipalmitoyl-sn-glycero-3-phosphoethanolamine-N-(biotinyl) (sodium salt) (biotinyl-DPPE) were purchased from Avanti Polar Lipids (Alabaster, AL, USA), 4-(2-Hydroxyethyl)piperazine-1-ethanesulfonic acid (HEPES), purity >99.5 %, was purchased from VWR chemicals (Germany). Sulforhodamine B (SRB) (230162, 75 %), N-hydroxysuccinimide (NHS) were purchased from Sigma Aldrich/Merck (Germany). Fetal Bovine Serum (FBS) (10270-106) was purchased from ThermoFisher Scientific (Germany) and human serum (HS) was provided by Microcoat Biotechnology GmbH (Bernried, Germany). 2-(N-

morpholino)ethanesulfonic acid (MES) and bovine serum albumin (BSA) (T844.2) was obtained from Carl Roth (Karlsruhe, Germany). Custom made lateral flow test strips as well as anti-digoxigenin and anti-IL-6 conjugates were kindly provided by Microcoat Biotechnology GmbH (Bernried, Germany) as well as recombinant human IL-6 (200-06, Peprotech, Germany), sheep anti-digoxigenin Fab (11214667001 (Roche), Sigma Aldrich, Germany). LFA running buffer (Art. No. 850003) and LFA 5 X serum buffer (ESS-2913). For all experiments ultrapure water was used. A more detailed list of standard chemicals and consumable is given in the SI.

4.1.2.2. Synthesis of sulforhodamine B liposomes

Liposomes, containing sulforhodamine B, with 6 mol% carboxy functionalization were prepared according to an established protocol from Edwards *et al.* with slight adjustments.[11] Shortly, encapsulant was prepared by dissolving sulforhodamine B (150 mmol L^{-1}) in 4.5 mL 0.02 mmol L^{-1} HEPES buffer, pH 7.5. DPPC (29.58 mg, 40.3 µmol), DPPG (15.64 mg, 21.0 µmol), cholesterol (19.99 mg, 51.7 µmol) and N-glutaryl-DPPE (6.2 mg, 7.0 µmol) were dissolved in 3 mL chloroform and 0.5 mL methanol and thoroughly sonicated in an ultrasonic bath (VWR ultrasonic cleaner, model USC 300 THD) at 60 °C. Subsequently, 2 mL of preheated (60 °C) encapsulant was added to the lipid solution and emulsified for 4 min at 60 °C, using an ultrasonic bath. After emulsification, residual solvent was evaporated at 60 °C under reduced pressure. The remaining 2 mL of encapsulant were added after gradual evaporation to 780 mbar and thoroughly vortexed before evaporation was continued to 400 mbar. The remaining solution was extruded at 60 °C successively through 1.0 µm, 0.4 µm and 0.2 µm membrane using a mini extruder (Avanti Polar Lipids, Inc.) to obtain unilamellar liposomes. Purification was first performed by size-exclusion chromatography with Sephadex® G-50 as stationary phase (column size: 2 cm x 8 cm) and HSS buffer (10 mmol L^{-1} HEPES, 200 mmol L^{-1} sodium chloride, 200 mmol L^{-1} sucrose, 0.01 wt% sodium azide), pH 7.5, osmolality 0.643 osmol kg^{-1} as mobile phase. Additionally, the liposomes were dialyzed against HSS buffer until the dialysis buffer remains colorless, pH 7.5, osmolality 0.643 osmol kg^{-1} before determination of the hydrodynamic diameter via DLS, phospholipid concentration via ICP-OES and zeta-potential was done.

4.1.2.3. Dynamic light scattering (DLS) and ζ-potential measurements

These measurements were done on a Malvern Zetasizer Nano-ZS (Malvern Panalytical, Germany). For all measurements, the temperature was set to 25 °C. Size determination was done in semi-micro polymethyl methacrylate (PMMA) cuvettes (Brand, Germany), and

ζ-potential was done in disposable folded capillary zeta cells (Malvern Panalytical, Germany). The liposomes were diluted 1:100 and measured in HSS buffer with the following settings: refractive index (RI) of the material of 1.34, material absorbance of zero, RI of 1.342 of the dispersant viscosity of 1.1185 mPa s were applied for DLS. For ζ-potential a refractive index of 1.342, viscosity of 1.1185 mPa s and a dielectric constant of 78.5 was used. An equilibration time of 60 s was applied before each measurement.

4.1.2.4. Phospholipid concentration

Here, inductively coupled plasma optical emission spectrometer (ICP-OES) was used with a SPECTROBLUE TI/EOP from (SPECTRO Analytical Instruments GmbH, Kleve, Germany). Phosphorous was detected at 177.495 nm and the device calibrated between 0 and 100 µmol L^{-1} phosphorous in 0.5 mol L^{-1} HNO_3. Before each measurement, the device was recalibrated with 0.5 mol L^{-1} HNO_3 and 50 µmol L^{-1} phosphorous. A 1:150 dilution of the liposomes (3 mL) in 0.5 mol L^{-1} HNO_3 was measured. ICP-OES measurements yielded a phospholipid concentration of 6.7 ± 0.04 mmol L^{-1}.

4.1.2.5. Protein coupling to liposomes

The N-glutaryl modified liposomes were mixed with EDC (10 mg mL^{-1} in 0.05 M MES buffer, pH 5.5) and NHS (10 mg mL^{-1} in 0.05 M MES buffer, pH 5.5) and incubated for 1 h at room temperature (RT) while shaking. The respective equivalent of protein (1 mg mL^{-1} in PBS) was added and incubated for 1.5 h at RT while shaking. A ratio of 1:17:42:0.017 (n(COOH):n(EDC):n(NHS):n(protein)) was applied for antibody coupling. For streptavidin a ratio of 1:100:180:0.23 was used. Lysine-HCl (1 mol L^{-1} in ultrapure water) was added to yield a final concentration of 10 mmol L^{-1} and again incubated for at least 10 min at RT while shaking to quench the reaction. The conjugated liposomes were purified via size exclusion chromatography using Sepharose CL-4B as stationary phase and HSS buffer (10 mmol L^{-1} HEPES, 200 mmol L^{-1} sodium chloride, 200 mmol L^{-1} sucrose, 0.01 wt% sodium azide), pH 7.5 as mobile phase and a flow rate of approximately 0.5 mL min^{-1}. The conjugates were subsequently characterized by optical density, hydrodynamic diameter and zeta potential measurements. Optical density was measured at 565 nm of a 1:100 dilution in demineralized water. DLS and zeta potential measurements were done on a Malvern Zetasizer Nano-ZS (Malvern Panalytical, Germany). For all measurements, the temperature was set to 25 °C. The liposomes were diluted 1:500 in demineralized water and measured with the following settings: refractive index (RI) of the material of 1.45, material absorbance of 0.001, RI of 1.330 of the dispersant viscosity of 0.8872 mPa s were applied for DLS. For

ζ-potential a refractive index of 1.330, viscosity of 0.8872 mPa s and a dielectric constant of 78.5 was used. An equilibration time of 60 s was applied before each measurement.

4.1.2.6. Lateral flow assay procedure.

The LFA with all reagents in solution was performed according to the following procedure if not stated differently. 36 µL of the respective dilution of recombinant IL-6 in serum and 9 µL serum buffer were mixed with 5 µL detection solution consisting of detection particles (colloidal gold and 350 nm liposomes (30 mOD per test), 190 nm liposomes (40 mOD per test)) and anti-IL-6 IgG-biotin (50 ng per test) and incubated 5 min at RT in a 2 mL reaction vessel prior to application on the test strip. After 15 min the test strip was evaluated with a ESEQuant LFR strip reader. The test strip consists of a transparent backed CN150 (colloidal gold and 190 nm liposomes) or CN95 (350 nm liposomes) nitrocellulose membrane (Sartorius, Göttingen, Germany) with a streptavidin (SA) test line (27 mm) and an anti-mouse IgG control line (36 mm). The LFA with the reagent solution applied on the test strip was done by adding the reagent solution (5 µL detection particles (colloidal gold and 350 nm liposomes (30 mOD per test), 190 nm liposomes (40 mOD per test)) and anti-IL-6 IgG-biotin (50 ng per test) to the overlap of sample pad and conjugate pad and placed directly into 45 µL IL-6 dilution including 9 µL serum buffer. The LFA was allowed to run for 15 min and was evaluated photometrically directly after the test run or allowed to dry before lysis with 2 µL absolute ethanol for fluorescence evaluation. Photometric detection was done directly after test run λ_{max} = 520 nm, fluorescence was measured before and after lysis of the dried strip with 2 µL absolute ethanol with λ_{ex} = 470 nm, λ_{em} = 600 nm if not stated otherwise.

4.1.2.7. Apparatus

Fluorescence measurements were performed with a Synergy Neo 2 microplate reader from BioTek (Bad Friedrichshall, Germany) for fluorescence measurements of liposomes or with the ESEQuant LFR strip reader from Qiagen (Hilden, Germany) for photometric and fluorescence measurements of the test strips.

4.1.3. Results and Discussion

4.1.3.1. Development of photometric and fluorescent liposomes

In view of a commercial application of liposomes in lateral flow assays, we studied modifications of previously reported SRB liposomes[9] on the synthesis level towards long-term stability in solution and dehydrated on a test strip. We designed them for excellent photometric and fluorescent performance. In theory, the larger the liposome, the more

encapsulant is present and hence can contribute to signal recording. Also, small size distribution of a liposome population enhances their colloidal stability during long-term storage. However, the synthesis of large unilamellar liposomes with small size distribution is difficult[12] and not that applicable to the POCT as it typically involves additional procedural steps and can become quite time consuming which rapidly increase the cost. We therefore chose the reverse phase evaporation method that is known for high encapsulation yields followed by size extrusion to quickly generate differently sized liposomes in a very simple, mass-producible manner. Furthermore, by varying the encapsulant concentration, we tailored the liposomes toward photometric (high SRB concentrations) or inherent fluorescent (low SRB concentrations that do not self-quench) detection strategies. A mandatory design feature is the creation of a single-step LFA procedures to maintain the dramatic advantage LFAs have over other POCT systems.

4.1.3.2. Inherently fluorescent liposomes

We developed inherently fluorescent liposomes by reducing the amount of encapsulant dye. It is known that 150 mmol L^{-1} SRB liposomes exhibit fluorescence self-quenching in their intact state.[9] Hence, high-performance fluorescence measurement with these liposomes is only possible through release of SRB by lysis of the liposomes. Consequently, the fluorescence signal of such intact liposomes is typically below 1 % of the fluorescence of its lysed pendant. While significant signal enhancement could be achieved, in a lateral flow assay this would be accompanied by an additional lysis step. Instead, liposomes which are already fluorescent in their intact state avoid any additional procedural step and are thus desirable for enhanced fluorescent LFA designs. Liposomes with 10, 50 and 150 mmol L^{-1} SRB maintained self-quenching. For these liposomes, the fluorescence intensity of the intact liposomes remained below 1 % (**Table 1 and 2**, I_{intact} (%)). However, the overall fluorescence performance (I_{lysed}) of the different batches when being lysed continuously decreases with decreasing encapsulant concentrations as expected (**Table 1**).

Table 1 Characteristics of small sulforhodamine B liposomes (extruded through 0.2 µm membrane)

encapsulant concentration	hydrodynamic diameter[a] (nm)	ζ-potential (mV)	Polydispersity index	I_{lysed}[b] × 10^3 (a. u.)	I_{intact}[c] (%)
0.1 mmol L^{-1}	141 ± 40	-37 ± 3	0.06 ± 0.01	0.059 ± 0.002	103 ± 4
1 mmol L^{-1}	136 ± 46	-39 ± 4	0.09 ± 0.01	1.25 ± 0.03	10.5 ± 0.2
10 mmol L^{-1}	116 ± 51	-32 ± 2	0.06 ± 0.01	8.1 ± 0.2	0.76 ± 0.02
50 mmol L^{-1}	197 ± 68	-30 ± 2	0.10 ± 0.01	15.9 ± 0.3	0.204 ± 0.004
150 mmol L^{-1}	204 ± 61	-31 ± 2	0.07 ± 0.01	39.5 ± 0.9	0.204 ± 0.005

[a]size by intensity of a 1:100 dilution, [b]I_{intact} was obtained by diluting liposomes to 100 µmol L^{-1} total lipid in HSS buffer (100 µL) and I_{lysed} by diluting the liposomes in 30 mmol L^{-1} *n*-octyl-*β*-*D*-glycopyranoside in HSS buffer, [c]$I_{intact} = I_{intact}/I_{lysed} \times 100$, data are presented as mean ± SD with n = 3

Only the liposomes with 0.1 and 1 mmol L^{-1} SRB showed increased fluorescence > 1 % in their intact state, yet their overall fluorescence performance (I_{lysed}) in solution was very poor with as little as three orders of magnitude lower signals when lysed (59 a. u. for the 0.1 mmol L^{-1} SRB liposomes in comparison to the 39500 a. u. for 150 mmol L^{-1} SRB liposomes). Thus, while the low-concentrated encapsulated dye prevented its self-quenching it consequently reduced the obtained lysed fluorescence signal, too (**Figure 1 a**). When using both inherently fluorescence liposomes in an interleukin 6 LFA test (**Figure 1 b**), it was found that the overall lower fluorescence signal outweighs the positive effect obtained through sensitive fluorescence detection. Specifically, consistent with the observations in solution, both liposomes performed poorly in their fluorescent LFA. Furthermore, in comparison to the photometric detection of the high encapsulant equivalents (150 mmol L^{-1}) both, 0.1 and 1 mmol L^{-1} SRB liposomes, are by a factor of 10 less sensitive in their fluorescent IL-6 assay.

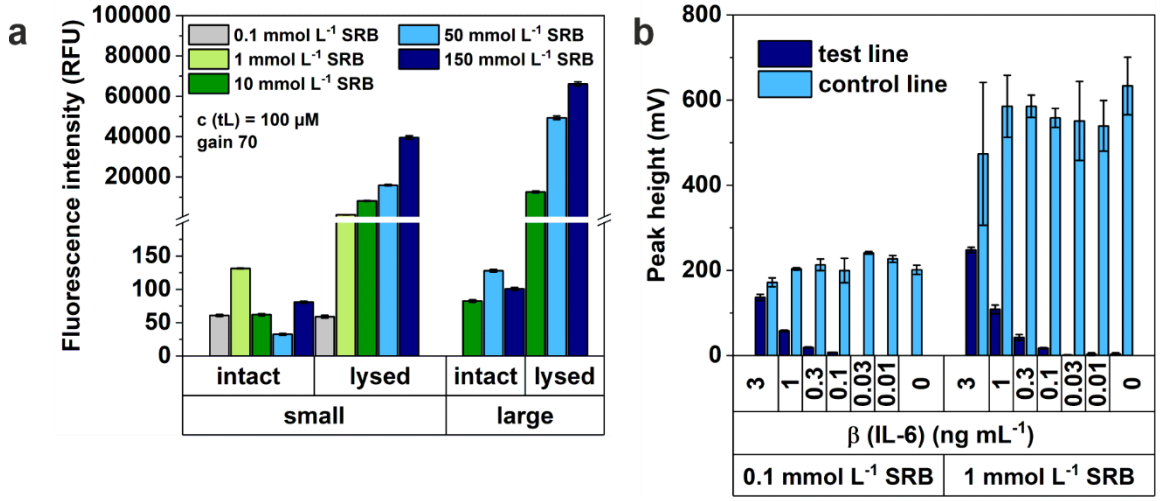

Figure 1 Fluorescence performance of large and small liposomes with varying encapsulation concentrations. (a) Fluorescence performance of intact and lysed large and small liposomes in solution of 100 µL liposome dilution (c (total lipid) = 100 µmol L^{-1}) in HSS buffer (intact) or 30 mmol L^{-1} *n*-octyl-*β*-D-glucopyranoside in HSS buffer (lysed) and (b) fluorescence performance of intact small 0.1 and 1 mmol L^{-1} SRB liposomes in an IL-6 LFA, data are presented as mean ± SD (error bar) with n = 3, fluorescence signal was recorded with λ_{ex} = 550 nm, λ_{em} = 600 nm

4.1.3.3. Optimization of photometric liposome detection

To fully harness the liposome signaling capability for the photometric approach, they were maximally loaded with SRB by increasing their size and thus the inner volume to increase their overall sensitivity. Furthermore, we were seeking to generate liposomes with small size variation to increase their colloidal stability during long-term storage. Liposomes can be synthesized using the reverse phase evaporation method and extruded to a desired size range through various sized membranes and extrusion steps (see **Table S 1** and **Figure S 1**) which is further supported by Szoka and colleagues[13]. Based on this information, we developed large liposomes in the range of 350 nm (PdI: 0.18) (**Table S 2**) by extrusion through only the 1 µm membrane and small liposomes in the range of 190 nm (PdI: 0.07) (**Table 1**) by extrusion through 0.4 and 0.2 µm membranes with varying SRB encapsulation concentrations. These liposomes showed in initial characterizations that the larger the liposome and the higher the SRB concentration is, the more SRB is encapsulated within the liposome, as evidenced by the fluorescent measurement of lysed liposomes (I_{lysed}) (**Table 2**). As these small and large 150 mmol L^{-1} SRB liposomes yielded the strongest fluorescence signal and are easy to manufacture, these two types of liposomes were chosen to evaluate their tolerance towards antibody coupling, dehydration and determine their overall performance in a regular LFA. Even larger liposomes could be investigated in the future, however, based on prior experiences (data not shown) it is assumed that more steric hindrance and less colloidal stability could hamper large liposomes.

Table 2 Overview of fluorescence intensities of large and small sulforhodamine B liposomes

large liposomes[a]	I_{lysed}[b] × 10^3 (a. u.)	I_{intact}[c] (%)	small liposomes[d]	I_{lysed}[b] × 10^3 (a. u.)	I_{intact}[c] (%)
10 mmol L^{-1}	12.5 ± 0.5	0.66 ± 0.03	10 mmol L^{-1}	8.1 ± 0.2	0.76 ± 0.02
50 mmol L^{-1}	49.3 ± 0.9	0.259 ± 0.005	50 mmol L^{-1}	15.9 ± 0.3	0.204 ± 0.004
150 mmol L^{-1}	66 ± 1	0.152 ± 0.002	150 mmol L^{-1}	39.5 ± 0.9	0.204 ± 0.005

[a]350 nm liposomes, [b]I_{intact} was obtained by diluting liposomes to 100 µmol L^{-1} total lipid in HSS buffer (100 µL) and I_{lysed} by diluting the liposomes in 30 mmol L^{-1} *n*-octyl-*β*-*D*-glycopyranoside in HSS buffer, [c]$I_{intact} = I_{intact}/I_{lysed} \times 100$, [d]190 nm liposomes, data are presented as mean ± SD with n = 3

4.1.3.4. Photometric and fluorescence lateral flow immunoassay

Previously optimized conditions for coupling streptavidin to liposomes were not directly transferrable to IgG coupling.[11] Thus, we used the relatively inexpensive anti-digoxigenin IgG (<Dig>) to identify the ideal coupling ratio of 1:17:42:0.17 (n(COOH):n(EDC):n(NHS): n(antibody)) and obtained already in this experiment a 4-times steeper slope and an order of magnitude lower detection limit of 1 ng mL^{-1} *vs.*10 ng mL^{-1}-with our liposome approach in contrast to commercial AuNPs (**SI, 2.3, Figure S 2**).

These coupling conditions were subsequently used for the covalent attachment of anti-interleukin 6 (<IL-6>) to the liposomes using a coupling ratio of 1:17:42:0.017 (n(COOH):n(EDC):n(NHS):n(antibody)) for anti-interleukin 6 (<IL-6>). Two different antibodies were tested, where one antibody showed an over 10-times higher sensitivity with over 20-times stronger signals especially for low concentrations (data not shown) which was consequently used in the following experiments. In the end, small and large liposomes were coupled accordingly to clone 2 (<IL-6>) and tested in the IL-6 LFA format towards the standard colloidal gold approach as illustrated in **Figure 2**. For the determination of the LOD, y_{LOD} = initial value (A1) + 3 × standard deviation of the blank (SD_{blank}) was chosen as it yields a more realistic LOD in contrast to the often-used linear approach. Already the small liposomes showed here significant improvement of the LOD with 4 pg mL^{-1} IL-6 in comparison to colloidal gold with an LOD of 0.025 ng mL^{-1} when detected photometrically (**Figure S 5**) with similar resolution ($slope_{190\ nm}$ = 0.7 mL pg^{-1}, $slope_{colloidal\ gold}$ = 0.5 mL pg^{-1}). Switching to large liposomes showed sensitivity enhancement not only by an even lower LOD (1 pg mL^{-1}) but also a significantly increased slope of 3.4 mL pg^{-1} (**Figure S 5**) was obtained, which is due to the increased inner volume of the liposomes and thus elevated amount of dye present (slopes were determined from the linear region).

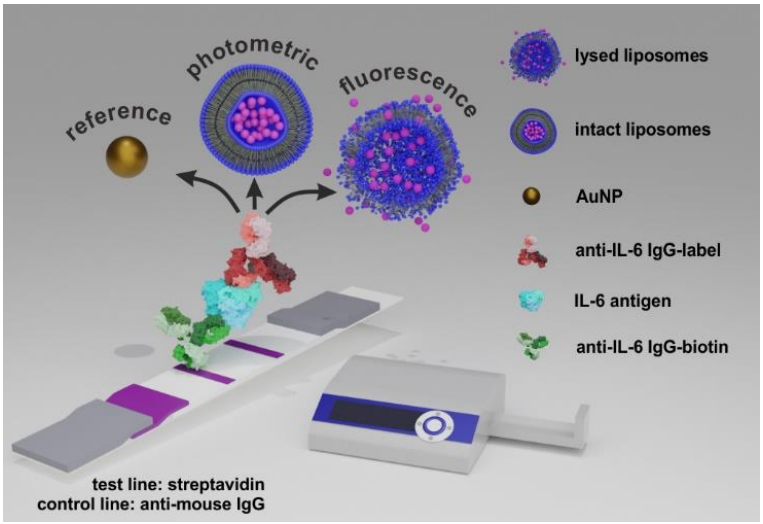

Figure 2 Illustration of applied analysis principle of developed interleukin 6 lateral flow assay

Furthermore, the large liposome approach had a dynamic range of almost three orders of magnitude. Even when measured photometrically in serum, the liposomes outperform commercial colloidal gold with slightly increased LOD toward the buffer conditions ($LOD_{190\ nm}$ = 23 pg mL^{-1}, $LOD_{350\ nm}$ = 7 pg mL^{-1}, $LOD_{colloidal\ gold}$ = 81 pg mL^{-1}) (**Figure 3 a**). Since the strategy to achieve a lower LOD using inherently fluorescent liposomes was not successful, a system was developed in which liposomes bound to test, and control lines were lysed through an additional step in order to harness their superior fluorescent capability.

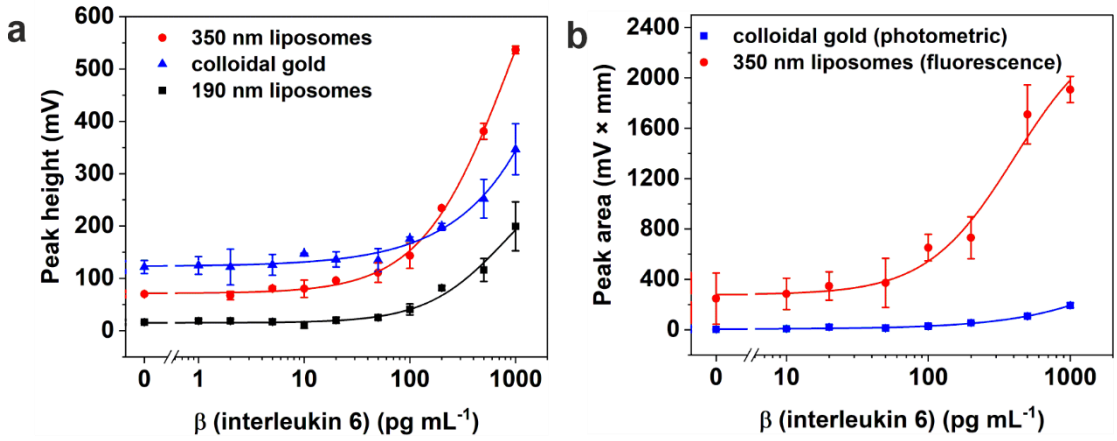

Figure 3 Titration of IL-6 with large and small liposome conjugates benchmarked to colloidal gold. (a) Photometric detection in human serum and (b) fluorescence detection of liposomes after lysis in human serum benchmarked to colloidal gold (photometric detection). In (a) preincubation of liposomes (5 min) with IL-6 and anti-IL-6-biotin IgG in running solution, in (b) liposomes on conjugate pad without preincubation. Photometric measurement was done at λ_{max} = 520 nm, fluorescence signal was recorded with λ_{ex} = 470 nm, λ_{em} = 600 nm, data are presented as mean ± SD (error bar) with n = 3, four-parameter logistic fitting with Origin2020 was done with in (a) R^2 = 0.9940 (red), R^2 = 0.9687 (blue) and R^2 = 0.9557 (black) and in (b) R^2 = 0.9493 (red) and R^2 = 0.9583 (blue), y_{LOD} = A1 + 3 SD_{blank}

In addition, pretests in a microtiter plate approach showed that the well-known fluorescence enhancement of SRB in human serum [14] could assist in enhancing the sensitivity (**SI, 2.4, Figure S 3, Table 3**). Yet, with the current assay design it is not possible to take advantage of this in the LFA format (**Figure S 4**). We assume that this is due to the absence of a bulk aqueous enviroment on the test strip which does not allow for a polarity change when introducing HSA into the system. Furthermore, surprisingly, the fluorescence approach did not yield a lower LOD (0.2 ng mL^{-1}) in contrast to the photometric approach. This is most likely due to the high background signal and the inherently introduced error of the additional procedural steps. The background signal can be lowered by changing the assay procedure and pre-applying the liposomes to the conjugate pads. However, as can be seen in **Figure 3**, the lack in pre-incubation time compensates any benefit obtained through lower background signals. Specifically, it led to an increased LOD not only with the liposomes but also with the AuNP (0.1 ng mL^{-1}) (**Figure 3 b**). In the future, other membrane materials that allow for more interactions such as slow running membranes (CN150) (**Figure S 6**) will be investigated along with developing an effective dehydration strategy for the large liposomes. When referencing to already published articles, our results are impressive as we show here several versions of LFA procedures that can be operated with undiluted real-world samples and yield already in its easiest form (photometrically) exceptional sensitivity with only 36 µL sample volume, whereas in literature often samples with only 10 % serum as matrix were employed, and typically more sample volume is needed (**Table 3**). Overall, only few articles are published which developed LFA-based IL-6 detection (**Table 3**), and most of them are limited to academic studies only and require sophisticated detection devices.

Table 3 Recently published techniques for sensitive detection of interleukin 6 with immuno-LFAs

detection method	LOD	Matrix	special remarks	Ref.
Fluorescence (Eu-NP[a])	0.37 pg mL^{-1}	buffer, human serum	70 µL sample LFA run 15 min, commercial strip reader	[15]
Fluorescence Quantum dots (QD)	100 pM (2.1 ng mL^{-1})[b]	buffer, 10 % serum	LFA run 20 min 100 µL sample, multiplex, protype detector with UV-LED	[16]
Photon-Upconverion (UCP)[c]	n. a.	diluted whole blood	50-fold diluted benchtop reader, UPCON, Labrox	[17]
SERS[d] Au/Au core satellite nanoparticels[e]	n. a.	PBS	proof of principle, multiplex, non-commercial portable SERS reader	[18]
Fluorescence (fluorescent microspheres[f])	7.15 pg mL^{-1} 48.5 pg mL^{-1}	human plasma, hydrogel samples	up to 33 µL, extra washing steps, commercial strip reader	[19]
Fluorescence (Near-infrared dye[g])	4 pg mL^{-1} (182 fmol L^{-1})	10 % human plasma	75 µL sample, LFA run ≥ 15 min, benchtop image scanner	[20]
Fluorescence Quantum dots (QD)	4.5 pM (0.09 ng mL^{-1})	buffer, 10 % human serum	120 µL sample, LFA run 20 min benchtop image scanner	[21]
Photometry (commercial colloidal gold)	0.025 ng mL^{-1} (buffer) 0.081 ng mL^{-1} (HS)	buffer, 100 % human serum (HS)	36 µL sample LFA run 15 min, commercial strip reader	this work
Photometry (dye-loaded liposomes)	1 pg mL^{-1} (buffer) 7 pg mL^{-1} (HS)	buffer, 100 % human serum (HS)	36 µL sample LFA run 15 min, commercial strip reader	this work

[a]europium(III)chelate-doped nanoparticles, [b]molecular weight of 21 kDa for IL-6 was presumed, [c]up-converting phosphor nanoparticles, [d]surface enhanced raman scattering, [e]core functionalized with Raman-active 4-nitrothiophenol for IL-6 or thio-2-naphthol for IL-8, [f]FluoSpheres®; fluorophore doped particles (200 nm), [g]IRDye 800CW (Li-Cor Biosciences),

Here, on the contrary, a commercially ready system was used and enhanced by refined liposomal reporter probes which, similarly to AuNP, can be used for a multitude of immuno-LFAs. Already the photometric readout competes with the sensitivity of most of the reported LFAs and the commercial colloidal gold approach. We envision simultaneous photometrical or fluorescent application in the future providing LODs in the LFA format that can rival signal generation in microtiter plate assays. In order to render a truly universal liposome label approach, we compared directly coupled <IL-6> liposomes to those indirectly

coupled to streptavidin-coated liposomes via <IL-6>-biotin. Such a universal reporter probe bypasses stability issues typically encountered with antibodies extending the overall shelf life of this reagent. We obtained no significant difference between the two strategies, as similar signal intensities, equal slopes ($slope_{indirect}$: 1.046 mL ng^{-1}, $slope_{direct}$: 1.069 mL ng^{-1}) and sensitivities (LOD_{direct}: 0.019 ng mL^{-1}, $LOD_{indirect}$: 0.026 ng mL^{-1}) were obtained with the direct and indirect approaches (**Figure 4**).

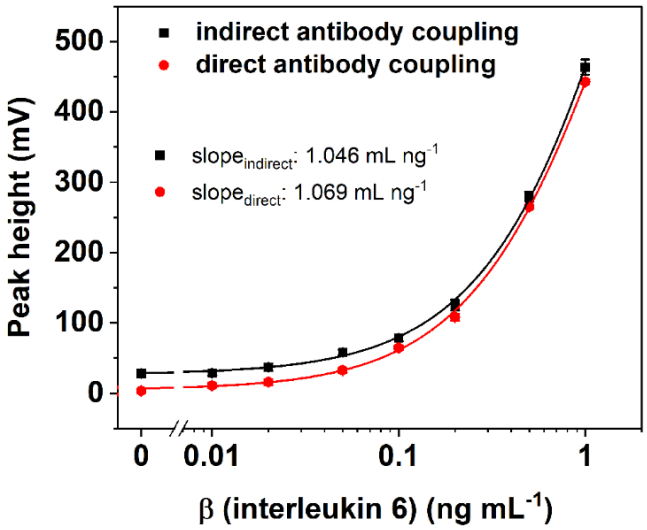

Figure 4 Performance test of universal streptavidin-modified liposomes towards direct coupled small liposomes with anti-interleukin 6 IgG (<IL-6>), four-parameter logistic fit with R^2 = 0.9970 (black) and R^2 = 0.9993 (red). 50 µL of a mixture of IL-6 and liposomes (40 mOD per test) in running solution were applied to the test strip (<IL-6> test line), test run for 15 min. Streptavidin-liposomes were mixed with anti-IL-6-biotin (equaling 0.2 µg anti-IL-6-biotin per test) and IL-6, photometric measurement was done at λ_{max} = 520 nm, data are presented as mean ± SD (error bar) with n = 3, $y_{LOD} = A1 + 3 \times SD_{blank}$, slope derived from four-parameter logistic fit function

4.1.3.5. Stability study and liposome dehydration

Since the direct and indirect coupling approach performed similar in the assay, the stability study was conducted with streptavidin-modified liposomes. In the end, these would be favored over the direct coupling approach in a commercial application as they can function as a generic label. These universal streptavidin-modified liposomes, that are independent from the durability of the antibody itself, were used in a long-term stability study assessing their stability in solution as well as in dehydrated form on the conjugate pad. Testing was conducted in a simple streptavidin biotin assay with the small (190 nm) streptavidin-modified liposomes. These liposomes remained stable in solution for at least 12 months at 2 – 8 °C and even 2 months at elevated temperatures up to 39 °C (**Figure 5 a**). The results from such an accelerated stability study translate roughly into 8 years when stored at 4 °C. [22]

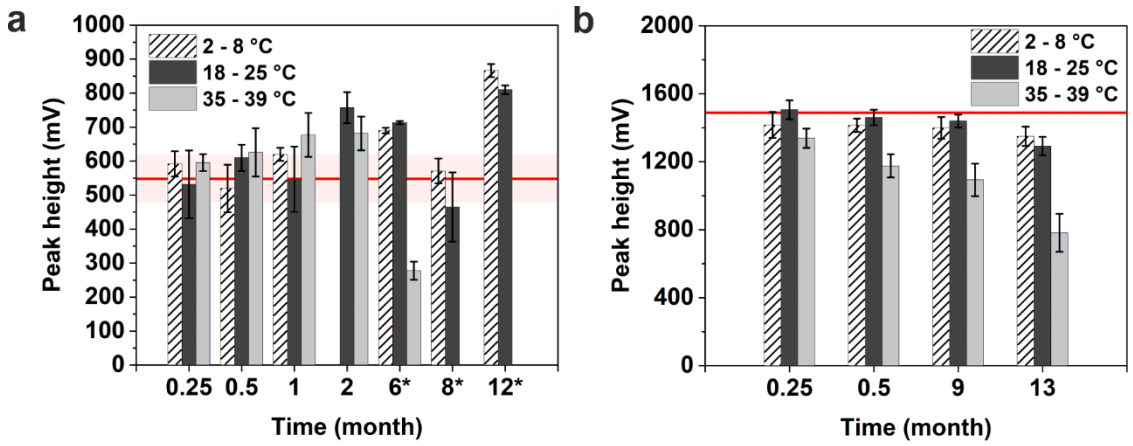

Figure 5 Long-term stability of small streptavidin liposomes in solution (a) or dehydrated on a test strip (b) before test run on LFA strips with biotin test line, red line indicates initial response at time point zero. Liposomes were diluted to 25 mOD per test in 90 µL (a), test run for 5 min, in (b) liposomes with 25 mOD per test were dehydrated on test strip and rehydrated by 50 µL running buffer, test run for 15 min. Photometric measurement was done at λ_{max} = 520 nm, data are presented as mean ± SD (error bar) with n = 5, times marked with an asterisk equals triplicates, reference line indicates initial response

Dehydration of the liposomes onto the conjugate pad was mainly motivated by the desire to reduce the number of assay steps and reagents needed to perform a LFA. In a first attempt, we identified the most suitable conjugate pad materials by simply drying our liposomes on different pad materials in HSS buffer at room temperature and 50 % air humidity for 1 h. The liposomes retained approximately 80 % of the liquid signal when dried on the conjugate pad made of fiber glass with binder (**Figure 6**), whereas all other pad materials studied showed meager performance (recovery <50 %). As manufacturers frequently pretreat membranes and pad material with inter alia detergents and typically use confidential binder formulations, this observation is not surprising and rather emphasizes the need of prescreening of LFA materials within the development process. For the follow up long-term stability study, liposomes were dispensed on the fiber glass conjugate pad with binder and dried in a drying cabinet at 37 °C for 1 h. After assembling, the test strips were stored at 2 - 8 °C, 18 - 25 °C and at 35 - 39 °C and tested periodically to assess reduction in the response. The test strips remain stable for at least nine months at temperatures between 2 - 25 °C with no significant reduction in the initial signal response and only a minor signal drop (<10 %) when retested after 13 months (**Figure 5 b**).

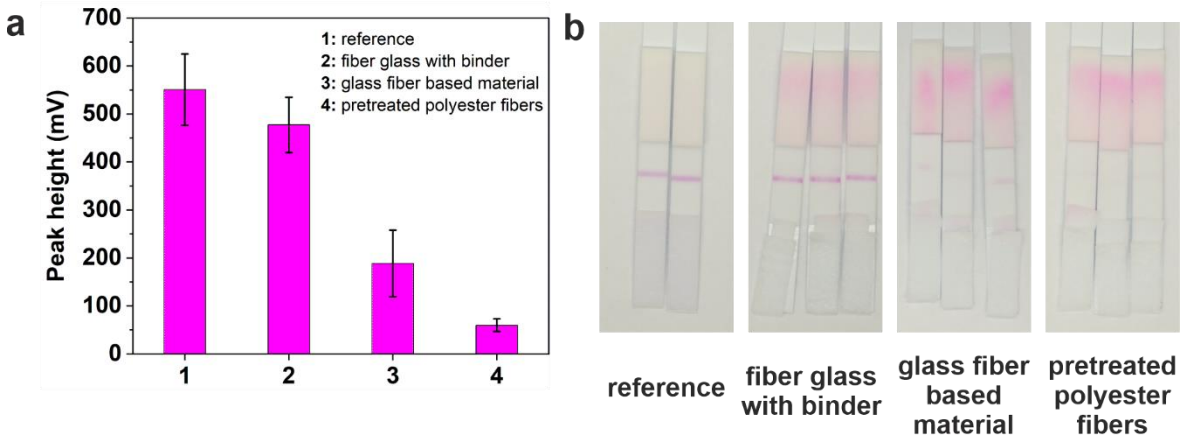

Figure 6 Evaluation of different conjugate pad materials for small liposome conjugates (a) obtained signal intensities and (b) real images. Test strips were prepared with 5 µL liposome dilution in conjugate pad buffer (80 mOD per test), test run for 5 min in 100 µL running buffer, photometric measurement was done at λ_{max} = 520 nm, data are presented as mean ± SD (error bar) with n ≥ 2

Harrigan and colleagues[23] stated that stability of vesicles critically depends on the vesicle size with the result, that smaller systems are most stable. We made similar observations as currently, only the small liposomes straightforwardly tolerate the dehydration process and were hence used for the long-term stability study. Dehydration of the large liposomes is currently under investigation as present data indicates that the liposomes are not fully destroyed (data not shown). Optimization of the drying conditions most likely provide the desired remedy, where we will apply protecting sugars as suggested previously by Martorell and colleagues[24]. They observed decreased recoveries for the larger liposomes as well but to a lesser extent (approx. 60 % in contrast to 75 % recovery with small liposomes). The results are not directly comparable as support material and size determination vary but it points to prosper when refining the dehydration conditions for our large liposomes.

4.1.4. Conclusion

The established commercial LFA system with colloidal gold for the detection of IL-6 shows already good sensitivity with 0.025 ng mL^{-1}. However, by replacing the gold nanoparticles with refined dye-loaded liposomes we were able to improve the sensitivity by over one order of magnitude to just 1 pg mL^{-1} with simple photometric detection. Furthermore, utmost care was taken to ensure that the liposomes are easily mass producible, could be dehydrated on the LFA membrane itself and hence be applied in the same, straight-forward, simple and easy-to-use LFA strategy that is so desirable. Further improvement of the LOD through fluorescent detection approaches, however, is not as easy to accomplish. Inherently fluorescent liposomes do not provide enough signal intensity and those that require an additional process step, as the dye has to be released from the liposome prior to detection, unfortunately compensate any gained signal intensity at the LOD by higher background

signals and less reproducibility due to the additional assay steps. Thus, while in a refined environment such as a microtiter plate, improved LODs can be obtained through fluorescence detection of these liposomes, this is not as easily translated to a robust, commercially-ready LFA approach. More experiments are needed to lower background signals, improve analyte-liposome interactions and hence lower the LOD effectively. However, already now the increased signal intensity afforded by the fluorescent liposomes will assist in the development of less sophisticated detection devices. Expanding on the applicability of these new reporter probes, our universal liposomes, which maintain sensitivity levels of directly conjugated liposomes, show remarkable long-term stability when stored in solution and dehydrated on a test strip of at least one year. These adaptable liposomes can easily be transferred to any other analyte of interest manifesting them as true alternative to standard colloidal gold. With this, a highly flexible and supersensitive toolset is provided for tailored assay development. Furthermore, in light of the importance of IL-6 detection with infectious diseases such as COVID-19, the here presented liposome-based LFA indicates that liposomes will rival the prevalence of colloidal gold as benchmark in LFA analysis.

4.1.5. Declarations

Acknowledgement

Thanks to Vanessa Tomanek and Anna Go for assisting in the liposome synthesis. Furthermore, special thanks to Roland Rist, Carolin Schrötel and Nora Schulte for assisting with the experimental execution.

Funding

The presented research was funded in part through the Central Innovation Program for small and medium-sized enterprises (SMEs) by the Federal Ministry of Economic Affairs and Energy according to a decision of the German Federal Parliament in cooperation with Microcoat Biotechnology (Germany)

Conflicts of interest/Competing interests

Antje J. Baeumner is Editor of *Analytical and Bioanalytical Chemistry* but was not involved in the peer review of this manuscript. The remaining authors declare no competing interests.

Ethics approval

The human serum samples involved in this study were obtained from voluntary donors with informed consent and were anonymized before usage. There was no association with a clinical trial and the studies have been performed in accordance with ethical standards.

4.1.6. References

[1] reports and data, "Point of Care (PoC) Diagnostics market size, share, trends and analysis, by product type (glucose monitoring, cardiometabolic testing, infectious disease), by platform type (lateral flow assays, biosensors), by prescription mode, by end user, forecasts To 2028.", can be found under https://www.reportsanddata.com/report-detail/point-of-care-poc-diagnostics-market, **2020**.

[2] N. Jiang, R. Ahmed, M. Damayantharan, B. Ünal, H. Butt, A. K. Yetisen, *Adv. Healthcare Mater.* **2019**, *8*, e1900244.

[3] G. A. Posthuma-Trumpie, J. Korf, A. van Amerongen, *Anal. Bioanal. Chem.* **2009**, *393*, 569.

[4] J. D. Bishop, H. V. Hsieh, D. J. Gasperino, B. H. Weigl, *Lab Chip* **2019**, *19*, 2486.

[5] Isalomboto Nkanga, C., Murhimalika Bapolisi, A., Ikemefuna Okafor, N., & Werner Maçedo Krause, R., *General Perception of Liposomes: Formation, Manufacturing and Applications. Liposomes - Advances and Perspectives.*, **2019**.

[6] K. A. Edwards, O. R. Bolduc, A. J. Baeumner, *Curr. Opin. Chem. Biol.* **2012**, *16*, 444.

[7] a) E. Morales-Narváez, C. Dincer, *Biosens. Bioelectron.* **2020**, *163*, 112274; b) L. Y. C. Chen, R. L. Hoiland, S. Stukas, C. L. Wellington, M. S. Sekhon, *Eur. Respir. J.* **2020**, *56*.

[8] J. M. Fernández-Real, M. Broch, J. Vendrell, C. Richart, W. Ricart, *J. Clin. Endocrinol. Metab.* **2000**, *85*, 1334.

[9] K. A. Edwards, A. J. Baeumner, *Anal. Bioanal. Chem.* **2006**, *386*, 1335.

[10] a) H.-W. Wen, W. Borejsza-Wysocki, T. R. DeCory, A. J. Baeumner, R. A. Durst, *Eur. Food Res. Technol.* **2005**, *221*, 564; b) H.-W. Wen, W. Borejsza-Wysocki, T. R. DeCory, R. A. Durst, *Anal. Bioanal. Chem.* **2005**, *382*, 1217; c) S. Shukla, H. Leem, M. Kim, *Analytical and bioanalytical chemistry* **2011**, *401*, 2581; d) E. Frohnmeyer, N. Tuschel, T. Sitz, C. Hermann, G. T. Dahl, F. Schulz, A. J. Baeumner, M. Fischer, *Analyst* **2019**, *144*, 1840.

[11] K. A. Edwards, K. L. Curtis, J. L. Sailor, A. J. Baeumner, *Anal. Bioanal. Chem.* **2008**, *391*, 1689.

[12] S. Shah, V. Dhawan, R. Holm, M. S. Nagarsenker, Y. Perrie, *Adv. Drug Delivery Rev.* **2020**, *154-155*, 102.

[13] F. Szoka, F. Olson, T. Heath, W. Vail, E. Mayhew, D. Papahadjopoulos, *Biochim. Biophys. Acta, Biomembr.* **1980**, *601*, 559.

[14] M. Kitamura, K. Murakami, K. Yamada, K. Kawai, M. Kunishima, *Dyes Pigm.* **2013**, *99*, 588.

[15] D. Huang, H. Ying, D. Jiang, F. Liu, Y. Tian, C. Du, L. Zhang, X. Pu, *Anal. Biochem.* **2020**, *588*, 113468.

[16] M. Mahmoud, C. Ruppert, S. Rentschler, S. Laufer, H.-P. Deigner, *Sens. Actuators, B* **2021**, *333*, 129246.

[17] A. van Hooij, M. Tió-Coma, E. M. Verhard, M. Khatun, K. Alam, E. Tjon Kon Fat, D. de Jong, A. Sufian Chowdhury, P. Corstjens, J. H. Richardus et al., *Front. Immunol.* **2020**, *11*, 1811.

[18] V. Tran, B. Walkenfort, M. König, M. Salehi, S. Schlücker, *Angew. Chem., Int. Ed. Engl.* **2019**, *58*, 442.

[19] G. J. Worsley, S. L. Attree, J. E. Noble, A. M. Horgan, *Biosens. Bioelectron.* **2012**, *34*, 215.

[20] C. Swanson, A. D'Andrea, *Clin. Chem. (Washington, DC, U. S.)* **2013**, *59*, 641.

[21] C. Ruppert, L. Kaiser, L. J. Jacob, S. Laufer, M. Kohl, H.-P. Deigner, *J. Nanobiotechnol.* **2020**, *18*, 130.

[22] S. S. Deshpande in *Enzyme immunoassays*. *From concept to product development* (Ed.: S. S. Deshpande), Chapman & Hall, New York, NY, **1996**, pp. 275–359.

[23] P. R. Harrigan, T. D. Madden, P. R. Cullis, *Chem. Phys. Lipids* **1990**, *52*, 139.

[24] D. Martorell, S. T. Siebert, R. A. Durst, *Anal. Biochem.* **1999**, *271*, 177.

4.1.7. Supporting Information

4.1.7.1. Experimental Section

4.1.7.1.1. Chemicals and consumables

Standard chemicals were purchased from Sigma Aldrich/Merck and used without purification. Chloroform and methanol were purchased from VWR chemicals (Germany). Milk powder, cholesterol, Sephadex® G 50, sucrose, sodium azide, glycine (purity >99.7 %), sodium hydroxide, TWEEN®20, Whatman Nucleopore™ Track-Etched membranes 1.0 µm, 0.4 µm and 0.2 µm, 19 mm diameter were purchased from Sigma Aldrich/Merck (Germany). Potassium hydrogen carbonate, *n*-octyl-*β*-*D*-glucopyranoside (CN23.2), dialysis tube Spectra/Por© 4 (2718.1) MWCO (12-14 kDa) were obtained from Carl Roth (Karlsruhe, Germany). Sepharose CL-4B was purchased from Cytiva Europe GmbH (Freiburg, Germany). Phosphorous standard was purchased from Bernd Kraft GmbH (Duisburg,Germany) and HNO_3 from Fisher Scientific GmbH (Schwerte, Germany). Synthetic sweat was purchased from synthetic urine (Eberdingen-Nussdorf, Germany). For all experiments ultrapure water was used.

4.1.7.1.2. Synthesis of sulforhodamine B liposomes.

The synthesis was done according to the procedure in the main article by using DPPC (29.58 mg, 40.3 µmol), DPPG (15.64 mg, 21.0 µmol), cholesterol (19.99 mg, 51.7 µmol) and N-glutaryl-DPPE (6.2 mg, 7.0 µmol). After rotary evaporation the remaining solution was split into 7 fraction and extruded at 65 °C. Each fraction was extruded with varying parameters with regard to the applied membranes (no membrane, only 1 µm, 1 µm and 0.4 µm or 1 µm, 0.4 µm and 0.2 µm) and the amount of extrusion steps (11 or 21 steps) using a mini extruder (Avanti Polar Lipids, Inc.). Each fraction was purified first by size-exclusion chromatography with Sephadex® G-50 as stationary phase (column size: 1 cm x 6 cm) and HSS buffer (10 mmol L^{-1} HEPES, 200 mmol L^{-1} sodium chloride, 200 mmol L^{-1} sucrose, 0.01 wt% sodium azide), pH 7.5, osmolality 0.643 osmol kg^{-1} as mobile phase. Additionally, the liposomes were dialyzed against HSS buffer until the dialysis buffer remains colorless before determining the respective hydrodynamic diameter via DLS, phospholipid concentration via ICP-OES and zeta-potential.

4.1.7.1.3. Matrix effect evaluation.

A series of liposome dilutions were prepared in HSS buffer containing 30 mmol L^{-1} *n*-octyl-*β*-D-glycopyranosid and 10 % (v/v) of the respective matrix. 100 µL of each dilution was measured in a black medium-binding microtiter plate (Greiner BioOne, Frickenhausen,

Germany) with a Synergy Neo 2 microplate reader from BioTek (Bad Friedrichshall, Germany). Fluorescence measurement was performed with λ_{ex} = 530 nm (10 nm), λ_{em} = 590 nm (10 nm) and gain 100 and a reading height of 4.5 mm.

4.1.7.1.4. Lateral flow assay procedure.

The LFAs were similarly performed to the procedure described in the main manuscript.

4.1.7.2. Results

4.1.7.2.1. Size adjustment of sulforhodamine B liposomes through variation of extrusion parameters

Here, the size of the liposomes was adjusted by varying the applied extrusion membranes and the extrusion steps. Whereas increasing extrusion steps generally lead to a lower polydispersity index (PdI), only extrusion to solely a 1 µm membranes leads to a significant size difference compared to those extruded through 0.4 µm and 0.2 µm membranes (**Table S 1**). This is also depicted in **Figure S 1** with more confined peaks for the fractions extruded with 21 steps and a shift of the peak for the fractions extruded through 0.4 µm and 0.2 µm membranes to smaller size distributions.

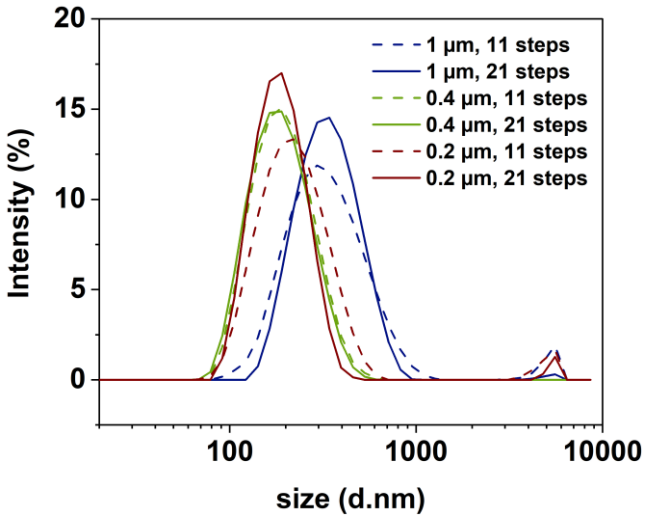

Figure S 1 Hydrodynamic diameter of 150 mmol L^{-1} sulforhodamine B liposomes synthesized with varying extrusion membranes and extrusion steps. DLS was carried out with a 1:100 dilution of liposomes in HSS buffer, data are presented as mean with n = 3, error bars not shown

Table S 1 Size parameters obtained for 150 mmol L^{-1} sulforhodamine B liposomes synthesized with varying extrusion conditions

Extrusion parameters	Size by Intensity (nm)	Size by Number (nm)	Z-average (nm)	Polydispersity index[a]
w/o extrusion[b]	n. a.	n. a	n. a.	n. a.
1 µm, 11 steps	356 ± 161	231 ± 111	323	0.20
1 µm, 21 steps	355 ± 132	277 ± 110	309	0.15
0.4 µm, 11 steps	205 ± 76	136 ± 52	189	0.14
0.4 µm, 21 steps	198 ± 74	131 ± 49	175	0.14
0.2 µm, 11 steps	232 ± 92	146 ± 63	219	0.16
0.2 µm, 21 steps	193 ± 60	141 ± 48	196	0.10

DLS was carried out with a 1:100 dilution of liposomes in HSS buffer; [a]polydispersity (PdI) was calculated for the corresponding peak according to PdI = $(\sigma_{size}/size)^2$, here the size by intensity values were used [1], [b]no reliable dataset was obtainable for liposomes without extrusion as they show too high variation in size; data are presented as mean ± SD with n = 3

4.1.7.2.2. Additional information to large sulforhodamine B liposomes with varying encapsulation concentration

Table S 2 lists the characteristics of the synthesized large sulforhodamine B liposomes with varying SRB encapsulation concentrations.

Table S 2 Characteristics of large sulforhodamine B liposomes

encapsulant concentration	hydrodynamic diameter[a] (nm)	ζ-potential (mV)	Polydispersity index	I_{lysed}[b] × 10^3 (a. u.)	I_{intact}[c] (%)
10 mmol L^{-1}	457 ± 170	-40 ± 3	0.24 ± 0.01	12.5 ± 0.5	0.66 ± 0.03
50 mmol L^{-1}	290 ± 146	-40 ± 1	0.23 ± 0.01	49.3 ± 0.9	0.259 ± 0.005
150 mmol L^{-1}	355 ± 132	-29.7 ± 0.7	0.18 ± 0.02	66 ± 1	0.152 ± 0.002

[a]size by intensity of a 1:100 dilution, [b]I_{intact} was obtained by diluting liposomes to 100 µmol L^{-1} total lipid in HSS buffer (100 µL) and I_{lysed} by diluting the liposomes in 30 mmol L^{-1} *n*-octyl-*β*-*D*-glycopyranoside in HSS buffer, [c]$I_{intact} = I_{intact}/I_{lysed} \times 100$, data are presented as mean ± SD with n = 3

4.1.7.2.3. Pretests for antibody coupling to liposomes

To define ideal coupling conditions antibody coupling was pretested with the model antibody anti-digoxigenin IgG (<Dig>). The liposomes contain 6 mol% of lipids bearing a glutaryl group available for EDC/NHS coupling chemistry, which limits the overall surface coverage obtainable in comparison to AuNPs. Nonetheless, with a coupling ratio of 1:17:42:0.17 (n(COOH):n(EDC):n(NHS):n(antibody)), the small liposomes outperformed commercial AuNPs (**Figure S 2 a, b**). In addition, a visibly lower limit of detection (**Figure S 2 c**) at 1 ng mL^{-1} was obtained for liposomes, and at 10 ng mL^{-1} for AuNPs. The overall lower signal intensity and earlier saturation obtained for the liposomes was caused by the maximally available loading of the surface, i.e. limited by the 6 mol% glutaryl groups. Fine-tuning of the final loading of the liposomes with <Dig> can overcome the lower signal intensity and saturation issue. However, this was not our primary focus in the present study.

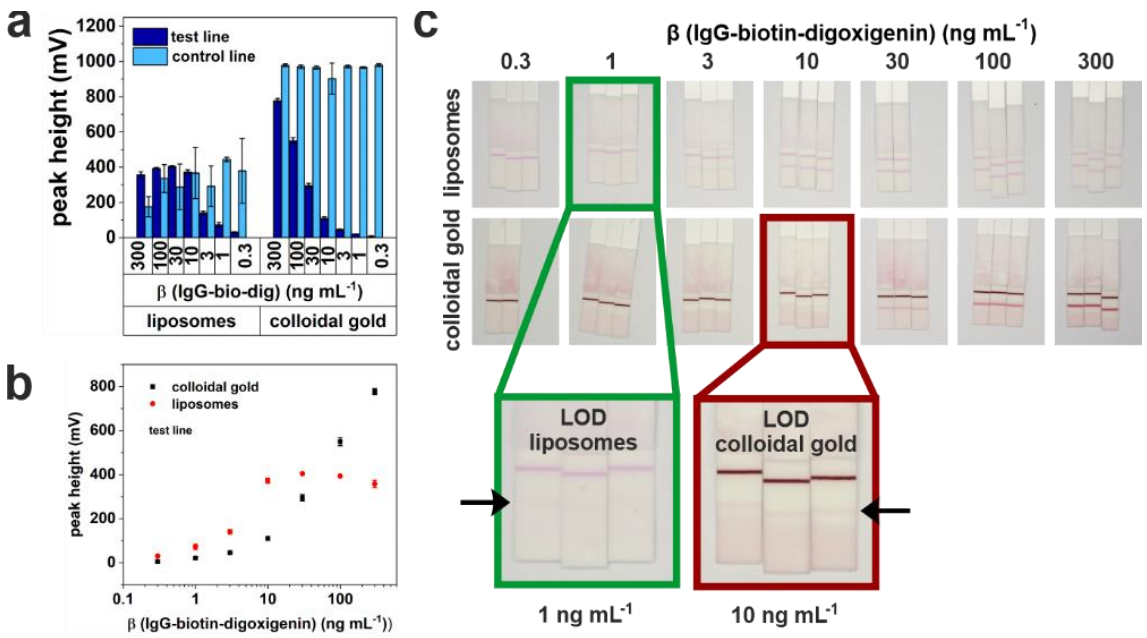

Figure S 2 Photometric titration of IgG-biotin-digoxigenin with anti-digoxigenin labeled liposomes in comparison to commercial gold nanoparticle with (a) illustrating the test and control line signals, (b) test line dose-response curve with small liposomes in direct comparison to colloidal gold and (c) images of lateral flow assays with visible limit of detection. Particles were preincubated (5 min) in running solution (85 µL IgG-biotin-digoxigenin dilution, 10 µL particles (80 mOD per test)), test run for 5 min, photometric measurement was done at λ_{max} = 520 nm, data are presented as mean ± SD (error bar) with n ≥ 2

4.1.7.2.4. Matrix effect on fluorescence signal (MTP-based)

For IL-6, human serum is the state-of-the-art matrix. It is proposed in literature that interaction of fluorophores with human serum albumin (HSA) can result in enhanced fluorescence due to non-covalent interaction of the fluorophore with binding side I in HSA[2]. Kitamura and colleagues[3] intensively studied the interaction between HSA and SRB and proposed that it binds through hydrophobic interaction to the Sudlow site I of HSA and the

accompanied change to a less polar environment benefits the fluorescence intensity of sulforhodamine B. Exploiting this fluorescence enhancement was intended to increase sensitivity not only in the microtiter plate approach but also in the LFA when measuring in human serum. However, as we also accomplished a universal liposome label, various analytes become accessible. Thus, we studied the influence of different matrices toward their effect on the fluorescence signal. We obtained fluorescence enhancement in human serum and in the presence of HSA, whereas no fluorescence enhancement was obtained in milk, synthetic sweat, fetal bovine serum and in the presence of BSA (**Figure S 3**) which is also mirrored in the obtained LODs.

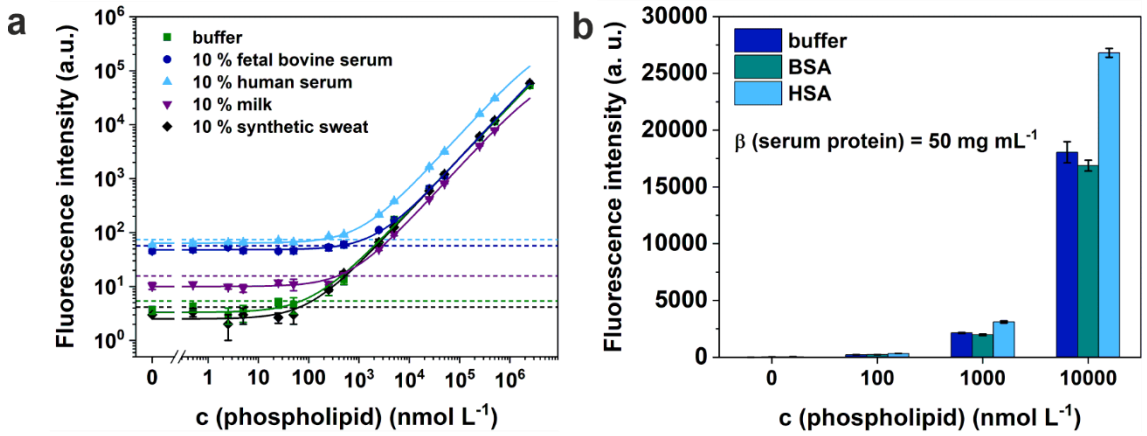

Figure S 3 Dose-response curve of fluorescence liposomes in various matrices and HSS buffer in (a) and enhancement obtained in presences of bovine serum albumin (BSA) and human serum albumin (HSA) in (b) and in HSS buffer. Fluorescence measurement was performed with λ_{ex} = 530 nm (10 nm), λ_{em} = 590 nm (10 nm) and gain 100 (RH 4.5), as fitting function, the four-parameter logistic fit from OriginLab 2020 was applied, data are presented as mean ± SD (error bar) with n = 3

As the binding site I in bovine serum albumin (BSA) is altered with an additional leucin residue, current assumptions are that this binding site is blocked in BSA and no enhancing proteins are present in the other tested matrices and thus fluorescence enhancement is only observed with HSA.[2] The obtained LODs with liposomes in the different matrices are listed in **Table S 3**.

Table S 3 Matrix effect on fluorescence signal

Matrix[a]	**LOD (pmol L^{-1})**
HSS buffer	59
fetal bovine serum	515
human serum	105
milk	300
synthetic sweat	70*

LOD: limit of detection (y_{LOD} = A1 + 3 × SD_{blank}), *LOD was calculated from 0.5 nmol L^{-1} phospholipid concentration sample

In solution a sensitivity enhancement with regard to other complex matrices (FBS or milk) was obtained. Unfortunately ,the enhancement effect from HSA (**Figure S 3**) in the microtiter plate was not obtained in the LFA approach. **Figure S 5** shows IL-6 titration with 350 nm liposomes in running buffer and serum to determine enhancement of fluorescence in human serum on an LFA and encountered sensitivity gain.

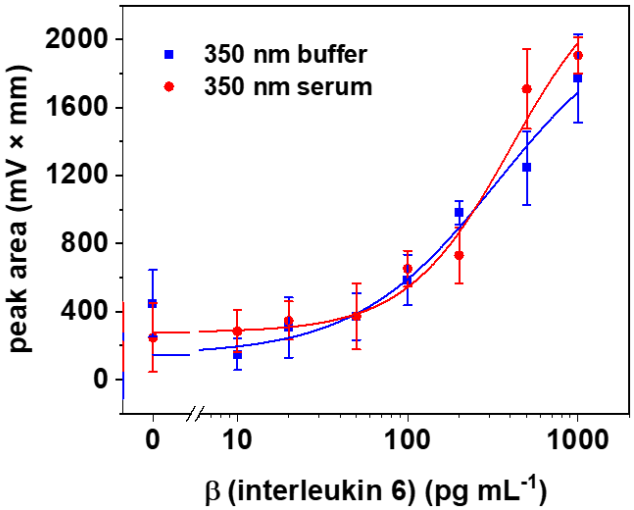

Figure S 4 Titration of IL-6 with large liposome conjugates after lysis in running buffer and serum, fluorescence signal was recorded with λ_{ex} = 470 nm, λ_{em} = 600 nm, data are presented as mean ± SD (error bar) with n = 3, four-parameter logistic fitting with Origin2020

4.1.7.2.5. Photometric and Fluorescence IL-6 Assay in running buffer

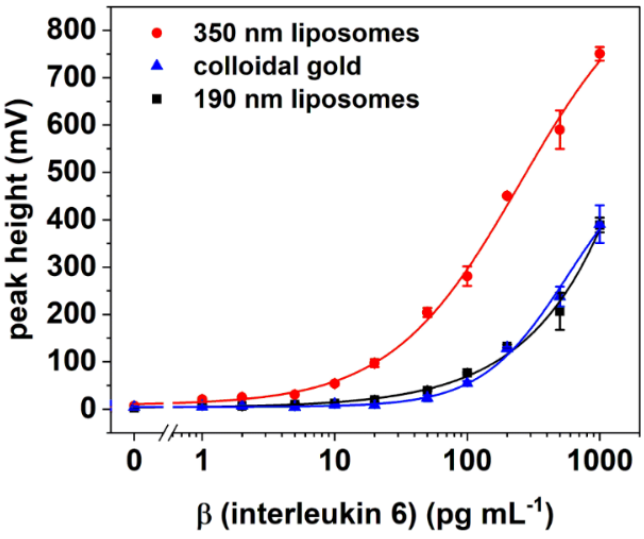

Figure S 5 Titration of IL-6 with large and small liposome conjugates benchmarked to colloidal gold. (a) Photometric detection in running buffer with preincubation of liposomes (5 min) with IL-6 and anti-IL6-biotin IgG in running solution, photometric measurement was done at λ_{max} = 520 nm, data are presented as mean ± SD (error bar) with n = 3, four-parameter logistic fitting with Origin2020, y_{LOD} = A1 + 3 SD_{blank}

Figure S 6 illustrates the pretest results for fluorescence and photometric IL-6 titrations with LFAs where the detection particles are directly dropped on the conjugate pad and the LFA run is immediately starting. Here, a slow running membrane (CN150) and a fast-running membrane (CN95) were tested.

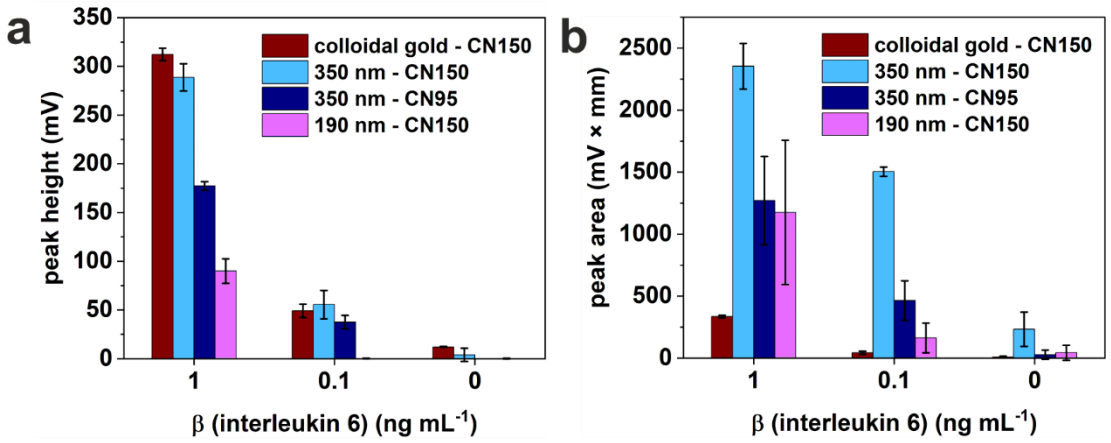

Figure S 6 Procedural pretests for IL-6 titration with large and small liposome conjugates benchmarked to colloidal gold. (a) Photometric detection and (b) fluorescence detection of liposomes after lysis benchmarked to colloidal gold. Liposomes were applied to conjugate pad and the assay performed in running buffer, photometric measurement was done at λ_{max} = 520 nm, fluorescence signal was recorded with λ_{ex} = 470 nm, λ_{em} = 600 nm, data are presented as mean ± SD (error bar) with n = 3

4.1.7.3. References

[1] N. Raval, R. Maheshwari, D. Kalyane, S. R. Youngren-Ortiz, M. B. Chougule, R. K. Tekade in *Basic Fundamentals of Drug Delivery*, Elsevier, **2019**, pp. 369–400.

[2] J. Fan, W. Sun, Z. Wang, X. Peng, Y. Li, J. Cao, *Chemical communications (Cambridge, England)* **2014**, *50*, 9573.

[3] M. Kitamura, K. Murakami, K. Yamada, K. Kawai, M. Kunishima, *Dyes Pigm.* **2013**, *99*, 588.

4.2. Changing from Standard Photometric and Fluorescence Detection to Chemiluminescence in Lateral Flow Assays

Graphical Abstract

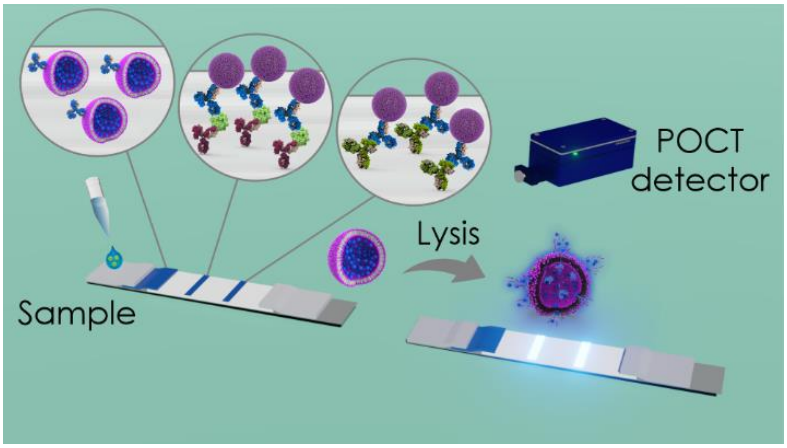

This chapter has not been published.

Abstract

Lateral flow assays (LFA) dominate as point-of-care (POC) detection platform in medical diagnostics due to their simplicity in use and comparably high analytical performance. The quest to lower limits of detection and hence broaden the range of clinically relevant analytes is therefore ever strong. Here, we investigate a new chemiluminescent (CL) approach combining liposomes as amplification tool and a highly water soluble new luminol derivative as exceptionally sensitive label. In this feasibility study the foundation for CL-based LFAs was developed along with a suitable point-of-care testing (POCT) detector and compared different detection techniques. Liposomes in general can outcompete commercial gold nanoparticles (AuNP) already when detected photometrically. Changing from photometric detection to fluorescence and chemiluminescence detection increased the sensitivity. Specifically, the CL approach yielded a significantly higher signal-to-noise (S/N) ratio of over 20 when studying an interleukin-6 immunoassay. Preliminary tests indicate that this can be further tuned by using higher CL dye loads. With fluorescence a S/N ratio of only 3.5 and surprisingly 12.8 for the colorimetric approach was achieved which already rivals the commercial AuNP approach. Liposomes in general outcompete the commercial AuNP with regard to sensitivity yet changing to CL detection could so far not considerably reduce the assay sensitivity compared to fluorescence detection. We assume this is because of non-specifically bound liposomes that interfere with the actual signal which is now subject to further studies.

4.2.1. Introduction

Within this study, the transfer from stable and highly loaded commercially ready sulforhodamine B (SRB) liposomes to similarly stable and sensitive chemiluminescence (CL) liposomes was investigated to introduce a new potent label for highly sensitive lateral flow assays (LFA) and expand the current POCT portfolio to low concentration biomarkers. Liposomes are very well known for years, as drug delivery system that is able to protect its cargo from non-specific protein interaction, degradation within the blood stream and unwanted dilution after administration.[1] Especially, their feature for incorporating hydrophilic, hydrophobic and amphiphilic molecules as well as encapsulating a variety of particles and biomolecules in large quantities raised interest not only in the pharmaceutical but also in the analytical field.[2] Liposomes have been used with great success in the development of sensitive biosensors as they are particularly interesting as signal amplification tool and detection particles to increase the overall assay sensitivity.[3,4] Their high surface area and large internal volume, together with easy surface modification and flexible adjustment of their physical characteristics such as fluidity through the lipid

composition, makes them ideal analytical reagents.[5] For optical detection, typical applied encapsulants are visible or fluorescent dyes such as SRB or carboxyfluorescein. These yield in photometric or fluorescent labels, which have pioneered in several different applications already.[5] With focus on the POCT field, photometric detection however often lacks sensitivity for low concentration biomarkers and is commonly applied in a qualitative way with simple yes/no answers. The emerging interest in monitoring changes of relevant biomarkers rather than conducting single measurements to obtain a more comprehensive picture of what is happening in the human body, impels the POCT field to advance from qualitative to quantitative responses as they offer the indisputable time advantage.[6] This allows doctors a more tailored therapy that ideally causes less side effects and reduces mortality by timely action. Monitoring, *e.g.,* the interleukin 6 values, a prognostic marker for inflammation, allows for early identification of changes in the baseline IL-6 concentration of patients and thus guarantees in-time treatment in case of an acute rise. IL-6 shows a fast response to incipient inflammation and thus allows for fast detection and early treatment.[7]

With fluorescence typically higher sensitivities are achieved but a higher instrumental demand is required for the inevitable detection device. Chemiluminescence (CL) on the contrary is known as highly sensitive detection technique and has been demonstrated to outperform absorbance and fluorescence with regard to sensitivity in several applications.[8] This is mainly attributed to the lower background signal as there is no need for external light sources.[9] Especially advantageous over other detection techniques, is the inherent generation of light through a chemical reaction which additionally allows for a significantly simplified instrumental setup while maintaining high detectability. This is uniquely attractive for the POCT field, as it reduces the overall costs and opens the field to diagnostic markers which can currently only be investigated through advanced laboratory techniques. Yet, a major drawback of chemiluminescence in general is the low quantum yield, that chemiluminescence probes typically have. In the previous chapter we investigated *m*-carboxy luminol, a highly water soluble luminol derivative that additionally exhibits a higher CL quantum yield, with regard to its performance in paper-based POCT applications. We demonstrated not only the simplicity of a CL-based POCT platform using a standard smartphone camera but also the leverage of a stronger emitting CL probe. The increased water solubility of *m*-carboxy luminol permits the successful encapsulation into the hydrophilic interior of liposomes to a high extend. Hence, combining the signal amplification properties of liposomes with chemiluminescence measurements has great potential for an exceptionally sensitive label that can bring POCT to the next level. We developed stable and highly loaded CL liposomes and studied different surface modifications to generate an

flexible and sensitive label. We tested these liposomes in model streptavidin-biotin LFAs and developed a procedure to facilitate CL detection with liposomes on common test strip. We adapted this procedure to evaluate the performance of a highly sensitive POCT detector for quantitative CL measurements on LFAs which has been developed in a parallel approach within this study. We finally tested these liposomes for the detection of interleukin 6 in comparison to our previously studied fluorescence and colorimetric detection particles.

4.2.2. Experimental Section

All chemicals were of commercial HPLC grade or higher and were used without purification.

4.2.2.1. Chemicals and consumables:

Standard chemicals were purchased from Merck. The phospholipids, 1,2-dipalmitoyl-sn-glycero-3-phosphocholine (DPPC), 1,2-dipalmitoyl-sn-glycero-3-phospho-(1′-rac-glycerol) (sodium salt) (DPPG), and 1,2-dipalmitoyl-sn-glycero-3-phosphoethanolamine-N-(glutaryl) (sodium salt) (N-glutaryl-DPPE), 1,2-dipalmitoyl-sn-glycero-3-phosphoethanolamine-N-(biotinyl) (sodium salt) (biotinyl-DPPE) were purchased from Avanti Polar Lipids (Alabaster, AL, USA), *m*-carboxy luminol (purity: 73.597 wt% ± 2.82 wt%) was customized synthesized by Taros Chemicals GmbH & Co. KG, 4-(2-Hydroxyethyl)piperazine-1-ethanesulfonic acid (HEPES, purity >99.5 %), chloroform and methanol were purchased from VWR chemicals, Germany. Milk powder, cholesterol, Sephadex® G 50, sucrose, sodium azide, glycine (purity >99.7 %), sodium hydroxide, sulforhodamine B (230162, 75 %), hemin, TWEEN®20, Whatman Nucleopore™ Track-Etched membranes 1.0 µm, 0.4 µm and 0.2 µm, 19 mm diameter were purchased from Sigma Aldrich/Merck, Germany. Fetal bovine serum (FCS), and human serum (HS) (NB-52-0856) was purchased from Biotrend (Cologne, Germany). Potassium hydrogen carbonate, *n*-octyl-β-D-glucopyranoside (CN23.2), dialysis tube Spectra/Por© 4 (2718.1), 2-(N-morpholino)ethanesulfonic acid (MES), sodium chloride and bovine serum albumin (BSA) (T844.2) was obtained from Carl Roth (Karlsruhe, Germany). Lateral flow test strips, recombinant human IL-6 and anti-IL-6 conjugates were kindly provided by Microcoat Biotechnology GmbH (Bernried, Germany). Synthetic sweat was purchased from synthetic urine e.K., Germany. For all experiments Milli-Q water was used and stock solutions were prepared for hemin (1 mmol L^{-1} in 0.1 mol L^{-1} carbonate buffer, pH 10.5). For H_2O_2 the stock solution (100 mmol L^{-1} in Milli-Q water) was freshly prepared before each measurement. Streptavidin plates (604500) were provided by Microcoat biotechnology GmbH (Bernried, Germany), white and black microtiter plates were

purchased from Greiner BioOne and depending on the experiment high or medium binding plates (655074, 655075, 655076) were applied.

4.2.2.2. Dynamic light scattering and zeta potential

Dynamic light scattering (DLS) and zeta potential measurements were done on a Malvern Zetasizer Nano-ZS (Malvern Panalytical, Germany). For all measurements, the temperature was set to 25 °C. Size determination was done in semi-micro polymethyl methacrylate (PMMA) cuvettes (Brand, Germany), and zeta potential was done in disposable folded capillary zeta cells (Malvern Panalytical, Germany). The liposomes were diluted 1:100 and measured in HSS buffer (10 mmol L^{-1} HEPES, 200 mmol L^{-1} sodium chloride, approximately 200 mmol L^{-1} sucrose, 0.01 wt% sodium azide) with the following settings, refractive index (RI) of the material of 1.34, material absorbance of zero, RI of 1.342 of the dispersant viscosity of 1.1185 mPa s were applied for DLS. For zeta potential a refractive index of 1.342, viscosity of 1.1185 mPa s and a dielectric constant of 78.5 was used. An equilibration time of 60 s was applied before each measurement.

4.2.2.3. Determination of phospholipid concentration through ICP-OES

Phospholipid concentration was determined through inductively coupled plasma optical emission spectrometer (ICP-OES) measurements with a SPECTROBLUE TI/EOP from (SPECTRO Analytical Instruments GmbH, Kleve, Germany). Phosphorous was detected at 177.495 nm and the device calibrated between 0 and 100 µmol L^{-1} phosphorous in 0.5 mol L^{-1} HNO_3. Before each measurement, the device was recalibrated with 0.5 mol L^{-1} HNO_3 and 50 µmol L^{-1} phosphorous. A 1:150 dilution of the liposomes (3 mL) in 0.5 mol L^{-1} HNO_3 was measured.

4.2.2.4. Synthesis of *m*-carboxy luminol liposomes

Anionic liposomes, containing *m*-carboxy luminol, with various surface modifications were prepared according to an established protocol from Mayer *et al.*[4] with adjustments towards the phospholipid composition. First, the respective lipids (**Table 2**) for a 120 µmol total lipid batch were dissolved in 3 mL chloroform and 0.5 mL methanol and thoroughly sonicated in an ultrasonic bath (VWR ultrasonic cleaner, model USC 300 THD) at 60 °C. Subsequently, 2 mL of preheated (60 °C) encapsulant was added to the lipid solution and emulsified for 4 min at 60 °C, using an ultrasonic bath. Encapsulant was previously prepared by dissolving 30 mmol L^{-1} or 75 mmol L^{-1} *m*-carboxy luminol in 4 mL 0.2 mmol L^{-1} HEPES buffer, pH 7.5, including 50 µL and 900 µL 1 mol L^{-1} NaOH, respectively. After emulsification, residual solvent was evaporated at 60 °C under reduced pressure. The remaining 2 mL of

encapsulant were added after the first evaporation step (780 mbar) and thoroughly vortexed before evaporation was continued (400 mbar). The remaining solution was extruded at 60 °C through 1.0 µm, 0.4 µm and finally 0.2 µm membranes to obtain unilamellar liposomes. Purification was first performed by size-exclusion chromatography with Sephadex® G-50 as stationary phase (column size: 2 cm x 8 cm) and outer buffer (glycine-NaOH buffer: (10 mmol L^{-1} glycine, 200 mmol L^{-1} sodium chloride, approximately 100 mmol L^{-1} sucrose or 200 mmol L^{-1}, 0.01 wt% sodium azide), pH 8.6, osmolality approximately 0.52 osmol kg^{-1} (30 mmol L^{-1} encapsulant) or 0.66 osmol kg^{-1} (75 mmol L^{-1} encapsulant)), pH 8.6, osmolality 0.52 osmol kg^{-1} as mobile phase. Additionally, the liposomes were dialyzed overnight against 0.01 mol L^{-1} outer buffer, pH 8.6, osmolality approximately 0.52 osmol kg^{-1} (30 mmol L^{-1} encapsulant) or 0.66 osmol kg^{-1} (75 mmol L^{-1} encapsulant)) in Spectra/Por© 4 dialysis tube (MWCO: 12 – 14 kDa). The were characterized by DLS measurements and zeta potential measurements. The total lipid (tL) concentration was determined by ICP-OES measurements. The results are summarized in **Table 2**.

Similarly, anionic liposomes, containing sulforhodamine B, were synthesized with the following adjustments. Here, the encapsulant was previously prepared by dissolving sulforhodamine B (522.59 mg, 150 mmol L^{-1}) in 4.5 mL 0.02 mmol L^{-1} HEPES buffer, pH 7.5. The remaining solution was extruded at 60 °C through at least 1.0 µm and 0.4 µm membranes. Purification by size-exclusion chromatography utilizes Sephadex® G-50 as stationary phase (column size: 2 cm x 8 cm) and outer buffer (HSS buffer: 10 mmol L^{-1} HEPES, 200 mmol L^{-1} sodium chloride, approximately 200 mmol L^{-1} sucrose, 0.01 wt% sodium azide), pH 7.5, osmolality of approximately 0.64 osmol kg^{-1} as mobile phase. Additionally, the liposomes were dialyzed overnight against outer buffer, pH 7.5, osmolality 0.64 osmol kg^{-1}. Likewise, the liposomes were characterized by DLS measurements and zeta potential measurements. The total lipid (tL) concentration was determined by ICP-OES measurements. The results are summarized in **Table 2**.

Table 1 Characteristics of synthesized anionic liposomes

Lipid composition	Surface	PdI[a]	Size[b] by Int (nm)	Zeta potential (mV)	Total lipid concentration (mmol L^{-1})
Encapsulant: 30 mmol L^{-1} *m*-carboxy luminol[c]					
batch 4 DPPC: 35.3 mol% DPPG: 17.7 mol% Cholesterol: 44.9 mol% biotin: 2.1 mol%	2 mol% biotin	0.08 ± 0.01	149 ± 47	-28.7 ± 1.6	15.27 ± 0.02
batch 2 DPPC: 33.3 mol% DPPG: 16.3 mol% Cholesterol: 42.5 mol% N-glutaryl-DPPE: 7.9 mol%	8 mol% N-glutaryl	0.08 ± 0.01	156 ± 48	-34.9 ± 1.8	15.47 ± 0.02
Encapsulant: 75 mmol L^{-1} *m*-carboxy luminol[c]					
batch 11 DPPC: 35.5 mol% DPPG: 17.4 mol% Cholesterol: 45.0 mol% biotin: 2.1 mol%	2 mol% biotin	0.12 ± 0.1	199 ± 67	-23.1 ± 1.0	8.6 ± 0.1
batch 12 DPPC: 35.4 mol% DPPG: 17.8 mol% Cholesterol: 44.8 mol% biotin: 2.0 mol%	2 mol% biotin	0.08 ± 0.02	164 ± 49	-24.6 ± 1.9	8.55 ± 0.06
batch 13 DPPC: 33.0 mol% DPPG: 16.6 mol% Cholesterol: 42.6 mol% N-glutaryl-DPPE: 7.8 mol%	8 mol% N-glutaryl	0.12 ± 0.01	132 ± 47	-30.6 ± 1.7	16.22 ± 0.07
batch 31 DPPC: 35.5 mol% DPPG: 17.5 mol% Cholesterol: 45.0 mol% N-glutaryl-DPPE: 2.0 mol%	2 mol% biotin	0.08 ± 0.01	113 ± 34	-25.7 ± 1.7	15.73 ± 0.04
batch 29 DPPC: 34.9 mol% DPPG: 17.1 mol% Cholesterol: 44.0 mol% N-glutaryl-DPPE: 4.0 mol%	4 mol% N-glutaryl DPPE	0.08 ± 0.02	125 ± 38	-25.6 ± 0.06	20.31 ± 0.09
batch 32 DPPC: 34.1 mol% DPPG: 16.8 mol% Cholesterol: 43.1 mol% N-glutaryl-DPPE: 6.1 mol%	6 mol% N-glutaryl DPPE	0.09 ± 0.01	116 ± 35	-28.2 ± 2.1	17.19 ± 0.05
batch 30 DPPC: 33.4 mol% DPPG: 16.5 mol% Cholesterol: 42.1 mol% N-glutaryl-DPPE: 8.0 mol%	8 mol% N-glutaryl DPPE	0.08 ± 0.01	111 ± 33	-28.8 ± 1.0	20.5 ± 0.2

Table 2 Characteristics of synthesized anionic liposomes (continued)

Lipid composition	Surface	PdI[a]	Size[b] by Int (nm)	Zeta potential (mV)	Total lipid concentration (mmol L^{-1})
Encapsulant: 150 mmol L^{-1} sulforhodamine B					
CF150[d] DPPC: 35.6 mol% DPPG: 17.8 mol% Cholesterol: 44.6 mol% DPPE-biotin: 2 mol%	2 mol% biotin	0.13 ± 0.01	231 ± 86	-21.4 ± 1.5	12.94 ± 0.03
MC2[c] DPPC: 33.5 mol% DPPG: 17.5 mol% Cholesterol: 43.0 mol% N-glutaryl-DPPE: 6.0 mol%	6 mol% N-glutaryl DPPE	0.07 ± 0.01	204 ± 61	-30.7 ± 1.9	11.69 ± 0.06

[a]PdI: Polydispersity index,[b]size refers to hydrodynamic diameter, [c]final extrusion membrane: 0.2 µm, [d]final extrusion membrane: 0.4 µm

4.2.2.5. Surface modification of liposomes

Protein coupling to the liposomes was done by microcoat biotechnology GmbH according to the following procedure. Streptavidin or anti-IL6 were coupled to the liposome surface by mixing N-glutaryl liposomes with EDC (10 mg mL^{-1} in 0.05 M MES buffer, pH 5.5) and NHS (10 mg mL^{-1} in 0.05 M MES buffer, pH 5.5) and incubation for 1 h at room temperature (RT) while shaking. The respective equivalent of protein (1 mg mL^{-1} in PBS) was added and incubated for 1.5 h at RT while shaking. Lysine-HCl (1 mol L^{-1} in ultrapure water) was added to yield a final concentration of 10 mmol L^{-1} and again incubated for at least 10 min at RT while shaking, to quench the reaction. For streptavidin a coupling ration of 0.23:1 streptavidin to carboxy groups was used. The conjugated liposomes were purified via size exclusion chromatography using Sepharose CL-4B as stationary phase and the respective outer buffer as mobile phase and a flow rate of approximately 0.5 mL min^{-1}. The conjugates were subsequently characterized by optical density (OD), hydrodynamic diameter and zeta potential measurements. Optical density was measured at 565 nm of a 1:100 dilution in demineralized water. Furthermore, the total lipid concentration was determined through ICP-OES.

4.2.2.6. Lateral flow assay procedure

4.2.2.6.1. with biotinylated liposomes

For the simple streptavidin biotin assay, model test strips with a streptavidin control and test line were used. For the proof of principle studies, we used LFAs which in contrary to the typical LFAs contain the same capture molecule on test and control line. The test strip consists of a white backed CN150 nitrocellulose membrane (Sartorius, Göttingen, Germany). The liposomes were diluted in outer synthesis buffer with 1 % (w/v) BSA and

5 µl of the respective dilution was applied to the conjugate pad directly before the LFA was placed in 100 µL outer buffer with 1 % (w/v) BSA. The LFA run was stopped after 5 min and for chemiluminescence detection, the test strips were allowed to dry before they were either cut into pieces for the detection with the Synergy Neo 2 microplate reader (BioTek) or scratched in defined areas for the POCT detector that has been developed within this study and is further referred to as CAU detector. Subsequently, 3 µL 1 mmol L^{-1} hemin in 0.1 mol L^{-1} carbonate buffer, pH 10.5 and 3 µL 1 % (w/v) TWEEN®20 in 0.1 mol L^{-1} carbonate buffer, pH 10.5 were added sequentially and allowed to dry in-between. For the measurements with the Synergy Neo 2 microplate reader (BioTek), test and control line together with a background piece were punched out and placed in a white MTP. After a blank read of the membrane, the CL measurement was directly started after 10 µL 10 mmol L^{-1} H_2O_2 in 0.1 mol L^{-1} carbonate pH 10.5 was added. The CL signal was integrated for 2 s at a read height of 1 mm. For measurement with the CAU detector the relevant areas were isolated by scratching the nitrocellulose membrane from the backing card in the flanking region. These so-called scratched strips were pretreated with hemin and TWEEN®20 similarly to the cut-out pieces if not stated differently. Here, 3 µL 10 mmol L^{-1} H_2O_2 in 0.1 mol L^{-1} carbonate pH 10.5 was added before the measurement was started. Through the customized software, the CL signals was recorded for 60 s after it reached an initial voltage of 0.01 V if not stated differently.

4.2.2.6.2. with anti-IL-6 liposomes

Standardly, the LFA was performed with all reagents in solution according to the following procedure if not stated differently. 36 µL of the respective dilution of recombinant IL-6 in serum and 9 µL serum buffer were mixed with 5 µL detection solution consisting of detection particles and anti-IL-6 IgG-biotin (50 ng per test) and incubated 5 min at RT in a 2 mL reaction vessel prior to application on the test strip. After 15 min, the test strip was evaluated with a flatbed scanner or the Synergy Neo 2 microplate reader (BioTek). The test strip consists of a white backed CN150 nitrocellulose membrane (Sartorius, Göttingen, Germany) with a streptavidin (SA) test line (27 mm) and an anti-mouse IgG control line (36 mm). The LFA with the reagent solution applied on the test strip was done by adding the reagent solution (5 µL detection particles) to the overlap of the sample and conjugate pad and placing it directly into 45 µL IL-6 dilution including 9 µL serum buffer. Again, the LFA was allowed to run for 15 min and was evaluated directly after the test run or allowed to dry before lysis with 3 µL absolute ethanol for fluorescence evaluation or 1 % (w/v) TWEEN®20 in 0.1 mol L^{-1} carbonate buffer, pH 10.5 for chemiluminescence detection. The CL intensity was recorded with the Synergy Neo 2 microplate reader

(BioTek) after the LFA was cut into background, test and control line and 10 µL 10 mmol L^{-1} H_2O_2 in 0.1 mol L^{-1} carbonate pH 10.5 was added. CL was measured for 2 s at read height 1 mm. Fluorescence was determined through an area scan of the cuts with 49 x 49 data points at a read height of 4.5 mm and with λ_{ex} = 530 nm, bp 10 and λ_{em} = 590 nm, bp 10. The fluorescence intensity was subsequently determined with Image J by converting the data point matrix into an image and subsequent evaluation of the areas of interest (1444 square pixel) by intensity measurements with Image J Fiji.

4.2.2.7. Competitive biotin assay

For the competitive biotin assay, a MTP was coated with BSA-biotin and 100 µL respective biotin dilution including StAv-modified liposomes (10 µmol L^{-1} total lipid concentration) in outer buffer were incubated for 1 h at room temperature while constant shaking before the final lysis of the liposomes. Specifically, 200 µL of 1 µg mL^{-1} BSA-biotin in carbonate-borate buffer (80 mmol L^{-1} Na_2CO_3 and 100 mmol L^{-1} H_3BO_3, pH 9.4) was added to the MTP and incubated overnight at 4 °C. Subsequently, the plate was washed 3-times with 200 µL 1X PBS (137 mmol L^{-1} NaCl, 2.7 mmol L^{-1} KCl, 10 mmol L^{-1} sodium phosphate dibasic, 1.8 mmol L^{-1} potassium phosphate monobasic, pH 7.4), 0.05 wt.-% Tween®20, for 5 min while shaking before blocking for 1 h with 200 µL blocking solution (1% BSA in 1X PBS, 0.05% Tween®20, pH 7.4) at room temperature and 300 rpm. Following the blocking, the plate was washed 3-times with 200 µL outer buffer pH 8.6 for 5 min while shaking before 100 µL liposomes (c(tL) = 10 µmol L^{-1})/biotin dilution in outer buffer was added and incubated for 1 h at room temperature. Finally, the plate was washed 3-times with 200 µL CBS buffer before the liposomes were lysed for 5 min while shaking with 100 µL 30 mmol L^{-1} OG in CBS. The chemiluminescence (CL) intensity was measured with 50 µL 40 mmol L^{-1} H_2O_2 and 50 µL 40 µmol L^{-1} hemin in CBS, pH 10.5 and gain 80, read height (RH) 1 mm and integration time (IT) 2 s. All measurement were done at 25 °C.

4.2.2.8. Performance and stability test

The liposomes were stored at 4 °C in the dark with c(tL) > 8 mmol L^{-1}. For the performance test, liposomes were diluted to c(tL) = 8.4 µmol L^{-1} in CBS buffer to measure the CL signal for intact liposomes and diluted in 30 mmol L^{-1} OG/CBS to measure the lysed CL signal. The liposome dilution contained in addition 2 µmol L^{-1} hemin. 100 µL of liposome dilution was first measured as blank read. After H_2O_2 was added and 5 s shaking (425 cpm), the CL intensity was measured at gain 80, RH 1 mm and IT 2 s. CL measurements were recorded with a microplate reader (Synergy Neo 2, BioTek). All measurement were done at

25 °C. The free dye was calculated according to (1) and the leakage was calculated according to (2) for each stability measurement:

$$\boldsymbol{free\ dye}\ (\%) = \frac{\boldsymbol{I_{intact\ liposomes}} \times \mathbf{100}}{\boldsymbol{I_{lysed\ liposomes}}} \quad (1)$$

with

$I_{intact\ liposomes}$: CL signal of intact liposomes

$I_{lysed\ liposomes}$: CL signal of lysed liposomes

$$\boldsymbol{leakage}\ (\%) = \boldsymbol{free\ dye_n} - \boldsymbol{free\ dye_0} \quad (2)$$

with

free dye$_0$: percentage of free dye at day 0

free dye$_n$: percentage of free dye at day of stability test

4.2.2.9. Apparatus

CL and fluorescence measurements were performed with a Synergy Neo 2 microplate reader from BioTek (Bad Friedrichshall, Germany) either in endpoint mode (CL measurement) or as area scan (fluorescence measurements). For CL measurements in POCT format the customized POCT detector[10] from Chung Ang University was used. For colorimetric evaluation a standard flatbed scanner (Tevion, P91010 (MD90093)).

4.2.3. Results and Discussion

4.2.3.1. Development of functionalized, stable and highly loaded reporter liposomes

Introducing CL liposomes to LFAs, inaugurated several avenues of investigation. A fundamental part of this project was to refine the reporter probe itself, besides integrating CL liposomes in a user-friendly LFA format, optimizing the immunoassay and establishing a suitable detection procedure. The ideal label in this context shows high dye loading, low non-specific binding or interaction with the various pad materials, high stability especially towards dehydration procedures and minimal batch to batch variation. Based on the results from chapter 4.1, large liposomes are the most promising candidates when optimizing towards high sensitivity due to the increased dye load. Yet, further optimization is required so that the liposomes tolerate the dehydration process. Hence within this line of research both, large and small liposomes, were initially considered. However, contrary to the previous findings with sulforhodamine B (SRB) containing liposomes, the synthesis of large liposomes by extrusion only through the 1 µm membrane was not straightforward. With

m-carboxy luminol as encapsulant, the difference in the hydrodynamic diameter when extrusion is only performed through the 1 µm membrane was less pronounced than for SRB liposomes and hence, requires more thorough investigation in the future. The following studies were thus limited to the investigation of the small liposomes which have been extruded through 1 µm, 0.4 µm and 0.2 µm during the synthesis. Initially the newly synthesized liposomes were tested towards their overall stability and fully characterized. The liposomes applied in this study expose either biotin or glutaryl groups on the surface. To evaluate the effect of varying coupling conditions, liposomes with varying N-glutaryl DPPE were synthesized, coupled with streptavidin as model protein and anti-interleukin 6 and tested in an LFA. In a parallel approach, the overall performance of the optimized liposomes in the LFA format was evaluated with a simple streptavidin biotin assay using biotin-modified liposomes. In the same way, the performance of the POCT detector was investigated, which has been developed for CL-based LFA analysis within the scope of this project.

4.2.3.1.1. Characteristics of the developed liposomes

Here, model anionic liposomes with 30 and 75 mmol L^{-1} *m*-carboxy luminol, approximately 45 mol% cholesterol and 2 mol% biotin were synthesized and characterized, together with the liposomes containing N-glutaryl DPPE for post modification. The hydrodynamic diameter, zeta potential, polydispersity index (PdI) and the total lipid (tL) concentration of these liposomes are listed in **Table 2**. Considering the variations in the lipid composition and the encapsulant concentration the synthesis of the CL liposomes is very stable and reproduceable. This is further validated by batch 11 and batch 12, which do not exhibit significant batch to batch variation within the error of the measurements (**Table 3**) but show double the signal compared to batch 4 with a lower encapsulant concentration. Additionally, a dilution series with batch 4, batch 11 and batch 12 was conducted and resulted in lower limits of detection (LOD) for batch 11 (LOD: 8 pmol L^{-1}) and batch 12 (LOD: 5 pmol L^{-1}) compared to batch 4 (LOD: 13 pmol L^{-1}). This gives a first indication that the high encapsulant liposomes can assist in improving the LOD of future assays.

Table 3 Comparison of signal intensity of *m*-carboxy luminol with 2 mol% biotin with high and low encapsulant concentration

liposome batch	encapsulant concentration	CL signal intact liposomes (× 10^4 RLU)	CL signal lysed liposomes (× 10^4 RLU)
batch 4	30 mmol L^{-1}	3.36 ± 0.03	127 ± 2
batch 11	75 mmol L^{-1}	1.89 ± 0.09	278 ± 20
batch 12	75 mmol L^{-1}	3.74 ± 0.08	259 ± 6

RLU: relative luminescence units, batch 4: 30 mmol L^{-1} *m*-carboxy luminol liposomes with 2 mol % biotin, batch 11 and 12: 75 mmol L^{-1} *m*-carboxy luminol liposomes with 2 mol % biotin

4.2.3.1.2. Performance of high load chemiluminescence liposomes

The LODs for the 75 mmol L^{-1} *m*-carboxy luminol liposomes (LOD: 8 pmol L^{-1}), that have been determined by the dilution series in the previous chapter (4.2.4.1.1.), were benchmarked to 150 mmol L^{-1} SRB liposomes (LOD: 43 pmol L^{-1}) and 30 mmol L^{-1} *m*-carboxy luminol liposomes (LOD: 13 pmol L^{-1}). Furthermore, additional calibrations were done in buffer, milk synthetic sweat, fetal bovine serum and human serum to simultaneously evaluate the matrix effect on the different detection techniques for the 75 mmol L^{-1} *m*-carboxy luminol liposomes and 150 mmol L^{-1} SRB liposomes (**Table 4**). These matrices represent typical matrices in bioanalysis. Even though the 75 mmol L^{-1} CL liposomes contain less dye encapsulated compared to the fluorescent liposomes, they excel with an LOD that is over 7-times lower compared to the fluorescent liposomes (**Table 4**) when measured in outer buffer or synthetic sweat.

Table 4 Matrix effect on chemiluminescence and fluorescence signal

Matrix[a]	$LOD_{CL\ liposomes}$ (pmol L^{-1})	$LOD_{FL\ liposomes}$ (pmol L^{-1})
outer synthesis buffer	8	59
fetal calf serum	96	515
human serum	510	105
milk	458	300
synthetic sweat	3	70

LOD: limit of detection, CL-liposomes: chemiluminescence liposomes, FL-liposomes: fluorescence liposomes, [a]the matrix measurements were performed by using 10 % (v/v) of the respective matrix in the final reaction mix

Yet, when measured in matrices that contain radical scavengers such as serum[11] or milk[12], the chemiluminescence is quenched which consequently increases the LOD (**Figure 1 A**, **Table 4**). Whereas an LOD for fetal bovine serum (FBS) remains at 0.1 nmol L^{-1} when

increasing the matrix content from 10 % (v/v) to 50 % (v/v), for milk the LOD drastically increases from 458 pmol L^{-1} to 138 nmol L^{-1} (**Figure 1 B**). This illustrates the antioxidant capacity of milk and its effect on a radical based detection mechanism and needs to be considered in a final assay.

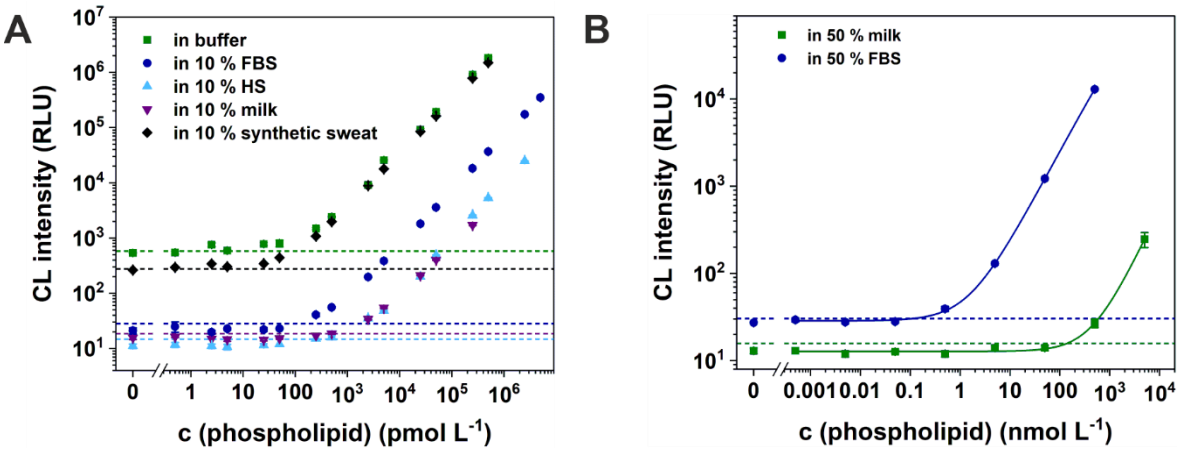

Figure 1 Dilution series of chemiluminescent and fluorescence liposomes to determine the limit of detection (dashed line), with A) illustrating the chemiluminescence liposomes in outer buffer, 10 %(v/v) fetal bovine serum, 10 %(v/v) milk, 10 %(v/v) synthetic sweat and 10 %(v/v) human serum including 30 mmol L^{-1} OG, B) illustrates the chemiluminescence liposomes in outer buffer, 50 %(v/v) fetal bovine serum and 50 %(v/v) milk including 30 mmol L^{-1} OG. Chemiluminescence measurement were recorded with gain 100, RH 1 mm, IT 2 s and at 25 °C, data are presented as mean ± SD, n = 3

4.2.3.1.3. Stability of new liposome formulations

Furthermore, the CL performance and thus the stability of the synthesized liposomes was monitored for approximately a year (**Figure 2**). Here, 30 and 75 mmol L^{-1} *m*-carboxy luminol liposomes which contain 2 mol% biotin and 75 mmol L^{-1} *m*-carboxy luminol liposomes which contain 8 mol% N-glutaryl DPPE were studied as representatives. Here, the stability of the new liposomes was studied when changing the encapsulant, its concentration and the lipid composition. As expected, the tested liposomes remained stable for at least 9 - 12 months with leakage values below 2 % and the adjusted encapsulant, as well as the integration of N-glutaryl DPPE does not negatively affect the stability of the liposomes.

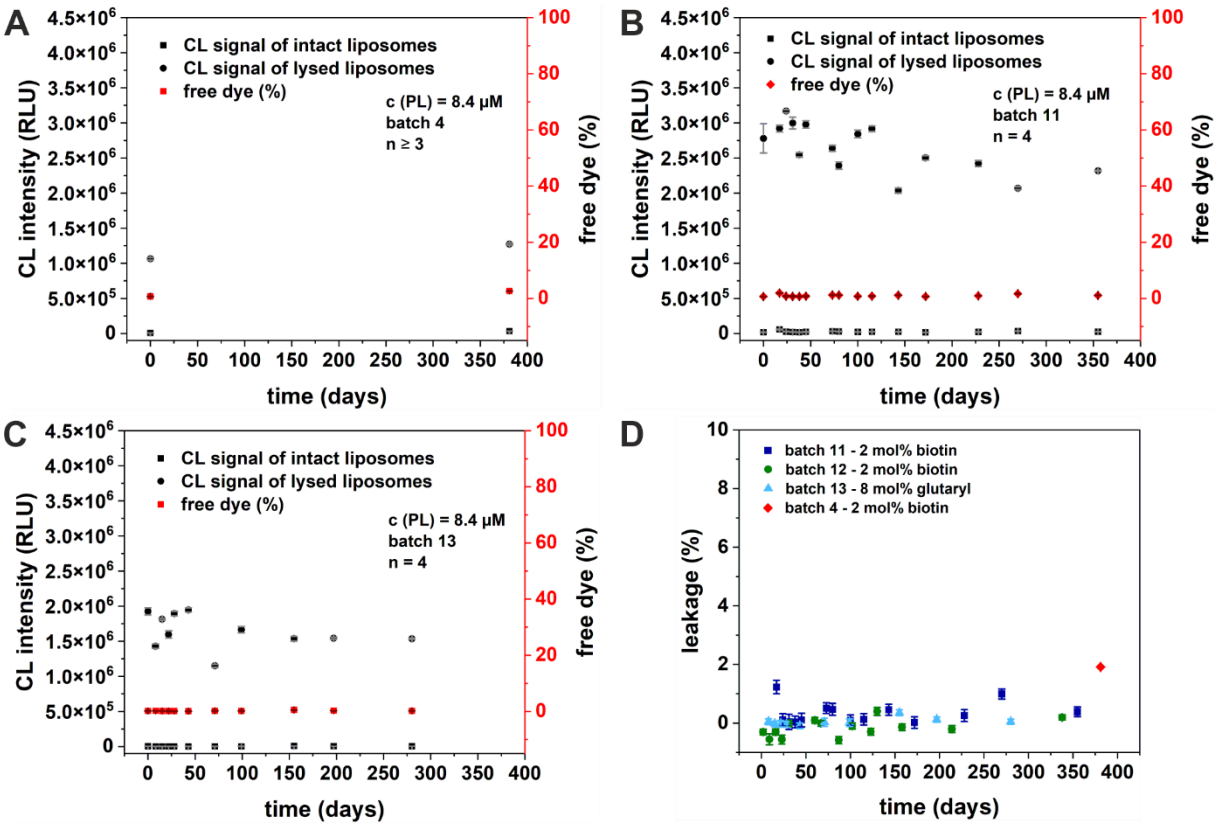

Figure 2 Stability study of A) 30 mmol L^{-1} *m*-carboxy luminol liposomes with 2 mol% biotin, B) 75 mmol L^{-1} *m*-carboxy luminol liposomes with 2 mol% biotin, C) 75 mmol L^{-1} *m*-carboxy luminol liposomes with 8 mol% N-glutaryl DPPE and D) dye leakage. Chemiluminescence measurement was performed by dilution of liposomes to c(PL) = 8.4 µmol L^{-1} either in CBS buffer or 30 mmol L^{-1} OG/CBS buffer including 2 µmol L^{-1} hemin. 100 µL of each liposome dilution was reacted with 100 µL 4 mmol L^{-1} H_2O_2 and measured first without H_2O_2 and after 5 s shaking with H_2O_2 with following settings: integration time 2 s, gain 80, read height 1 mm, data are presented as mean ± SD, n ≥ 4

4.2.3.1.4. Characterization of the liposomes with varying N-glutaryl DPPE content

Liposomes with 75 mmol L^{-1} *m*-carboxy luminol and 2 mol% to 8 mol% N-glutaryl DPPE content were tested. First, the liposomes were diluted to 10 µmol L^{-1} total lipid content and the CL signal was recorded upon lysis. The liposomes with 6 mol% (100 %) show the highest CL intensity followed by 4 mol% (99.6 %) and 8 mol% N-glutaryl DPPE (87.9 %). The liposomes with 2 mol% N-glutaryl DPPE show only 70 % of the CL signal of the value, obtained with the 6 mol% N-glutaryl liposomes. This indicates a slight variation in the encapsulation efficiency with varying lipid composition.

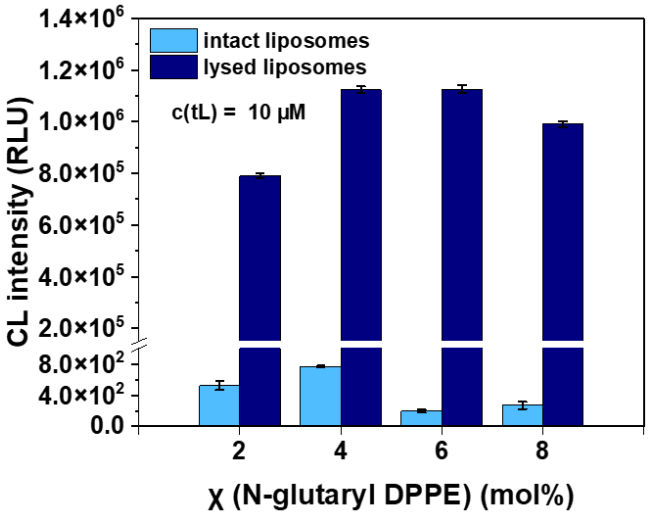

Figure 3 Chemiluminescence intensity of intact and lysed liposomes in CBS and CBS with 30 mmol L^{-1} OG buffer, respectively. Chemiluminescence measurement were recorded with gain 80, RH 1 mm, IT 2 s and at 25 °C, c(tL) = 10 µmol L^{-1}, data are presented as mean ± SD, n = 4

These liposomes were coupled initially to streptavidin to determine adequate coupling conditions and characterized before and after coupling (**Table 5**). The total lipid concentration was measured via ICP-OES.

Table 5 Characteristics of *m*-carboxy luminol liposomes before and after coupling measured by microcoat biotechnology GmbH

lipid composition	**Surface**	**Size** before coupling **(nm)**	**Size** after coupling **(nm)**	**Zeta potential** before coupling **(mV)**	**Zeta potential** after coupling **(mV)**
batch 31 DPPC: 35.5 mol% DPPG: 17.5 mol% Cholesterol: 45.0 mol% N-glutaryl-DPPE: 2.0 mol%	2 mol% N-glutaryl DPPE	111.9	144.8	-45	-27.8
batch 29 DPPC: 34.9 mol% DPPG: 17.1 mol% Cholesterol: 44.0 mol% N-glutaryl-DPPE: 4.0 mol%	4 mol% N-glutaryl DPPE	123	145.8	-49.6	-31.4
batch 32 DPPC: 34.1 mol% DPPG: 16.8 mol% Cholesterol: 43.1 mol% N-glutaryl-DPPE: 6.1 mol%	6 mol% N-glutaryl DPPE	115.9	124.9	-42.3	-32.9
batch 30 DPPC: 33.4 mol% DPPG: 16.5 mol% Cholesterol: 42.1 mol% N-glutaryl-DPPE: 8.0 mol%	8 mol% N-glutaryl DPPE	111.4	142	-48.1	-23

All liposomes, show a reduction in the zeta potential after the protein coupling and an increase in the hydrodynamic diameter, which is a first indication for successful coupling.

4.2.3.2. Optimization of surface functionalization through protein coupling and performance on LFA

To further validate the successful coupling of streptavidin a binding assay to a BSA-biotin modified MTP was conducted (**Figure 4 A**). Additionally, a competitive binding assay was performed to estimate the surface coverage of the liposomes with streptavidin (**Figure 4 B**).

4.2.3.2.1. Binding behavior of streptavidin-modified *m*-carboxy luminol liposomes in MTP

For the binding assay, varying liposome concentrations were bound to a BSA-biotin modified MTP (**Figure 4 A**) and at 40 µmol L^{-1} total lipids the 4 mol% and 6 mol% N-glutaryl DPPE modified liposomes yield the strongest CL signal. This indicates better immobilization compared to the liposomes with 8 mol% and 2 mol% N-glutaryl DPPE. In the competitive biotin assay the streptavidin liposomes were mixed with free biotin and incubated on a BSA-biotin MTP. The EC_{50} was used to estimate the streptavidin coverage. Assuming that the N-glutaryl DPPE is fully integrated into the liposome bilayer membrane, an increasing amount of N-glutaryl DPPE would yield a higher amount of carboxy groups on the surface to which a streptavidin molecule can be coupled. With an higher number of streptavidin molecules on the surface a higher amount of free biotin is required to successfully compete with the immobilized biotin. Indeed, with increasing N-glutaryl DPPE amount we observed an increase in the EC_{50} value (**Figure 4 B**, **Table 6**).

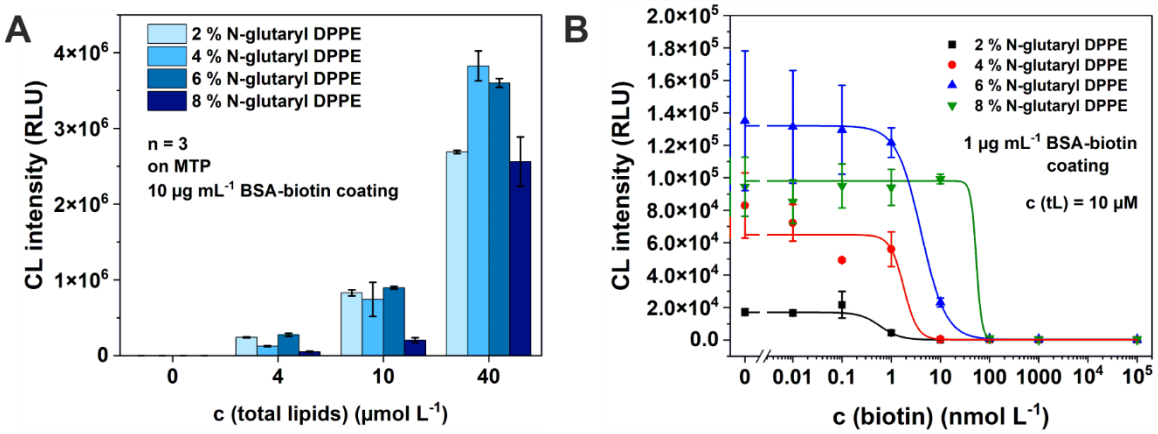

Figure 4 Binding study of streptavidin-modified liposomes A) streptavidin-biotin interaction with varying total lipid concentrations with liposome binding overnight and B) competitive biotin assay with 1 h liposome binding. Chemiluminescence measurement were recorded with gain 80, RH 1 mm, IT 2 s and at 25 °C, data are presented as mean ± SD, n = 3

This confirms that with higher N-glutaryl DPPE content more streptavidin can be coupled to the liposomes. However, a maximum of effective streptavidin on the surface is reached at 6 mol% N-glutaryl DPPE. Exceeding this amount, probably steric hindrance prevents more

efficient immobilization which is indicated by the upper asymptote value reaching its maximum at 6 mol% N-glutaryl DPPE (**Table 6**). Furthermore, the decreased CL signal in the binding experiment (**Figure 4 A**) for 8 mol% N-glutaryl DPPE for each liposome concentration supports this conclusion.

Table 6 Results of competitive biotin assay using liposomes with varying N-glutaryl DPPE content

N-glutaryl DPPE content	upper Asymptote ($\times 10^4$ RLU)	EC_{50} (nmol L^{-1})
2 mol%	1.71 ± 0.07	0.60
4 mol%	6.5 ± 0.7	1.8
6 mol%	13.2 ± 0.8	4.1
8 mol%	9.8 ± 0.4	54

4.2.3.2.2. Binding behavior of streptavidin-modified liposomes in an LFA format

Similarly, to the experiment in the MTP, the binding behavior as a function of the N-glutaryl DPPE content was tested in an LFA. The streptavidin liposomes were applied to the test strips with biotin-modified test and control lines. Here, BSA and BSA/TWEEN®20 blocked nitrocellulose membranes were used besides the standard nitrocellulose membrane to investigate their effect with regard to non-specific binding and the lipid composition. Here, the liposomes were applied to the conjugate pad and washed across the membrane with outer synthesis buffer including 1 % BSA. Liposomes with 6 mol% N-glutaryl DPPE showed the strongest CL signal, independent of the applied membrane (**Figure 5 A**, green). The signal-to-noise (S/N) ratios (**Figure 5 A**, blue), show that without preblocking of the membrane the measurements were prone to errors for all four N-glutaryl DPPE contents. Still, a slight trend towards 4 mol% and 6 mol% N-glutaryl DPPE with the highest S/N ratio was obtained for the untreated nitrocellulose membrane, however due to the high standard deviation, which is significantly influenced by the strong variation in the background measurement (**Figure 5 B**), no final statement can be made and further investigation is necessary. Less error prone, but a similar trend was observed when applying the BSA/TWEEN®20 preblocked membranes but with considerably lower overall S/N ratios. Here, 4 mol% and 6 mol% appear to work best. Although the background signal rises with increasing the N-glutaryl DPPE content from 4 mol% to 6 mol%, the test line signal doubles as well. With BSA preblocked membranes 6 mol% N-glutaryl DPPE liposomes clearly show the best S/N ratio. Overall, a trend towards 6 mol% N-glutaryl DPPE content was obtained. These liposomes show the best binding abilities in the MTP as well as in the LFA

experiment. A clear and significant improvement of non-specific binding of the liposomes to the nitrocellulose membrane with the preblocking of membranes, however, was not obtained.

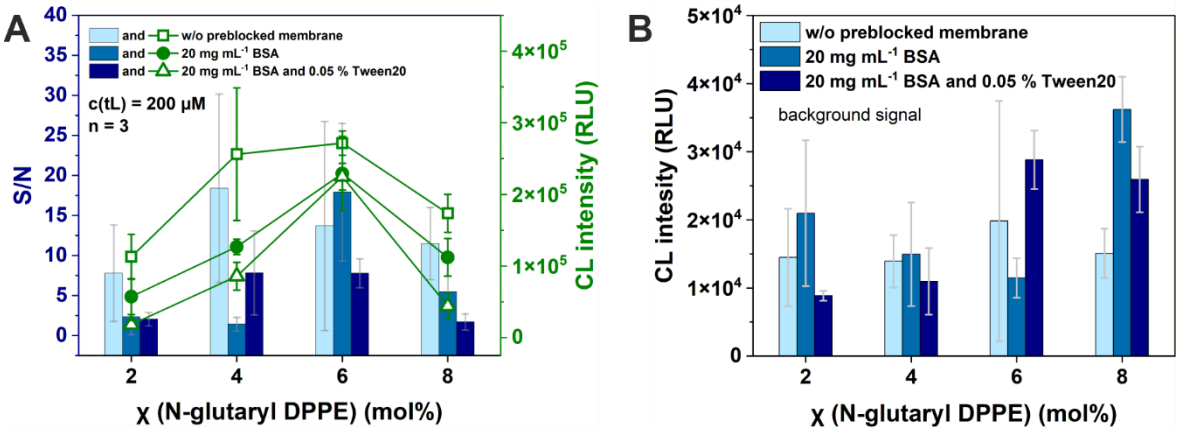

Figure 5 Comparison of preblocked membranes with streptavidin-modified 75 mmol L^{-1} *m*-carboxy luminol liposomes with varying N-glutaryl DPPE content in a streptavidin-biotin LFA using outer synthesis buffer with 1 % BSA. A) illustrates the obtained signal-to-noise ratios for the tested liposomes together with the absolute CL signals, B) illustrates the obtained background signal for each liposome type on the pretreated LFAs. Chemiluminescence was measured using 3 µL 1 mmol L^{-1} hemin and 3 µL 1 % Tween20 and 10 µL 10 mmol L^{-1} H_2O_2 all in 0.1 M carbonate buffer and was recorded with **gain 70**, RH 1 mm, IT 2s and at 25 °C, 3 µL ethanol, 4 µL 0.25 M hemin and 100 µL 10 mmol L^{-1} H_2O_2 in 0.1 M carbonate buffer, data are presented as mean ± SD, n = 3

4.2.3.3. IL-6 assay

In parallel, the CL liposomes were applied for the detection of interleukin 6 (IL-6), an inflammatory biomarker that is typically present in low concentration in human serum and rises when an inflammation is developed in the body.[13] Typical baseline concentrations of IL-6 in healthy people are <10 pg mL^{-1}, values above this threshold are considered as indication of inflammation.[13] We showed in the previous chapter that IL-6 detection with large sulforhodamine B liposomes already outperforms standardly used gold nanoparticles (AuNP) as label, when detected photometrically in undiluted human serum (chapter 4.1). Furthermore, we showed that by changing to fluorescent detection this offers an even greater potential to increase the sensitivity due to the significantly gain in signal intensity. However, we also obtained a strong increase in the background signal, that is most likely cause by two events. Firstly, non-specifically bound liposomes can now be detected more sensitively due to the higher sensitivity of the detection method and the release from the liposome itself. Secondly, autofluorescence and scattering of the applied membrane material or the matrix can interfere with the actual signal.[14] Hence, we tested in tandem our chemiluminescence liposomes within this assay, due to its special feature to emit light without external excitation. Hence, no, or only minimal straylight is expected and thus higher S/N ratios and higher sensitivities are envisioned. Similarly, the anti-interleukin 6 was

covalently coupled to the liposome surface and the LFA was conducted in a sandwich assay format. Contrary, to the detection in the previous chapter and to minimize variations due to different detection devices and their built-in components, we switched from a commercial LFA reader to a benchtop MTP reader for fluorescence and chemiluminescence measurements and a benchtop scanner for colorimetric detection. As these detection devices are not primarily intended for LFA readouts, overall higher LOD were obtained and thus should be considered as relative key figures rather than absolute LODs. For the CL and FL measurements, we punched out the background as well as the test and control line area and lysed the liposomes before the measurement, to release the encapsulated dye for analysis. Thus, we were able to compare the background fluorescence of the membrane with the actual responses. We applied sulforhodamine B (SRB) liposomes with 6 mol % and chemiluminescence liposomes with 8 mol % N-glutaryl content together with commercial gold nanoparticles and compared their overall performance (**Figure 6 A**). As expected, the fluorescence approach shows an significantly reduced S/N ratios compared to the CL approach (**Figure 6 B**). Yet, considering the sensitivity, fluorescence and chemiluminescence detection yield in similar LODs ($LOD_{CL\ liposomes}$: 0.1 ng mL^{-1}, $LOD_{SRB\ liposomes(FL)}$: 0.1 ng mL^{-1}), whereas the colorimetric approaches show higher LODs ($LOD_{gold\ nanoparticles}$: 1.5 ng mL^{-1}, $LOD_{SRB\ liposomes\ (Col)}$: 0.2 ng mL^{-1}). Surprisingly, the LOD difference between the colorimetric detection of the SRB liposomes and the fluorescence detection is not large and at higher concentration the S/N ratios obtained with the colorimetric detection is significantly better compared to the fluorescence approach. We assume that this is an effect of the limited sensitivity of the benchtop scanner, that is not able to detect the non-specifically bound liposomes on the background area which works in favor of the determined S/N ratio.

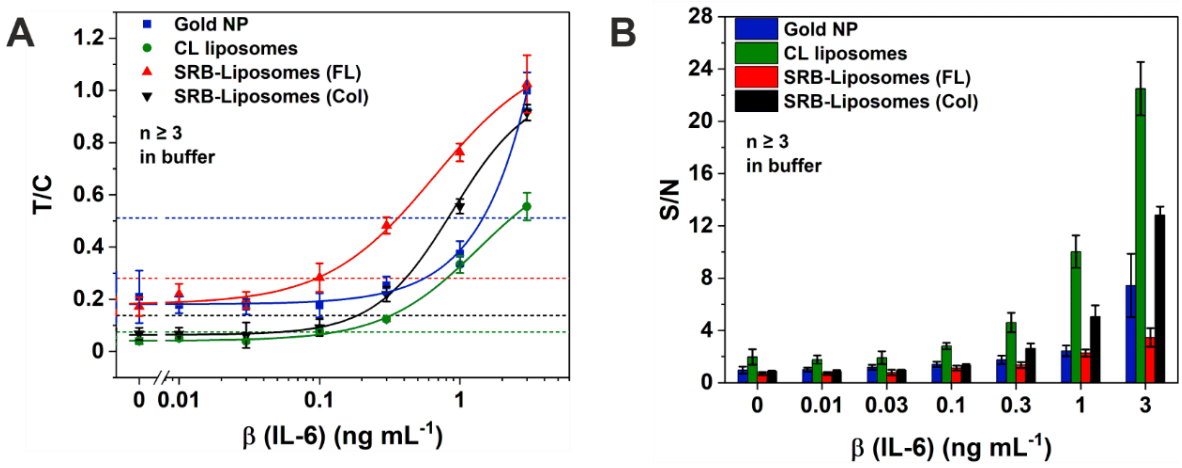

Figure 6 Comparison of different labels and detection techniques within a lateral flow assay (LFA) for the detection of Interleukin-6. A) illustrates the dose-response curve of the normalized test line signals using the control line as internal control and B) shows the signal-to-noise ratio for the IL-6 assay with comparison of the test line to background signal (S/N). The LFAs were conducted with similar procedure including an additional washing step and liposomes were applied with c(PL) = 200 µmol L^{-1}, the gold nanoparticles were used in a concentration of 8 OD mL^{-1}. The 30 mmol L^{-1} *m*-carboxy luminol liposomes were lysed with 3 µL 1 % (w/v) TWEEN®20 before the chemiluminescence (CL) reaction was initiated with 2 µL 1 mmol L^{-1} hemin and 3 µL 10 mmol L^{-1} H_2O_2. CL signal was integrated for 2 s (RH 1 mm), gain 100. The sulforhodamine B liposomes were measured in the fluorescence mode after lysis and colorimetrically before lysis. Fluorescence measurement was performed by an area scan of the respective lines (49 × 49 matrix) with λ_{ex} = 530 nm (10 nm), λ_{em} = 590 nm (10 nm) and subsequently evaluated with ImageJ Fiji. Colorimetric measurements were performed by taking an image and subsequent evaluation with Image J Fiji. As fitting function, the four-parameter logistic fit from OriginLab 2020 was applied, data is represented as mean ± SD, the dashed lines in A) indicates the limit of detection, n ≥ 3

Considering, that substantially more dye is encapsulated in the SRB liposomes (150 mmol L^{-1}) and that the 6 mol% N-glutaryl DPPE lipid composition was used, which were determined to bind more efficiently, these results are very promising for the CL approach. The 75 mmol L^{-1} *m*-carboxy luminol liposomes could even further improve the LOD in the future. First experiment, however, showed already higher background signals, which indicated non-specific binding of the liposomes to the membrane. Hence, further optimization of the LFA is needed before a true improvement of CL over FL can be obtained and the non-specific binding of the liposomes to the membrane needs to be addressed first.

When switching from buffer conditions to human serum we obtained a significant increase of the background signal for the fluorescence approach when measuring in human serum (**Figure 7**). This increase is either caused by the autofluorescence of human serum itself[15] or by the enhanced fluorescence of SRB in human serum[16] together with non-specifically bound liposomes. This fluorescence enhancement of SRB in human serum was previously observed in solution (**chapter 4.1**, **Figure S 3**). Interestingly, it was not obtained on LFAs when the fluorescence was measure with a commercial LFA reader (**Figure S 4**). On the contrary to the LFA reader, the recording in this experiment was done by an area scan of the cut-out pieces of the LFA allowing the conversion of the data into an image (**Figure 7**)

to visualize the important areas of the LFA. Non-specific binding of the liposomes to the nitrocellulose membrane was obtained in buffer and serum (**Figure 7,** background). They yield a significantly smaller signal in buffer than in human serum at equal assay conditions. Although it seems at first that fluorescence enhancement of SRB in human serum causes this difference, the intensity values of the control line signals remain similar in intensity to the experiment in buffer. With the previous data using the LFA reader, this would rather support the observation of autofluorescence of human serum. Yet, it should be noted, that in both cases the LFAs were washed with buffer after the actual run to remove the matrix from the LFA before the measurement. For a definite answer, on the nature of the increased background signal, a more thorough study is needed, but was not the primary focus in this work. The important finding here was, that when using fluorescence detection, the overall S/N ratio was strongly decreased due to the increased background signal in human serum.

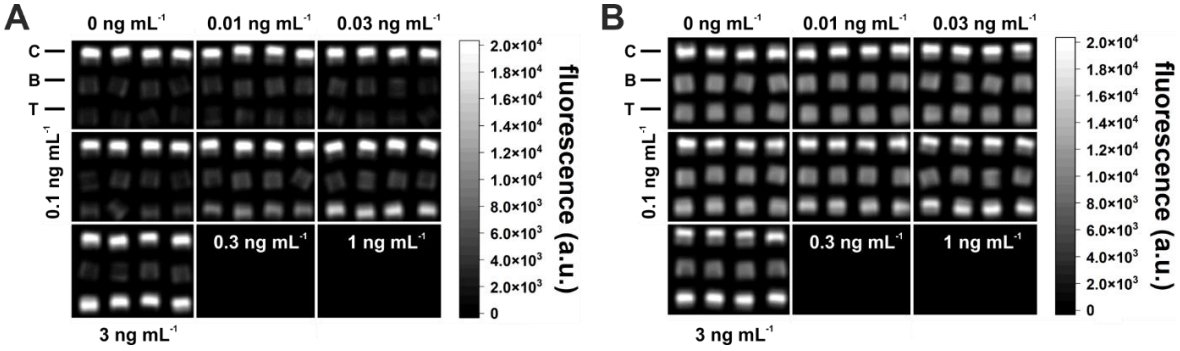

Figure 7 Images of the cut lateral flow assays (LFA) for the detection of Interleukin-6 at different concentrations (0 – 3 ng mL^{-1}). In A) the LFA was performed in running buffer whereas in B) the LFA was performed in human serum. Fluorescence measurement was performed by an area scan of the respective lines (49 × 49 matrix) with λ_{ex} = 530 nm (10 nm), λ_{em} = 590 nm (10 nm) and subsequently evaluated with ImageJ Fiji, C equal control line, B equals background and T equals test line area, (n = 4)

Using CL as detection technique allows signal generation in the absence of an external light source avoiding interferences by autofluorescence and thus non-specific background signals. Unfortunately, detecting the CL liposomes in human serum, yielded in an overall reduced signal response due to radical scavengers in the matrix, inhibiting the chemiluminescence reaction. This is in accordance with the experiments in solution (**Figure 1**) but less apparent on the LFA. These findings express the need of further optimizations to guarantee successful CL detection in real samples for future application with high sensitivity.

4.2.3.4. Comparison of high and low encapsulant chemiluminescence liposomes in a lateral flow assay

Within this study, liposomes with low (30 mmol L^{-1} *m*-carboxy luminol) and high (75 mmol L^{-1} *m*-carboxy luminol) encapsulant concentration were developed. In the

following, biotinylated high and low encapsulant liposomes were investigated with regard to their performance in a simple streptavidin-biotin LFA by using the Synergy Neo 2 microplate reader (BioTek) to detect the CL intensity. Here, the liposomes were applied to the conjugate pad and allowed to run along the membrane with 1 % BSA in outer liposome buffer (pH 8.6) (**Figure 9 A and B**). Subsequently, the respective areas were punched out the LFA strip before the measurement. Here, we invented an adaptor for a benchtop press to reproducibly punch out membrane pieces with the same size (**Figure 8**).

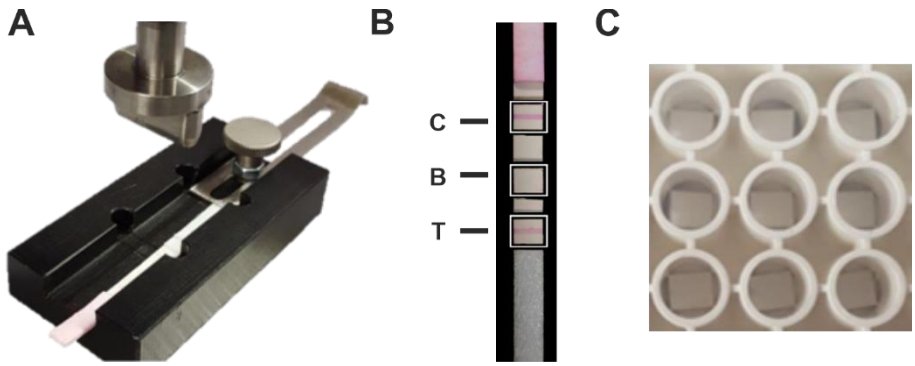

Figure 8 LFA preparation for chemiluminescence detection with Synergy Neo 2 microplate reader (BioTek). In A) the adaptor for the benchtop press is depicted consisting of a puncher and a counter plate, in B) the LFA after the punching process is shown with sulforhodamine liposomes to visualize the test (T) and control (C) line on the LFA and the respective background (B) piece and in C) the positioning of the punched out 4 × 5 mm nitrocellulose membranes pieces into a white 96-well microtiter plate is shown

We conducted a dilution series of both liposome types and recorded the background signal together with the test and control line signal. At a phospholipid concentration of 400 µmol L^{-1}, the S/N ratio was improved by a factor of 2.3 (**Figure 9 C**) which results in a reduced limit of detection (LOD). The limit of detections were approximated from the dose-response curve and equal the concentration that yields a signal on the test and control line larger than $mean_{background}$ + 3 × standard deviation of the background ($SD_{background}$). For the high encapsulant liposomes an LOD of 4 µmol L^{-1} (**Figure 9 B**) was obtained, whereas the LOD for the low encapsulant liposomes was at approximately 8 µmol L^{-1} phospholipid concentration (**Figure 9 A**).

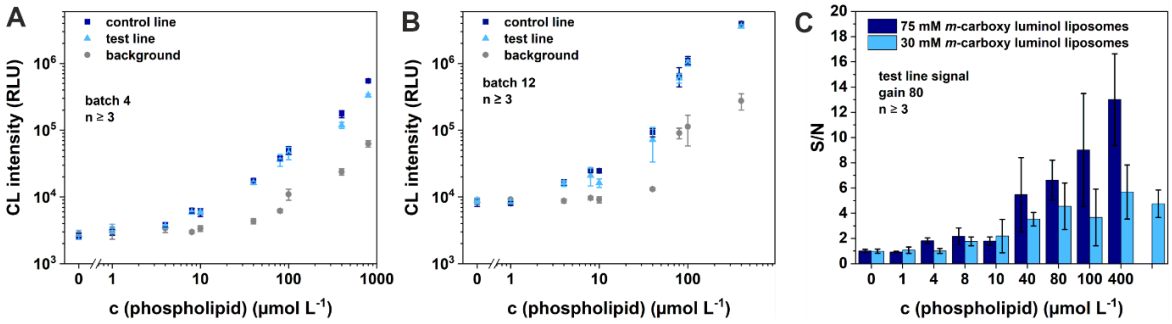

Figure 9. Performance of (A) 30 mmol L^{-1} *m*-carboxy luminol liposomes and (B) 75 mmol L^{-1} *m*-carboxy luminol liposomes within an LFA format, dose-response curve of liposomes in a streptavidin-biotin assay, (C) illustrates the obtained signal-to-noise ratios, CL measurement was performed with 3 µL 1 % (w/v) Tween20, 3 µL hemin 1 mmol L^{-1}, 3 µL H_2O_2 10 mmol L^{-1}, integration time: 2 s, read height: 1 mm, gain 80, data are presented as mean ± SD, n = 3

The dose-response curve for the background and the test and control line of high encapsulant liposomes, however, was overall shifted to higher CL intensities, which corroborates with previously suspected non-specific binding of the liposomes to the nitrocellulose membrane.

4.2.3.5. Evaluation of CAU detector prototype first and second generation

Besides the development of the chemiluminescent lateral flow assay itself, designing and constructing a POCT detection device for chemiluminescent lateral flow assays was also part of the work. We obtained two prototypes[10] from our collaboration partner and investigated their performance with our simple streptavidin-biotin system using streptavidin modified test strips and biotinylated liposomes. The CAU detector contains photodiodes to convert the CL intensity into a voltage signal. With a customized computer-based software (compilation_dual_ut71v3, and adjusted versions), the time course of the voltage change was recorded over time. Whereas the first generation of the CAU detector (**Figure 10 A**) requires external multimeters for the data acquisition, the second generation (**Figure 10 B**) was improved by an enhanced circuit, an additional shutter to avoid interfering light while inserting the cassette, an integrated data acquisition unit, Bluetooth connectivity and full battery mode.

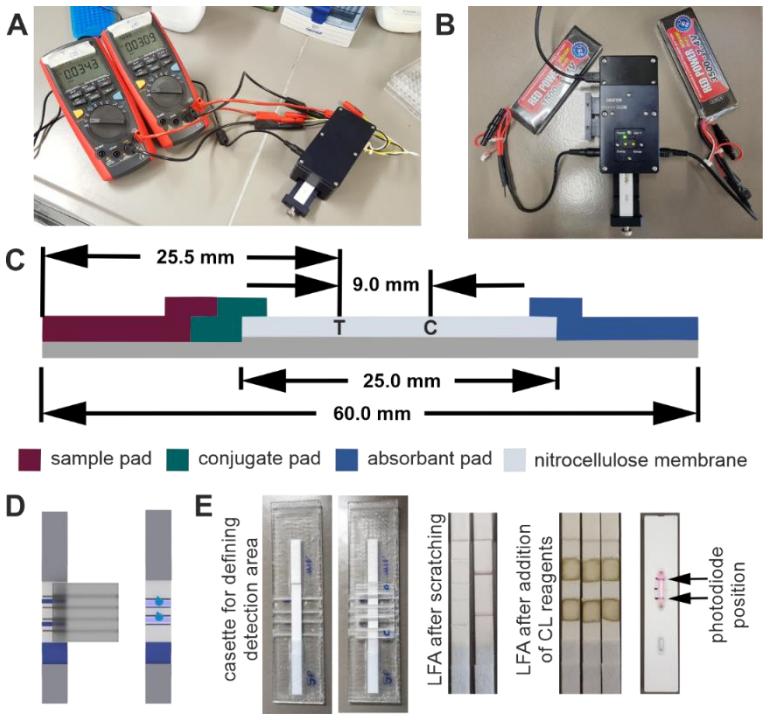

Figure 10. CAU detector prototypes and LFA dimensions and preparation. A) real image of CAU detector first generation with multimeters for computer-aided evaluation, B) real image of battery powered second generation of the CAU detector with android based data acquisition through bluetooth, C) LFA dimension requirements for application with the CAU detector, D) scheme of LFA preparation for chemiluminescence measurement with CAU detector, E) real images of the LFA preparation

Both detectors require LFA with the position of the test and control line at 25.5 mm and 34.5 mm, respectively (**Figure 10 C**). The measurements were conducted following the procedure for the Synergy Neo 2 microplate reader (BioTek). Yet, small adjustment were necessary. In contrary to the detection with the Synergy Neo 2 microplate reader (BioTek), the intact LFA strip is inserted into the detector and two photodiodes are positioned on top of the test and control line. Due to the absence of a third photodiode, the detection of the background signal is not possible within this setup. In order to apply the CL reagents reproducibly, the detection areas were first isolated by the developed scratching method, before the reagents were applied (**Figure 10 D,E**). A dilution series of 75 mmol L^{-1} encapsulant liposomes was recorded on both prototypes. With the enhanced circuit, higher voltages were determined. Whereas with the first prototype an LOD of approximately 4 µmol L^{-1} total lipid concentration was determined (**Figure 11 A**), a 10-fold reduction to 0.4 µmol L^{-1} was obtained for the second generation (**Figure 11 B**). The LOD was determined only for the test line signal by $mean_{blank}$ + 3 × standard deviation of the blank (SD_{blank}) for the second prototype. For the first generation the lowest concentration that yielded an integral was used instead of the blank value to calculate the LOD as no signal was obtained for the blank value.

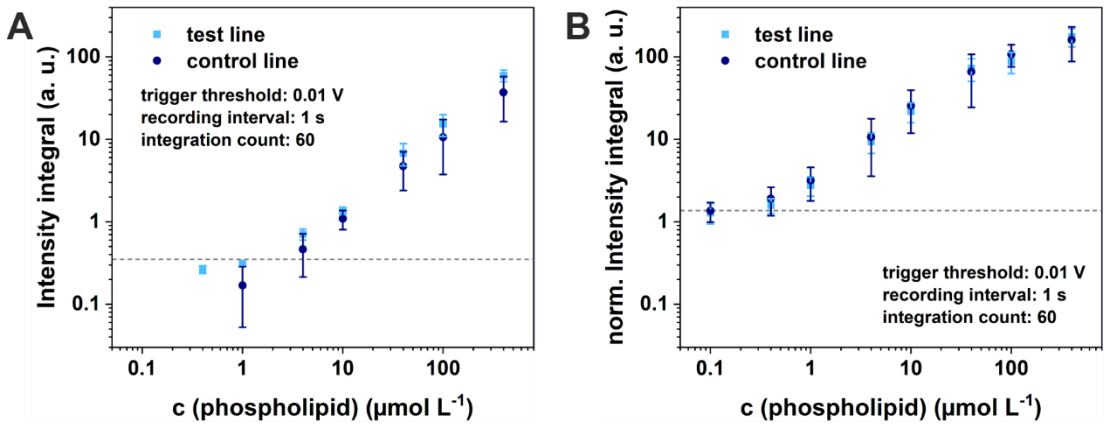

Figure 11. Evaluation of CAU detector prototypes through dilution study of high encapsulant liposomes through a simple biotin-streptavidin LFA. A) illustrates the dilution series of 75 mmol L^{-1} encapsulant liposomes when detected with prototype 1 and B) illustrates the dilution series of 75 mmol L^{-1} encapsulant liposomes when detected with prototype 2. For the chemiluminescence measurement, 3 µL 1 % (w/v) TWEEN®20, 3 µL 1 mmol L^{-1} hemin and 2 µL 10 mmol L^{-1} H_2O_2 in 0.1 mmol L^{-1} carbonate buffer were applied and the signal was integrated over 60 measurements after 0.01 V was initially reached, data are presented as mean ± SD, reference line illustrates LOD, n = 4

Finally, we benchmarked the results obtained with the CAU detector with photodiodes with a high-end photomultiplier tube in the Synergy Neo 2 microplate reader (BioTek), which is known as detector of choice[17] for sensitive low light detection. Here, the CAU detector slightly overestimates the applied concentrations whereas the Synergy Neo 2 microplate reader (BioTek) reader slightly underestimates the applied concentration (slope = 2) (**Figure 12**). Due to several manual steps that are involved in both processes, the experimental error was relatively high and further optimization of the lysis process and automation of the overall procedure including a reduction of the manual steps, would allow for more precise measurement. However, comparing the determined LODs, the second prototype outperforms the BioTek reader by a factor of 10 (**Figure 9 B, Figure 11 B**). Furthermore, when comparing the performance of the photodiodes with a photomultiplier, a dose-dependent signal was obtained (**Figure 12**) in both cases with a linear dependency and good correlation (R^2 = 0.909) making the photodiodes and the CAU detector a promising future POCT detector.

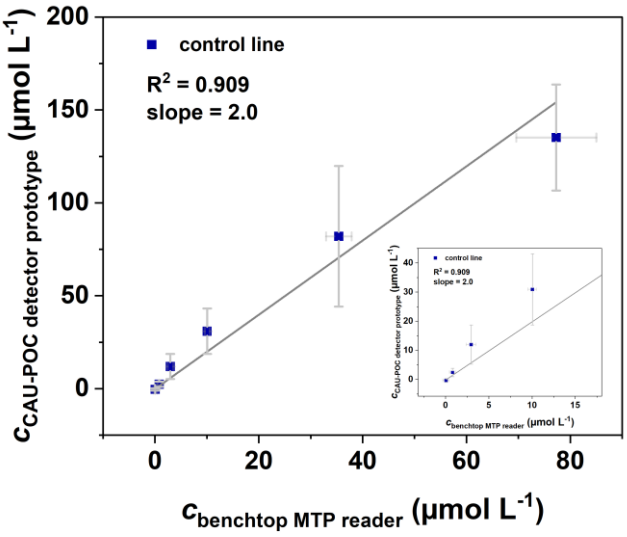

Figure 12. Comparison of second generation CAU detector with Synergy Neo 2 microplate reader (BioTek) for the detection of a dilution series of 75 mmol L^{-1} *m*-carboxy luminol liposomes. Data are presented as mean ± SD, n = 4

4.2.4. Conclusion

Within this chapter, we refined previously reported *m*-carboxy luminol liposomes toward a highly sensitive label in lateral flow assays. In this pilot study we investigated CL liposomes toward a qualitative LFA approach. For this, we developed stable and functional liposomes that can be easily modified and stored for at least 9 months. Furthermore, coupling to proteins such as streptavidin and antibodies is straightforward. Here, we further determined the ideal N-glutaryl DPPE content for post coupling of functional biomolecules and tested these liposomes in an MTP approach. We further developed a procedure that enables the detection of chemiluminescence and fluorescence on a benchtop MTP reader to compare both detection techniques. Direct comparison of the chemiluminescence liposomes with the fluorescence liposomes showed, that albeit no reduction in the limit of detection was obtained, a significantly higher signal-to-noise ratio for the chemiluminescence liposomes was determined. Considering, that fluorescent liposomes were applied with 5-times higher encapsulant concentration and the more efficient lipid composition, the results are still highly promising, already with the low encapsulant liposomes. By increasing the encapsulant concentration to 75 mmol L^{-1} *m*-carboxy luminol, sensitivity enhancement in solution was obtained. Direct comparison of the fluorescent and the refined high load chemiluminescent liposomes in solution yielded a 5-times lower LOD. However, within this study it was not directly transferable to the LFA approach. A major issue during LFA experiments was that with more sensitive detection techniques also the non-specific binding of the liposomes to the nitrocellulose membrane became more pronounced and prevented sensitivity improvements. Yet, despite non-specific binding of the liposomes to the nitrocellulose

membrane, switching from fluorescence to chemiluminescence allows for a significant improvement of the signal-to-noise ratios which is probably attributed to the absence of autofluorescence and scattering in chemiluminescence measurements. Modifying the liposome surface with polyethylenglycol could help to prevent non-specific binding, besides pretreatment of the membrane with blocking agents. Within this work we were not able to show the benefit of BSA or TWEEN®20 preblocked membranes with regard to sensitivity enhancement, yet when using the preblocked membranes a more homogenous signal response was obtained even though it was at the expense of a high signal intensity. This indicates potential for improvement and further optimization with regard to the concentration and the blocking reagents and may lead to the desired advances of CL LFA. Hence, together with the refined liposomes and optimized surface functionalization, chemiluminescence detection has the potential to outcompete fluorescence detection in LFAs not only through the improved signal-to-noise ratio but also by improved sensitivities. However, before CL liposomes can become the new label of choice in POCT a few open questions have to be addressed first. For example, a user-friendly strategy to release the marker molecules from the liposomes is important to overall adhere to the POCT concept. Besides, a reduction of the non-specific binding of the liposomes to the nitrocellulose membrane is necessary to truly obtain a sensitivity enhancement. Furthermore, a proper solution to avoid the reduction of CL intensity in matrices that contain radical scavengers would reinforce the power of CL in diagnostic in general. Here, masking agents for ascorbate or other antioxidants in such matrices could be an option for a workaround. This would finally allow simplified detection devices that fit better to the budget of POCT but offer sensitivities comparable to laboratory devices. We demonstrate already in a second line of research, the powerful performance of a newly developed CL strip reader towards a standard benchtop reader. Here, the POCT detector outperformed the benchtop reader with regard to sensitivity by a factor of 10 for the LFA readout. Together with an optimized LFA method, the combination of the newly developed POCT detector with our chemiluminescence approach can yield in a highly sensitive and truly portable POCT system with sensitivities that can rival laboratory approaches with faster analysis times.

4.2.5. References

[1] L. Sercombe, T. Veerati, F. Moheimani, S. Y. Wu, A. K. Sood, S. Hua, *Frontiers in pharmacology* **2015**, *6*, 286.

[2] A. Gómez-Hens, J. Manuel Fernández-Romero, *TrAC Trends in Analytical Chemistry* **2005**, *24*, 9.

[3] a) Q. Liu, B. J. Boyd, *The Analyst* **2013**, *138*, 391; b) S. Rink, B. Kaiser, M.-S. Steiner, A. Duerkop, A. J. Baeumner, *Analytical and bioanalytical chemistry* **2022**, *414*, 3231.

[4] M. Mayer, S. Takegami, M. Neumeier, S. Rink, A. Jacobi von Wangelin, S. Schulte, M. Vollmer, A. G. Griesbeck, A. Duerkop, A. J. Baeumner, *Angew. Chem., Int. Ed.* **2018**, *57*, 408.

[5] K. A. Edwards, A. J. Baeumner, *Talanta* **2006**, *68*, 1421.

[6] A. Sharma, A. I. Y. Tok, P. Alagappan, B. Liedberg, *TrAC Trends in Analytical Chemistry* **2021**, *142*, 116327.

[7] M. Song, J. A. Kellum, *Critical care medicine* **2005**, *33*, S463-5.

[8] K. Tsukagoshi, H. Akasaka, Y. Okumura, R. Fukaya, M. Otsuka, K. Fujiwara, H. Umehara, R. Maeda, R. Nakajima, *ANAL. SCI.* **2000**, *16*, 121.

[9] X. Zhu, T. Gao in *Nano-Inspired Biosensors for Protein Assay with Clinical Applications*, Elsevier, **2019**, pp. 237–264.

[10] H. T. Kim, E. Jin, M.-H. Lee, *Biosensors* **2021**, *11*.

[11] G. Cao, R. L. Prior, *Clinical Chemistry* **1998**, *44*, 1309.

[12] A. Zulueta, A. Maurizi, A. Frígola, M. J. Esteve, R. Coli, G. Burini, *International Dairy Journal* **2009**, *19*, 380.

[13] J. M. Fernández-Real, M. Broch, J. Vendrell, C. Richart, W. Ricart, *J. Clin. Endocrinol. Metab.* **2000**, *85*, 1334.

[14] K. G. Shah, P. Yager, *Analytical chemistry* **2017**, *89*, 12023.

[15] O. S. Wolfbeis, M. Leiner, *Anal. Chim. Acta* **1985**, *167*, 203.

[16] M. Kitamura, K. Murakami, K. Yamada, K. Kawai, M. Kunishima, *Dyes Pigm.* **2013**, *99*, 588.

[17] A. Roda, P. Pasini, M. Guardigli, M. Baraldini, M. Musiani, M. Mirasoli, *Fresenius' journal of analytical chemistry* **2000**, *366*, 752.

5. Investigation of Architectural Features of Liposomes in Terms of Their Interaction with the Human Complement System to Establish a Straightforward Neutralization Assay for SARS-CoV-2

Graphical Abstract

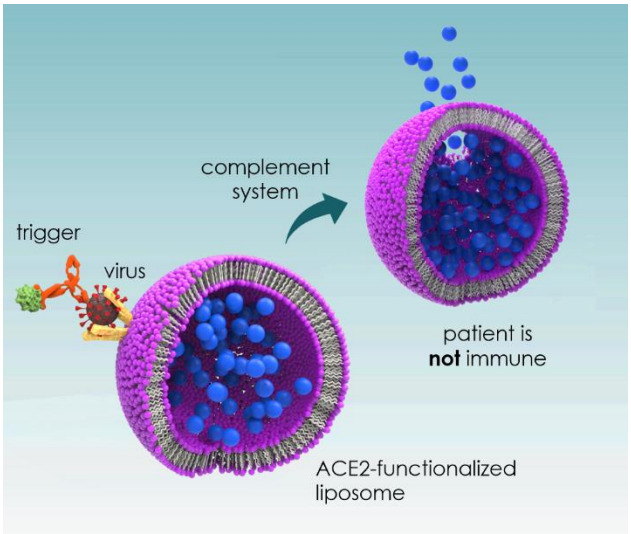

This chapter is intended for publication in part.

Abstract

Accurate diagnosis of viral infection and immunity mostly requires advanced laboratory testing with stringent safety requirement. Yet, in case of a global pandemic the capacities of analysis laboratories are limited, and besides the initial diagnosis, information of the population's immunity status and effective immunization is of essence for managing a pandemic. Typically, a neutralization assay is performed to identify neutralizing antibodies that prevent the virus from invading the host cell and thus viral reproduction. However, this kind of tests are time and cost intensive and if pathogen viruses are included special biosafety restrictions apply. Nevertheless, the neutralization assay currently represents the gold standard to identify neutralizing antibodies and no adequate alternatives are available up to now. Hence, we studied a new assay system based on the principle of the standard neutralization assay using liposomes that are specifically lysed through the complement system. This work reports initial proof-of-concept studies, which confirm specific lysis of liposomes through a trigger molecule. Particularly, antibodies or lipopolysaccharide were tested for their ability to function as trigger. We further demonstrated in a bystander assay that the complement system only attacks liposomes which bear a trigger molecule on the surface or directly bind to a trigger molecule. Liposomes without a trigger in close proximity to the surface remain unaffected. Finally, successful surface modification of liposomes with ACE2 as recognition molecule was demonstrated and the suitability of side-directed versus random coupling evaluated.

5.1. Introduction

In 2020 the corona pandemic emerged and continues to pose great challenges to humanity. To get the situation under control, one essential tool is immunization of the population either through vaccination or through surviving a natural infection. This is not only true for the SARS-CoV-2 virus but for many pathogens in general. In order to assess the potential danger that a population is exposed to and to evaluate the effectiveness of new vaccines or anti-viral drugs, knowledge over the protective immunity status is an essential criterion.[1] The prevalence of an immunity is mainly extracted from neutralization assays which determine the amount of neutralizing antibodies, a patient generates after the encounter, either with the vaccine or the natural virus itself. Especially in the long-term management of a viral outbreak, this information is key to define an appropriate course of action. The live virus neutralization assay for determining infections is still the gold standard due to its accuracy.[2] Yet, in particularly the gold standard but also the current alternative such as the

pseudo neutralization assay are elaborate with assay times up to four days and the necessity to work under stringent safety specification.[2] Alternatives such as surrogate virus neutralization test often lack in sensitivity or specificity as they typically focus on blocking the binding between the cellular receptor angiotensin converting enzyme 2 (ACE 2) and the receptor binding domain (RBD) in case of the SARS-CoV-2 virus.[2,3] Hence, fast and easy to handle alternatives are still urgently needed. Instead of using the natural virus, using virus-like particle mimicking the natural virus, together with liposomes as reporter particles, allows for a safer, more rapid and still highly sensitive assay format. Hence, they were studied in the following towards a straightforward neutralization assay. A homogenous system using liposomes as detection particles that can bind a virus-like particle (VLP) upon exposure was envisioned. In the homogenous assay, liposomes with a fluorescence dye were used. Here, the fluorescence is quenched in intact liposomes when encapsulated in high concentrations in the liposome interior. In case of a binding event between the virus-like particle and the liposomes, the liposomes are specifically lysed through the human complement system (**Figure 1**).

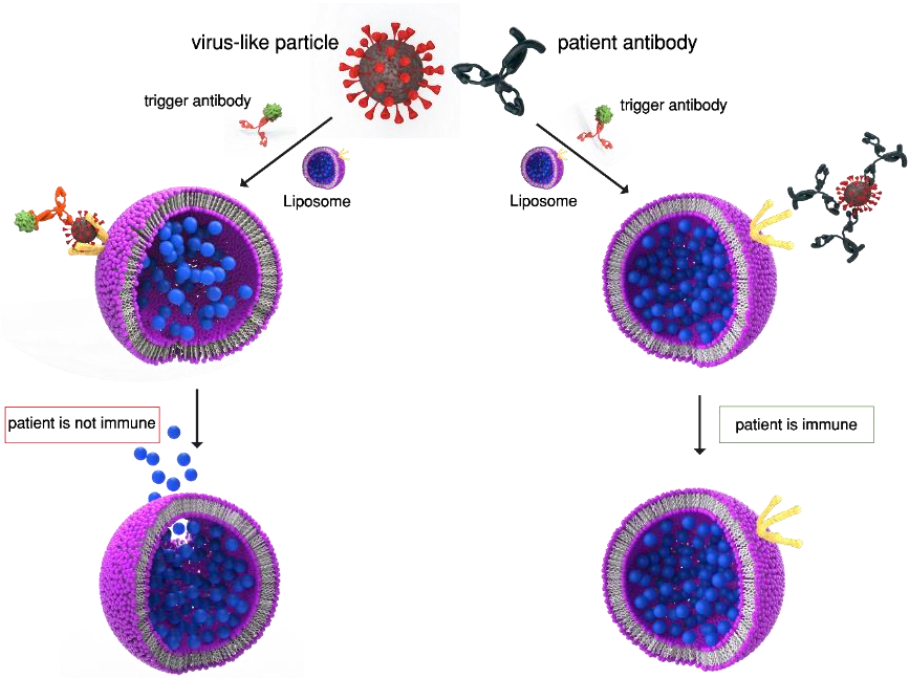

Figure 1 Concept of developed neutralization assay using liposomes as detection particle and the human complement system for triggered lysis upon binding of the virus-like particle

Lysis of the liposomes takes place if the serum sample does not contain neutralizing antibodies against the VLP. The virus can then bind to the modified liposomes together with a complement trigger which initiates the lytic process through the complement system. The

encapsulated dye is subsequently released, the fluorescence quenching is repealed and can hence be monitored. If the patient's sample contains neutralizing antibodies, the virus cannot bind to the liposome surface and hence the trigger antibody will not be in close proximity of the liposomes to allow the complement induced lysis to proceed.[4] For chemiluminescence liposomes, a heterogenous approach was developed due to to the incompatibility of chemiluminescence measurements in the presence of serum. Although the overall strategy remains similar, in the heterogenous assay format, a decline in the signal intensity is obtained when complement lysis occurs. In contrary to the homogenous assay, the liposomes are first bound to a microtiter plate and after the assay the remaining intact liposomes are measured.

The complement system is part of the mammalian innate immune defense that consists of over 60 plasma proteins which lead to opsonization, inflammation and lysis of pathogens upon activation.[5] Opsonization, inflammation and lysis of the pathogen can occur through three pathways, namely the classical, the alternative and the lectin pathway (**Figure 2**).

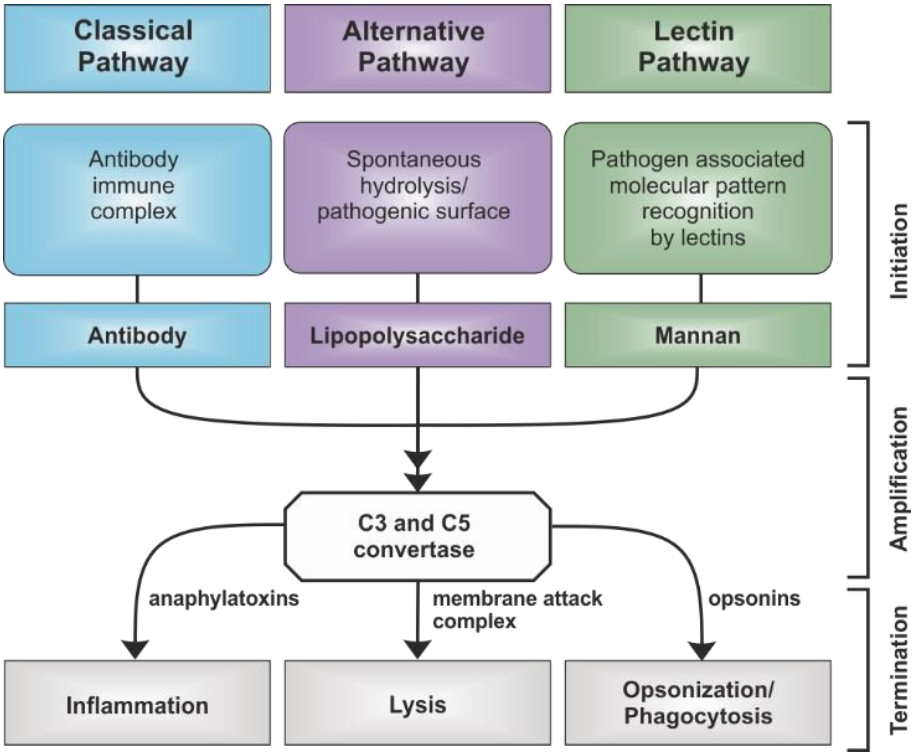

Figure 2 Simplified complement pathways with respective trigger molecules for classical, alternative and lectin pathway initiating the enzymatic cascade which ends up in the formation of C3 and C5 convertase in all three pathways. The convertase generates subsequently the major effectors for the terminal stage which lead to inflammation, lysis and phagocytosis, adapted from Dunkelberger *et al.* [6]

Each pathway is activated by specific components that are either part of the immune response such as antibodies or are exposed on the surface of the invader. These virulence factors like lipopolysaccharides (LPS), bacterial outer membrane proteins or bacterial capsular polysaccharides containing mannan, are part of pathogen associated molecular patterns which can be recognized by the complement system.[5,6] Liposomes have been identified as activators for all three pathways of the complement system in the course of evaluating them as novel drug delivery system to overcome their rapid clearance from the blood stream.[7] The complement induced liposome lysis is mainly attributed to the formation of the membrane attack complex (MAC) which is an assembly of soluble complement proteins forming a pore in the lipid membrane leading to leakage of the entrapped molecules.[7,8] It is known that the complement lysis is dependent on the surface charge, surface coating, size and stability of the liposomes.[9] Hence, the initial focus in this study was to develop liposome formulation that can only be lysed by the complement system within the presence of a specific trigger molecule. Moghimi *et al.* reviewed in detail the interaction of liposomes with the complement system and the presumed processes that are associated with complement-mediated liposome lysis.[7] In analytical chemistry, the specific lysis in contrary to the typical solvent or surfactant-based lysis of liposomes, has already been utilized in the late 20th century for several homogenous complement-mediated liposome immunoassays and offers some advantages.[10] For example, Ishimori *et al.* developed and homogenous immunoassay for the detection of ferritin through a sandwich complex on the liposome surface that activated the complement system and released the encapsulated carboxyfluorescein.[11] Although, the complement induced lysis is typically significantly slower compared to the generic chemical-based one, targeted lysis of liposomes with the complement system is possible.

Within this study, we conducted a proof of principle tests toward the final homogeneous assay including the identification of suitable lipid compositions, potent trigger molecules, evaluation of feasible surface functionalization and realizable assay formats and conditions. Specifically, LPS and antibodies were evaluated as trigger molecules and were tested with stealth liposomes either containing a fluorescence (sulforhodamine B) or a chemiluminescence dye (*m*-carboxy luminol). *m*-Carboxy luminol liposomes were investigated exclusively in the heterogenous format to avoid inconsistencies originating from the diminished chemiluminescence signals in serum, whereas the fluorescent liposomes were exclusively studied in the homogenous format. Furthermore, liposomes were functionalized with biotin, anti-Ankyrin repeat-rich membrane spanning (ARMS)

peptide and ACE2 either as immobilization or recognition moiety for the virus or the trigger in proof-of-concept experiments.

5.2. Experimental Section

All chemicals were of commercial HPLC grade or higher and were used without purification.

5.2.1. Chemicals and consumables:

1,2-dipalmitoyl-sn-glycero-3-phosphocholine (DPPC), 1,2-dipalmitoyl-sn-glycero-3-phospho-(1'-rac-glycerol) (sodium salt) (DPPG), 1,2-dipalmitoyl-sn-glycero-3-ethylphosphocholine (chloride salt) (EDPPC), 1,2-dipalmitoyl-sn-glycero-3-phosphoethanolamine-N-(glutaryl) (sodium salt) (N-glutaryl-DPPE), 1,2-dipalmitoyl-sn-glycero-3-phosphoethanolamine-N-(biotinyl) (sodium salt) (DPPE-biotin) were purchased from avanti polar lipids (Alabaster, AL, USA), 1,2-dimyristoyl-sn-glycero-3-phosphoethanolamine-N-[biotinyl(polyethylene glycol)-2000] (DMPE-PEG-2000-biotin), 1,2-dimyristoyl-sn-glycero-3-phosphoethanolamine-N-[methoxy(polyethylene glycol)-2000] (DMPE-PEG2000) were purchased from tebubio GmbH (Offenbach, Germany). Lipopolysaccharide (LPS) (L6011), bovine serum albumin (BSA)-biotin (A8549), Streptavidin (StAv) (85878), goat anti-biotin polyclonal IgG (B3640), cholesterol (C8667), Sephadex® G 50, sucrose, sodium azide, glycine (purity >99.7 %), sodium hydroxide, Lysin-HCl, hemin, Ethylenediaminetetraacetic acid (EDTA), Ethylenebis(oxyethylenenitrilo)tetraacetic acid (EGTA), Tween®20, potassium chloride, sodium phosphate dibasic, potassium phosphate monobasic, boric acid, sodium carbonate and Whatman Nucleopore™ Track-Etched membranes 1.0 µm, 0.4 µm and 0.2 µm were purchased from Sigma Aldrich/Merck KGaA (Darmstadt,Germany). Sulforhodamin B (S1307) was purchased from Thermo Fisher Scientific (Darmstadt,Germany). *m*-Carboxy luminol (purity: 73.597 wt% ± 2.82 wt%) was custom-made by Taros Chemicals GmbH & Co. KG (Germany). ACE2, ACE2-biotin and RBD were kindly provided by Prof. Dr. Wagner (University Hospital Regensburg, Germany) and Mikrogen GmbH (Neuried, Germany). anti-Ankyrin repeat-rich membrane spanning (ARMS) peptide (Peptide Sequence: IHTELCLPAFFSPAGTQRRFQQPQHHLTLSIIHTAAR) and anti-ARMS antibodies (A626, A375) were provided by Prof. Dr. Pauly (University of Marburg, Germany), human serum was donated by voluntary donors and pooled before used (1/6 S1, 1/6 S2, 1/3 S3, 1/3 S4). The human serum samples involved in this study were obtained from voluntary donors with informed consent and were anonymized before usage. There was no association with a

clinical trial and the studies have been performed in accordance with ethical standards. Streptavidin plates (604500) were provided by microcoat biotechnology GmbH (Bernried, Germany), white or black microtiter plates were purchased from Greiner BioOne and depending on the experiment high or medium binding plates (655074, 655075, 655076) were applied. Potassium hydrogen carbonate, dialysis tube Spectra/Por© 4 (2718.1), *n*-octyl-*β*-D-glucopyranosid (OG) (CN23.2), BSA (T844.2), 2-(N-morpholino)ethanesulfonic acid (MES), sodium chloride was purchased from Carl Roth (Karlsruhe, Germany). 4-(2-Hydroxyethyl)piperazine-1-ethanesulfonic acid (HEPES) (purity >99.5 %), chloroform and methanol were purchased from VWR chemicals (Germany). For all experiments Milli-Q water was used and stock solutions were prepared for hemin (1 mmol L^{-1} in 0.1 mol L^{-1} carbonate buffer, pH 10.5). For H_2O_2 the stock solution (100 mmol L^{-1} in Milli-Q water) was freshly prepared before each measurement.

5.2.2. Synthesis of *m*-carboxy luminol liposomes

Liposomes, containing *m*-carboxy luminol, with various surface modifications were prepared according to an established protocol from Mayer *et al.*[12] with adjustments towards the phospholipid composition. First, the respective lipids (**Table 2**) for a 60 µmol total lipid batch were dissolved in 3 mL chloroform and 0.5 mL methanol and thoroughly sonicated in an ultrasonic bath (VWR ultrasonic cleaner, model USC 300 THD) at 60 °C. Subsequently, 2 mL of preheated (60 °C) encapsulant was added to the lipid solution and emulsified for 4 min at 60 °C, using an ultrasonic bath. Encapsulant was previously prepared by dissolving *m*-carboxy luminol (30 mmol L^{-1}) in 3.95 mL 0.2 mmol L^{-1} HEPES buffer, pH 7.5, and 50 µL 1 mol L^{-1} NaOH. After emulsification, residual solvent was evaporated at 60 °C under reduced pressure. The remaining 2 mL of encapsulant were added after the first evaporation step (780 mbar) and thoroughly vortexed before evaporation was continued (400 mbar). The remaining solution was extruded at 60 °C through 1.0 µm, 0.4 µm and finally 0.2 µm membranes to obtain unilamellar liposomes. Purification was first performed by size-exclusion chromatography with Sephadex® G-50 as stationary phase (column size: 2 cm x 8 cm) and 0.01 mol L^{-1} outer buffer (glycine-NaOH buffer: 10 mmol L^{-1} glycine, 200 mmol L^{-1} NaCl, approximately 100 mmol L^{-1} sucrose, 0.01 % (w/v) sodium azide), pH 8.6, osmolality 0.52 osmol kg^{-1} as mobile phase. Additionally, the liposomes were dialyzed overnight against 0.01 mol L^{-1} glycine-NaOH buffer, pH 8.6, osmolality 0.52 osmol kg^{-1} in Spectra/Por© 4 dialysis tube (MWCO: 12 – 14 kDa). The 30 mmol L^{-1} *m*-carboxy luminol liposomes with 5 mol% cholesterol were characterized by DLS

measurements and zeta potential measurements. The total lipid (tL) concentration was determined by ICP-OES measurements. The results are summarized in **Table 2**.

Table 2 Characteristics of synthesized liposomes

Lipid composition	Surface	PdI[a]	Size[b] by Int (nm)	Size[b] by Num (nm)	Zeta potential (mV)	Total lipid concentration (mmol L^{-1})
Encapsulant: 30 mmol L^{-1} *m*-carboxy luminol[c]						
batch 14 DPPC: 73.1 mol% DPPG: 18.0 mol% Cholesterol: 4.9 mol% N-glutaryl-DPPE: 4.0 mol%	anionic, N-glutaryl	0.08 ± 0.01	125 ± 39	87 ± 25	-28.4 ± 2.38	17.04 ± 0.04
batch 15 DPPC: 74.3 mol% EDPPC: 18.3 mol% Cholesterol: 5.3 mol% DPPE-biotin: 2.1 mol%	cationic, biotin	0.10 ± 0.02	136 ± 43	92.6 ± 27	13.8 ± 1.34	9.40 ± 0.04
batch 16 DPPC: 72.6 mol% EDPPC: 18.4 mol% Cholesterol: 5.0 mol% DMPE-PEG-biotin: 2.0 mol% DMPE-PEG: 2.0 mol%	cationic, PEG-biotin	0.07 ± 0.01	131.9 ± 40	92.4 ± 26	0.05 ± 0.6	11.9 ± 0.1
batch 17 DPPC: 74.9 mol% DPPG: 17.5 mol% Cholesterol: 5.6 mol% DPPE-biotin: 2.0 mol%	anionic, biotin	0.09 ± 0.01	135 ± 42	120 ± 44	-19 ± 1	9.60 ± 0.04
batch 18 DPPC: 71.7 mol% DPPG: 19.3 mol% Cholesterol: 4.9 mol% DMPE-PEG-biotin: 2.0 mol% DMPE-PEG: 2.1 mol%	anionic, PEG-biotin	0.05 ± 0.02	127 ± 35	113 ± 37	-3.1 ± 1.4	9.20 ± 0.05
batch 19 DPPC: 73.7 mol% DPPG: 17.8 mol% Cholesterol: 5.7 mol% DPPE-biotin: 1.9 mol% LPS: 0.9 mol%	anionic, biotin, LPS	0.05 ± 0.01	135 ± 37	123 ± 39	-9.3 ± 2.1	11.77 ± 0.04
batch 20 DPPC: 74.2 mol% DPPG: 17.9 mol% Cholesterol: 5.0 mol% DMPE-PEG-biotin: 1.9 mol% LPS: 1.0 mol%	anionic, PEG-biotin, LPS	0.07 ± 0.02	142.8 ± 40	104.3 ± 30	-5.9 ± 0.7	12.29 ± 0.07

Table 2 Characteristics of synthesized liposomes (continued)

Lipid composition	Surface	PdI[a]	Size[b] by Int (nm)	Size[b] by Num (nm)	Zeta potential (mV)	Total lipid concentration (mmol L^{-1})
Encapsulant: 10 mmol L^{-1} sulforhodamine B[d]						
CG210327-1H DPPC: 72 mol% DPPG: 18 mol% Cholesterol: 5 mol% N-glutaryl-DPPE: 4 mol%	anionic, N-glutaryl	0.191 ± 0.004	187 ± 17 5000 ± 52	105 ± 10	-21 ± 2	12.54 ± 0.14
CG210331-1H DPPC: 73 mol% DPPG: 19 mol% Cholesterol: 5 mol% DPPE-biotin: 2 mol%	anionic, biotin	0.18 ± 0.01	218 ± 13 4574 ± -	119 ± 8	-17.3 ± 1	13.39 ± 0.09
KH210218-H DPPC: 74 mol% DPPG: 17 mol% Cholesterol: 5 mol% DPPE-biotin: 2 mol% LPS: 1 mol%	anionic, biotin, LPS	0.210 ± 0.002	271 ± 22 5103 ± 185	181 ± 82	-10 ± 1	8.11 ± 0.04

[a]PdI: Polydispersity index, [b]size refers to hydrodynamic diameter, [c]final extrusion membrane: 0.2 µm, [d]final extrusion membrane: 0.4 µm

5.2.3. Dynamic light scattering and zeta potential

Dynamic light scattering (DLS) and zeta potential measurements were done on a Malvern Zetasizer Nano-ZS (Malvern Panalytical, Germany) at 25°C. Size determination was done in semi-micro polymethyl methacrylate (PMMA) cuvettes (Brand, Germany), and zeta potential was done in disposable folded capillary zeta cells (Malvern Panalytical, Germany). The liposomes were diluted 1:100 and measured in HSS buffer with the following settings, refractive index (RI) of the material of 1.34, material absorbance of zero, RI of 1.342 of the dispersant viscosity of 1.1185 mPa s were applied for DLS. For zeta potential a refractive index of 1.342, viscosity of 1.1185 mPa s and a dielectric constant of 78.5 was used. An equilibration time of 60 s was applied before each measurement.

5.2.4. Determination of phospholipid concentration through ICP-OES

Phospholipid concentration was determined through inductively coupled plasma optical emission spectrometer (ICP-OES) measurements with a SPECTROBLUE TI/EOP from (SPECTRO Analytical Instruments GmbH, Kleve, Germany). Phosphorous was detected at 177.495 nm and the device calibrated between 0 and 100 µmol L^{-1} phosphorous in 0.5 mol L^{-1} HNO_3. Before each measurement, the device was recalibrated with 0.5 mol L^{-1} HNO_3 and 50 µmol L^{-1} phosphorous. A 1:150 dilution of the liposomes (3 mL) in 0.5 mol L^{-1} HNO_3 was measured.

5.2.5. Surface modification of liposomes

Liposomes were surface modified through 1-Ethyl-3-(3-dimethylaminopropyl)carbodiimide (EDC) and N-Hydroxysulfosuccinimide sodium salt (sulfo-NHS) chemistry. The respective volume of liposome solution was mixed with EDC (10 mg mL^{-1} in 0.1 mol L^{-1} MES buffer, pH 6.0) and sulfo-NHS (10 mg mL^{-1} in 0.1 M MES buffer, pH 6.0) and incubated for 1 h at room temperature and 300 rpm. The respective equivalent of protein (ARMS peptide, streptavidin, ACE2) was added and incubated for 3 h at room temperature and 300 rpm. Lysin-HCl (1 M in ultrapure water) was added and again incubated for 15 min at room temperature and 300 rpm. The reaction mix was dialyzed 3-times against 300 mL outer buffer of the respective liposomes overnight. Several coupling ratios of the relevant protein have been explored and are given in detail in the respective section. The equivalent of liposomes:EDC:sNHS:lysin-HCl were kept constant at 1:2.1:3.8:6.7.

5.2.6. Binding assay

Simple binding assays were performed to confirm successful surface modification of liposome with biomolecules. The described binding assays were done with functionalized 96-well high binding microtiter plate (MTP). For antibodies and RBD, phosphate buffered saline (1 X PBS, 137 mmol L^{-1} NaCl, 2.7 mmol L^{-1} KCl, 10 mmol L^{-1} sodium phosphate dibasic, 1.8 mmol L^{-1} potassium phosphate monobasic, pH 7.4) was used as coating buffer whereas for BSA-biotin a carbonate/borate buffer was used (80 mmol L^{-1} Na_2CO_3 and 100 mmol L^{-1} H_3BO_3, pH 9.4). Firstly, the MTP was coated overnight at 4 °C.

5.2.6.1. for streptavidin liposomes

Here, 200 µL of a 1 µg mL^{-1} BSA-biotin dilution in carbonate-borate buffer (80 mmol L^{-1} Na_2CO_3 and 100 mmol L^{-1} H_3BO_3, pH 9.4) was added to the MTP and incubated overnight at 4 °C. Subsequently, the plate was washed 3-times with 200 µL 1X PBS, 0.05 wt.-% Tween®20, pH 7.4 for 5 min while shaking before blocking for 1 h at room temperature with 200 µL blocking solution (1% BSA in 1X PBS, 0.05% Tween®20, pH 7.4) while constant shaking. Following the blocking, the plate was washed twice with 200 µL 1X PBS, 0.05% Tween®20, pH 7.4 and once with 200 µL outer buffer (10 mmol L^{-1} glycine, 200 mmol L^{-1} NaCl, 100 mmol L^{-1} sucrose, 0.01% (w/v) NaN_3, pH 8.6, osmolality 0.520 osmol kg^{-1}) for 5 min while shaking before 100 µL modified liposomes with respective total lipid concentration (c(tL)) in outer buffer was added and incubated for 1 h at room temperature or overnight at 4 °C. Finally, the plate was washed 3-times with 200 µL CBS buffer for 5 min

before the liposomes were lysed for 5 min while shaking with 100 µL 30 mmol L^{-1} OG in CBS. The chemiluminescence (CL) intensity was measured with a microplate reader (Syngene2, BioTek) after adding 50 µL 40 mmol L^{-1} H_2O_2 and 50 µL 4 µmol L^{-1} hemin in CBS, pH 10.5. A blank reading was done prior to the H_2O_2 addition and later subtracted from the final measurement to correct for stray light. After H_2O_2 was added a 5 s shaking (425 cpm) was started and if not stated differently the CL intensity was measured at read height (RH) 1 mm and integration time (IT) 2 s. All measurement were done at 25 °C.

5.2.6.2. for ARMS liposomes

The binding assay for ARMS liposomes was done according to the procedure for the StAv liposomes. Deviating from this procedure, 100 µL of a 10 µg mL^{-1} anti-ARMS (A626 or A375) in 1X PBS, pH 7.4 were used for coating. Furthermore, 100 µL liposomes with c(tL) = 50 µmol L^{-1} were used for binding overnight at 4 °C. The chemiluminescence (CL) intensity was measured similarly to the binding assay with StAv liposomes.

5.2.6.3. for ACE2 liposomes

The binding assay for ACE2 liposomes was done according to the procedure for the StAv liposomes. The RBD coating was adapted from an already published procedure.[13] Here, 50 µL of 2 µg mL^{-1} RBD in 1 X PBS, pH 7.4 was incubated overnight at 4 °C and blocked for 1 h at room temperature while shaking with 200 µL 5 % Milk (w/v) in 1X PBS, 0.1% Tween®20, pH 7.4. Subsequently the plate was washed 3-times with 200 µL outer buffer for 5 min while shaking before 100 µL liposomes (c(tL) = 50 µmol L^{-1}) in outer buffer were allowed to bind. The chemiluminescence (CL) intensity was measured similarly to the binding assay with StAv liposomes.

5.2.7. Competitive assay

Competitive assays were performed to estimate the degree of surface functionalization of the liposomes.

5.2.7.1. with biotinylated liposomes

The competitive biotin assay was done in a StAv-coated 96-well microtiter plate (MTP). Firstly, the StAv-plate was washed with 200 µL outer liposome buffer for 5 min at constant agitation before 100 µL respective biotin dilution including biotin-modified liposomes (10 µmol L^{-1} total lipid concentration) in outer buffer (10 mmol L^{-1} glycine, 200 mmol L^{-1} NaCl, 100 mmol L^{-1} sucrose, 0.01% (w/v) NaN_3, pH 8.6, osmolality 0.520 osmol kg^{-1}) were

incubation for 1 h while shaking. After the incubation the biotin dilutions were removed and the MTP was washed 3-times with 200 µL CBS buffer before the liposomes were lysed for 5 min while shaking with 100 µL 30 mmol L^{-1} OG in CBS. The chemiluminescence (CL) intensity was measured with a microplate reader (Syngene2, BioTek) after adding 50 µL 40 mmol L^{-1} H_2O_2 and 50 µL 40 µmol L^{-1} hemin in CBS, pH 10.5. A blank reading was done prior to the H_2O_2 addition and later subtracted from the final measurement to correct for stray light. After H_2O_2 was added a 5 s shaking (425 cpm) was started and if not stated differently the CL intensity was measured at gain 100, read height (RH) 1 mm and integration time (IT) 2 s. All measurement were done at 25 °C.

5.2.7.2. with ARMS-modified liposomes

For the competitive ARMS assay, an anti-ARMS (A626 or A375) coated 96-well white high binding MTP was used. Here, 100 µL of a 10 µg mL^{-1} antibody dilution in 1X PBS, pH 7.4 was added to the MTP and incubated overnight at 4 °C. Subsequently, the plate was washed 3-times with 200 µL 1X PBS (137 mmol L^{-1} NaCl, 2.7 mmol L^{-1} KCl, 10 mmol L^{-1} sodium phosphate dibasic, 1.8 mmol L^{-1} potassium phosphate monobasic, pH 7.4), 0.05 wt.-% Tween®20, for 5 min while shaking before blocking for 1 h with 200 µL blocking solution (1% BSA in 1X PBS, 0.05% Tween®20, pH 7.4) at room temperature while constant shaking. Following the blocking, the plate was washed once with 200 µL 1X PBS, 0.05% Tween®20, pH 7.4 and 2-times with 200 µL outer buffer pH 8.6 for 5 min while shaking before 100 µL liposomes (c(tL) = 50 µmol L^{-1})/antibody dilution in outer buffer was added and incubated overnight (approx. 17 h) at 4 °C. Finally, the plate was washed 3-times with 200 µL CBS buffer before the liposomes were lysed for 5 min while shaking with 100 µL 30 mmol L^{-1} OG in CBS. The chemiluminescence (CL) intensity was measured similarly to the competitive biotin assay with 50 µL 40 mmol L^{-1} H_2O_2 and 50 µL 40 µmol L^{-1} hemin in CBS, pH 10.5 and gain 80, read height (RH) 1 mm and integration time (IT) 2 s. All measurement were done at 25 °C.

5.2.7.3. with streptavidin-modified liposomes

The competitive streptavidin assay was done according to the competitive assay with the ARMS antibodies. Here, the MTP was coated with 200 µL of 1 µg mL^{-1} BSA-biotin in carbonate-borate buffer (80 mmol L^{-1} Na_2CO_3 and 100 mmol L^{-1} H_3BO_3, pH 9.4) and 100 µL respective biotin dilution including StAv-modified liposomes (10 µmol L^{-1} total lipid concentration) in outer buffer were incubated for 1 h at room temperature while constant

shaking before the final lysis. The chemiluminescence (CL) intensity was measured similarly to the competitive biotin assay.

5.2.8. Heterogenous complement assay

The heterogenous complement assay was performed in a StAv-coated 96-well microtiter plate (MTP). Firstly, the StAv-plate was washed with 200 µL outer liposome buffer (10 mmol L^{-1} glycine, 200 mmol L^{-1} NaCl, 100 mmol L^{-1} sucrose, 0.01% (w/v) NaN_3, pH 8.6, osmolality 0.520 osmol kg^{-1}) for 5 min while shaking before 100 µL respective biotin-modified liposomes in outer buffer (50 µmol L^{-1} total lipid concentration) were incubated overnight. The unbound liposomes were removed and the MTP was washed 3-times with 200 µL outer buffer for 5 min. For the complement assay, the bound liposomes were incubated with 100 µL outer buffer, Paul Morgan buffer (PMB, 10 mmol L^{-1} HEPES, 150 mmol L^{-1} NaCl, 135 nmol L^{-1} $CaCl_2$, 1 mmol L^{-1}, $MgCl_2$, pH 7.4), inactivated serum in PMB, and activated serum in PMB and incubated for 1 h at 37 °C and gently shaking. Serum was inactivated by mixing with inactivation complement buffer (iaCB, 200 mmol L^{-1} EDTA, 0.5 µmol L^{-1} EGTA and 90 % Paul Morgan complement buffer, pH 8). Standardly, 10 vol.-% serum was used in the complement assay if not stated differently and only added to the active and inactive serum sample. After the incubation the MTP was washed 3-times with 200 µL CBS (10 mmol L^{-1} $KHCO_3$, 200 mmol L^{-1} NaCl, 100 mmol L^{-1} sucrose, pH 10.5) for 5 min before the liposomes were lysed for 5 min while shaking with 100 µL 30 mmol L^{-1} OG in CBS. The lysed liposomes were transferred into a white MTP. The chemiluminescence (CL) intensity was measured with a microplate reader (Syngene2, BioTek) after adding 50 µL 40 mmol L^{-1} H_2O_2 and 50 µL 4 µmol L^{-1} hemin in CBS, pH 10.5. A blank reading was done prior to the H_2O_2 addition. After H_2O_2 was added a 5 s shaking (425 cpm) was started and if not stated differently the CL intensity was measured at gain 80, read height (RH) 1 mm and integration time (IT) 2 s. All measurement were done at 25 °C.

5.2.9. Heterogenous complement assay with trigger

Here, specific lysis of the liposomes through the complement system in presence of a complement trigger was tested with different trigger molecules.

5.2.9.1. simple antibody trigger

The antibody trigger assay was based on a standard complement assay. In addition to the standard complement assay the liposomes were incubated with 100 µL goat anti-biotin

antibody (0.015 mg mL^{-1} in 1X PBS, pH 7.4 (equaling 0.2 mol% towards total lipid concentration) for 1 h at room temperature after the liposomes were bound to the MTP and washed twice with 200 µL outer buffer and once with 200 µL 1X PBS buffer pH 7.4. The complement assay was performed with 5,10 or 25 vol.-% pooled serum.

5.2.9.2. LPS-modified liposomes as trigger

Here, a standard complement assay with 5, 10 or 25 vol.-% serum was performed with liposomes that have been modified with LPS as trigger through the synthesis.

5.2.9.3. Bystander assay with antibody

A variation of the standard complement assay was applied. In the bystander assay, liposomes that can be lysed specifically through the complement system are mixed with liposomes that cannot be lysed and are tested in a standard complement assay. To distinguish between the signals of the different liposome types, sulforhodamine B and *m*-carboxy luminol liposomes as encapsulants were combined with the respective criteria. Before performing the complement assay, the liposomes were prepared with 0.2 mol% antibody towards the total lipid concentration. For the immobilized liposomes (*m*-carboxy luminol) 100 µL goat anti-biotin antibody (0.015 mg mL^{-1} in 1X PBS, pH 7.4) was incubated with the liposomes for 1 h at room temperature after they were bound to the MTP (100 µL, c(tL) = 50 µmol L^{-1}). The unbound liposomes (sulforhodamine B), c(tL) = 100 µmol L^{-1}) were separately prepared with 0.2 mol% goat anti-biotin antibody in a 10-times concentrated solution to end up with c(tL) = 10 µmol L^{-1} sulforhodamine B liposomes in the final assay. Deviating from the standard heterogenous complement assay, the sample in outer buffer was replaced by the positive control in the homogenous complement assay. Here, the liposomes were diluted in 30 mmol L^{-1} OG in PMB containing the respective amount of serum and were incubated for 1 h at 37 °C together with the PMB, inactive serum and active serum sample. After the 1 h incubation, the standard procedure was continued. Additionally, to the bystander assay two control assays with trigger antibody were performed containing only one liposome species. Here, sulforhodamine B liposomes were replaced by HSS buffer (10 mmol L^{-1} HEPES, 200 mmol L^{-1} NaCl, 200 mmol L^{-1} sucrose, 0.01% (w/v) NaN_3, pH 7.5) in the control with *m*-carboxy luminol liposomes whereas the sulforhodamine B liposome control was tested in an unmodified MTP. The fluorescence was monitored for 1 h at 37 °C in 2.5 min intervals in a transparent plate (gain 150, RH 4.5 mm, λ_{ex} = 565 (5) nm, λ_{em} = 585 (5) nm) whereas the bound liposomes were transferred after 3-times washing with

200 µL CBS and subsequent lysis into a white MTP before measuring, similar to the complement assay procedure. The chemiluminescence (CL) intensity was measured with a microplate reader (Syngene2, BioTek) after adding 50 µL 40 mmol L^{-1} H_2O_2 and 50 µL 4 µmol L^{-1} hemin in CBS, pH 10.5. A blank reading was done prior to the H_2O_2 addition. After H_2O_2 was added a 5 s shaking (425 cpm) was started and if not stated differently the CL intensity was measured at gain 80, read height (RH) 1 mm and integration time (IT) 2 s. All measurement were done at 37 °C.

5.2.9.4. Bystander assay with LPS-modified liposomes

Similarly to the bystander assay with the antibody, the bystander assay with the internal trigger LPS was performed as alteration of a standard complement assay. Deviating from the standard heterogenous complement assay, the sample in outer buffer was replaced by the positive control in the homogenous complement assay. Here, the liposomes were diluted in 30 mmol L^{-1} OG in PMB containing the respective amount of serum and were incubated for 1 h at 37 °C together with the PMB, inactive serum and active serum sample.100 µL of *m*-carboxy luminol liposome dilutions with a c(tL) = 50 µmol L^{-1} were immobilized overnight, 4°C, on a StAv-MTP and 10 µmol L^{-1} sulforhodamine B liposomes were added for the final complement assay. Two perspectives were investigated. Firstly, the bound liposomes contain LPS (anionic, PEG, LPS) and the unbound liposomes poses the stealth liposomes (anionic, N-glutaryl). Secondly the bound liposome represents the stealth liposomes (anionic, biotinylated) and the unbound liposome contains the trigger (anionic, biotinylated, LPS). Similar to the procedure with the antibody trigger, the fluorescence was monitored for 1 h at 37°C in 2.5 min intervals in a transparent plate (gain 150, RH 4.5 mm, λ_{ex} = 565 (5) nm, λ_{em} = 585 (5) nm) whereas the bound liposomes were transferred after 3-times washing with 200 µL CBS and lysis into a white MTP before measuring. The chemiluminescence (CL) intensity was measured with a microplate reader (Syngene2, BioTek) after adding 50 µL 40 mmol L^{-1} H_2O_2 and 50 µL 4 µmol L^{-1} hemin in CBS, pH 10.5. A blank reading was done prior to the H_2O_2 addition. After H_2O_2 was added a 5 s shaking (425 cpm) was started and if not stated differently the CL intensity was measured at gain 80, RH 1 mm and IT 2 s. All measurement were done at 37 °C.

5.2.10. Performance and stability test

The liposomes were stored at 4 °C in the dark with c(tL) > 9 mmol L^{-1}. For the performance test liposomes were diluted to c(tL) = 15 µmol L^{-1} or 10 µmol L^{-1} in CBS buffer to measure

the CL signal for intact liposomes and in 30 mmol L^{-1} OG diluted in CBS to measure the CL signal lysed. The liposome dilution contained in addition 2 µmol L^{-1} hemin. 100 µL of liposome dilution was first measured as blank read and afterwards 100 µL of H_2O_2 (4 mmol L^{-1}) was added directly before the second CL read. CL measurements were recorded with a microplate reader (Syngene2, BioTek). A blank reading was done prior to the H_2O_2 addition. After H_2O_2 was added and 5 s shaking (425 cpm), the CL intensity was measured at gain 80, RH 1 mm and IT 2 s. All measurement were done at 25 °C. Leakage was calculated according to (1) for each stability measurement:

$$\boldsymbol{free\ dye}\ (\%) = \frac{\boldsymbol{I_{intact\ liposomes}} \times \mathbf{100}}{\boldsymbol{I_{lysed\ liposomes}}} \quad (1)$$

with

$I_{intact\ liposomes}$: CL signal of intact liposomes

$I_{lysed\ liposomes}$: CL signal of lysed liposomes

5.3. Results and Discussion

5.3.1. Development of stealth liposomes through variation of the lipid composition

Initially, for the development of liposomes as reporter probes in the intended assay format, the lipid composition and architectural features of the liposomes were investigated towards their effect on the human complement system. Prior studies, which are not subject to this work, revealed that cholesterol, although known for having a stabilizing effect on the liposomal membrane[14], plays also an important role in inducing complement related responses[15]. Testing the 30 and 75 mmol L^{-1} *m*-carboxy luminol liposomes with 45 mol% cholesterol showed complement induced lysis already in absence of a complement trigger. Hence, the initial lipid composition with ≥ 40 mol% cholesterol was refined to 5 mol% and different surface charges, functional groups and alternate stabilizers such as polyethylene glycol (PEG) were investigated. Their effect on the complement system was studied to deduce the boundaries for stealth liposomes that can be specifically lysed by the complement system in an heterogenous assay format using chemiluminescence as highly sensitive detection strategy.

5.3.1.1. Liposome characteristics

Therefore, model liposomes with 30 mmol L^{-1} *m*-carboxy luminol, 5 mol% cholesterol and 2 mol% biotin with different surface charges were synthesized, characterized, and

evaluated towards their binding ability and complement activity. The hydrodynamic diameter, zeta potential, polydispersity index (PdI) and the total lipid (tL) concentration of these liposomes are listed in **Table 2**. Furthermore, the CL performance and thus the stability of the newly synthesized liposomes was monitored for several weeks (**Figure 3**). Overall, all liposomes remained stable for at least 6 months. Yet, the pegylated liposomes exhibit from the beginning a higher percentage of free dye of 10 to 20 %. Along with this observation, liposomes with cationic surface charge tend to attract the encapsulant dye more than their anionic equivalent which is evident by the amount of free dye for anionic (≤ 2%), anionic pegylated (≤ 11%), cationic (≤ 4%) and cationic pegylated liposomes (≤ 20 %).

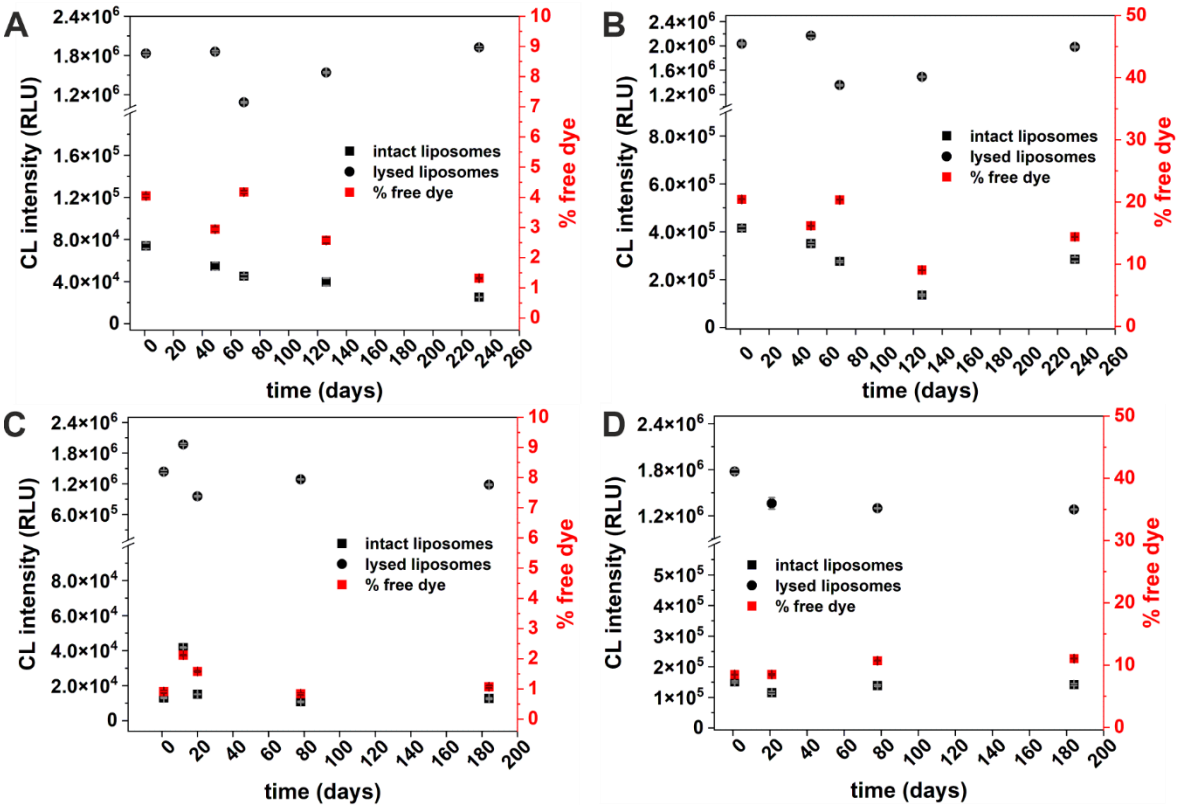

Figure 3 Stability study of A) cationic, B) cationic-PEG, C) anionic and D) anionic-PEG biotin tagged 30 mmol L^{-1} *m*-carboxy luminol liposomes by measuring the chemiluminescence intensity of liposomes in solution. Chemiluminescence properties of the *m*-carboxy luminol liposome measurement was performed by dilution of liposomes to c(tLipids) = 10 µmol L^{-1} either in CBS buffer or 30 mmol L^{-1} OG/CBS buffer including 2 µmol L^{-1} hemin. 100 µL of each liposome dilution was reacted with 100 µL 4 mmol L^{-1} H_2O_2 and measured first without H_2O_2 and after 5 s shaking with H_2O_2 with following settings: integration time 2 s, gain 80, read height 1 mm, n = 4

In addition, a competitive biotin assay was performed to assess the immobilization ability of the different liposome types. Here, six to seven-times higher EC_{50} value for the pegylated

liposomes were determined in direct comparison to their non-pegylated equivalents (**Figure 4**).

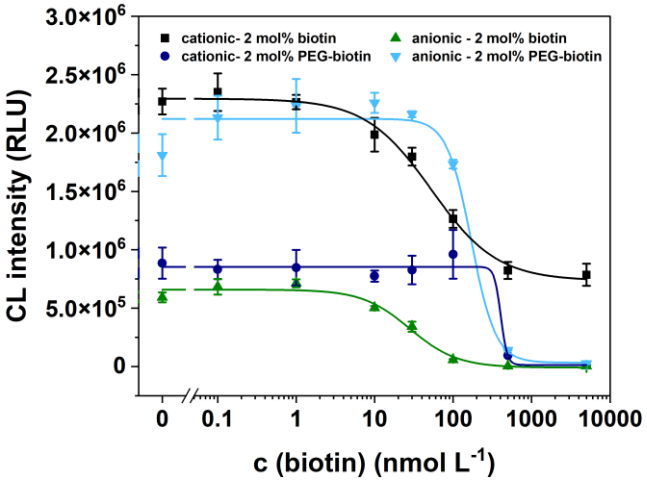

Figure 4 Competitive biotin assay with biotin-modified *m*-carboxy luminol liposomes, washing with outer buffer, incubation of biotin dilution including liposomes (total lipid concentration = 10 µmol L^{-1}) for 1 h, three times washing with CBS buffer, lysis for 5 min with 30 mmol L^{-1} OG/CBS, addition of 50 µL 40 mmol L^{-1} H_2O_2 and 50 µL 40 µmol L^{-1} hemin in CBS, pH 10.5). Chemiluminescence measurement: 5 s shaking (425 cpm), gain 100, RH 1 mm, IT 2 s, T 25°C, n = 4

The pegylated liposomes exhibit similar EC_{50} values regardless of the surface charge. This behavior is observed for the non-pegylated liposomes as well. The overall immobilization, however, varies between anionic, cationic, pegylated and non-pegylated liposomes (**Table 3**).

Table 3 Summary of key figures of competitive biotin assay with biotinylated liposomes and data for dye load comparison

Batch	Surface	I_{intact}[a] (× 10^5 RLU)	I_{lysed}[b] (× 10^5 RLU)	upper asymptote (× 10^5 RLU)	EC_{50} (biotin) (nmol L^{-1})
batch 15	cationic, biotin	0.45 ± 0.02	10.8 ± 0.1	22.9	53
batch 16	cationic, PEG-biotin	2.76 ± 0.04	13.6 ± 0.09	8.54	405
batch 17	anionic, biotin	0.151 ± 0.001	9.6 ± 0.1	6.59	28
batch 18	anionic, PEG-biotin	1.16 ± 0.04	13.6 ± 0.7	21.2	170

[a]CL intensity of intact liposomes (c(tL) = 10 µmol L^{-1}) in solution, [b]CL intensity of lysed liposomes (c(tL) = 10 µmol L^{-1}) in solution

Here, the competitive binding event was performed for 1 h. The cationic non-pegylated liposomes show similar binding efficiency to the anionic pegylated once and the cationic pegylated to the anionic non-pegylated liposomes (**Figure 4**). When measuring the liposomes in solution, similar CL intensities (**Table 3**) were obtained for all four liposome

types, hence the variation in the upper asymptote value is not an artefact of varying dye load of the liposomes but rather indicates varying immobilization behavior.

Furthermore, a higher EC_{50} value for the pegylated liposomes suggests that more streptavidin binding sides are covered with biotinylated liposomes. Due to the PEG2000 spacer the biotin on the liposome surface is less sterically hindered and a greater number of biotin functionalized lipids from the lipid bilayer have access to streptavidin binding sides. Consequently, a higher biotin concentration is needed to displace the biotinylated liposomes with free biotin. For the non-pegylated liposomes, however, DPPE-biotin was used as biotinylated lipid. Here, the biotin is directly attached to the headgroup of the phospholipid and thus after proper integration of this lipid into the bilayer, the biotin is exposed directly at the liposome surface, minimizing its steric flexibility.

5.3.1.2. Complement Assay with biotin-modified anionic and cationic CL-liposomes

After characterization of the liposomes and evaluation of the binding efficiency, the stability of the modified liposomes in human serum was evaluated in a complement assay. Identification of the fundamental factors of complement-activating liposomes are still very challenging to pinpoint due to the limitation of very few diverse liposome compositions within each single complement system study. Yet, Chonn *et al.* have found that the surface charge has an effect on the activation of different pathways of the complement system.[16] Both, positively and negatively charged liposomes activate the complement system but through different pathways. Additionally, Chonn *et al.* have shown that the complement activation is dependent on the lipid concentration. Hence, we tested all synthesized liposomes with regard to their behavior in presence of the human complement system in order to determine if the chosen lipid composition withstand the human complement system. For this, the liposomes were bound to a streptavidin MTP in outer buffer overnight and incubated for 1 h at 37 °C with either outer buffer (OB), Paul Morgan buffer (PMB), inactive serum (iaS) or active serum (aS) (5 and 10 vol.-%) (**Figure 5**).

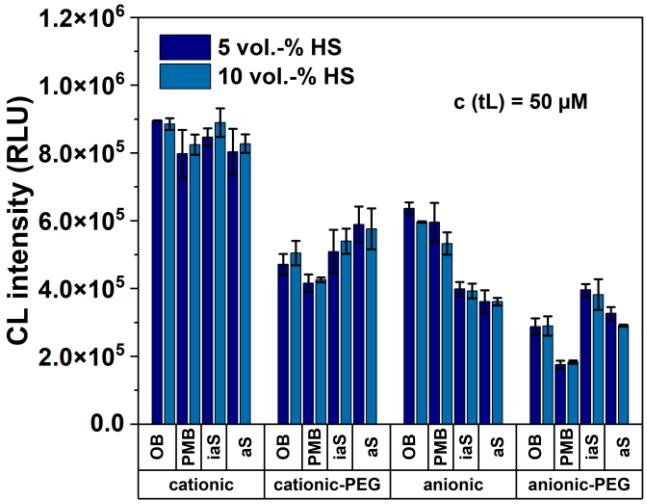

Figure 5 Heterogenous complement assay with biotin-modified pegylated and non-pegylated, anionic and cationic chemiluminescence liposomes. Liposomes with a total lipid concentration of 50 µmol L^{-1} were immobilized overnight on a streptavidin coated MTP and incubated for 1 h at 37 °C in either outer liposome buffer, Paul Morgan buffer (PMB), inactive serum (iaS) and active serum (aS) (varying human serum (HS) concentrations 5 and 10 vol.-%). Chemiluminescence measurement was performed by adding 50 µL of 4 µmol L^{-1} hemin and 50 µL 40 mmol L^{-1} H_2O_2 in 0.01 M CBS, pH 10.5, 2 s integration time, gain 80, RH 1 mm, T = 25 °C, n = 3

Only the inactive and active serum samples contain human serum, outer buffer and Paul Morgan buffer were used as internal control for the liposome stability. Here, increasing the incubation time from 1 h to overnight together with the 1 h incubation at 37 °C changes the previously determined order from cationic non-pegylated liposomes being the most stable and best immobilizing type, followed by anionic non-pegylated, cationic pegylated, and anionic pegylated liposomes (**Figure 4**, OB signal). If complement induced lysis occurs, the CL signal of the active serum sample will drop compared to the inactive serum sample. The outer buffer and PMB sample pose internal controls to monitor the overall stability of the liposomes in the assay format. Only the anionic pegylated liposomes show a reduced signal in active serum. Hence, the herein synthesized cationic, anionic and cationic pegylated liposomes were identified to be stealth in up to at least 10 vol.-% human serum (HS) in the applied complement assay. Here, cationic liposomes show the most efficient immobilization followed by the anionic and cationic PEG liposomes. The anionic pegylated liposomes were the least efficient to be immobilized and most instable once in contrast to the other liposomes, demonstrated by their reduced signal in outer buffer and PMB. The trend in the binding behavior is most likely attributed to the varying surface charges of the different liposome types. Through Atomic Force Microscopy – Force Spectroscopy, Almonte *et al.* showed that streptavidin (pI 6.3)[17] in contrast to avidin (pI 10.5) exhibits a more negative experimental charge density at neutral pH. These findings together with the study of

Sivasankar *et al.*, who studied the surface charge density of streptavidin in dependency of the pH, suggest that the different immobilization behavior of the tested liposomes originate from electrostatic interaction. Liposomes with a negative surface charge are stronger repelled from the inherent negative surface charge of streptavidin in neutral to alkaline solution than cationic liposomes. Pegylation on the other hand shields the inherent charge from the lipids to a certain degree, which is supported by the respective zeta potential measurement (**Table 2**).

5.3.2. Development of liposome trigger

Even though the cationic liposomes pose the most stable lipid composition within the complement assay, in order to achieve complement induced lysis in the presence of a trigger molecule, a lipid composition that remains stealth within human serum and yet, at the same time, can be lysed specifically through the complement system is inevitable. Hence, for first studies the anionic liposomes were investigated, as they show marginal vulnerability to lysis when serum is present, although this lysis is independent of the complement system. Having identified the lipid composition, which is suitable to generate perfectly balanced stealth liposomes, a proof of principle study for triggered lysis through the complement system was conducted. For this, different strategies were pursued.

5.3.2.1. through an internal trigger - anionic LPS liposomes

It is commonly accepted that bacterial lipopolysaccharide (LPS), an essential component of the outer membrane of gram-negative bacteria, shows complement activating properties.[18] As it is a large glycolipid that is composed of three structural units, lipid A, the hydrophilic core oligosaccharides and the o-antigens[19], mimicking the structural properties of a phospholipid, it suites well for integration into the lipid bilayer membrane of liposomes. Simultaneously, the incorporation of LPS into the membrane of liposomes allows to generate a positive control for complement induced lysis through an internal trigger.

5.3.2.1.1. Synthesis and characterization of LPS liposomes

Besides the triggered activation of the complement system through the integrated LPS, a key feature of the liposomes is the immobilization on the MTP for the heterogenous complement assay. Hence, the anionic liposome formulation with DPPE-biotin (batch 19) and DMPE-PEG2000-biotin (batch 20) together with 1 mol% LPS were synthesized and characterized (**Table 4**). For the non-pegylated liposomes, similar sizes and EC_{50} (biotin) values towards their parent liposome were obtained. For the pegylated species

liposomes a slightly higher EC_{50} value was obtained for liposomes with LPS in contrast to the parent liposome without LPS.

Table 4 Summary of key figures of LPS liposomes and respective parent liposomes

Lipid composition	Surface	PdI[a]	Size[b] by Int (nm)	Zeta potential (mV)	upper asymptote (× 10^5 RLU)	EC_{50} (biotin) (nmol L^{-1})
batch 17 DPPC: 74.9 mol% DPPG: 17.5 mol% Cholesterol: 5.6 mol% DPPE-biotin: 2.0 mol%	anionic, biotin	0.09 ± 0.01	135 ± 42	-19 ± 1	6.59	28
batch 18 DPPC: 71.7 mol% DPPG: 19.3 mol% Cholesterol: 4.9 mol% DMPE-PEG-biotin: 2.0 mol% DMPE-PEG: 2.1 mol%	anionic, PEG-biotin	0.05 ± 0.02	127 ± 35	-3.1 ± 1.4	21.2	170
batch 19 DPPC: 73.7 mol% DPPG: 17.8 mol% Cholesterol: 5.7 mol% DPPE-biotin: 1.9 mol% LPS: 0.9 mol%	anionic, biotin, LPS	0.05 ± 0.01	135 ± 37	-9.3 ± 2.1	0.75	21
batch 20 DPPC: 74.2 mol% DPPG: 17.9 mol% Cholesterol: 5.0 mol% DMPE-PEG-biotin: 1.9 mol% LPS: 1.0 mol%	anionic, PEG-biotin, LPS	0.07 ± 0.02	142.8 ± 40	-5.9 ± 0.7	15.1	105

[a]PdI: Polydispersity index, [b]size refers to hydrodynamic diameter

The stability of the LPS liposomes was monitored for at least 72 days. The percentage of free dye remains below 13 % within the tested period (**Figure 6**). This is higher compared to the anionic liposomes without LPS but still lower as for the pegylated cationic liposomes and remains constant throughout the tested period confirming that the synthesized liposomes are stable.

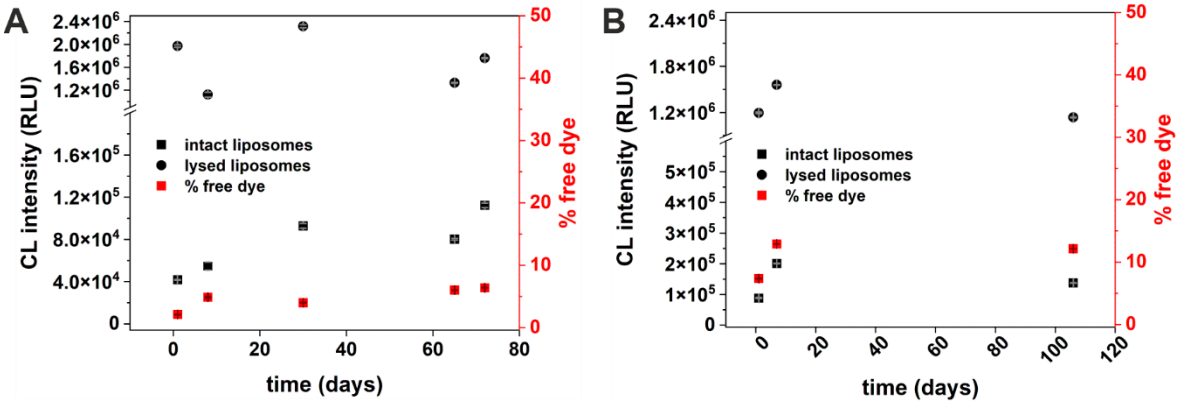

Figure 6 Stability study of LPS modified 30 mmol L^{-1} *m*-carboxy luminol liposomes with A) DPPE-biotin and in B) DMPE-PEG2000-biotin as anchoring lipid by measuring the chemiluminescence intensity of liposomes in solution. Chemiluminescence properties of the *m*-carboxy luminol liposome measurement was performed by dilution of liposomes to c(tLipids) = 10 µmol L^{-1} either in CBS buffer or 30 mmol L^{-1} OG/CBS buffer including 2 µmol L^{-1} hemin. 100 µL of each liposome dilution was reacted with 100 µL 4 mmol L^{-1} H_2O_2 and measured first without H_2O_2 and after 5 s shaking with H_2O_2 with following settings: integration time 2 s, gain 80, read height 1 mm, n = 4

5.3.2.1.2. Complement Assay with biotin-modified anionic LPS CL-liposomes

Compared to the liposomes without LPS, the newly synthesized LPS-containing liposomes show overall reduced CL intensity, especially in OB and PMB. Interestingly, the inactive serum samples show for both liposome types a higher CL signal compared to the controls, indicating that the serum proteins may have a stabilizing effect on these liposomes. LPS is known for its distinct interaction with monovalent and divalent cations to either stabilize LPS or form negatively-charged aggregates indicating that due to its size and charge, steric and electrostatic repulsion maybe the reason for the reduced signal in high salt buffers such as OB and PMB.[20] When using DMPE-PEG2000-biotin over DPPE-biotin, the CL signal in inactive serum approaches almost the intensities of the liposomes without LPS (**Figure 7 A**), supporting the theory that the huge hydrophilic part of LPS shields the biotin from binding to streptavidin when DPPE-biotin is used.

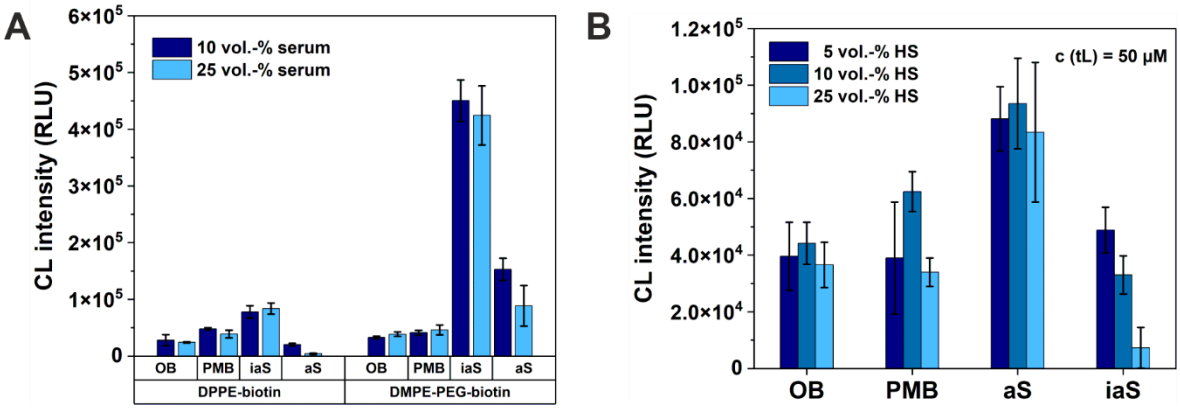

Figure 7 Heterogenous complement assay with biotin-modified anionic chemiluminescence liposomes with 1 mol% LPS. Liposomes with a total lipid concentration of 50 µmol L^{-1} were immobilized overnight on a streptavidin coated MTP and incubated for 1 h at 37 °C in either outer liposome buffer (OB), Paul Morgan buffer (PMB), inactive serum (iaS) and active serum (aS). A) shows DPPE-biotin and DMPE-PEG2000-biotin functionalized LPS liposomes at serum concentrations 10 and 25 vol.-% and B) illustrates a serum titration from 5 - 25 vol.-% within the complement assay with LPS liposome containing DPPE-biotin. Chemiluminescence measurement was performed by adding 50 µL of 4 µmol L^{-1} hemin and 50 µL 40 mmol L^{-1} H_2O_2 in 0.01 M CBS, pH 10.5, 2 s integration time, gain 80, RH 1 mm, T = 25 °C, n = 3

When using DMPE-PEG2000-biotin with a PEG2000 linker the biotin is more exposed to the surface, yielding in better immobilization properties (**Table 4**). Furthermore, for both liposome types a reduction of the active serum sample was obtained confirming at the same time the successful modification with LPS and its trigger properties. Following the standard complement protocol, the performance of the LPS liposomes with DPPE-biotin were finally tested with 5 - 25 vol.-% human serum. Increasing the serum concentration to 25 vol.-%, the complement related lysis approaches almost 100 % (**Figure 7 B**), considering only the active and inactive serum value (**Table 5**). Furthermore, the lysis increases linear with the serum concentration.

Table 5 Serum dependency of the lysis values obtained for chemiluminescence LPS liposomes in a standard complement assay

Liposome type	serum conc. (vol.-%)	I_{iaS}[a]	I_{aS}[b]	% lysis[c]	% CL signal towards iaS[d]
anionic LPS liposomes	5	$(8.8 \pm 1.1) \times 10^4$	$(4.9 \pm 0.8) \times 10^4$	45 %	55 %
	10	$(9 \pm 2) \times 10^4$	$(3.3 \pm 0.7) \times 10^4$	65 %	35 %
	25	$(8 \pm 2) \times 10^4$	$(0.7 \pm 0.7) \times 10^4$	91 %	9 %

[a] CL signal in inactivated serum, [b] CL signal in activated serum, [c]was determined according to $(I_{iaS} - I_{aS})/ I_{iaS} \times 100$, [d] was determined according $I_{aS}/ I_{iaS} \times 100$

Using DMPE-PEG2000-biotin for biotin functionalization of the liposomes allows to improve the performance of the LPS liposomes in a complement assay (**Table 6**). They are still triggerable but more stable towards the complement assay conditions than the liposomes

with DPPE-biotin. They show five-times higher CL signal in inactivated serum. We assume that the complement lysis is a sensitive process that requires perfectly balanced serum to liposome ratio which is supported by this experiment and the obtained reduced lysis values with the more efficiently immobilized liposomes.

Table 6 Overview of lysis values with chemiluminescent biotin and PEG2000-biotin LPS liposomes in a standard complement assay

Liposome type	serum conc. (vol.-%)	I_{iaS}[a]	I_{aS}[b]	% lysis[c]	% CL signal towards iaS[d]
anionic LPS liposomes	10	$(7.8 \pm 1.1) \times 10^4$	$(2.0 \pm 0.2) \times 10^4$	73 %	27 %
	25	$(8.4 \pm 1.0) \times 10^4$	$(0.4 \pm 0.1) \times 10^4$	95 %	5 %
anionic PEG LPS liposomes	10	$(45 \pm 4) \times 10^4$	$(15 \pm 2) \times 10^4$	66 %	34 %
	25	$(42 \pm 5) \times 10^4$	$(9 \pm 4) \times 10^4$	79 %	21 %

[a] CL signal in inactivated serum, [b] CL signal in activated serum, [c]was determined according to $(I_{iaS} - I_{aS})/ I_{iaS} \times 100$, [d] was determined according $I_{aS}/ I_{iaS} \times 100$

5.3.2.2. through an external trigger - antibodies

An alternative approach to trigger the complement system is through antibodies, mainly the IgG and IgM antibodies, which are also intended to be the trigger molecule in the final assay format. The reported accepted reference ranges of total IgG and IgM in human serum is 7-16 mg mL^{-1} and 0.4 - 2.3 mg mL^{-1}, respectively.[21] It is well known that IgG and IgM antibodies successfully activate the classical pathway when the complement protein complex C1q binds to the Fc region of the antibody.[22] Yet, there are differences within the IgG subtypes with regard to their complement activation ability. Studies, which are not subject to this thesis, prescreened a variety of antibodies and found a polyclonal anti-biotin antibody that is able to activate the complement system and lyse biotinylated liposomes specifically in the homogenous format. Due to the concentration dependency of this system within the internal trigger study, a proof-of-concept study of the antibody trigger in the heterogenous format was conducted testing the effect of different surface charges of the liposomes, antibody concentrations and serum concentrations.

5.3.2.2.1. Serum titration and evaluation of liposome type

The experiments in the homogenous assay format revealed, that 0.2 mol% anti-biotin antibody toward the applied total lipid concentration initiates complement induced lysis. Hence, the effect of different surface charges and pegylation was studied with this concentration in the heterogenous format. Here, a standard complement assay was

performed with c(total lipids) = 50 µmol L^{-1} with prior incubation with the anti-biotin antibody before 5 vol.-% (**Figure 8 A**), 10 vol.-% (**Figure 8 B**) and 25 vol.-% serum (**Figure 8 C**) was applied. The respective control experiment with the standard complement assay is shown in (**Figure 8 D**)**.**

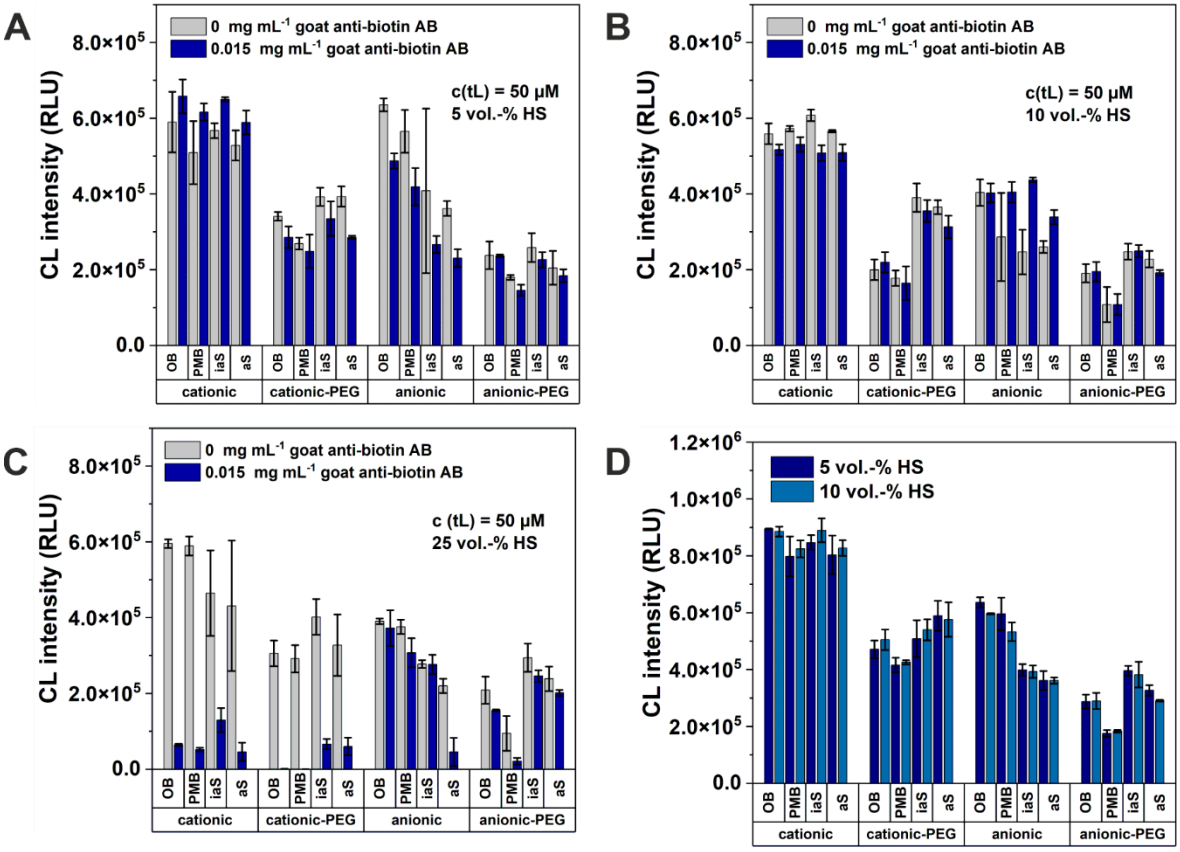

Figure 13 Heterogenous complement assay with biotin-modified anionic and cationic chemiluminescence liposomes. Liposomes with a total lipid concentration of 50 µmol L^{-1} were immobilized overnight on a streptavidin coated MTP and incubated for 1 h at 37 °C in either outer liposome buffer, Paul Morgan buffer (PMB), inactive serum (iaS) and active serum (aS) (varying serum concentrations 5 - 25 vol.-%). Cationic, cationic-PEG, anionic and anionic-PEG were tested with and without 0.015 mg mL^{-1} goat anti-biotin trigger antibody (0.2 mol%) in A) with 5 vol.-% serum, in B) with 10 vol.-% serum and in C) with 25 vol.-% serum. D) shows the tested liposomes in the standard complement assay without trigger. Chemiluminescence measurement was performed by adding 50 µL of 4 µmol L^{-1} hemin and 50 µL 40 mmol L^{-1} H_2O_2 in 0.01 M CBS, pH 10.5, 2 s integration time, gain 80, RH 1 mm, T = 25 °C, n = 3

The obtained lysis values of the tested liposomes and the CL intensities in the antibody-triggered complement assay (**Figure 8 A-C**) correlate well within the standard (**Figure 8 D**) complement assay. No antibody-triggered lysis of the tested liposomes was observed with 5 vol.-% human serum (**Figure 8 A**). At 10 vol.-% serum, the anionic liposomes show a tendency to antibody induced lysis, whereas the reduction of CL intensity of cationic-PEG and anionic-PEG liposomes cannot be clearly attributed to antibody triggered lysis. Here, the decline of CL intensity occurs to a similar degree in the samples

that were not treated with the antibody. Applying 25 vol.-% human serum, the antibody induced lysis for the anionic liposomes was verified by an increased lysis value (83 %). At 25 vol.-% serum, the cationic liposomes show triggered lyses as well. However, the lysis only approaches 65 % with the cationic liposomes, whereas the anionic liposomes show over 80 % (**Table 7**).

Table 7 Lysis values for various types of chemiluminescent liposomes in antibody triggered complement assay

Liposome type	antibody conc. (mg mL^{-1})	serum conc. (vol.-%)	I_{iaS}[a] (× 10^5 RLU)	I_{aS}[b] (× 10^5 RLU)	% lysis[c]	% CL signal towards iaS[d]
cationic	0	5	5.7 ± 0.2	5.3 ± 0.4	7 % (5 %)	93 % (95 %)
	0.015	5	6.50 ± 0.05	5.9 ± 0.3	9 %	91 %
cationic-PEG	0	5	3.9 ± 0.2	3.9 ± 0.3	0 % (-16 %)	100 % (116%)
	0.015	5	3.4 ± 0.5	2.9 ± 0.4	15 %	85 %
anionic	0	5	4.1 ± 2.2	3.6 ± 0.2	11 % (9 %)	89 % (91 %)
	0.015	5	2.7 ± 0.2	2.3 ± 0.2	14 %	86 %
anionic-PEG	0	5	2.6 ± 0.4	2.1 ± 0.4	21 % (17 %)	79 % (83 %)
	0.015	5	2.3 ± 0.2	1.8 ± 0.2	19 %	81 %
cationic	0	10	6.1 ± 0.2	5.66 ± 0.03	7 % (7 %)	93 % (93 %)
	0.015	10	5.1 ± 0.2	5.1 ± 0.2	0 %	100 %
cationic-PEG	0	10	3.9 ± 0.4	3.7 ± 0.2	6 % (-7 %)	94 % (107 %)
	0.015	10	3.6 ± 0.3	3.1 ± 0.3	12 %	88 %
anionic	0	10	2.5 ± 0.6	2.6 ± 0.2	-5 % (8 %)	105 % (92 %)
	0.015	10	4.37 ± 0.06	3.4 ± 0.2	22 %	78 %
anionic-PEG	0	10	2.5 ± 0.2	2.3 ± 0.2	8 % (24 %)	92 % (76 %)
	0.015	10	2.5 ± 0.2	1.92 ± 0.07	23 %	77 %

Table 7 Lysis values for various types of chemiluminescent liposomes in antibody triggered complement assay (continued)

Liposome type	antibody conc. (mg mL^{-1})	serum conc. (vol.-%)	I_{iaS}[a] (× 10^5 RLU)	I_{aS}[b] (× 10^5 RLU)	% lysis[c]	% CL signal towards iaS[d]
cationic	0	25	4.7 ± 1.1	4.3 ± 1.7	7 % (7 %)	93 % (93 %)
	0.015	25	1.3 ± 0.3	0.5 ±0.2	65 %	35 %
cationic-PEG	0	25	4.0 ± 0.5	3.3 ± 0.8	19 % (-7 %)	81 % (107 %)
	0.015	25	0.6 ± 0.1	0.6 ± 0.2	9 %	91 %
anionic	0	25	2.8 ± 0.1	2.2 ± 0.2	21 % (8 %)	79 % (92 %)
	0.015	25	2.8 ± 0.1	0.5 ± 0.4	83 %	17 %
anionic-PEG	0	25	2.9 ± 0.4	2.4 ± 0.3	19 % (24 %)	81 % (76 %)
	0.015	25	2.5 ± 0.2	2.0 ± 0.08	18 %	82 %

[a] CL signal in inactivated serum, [b] CL signal in activated serum, [c]was determined according to (I_{iaS} - I_{aS})/ I_{iaS} × 100, [d] was determined according I_{aS}/ I_{iaS} × 100, [c,d] values in brackets correlate to lysis values in standard complement assay, negative lysis values are interpreted with the absence of lysis

Similarly, to the LPS liposomes, the trigger ability increases with increasing serum content. The anionic liposomes appear to be the most suited liposomes to be triggered by the anti-biotin antibody. The cationic liposomes show triggered lysis as well but only at 25 vol.-% serum. However, the elevated serum concentration in turn interferes with the immobilization and stability of these liposomes and are probably caused by electrostatic interferences between the involved proteins and the liposomes. Furthermore, the assay results were verified with at least one repetition. The pegylated liposomes show overall inhomogeneous behavior in the heterogenous assay leading to inconclusive results (**Table 8**). This might be caused by their overall instable binding properties. Hence, they are not suitable for the intended assay and were not further investigated. The anionic liposomes give a relatively reproducible lysis value of around 80 % which is also the highest obtained value. The cationic liposomes are the second species which can be lysed by an antibody trigger. However, the cationic liposomes show more divergent results in the control experiments (OB and PMB) making interpretation controversial. In addition, the cationic liposomes show only half of the lysis of the anionic liposomes with a lysis value of around 45 % which varies stronger from assay to assay (**Table 8**).

Table 8 Validation of lysis values for various types of chemiluminescence liposomes in the antibody triggered complement assay

Liposome type	β (antibody) (µg mL^{-1})	lysis in standard complement assay	lysis[a] (1)	lysis[a] (2)	lysis[a] (3)	lysis[a] (4)
cationic	0	7 %	7 %	**-7 %**	-7 %	2 %
	15	-	65 %	46 %	32 %	36 %
cationic-PEG	0	-7 %	19 %	-10 %	-	44 %
	15	-	9 %	5 %	-	25 %
anionic	0	8 %	21 %	20 %	13 %	-
	15	-	83 %	83 %	74 %	-
anionic-PEG	0	24 %	19 %	7 %	-	-
	15	-	18 %	58 %	-	-

[a]was determined according to (I_{iaS} - I_{aS})/ I_{iaS} × 100, negative lysis values are interpreted with the absence of lysis

5.3.2.2.2. Antibody titration

After determining the liposome species that can be lysed and the serum concentration that is required for antibody triggered lysis, the required antibody concentration was verified. Antibody induced lysis is only obtained when using 0.2 mol% (equals 15 µg mL^{-1}) goat anti-biotin antibody for both, cationic and anionic liposomes (**Figure 9**). Lower concentrations do not initiate antibody-triggered lysis and further support the concentration dependency of the system.

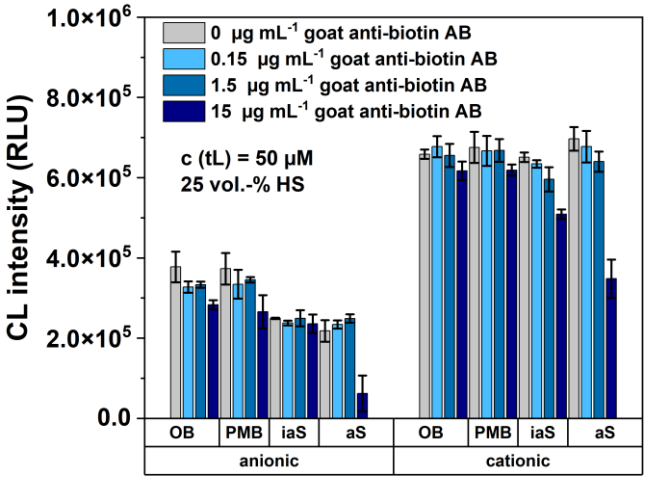

Figure 9 Antibody-titration within triggered complement assay using biotin-modified anionic and cationic 30 mmol L^{-1} *m*-carboxy luminol liposomes. Liposomes with a total lipid concentration of 50 µmol L^{-1} were immobilized overnight on a streptavidin coated MTP and incubated for 1 h with goat anti-biotin antibody before incubation in either outer liposome buffer (OB), Paul Morgan buffer (PMB), inactive serum (iaS) and active serum (aS) (25 vol.-% human serum (HS)) for 1 h at 37 °C. Chemiluminescence measurement was performed by adding 50 µL of 4 µmol L^{-1} hemin and 50 µL 40 mmol L^{-1} H_2O_2 in 0.01 M CBS, pH 10.5, 2 s integration time, gain 80, RH 1 mm, T = 25 °C, n = 3

5.3.3. Innocent bystander assay – localized and targeted lysis of liposomes

A fundamental requirement for the final assay format is the localized and specific lysis of the targeted liposomes thorough the complement system as a result of the intended binding events. Even though about 100-times more complement is needed for non-specific complement lysis[23], the so-called innocent bystander lysis, in which non-targeted cells in close proximity are also affected, would interfere with the final assay format. Hence, the triggered lysis of liposomes through the complement system was studied in more detail using liposomes that can be lysed through an external or internal trigger together with their stealth counterpart. In order to resolve the response of the respective liposomes fluorescent and chemiluminescent liposomes were used. The trigger was either LPS on the surface of the liposomes or the goat anti-biotin antibody. Within the tested systems the bystander liposomes were not affected by the localized complement activation.

5.3.3.1. Key characteristics of the tested liposomes

Here, the following 30 mmol L^{-1} *m*-carboxy luminol and 10 mmol L^{-1} SRB, 210 mmol L^{-1} NaCl liposomes were applied. The main characteristics of these liposomes are listed in **Table 9**.

Table 9 Key figures of liposomes applied for bystander complement assay

Liposome batch	Surface	Encapsulant	Extrusion membrane	PdI[a]	Size[b] by Int (nm)	Zeta potential (mV)
batch 17	anionic, biotin	*m*-carboxy luminol	0.2 µm	0.09 ± 0.01	135 ± 42	-19 ± 1
batch 20	anionic, PEG-biotin, LPS	*m*-carboxy luminol	0.2 µm	0.07 ± 0.02	143 ± 40	-5.9 ± 0.7
CG210327-1H	anionic, N-glutaryl	SRB[c]	0.4 µm	0.191 ± 0.004	187 ± 17 5000 ± 52	-21 ± 2
CG210331-1H	anionic, biotin	SRB[c]	0.4 µm	0.18 ± 0.01	218 ± 13 4574 ± -	-17.3 ± 1
KH210218-H	anionic, biotin, LPS	SRB[c]	0.4 µm	0.210 ± 0.002	271 ± 22 5103 ± 185	-10 ± 1

[a]Polydispersity index, [b]size refers to hydrodynamic diameter, [c]sulforhodamine B

5.3.3.2. Bystander Assay

Liposome lysis through the complement system is associated with the formation of the membrane attack complex that generates pores in the lipid bilayer. To evaluate if the membrane attack complex, binds non-specifically to nearby liposome surfaces, and lyses those after complement activation, a bystander assay was performed. Here, two different approaches were pursued. The first approach utilized an antibody, activating the complement system and induces liposome lysis after binding to the biotinylated liposome surface. The second approach uses liposomes which are decorated with lipopolysaccharide (LPS) on the surface for complement activation. Both complement active liposomes were mixed with their complement inactive counterpart.

5.3.3.2.1. employing an antibody as trigger

In the goat anti-biotin antibody bystander assay the trigger binds only to the biotinylated chemiluminescence liposomes, whereas the non-biotinylated SRB liposomes remain idle. No lysis of the bystander liposome (SRB liposome) was obtained by the localized activation of the complement system in vicinity of the biotinylated chemiluminescence liposome (**Figure 10 A**). To validate the results obtained by the bystander assay, both liposome types were simultaneously tested independently in a complement assay (**Figure 10 B, Figure 11**).

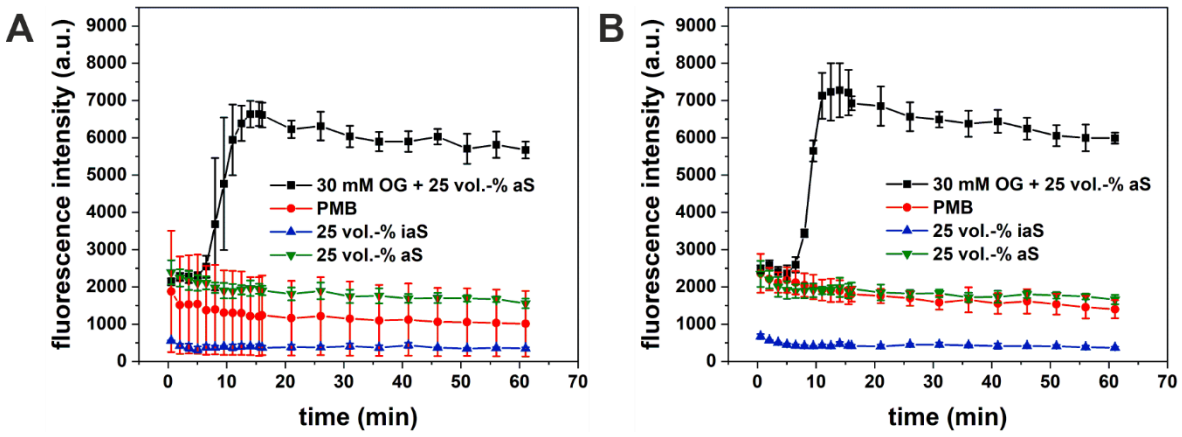

Figure 10 Fluorescent bystander complement assay with stealth SRB liposomes (N-glutaryl modified, anionic, c (tL) = 10 µmol L^{-1}) and antibody triggerable chemiluminescent liposomes (biotinylated, anionic, c (tL) = 50 µmol L^{-1}). The liposomes were preincubated with 0.015 mg mL^{-1} goat anti-biotin antibody before the complement assay. A) depicts the bystander assay including stealth and triggerable liposomes, B) depicts the independent complement assay of the stealth SRB liposomes. Fluorescence was monitored for 1 h at 37 °C with gain 150, RH 4.5 mm, λ_{ex} = 565 (5) nm, λ_{em} = 585 (5) nm, n = 3

Whereas the chemiluminescence liposomes show complement induced lysis (98 % in the bystander assay and 95 % in the independent complement assay, **Figure 11,Table 10**) the bystander liposomes remain stealth (28 % in the bystander assay and the independent complement assay, **Table 11**).

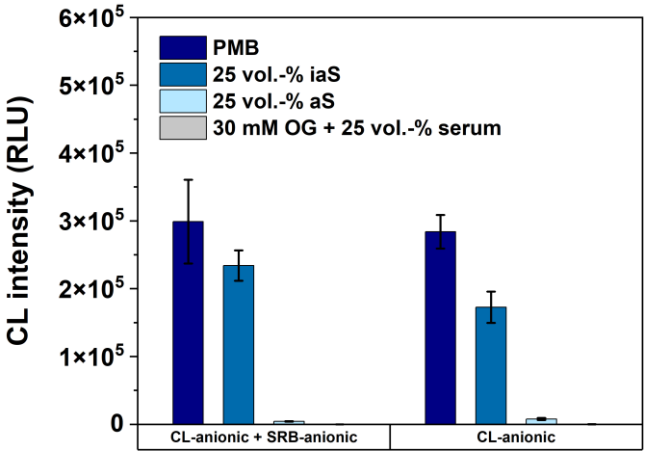

Figure 11 Chemiluminescent bystander complement assay with stealth SRB liposomes (N-glutaryl modified, anionic, c (tL) = 10 µmol L^{-1}) and antibody triggerable chemiluminescent liposomes (biotinylated, anionic, c (tL) = 50 µmol L^{-1}) with control independent assay with only chemiluminescent liposomes. The liposomes were preincubated with 0.015 mg mL^{-1} goat anti-biotin antibody before the complement assay. Chemiluminescence measurement was performed by adding 50 µL of 4 µmol L^{-1} hemin and 50 µL 40 mmol L^{-1} H_2O_2 in 0.01 M CBS, pH 10.5, 2 s integration time, gain 80, RH 1 mm, T = 37 °C, n = 3

Furthermore, the liposomes in the bystander assay behave similar to the independent complement assay with similar signal and lysis values (**Table 10**, **Table 11**).

Table 10 Lysis values obtained for chemiluminescence liposomes after complement assay with 25 vol.-% serum

Liposome combination	I_{iaS}[a]	I_{aS}[b]	% lysis[c]
CL-anionic, biotin (batch 17) **+ SRB-anionic** (CG210327)	$(2.3 \pm 0.2) \times 10^5$	$(0.044 \pm 0.003) \times 10^5$	98 %
CL-anionic, biotin (batch 17)	$(1.7 \pm 0.2) \times 10^5$	$(0.08 \pm 0.01) \times 10^5$	95 %

[a]CL signal in inactivated serum, [b] CL signal in activated serum, [c]was determined according to $(I_{iaS} - I_{aS})/ I_{iaS} \times 100$

It should be noted that the SRB liposomes were tested in the antibody employing bystander assay with a serum concentration of 25 vol.-% which deviates from the standardly used 10 vol.-% in the homogeneous complement assay, as this is needed for the antibody mediated triggering of the chemiluminescence liposomes. The independent complement assay with SRB liposomes ensures that 25 vol.-% serum was tolerated by these liposomes as no lysis was obtained (**Table 11**).

Table 11 Lysis values obtained for SRB liposomes after complement assay with 25 vol.-% serum

Liposome combination	PMB[a] (%)	aS[b] (%)	iaS[c] (%)	OG[d] (%)
CL-anionic, biotin (batch 17) **+ SRB-anionic** (CG210327)	18 ± 15	28 ± 2	6 ± 1	100 ± 6
SRB-anionic (CG210327)	23 ± 4	28 ± 2	6 ± 1	100 ± 3

[a]Paul Morgan buffer signal in % normalized to OG signal at minute 61, [b] active serum signal in % normalized OG signal at minute 61, [c] inactive serum signal in % normalized to OG signal at minute 61, [d] *n*-octyl-*β*-D-glucopyranoside signal in %, normalized to OG signal at minute 61

5.3.3.2.2. employing lipopolysaccharide as trigger

The bystander assay using complement activating LPS liposomes and the corresponding liposome without LPS confirmed the results of the bystander assay with the antibody trigger. Here, the bystander assay was performed once with SRB liposomes and once with chemiluminescence liposomes bearing the LPS trigger. In both combinations, the bystander (liposome without LPS) was not affected by the local activation of the complement system (**Figure 12 B, E**), whereas the liposome with trigger showed complement induced lysis (**Figure 12 A, F**). To validate the obtained results by the LPS bystander assay, the employed liposome types were tested independently in a standard complement assay (**Figure 12 C-F**).

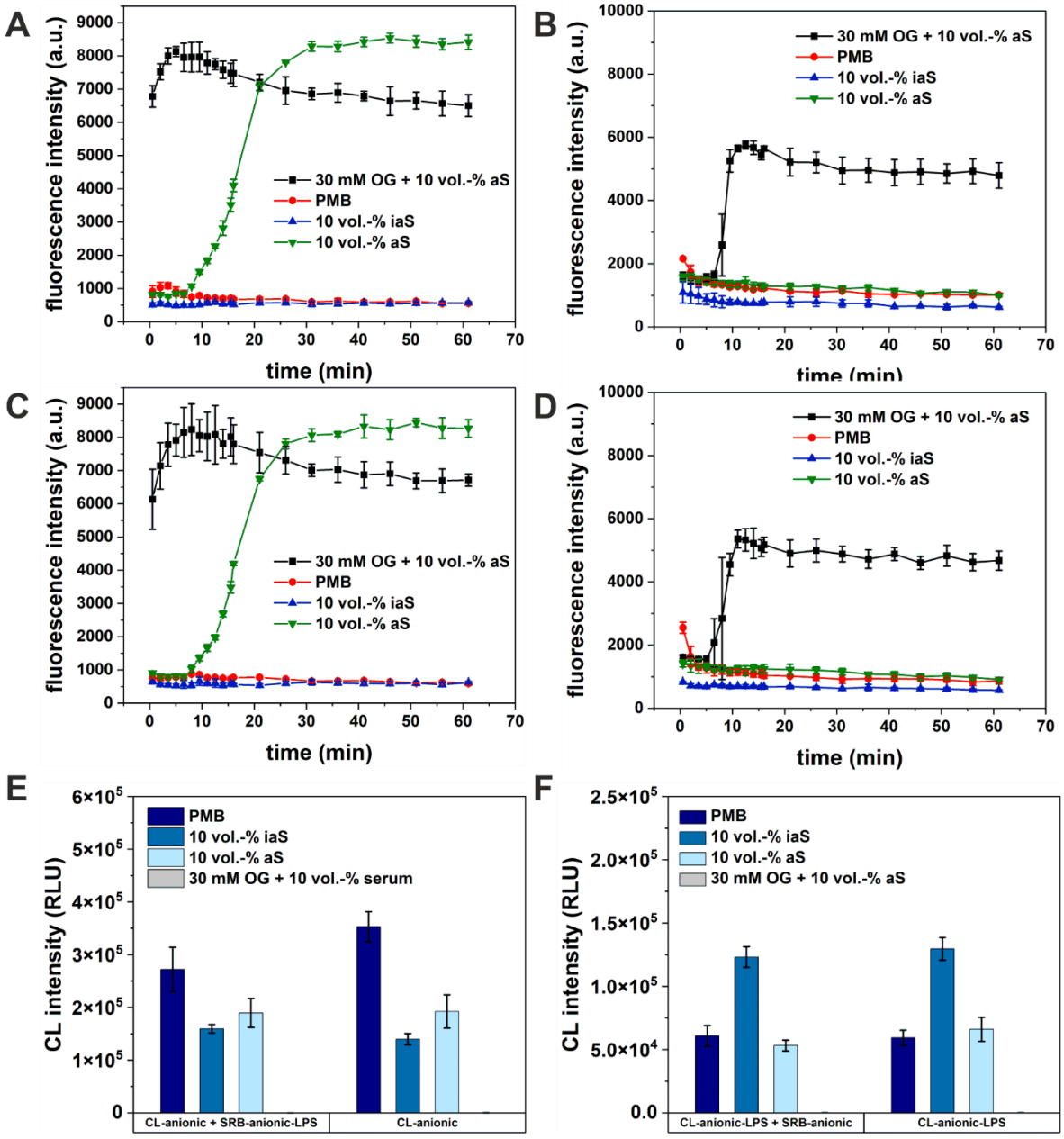

Figure 12 Bystander assay with triggerable SRB liposomes (anionic-LPS, c (tL) = 10 µmol L^{-1}) and stealth CL-liposomes (anionic, c (tL) = 50 µmol L^{-1}) with independent controls (A, C, E) and triggerable CL-liposomes (anionic-LPS) and stealth SRB liposomes (anionic) with independent controls (B, D, F). A and B show the bystander assay including stealth and triggerable liposomes, C and D show the complement assay of the respective SRB liposomes, E and F show the complement assay of the respective chemiluminescence liposomes. Chemiluminescence measurement was performed by adding 50 µL of 4 µmol L^{-1} hemin and 50 µL 40 mmol L^{-1} H_2O_2 in 0.01 M CBS, pH 10.5, 2 s integration time, gain 80, RH 1 mm, T = 37 °C, fluorescence was monitored for 1 h at 37 °C with gain 150, RH 4.5 mm, λ_{ex} = 565 (5) nm, λ_{em} = 585 (5) nm, n = 3

Whereas the chemiluminescence LPS liposomes show complement induced lysis (57 % in the bystander assay and 49 % in the independent complement assay, **Table 12**) the bystander SRB liposomes remain stealth (21 % in the bystander assay and 20 % the independent complement assay, **Table 13**). Here, 10 vol.-% human serum was applied

according to the standard conditions of the complement assay which causes lysis values of the chemiluminescence liposomes of only approximately 50 %. The chemiluminescent liposomes are bound to the MTP in the complement assay, shielding a large extend of the liposome surface from the interaction with the complement proteins. Hence, in order to fully lyse the liposomes, a higher concentration of complement complex and thus serum is needed to allow the formation of a higher number of MAC pores per area. This most likely causes the limited lysis within 10 vol.-% serum in contrary to the obtained full lysis of unbound SRB liposomes in the homogenous complement assay (**Table 13**).

Table 12 Lysis values obtained for chemiluminescence liposomes after complement assay with 10 vol.-% serum

Liposome combination	I_{iaS}[a]	I_{aS}[b]	% lysis[c]
CL-anionic-LPS (batch 20) **+ SRB-anionic** (CG210331)	$(1.23 \pm 0.08) \times 10^5$	$(0.53 \pm 0.04) \times 10^5$	57
CL-anionic-LPS (batch 20)	$(1.30 \pm 0.09) \times 10^5$	$(0.66 \pm 0.1) \times 10^5$	49
CL-anionic (batch 17) **+ SRB-anionic-LPS** (KH210218)	$(1.59 \pm 0.08) \times 10^5$	$(1.9 \pm 0.3) \times 10^5$	-19 %
CL-anionic (batch 17)	$(1.4 \pm 0.1) \times 10^5$	$(1.9 \pm 0.3) \times 10^5$	-37 %

[a] CL signal in inactivated serum, [b] CL signal in activated serum, [c]was determined according to $(I_{iaS} - I_{aS})/ I_{iaS} \times 100$, negative lysis values are interpreted with the absence of lysis

Vice versa the SRB LPS liposomes show complement induced lysis (129 % in the bystander assay and 123 % in the independent complement assay, **Table 13**) whereas the bystander chemiluminescence liposomes remain stealth (-19 % in the bystander assay and -37 % the independent complement assay, **Table 12**).

Table 13 Lysis values obtained for SRB liposomes after complement assay with 10 vol.-% serum

Liposome combination	PMB[a] (%)	aS[b] (%)	iaS[c] (%)	OG[d] (%)
CL-anionic-LPS (batch 20) **+ SRB-anionic** (CG210331)	21 ± 2	21 ± 2	13 ± 1	100 ± 12
SRB-anionic (CG210331)	18 ± 2	20 ± 1	12 ± 1	100 ± 9
CL-anionic (batch 17) **+ SRB-anionic-LPS** (KH210218)	9 ± 1	129 ± 7	9 ± 1	100 ± 7
SRB-anionic-LPS (KH210218)	9 ± 1	123 ± 5	9 ± 0	100 ± 4

[a]Paul Morgan buffer signal in % normalized to OG signal at minute 61, [b] active serum signal in % normalized OG signal at minute 61, [c] inactive serum signal in % normalized to OG signal at minute 61, [d] *n*-octyl-β-D-glucopyranoside signal in % normalized to OG signal at minute 61

The bystander assay verifies that the complement induced lysis occurs only in close vicinity of the trigger molecule. Liposomes that do not bear a trigger are not affected.

5.3.4. Surface functionalization of liposomes

Simultaneously, the modification of the liposomes with a variety of binding molecules was studied to determine a suitable coupling strategy and ideal coupling conditions. For the final assay, the liposome surface needs to be functionalized with a receptor in order to bind the virus-like particle (VLP) which mimics the SARS-CoV-2 virus. By now it is commonly accepted, that the angiotensin-converting enzyme 2 (ACE2) acts as receptor in the cellular membrane that binds the S-glycoprotein which is exposed on the SARS-CoV-2 surface.[24] More precisely, the receptor binding domain (RBD) of the S-glycoprotein mediates receptor recognition by ACE2.[24] Here, we exploit this molecular recognition and modified the liposome surface with ACE2 by covalent binding and through streptavidin (StAv) biotin interaction with streptavidin-modified liposomes and biotinylated ACE2. These liposomes are precursors to the final liposome type to study their interaction with the complement system. In a parallel proof-of-concept study, the interaction of complement activating anti-Ankyrin repeat-rich membrane spanning (ARMS) antibodies were tested with ARMS liposomes bearing an ARMS peptide on the surface. For the following coupling experiments the 30 mmol L^{-1} *m*-carboxy luminol liposomes with 5 mol% cholesterol and 4 mol% N-glutaryl DPPE were used. The main characteristics of this liposome are listed in **Table 14**.

Table 14 Characteristics of *m*-carboxy luminol liposomes applied for streptavidin coupling

lipid composition	encapsulant	Surface	PdI[a]	Size[b] by Int (nm)	Size[b] by Num (nm)	Zeta potential (mV)
Batch 14 DPPC: 73.1 mol% DPPG: 18.0 mol% Cholesterol: 4.9 mol% glutaryl-DPPE: 4.0 mol%	30 mmol L^{-1} *m*-carboxy luminol	anionic glutaryl	0.08 ± 0.01	125 ± 39	87 ± 25	-28.4 ± 2.38

[a]PdI: Polydispersity index, [b]size refers to hydrodynamic diameter

The stability of these liposomes was monitored over 9 months. The percentage of free dye outside of the liposomes remains below 1 % (**Figure 13**) when stored highly concentrated at 4° C. Simultaneously, the total CL signal remains stable within the tested period rendering these liposomes stable for at least 9 months.

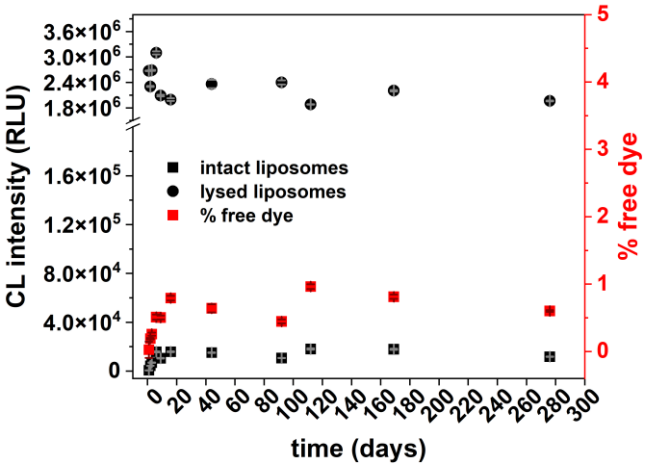

Figure 13 Stability study of N-glutaryl tagged 30 mmol L^{-1} *m*-carboxy luminol liposomes (batch 14) by measuring chemiluminescence intensity. Chemiluminescence properties of the *m*-carboxy luminol liposome measurement was performed by dilution of liposomes to c(tLipids) = 15 µmol L^{-1} either in CBS buffer or 30 mmol L^{-1} OG/CBS buffer including 2 µmol L^{-1} hemin. 100 µL of each liposome dilution was reacted with 100 µL 4 mmol L^{-1} H_2O_2 and measured first without H_2O_2 and after 5s shaking with H_2O_2 with following settings: integration time 2 s, gain 80, read height 1 mm, n = 4

5.3.4.1. ARMS coupling Results

Finally, in order to evaluate the trigger ability of anti-ARMS antibodies within the system, liposomes with covalently bound 0.2 mol% and 0.5 mol% ARMS peptide were synthesized.

5.3.4.1.1. Loading study of ARMS-modified liposomes to anti-ARMS coated microtiter plate

To determine an ideal anti-ARMS concentration for antibody subtype A626 and A375 and to obtain sufficient coverage of the MTP with antibody for the later competitive assay, a loading study was performed (**Figure 14**).

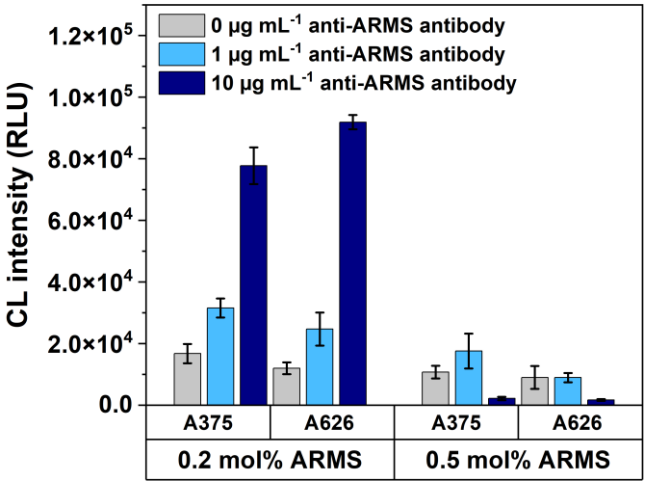

Figure 14 Anti-ARMS loading study of ARMS-modified 30 mmol L^{-1} *m*-carboxy luminol liposomes. 50 µmol L^{-1} total lipid concentration, of the respective ARMS-modified liposomes was applied to varying anti-ARMS coating concentrations. Binding of the liposomes to the anti-ARMS MTP was performed in outer liposome buffer, chemiluminescence measurement was performed by adding 50 µL of 4 µmol L^{-1} hemin and 40 mmol L^{-1} H_2O_2 in 0.01 M CBS, pH 10.5, 2 s integration time, gain 80, RH 1 mm, n = 3

For this, varying ARMS concentration were tested with the ARMS-modified liposomes with 50 µmol L^{-1} total lipid concentration incubated in outer buffer (**Figure 14**). With 50 µmol L^{-1} total lipid amount and increasing anti-ARMS concentration, the chemiluminescence (CL) signal increases for the liposomes modified with 0.2 mol% ARMS. An anti-ARMS coating of 10 µg mL^{-1} resulted in the highest CL intensity with in the tested antibody coating concentrations. Changing from A375 to A626 shows even higher CL intensities for the highest coating concentration. This indicates that the ARMS-modified liposomes bind more effectivly to the A626 antibody. However, a relatively high blank signal was obtained as well. Modification with 0.5 mol% ARMS unexpectedly showed overall less efficient binding to the antibody regardless of the coating concentration. This is supposingly again a result of crosslinking of the ARMS peptide at higher coupling concentrations.

5.3.4.1.2. Antibody binding study

In the competitive ARMS antibody assay (**Figure 15**) competition of free ARMS-antibody with to the MTP bound ARMS-antibody for binding to 0.2 mol% ARMS-modified anionic CL-liposomes were investigated. The competitive assay was performed with both antibody subtypes (A626 and A375) to find a measure for the saturation of liposome with ARMS antibodies. Initial thought on the activation potential suspected different binding properties of the antibodies. Considering that for each antibody subtypes the same liposomes and equal conditions were applied, the competitive ARMS antibody assay leads to the following conclusion: A375 antibody is needed in higher concentrations to observe a competition.

This is indicated by the higher LOD (2.1 µg mL^{-1} for A375 vs. 0.3 µg mL^{-1} for A626) and the higher EC_{50} value ((5.2 ± 0.9) µg mL^{-1} for A375 vs. (1.6 ± 0.2) µg mL^{-1} for A626) (**Table 15**).

Table 15 Summary of EC_{50} values and limit of detection obtained from competitive ARMS antibody assay

applied antibody	EC_{50} (ARMS) (µg mL^{-1})	LOD[a] (µg mL^{-1})
A626	1.6 ± 0.2	0.3
A375	5.2 ± 0.9	2.1

[a]limit of detection (y_{LOD}: A1 + 3 × SD_{blank})

On the contrary, for full saturation of the liposome surface similar amounts of both antibody subtypes were needed. With 0.2 mol% antibody (0.015 mg mL^{-1}), saturation is nearly reached for both antibody subtypes. This equals the amount of antibody used in the antibody triggered complement assay. Yet, the A626 induces complement lysis whereas A375 is not able to trigger the complement system. This could be a consequence of the different binding constants or varying complement activation properties.

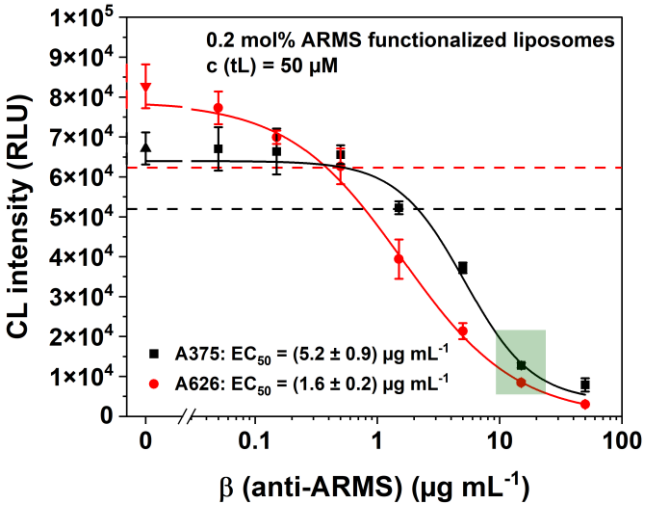

Figure 15 Competitive anti-ARMS assay with 0.2 mol% ARMS-modified *m*-carboxy luminol liposomes, washing once with 1 X PBS, 0.05 % Tween®20, two times with outer buffer, incubation of anti-ARMS antibody dilution including liposomes (total lipid concentration = 50 µmol L^{-1}) overnight at 4 °C in outer liposomes buffer, three times washing with CBS buffer, lysis for 5 min with 30 mmol L^{-1} OG/CBS, addition of 50 µL 40 mmol L^{-1} H_2O_2 and 50 µL 40 µmol L^{-1} hemin in CBS, pH 10.5. Chemiluminescence measurement: 5 s shaking (425 cpm), gain 80, RH 1 mm, IT 2 s, T = 25°C, n = 3, green square indicates the 0.2 mol% antibody equivalent which was used for trigger experiments, the dashed lines illustrate the limit of detection

The A375 exhibits a higher EC_{50} compared to the A626 which indicates less efficient binding of the A375 antibody compared to the A626 antibody. For a definite statement, however, further studies are required. The competition reaction was allowed >12 h at 4 °C.

5.3.4.2. Streptavidin functionalization

Streptavidin (StAv) was intended as anchoring group for biotinylated ACE2. To determine suitable coupling conditions, liposomes with 0.01 mol%, 0.05 mol% and 0.5 mol% streptavidin were synthesized and their binding ability and stability in an complement assay evaluated.

5.3.4.2.1. Loading study of StAv-modified liposomes

Immobilization of StAv liposomes was realized on bovine serum albumin (BSA)-biotin functionalized MTPs. To determine the ideal BSA-biotin and liposome loading concentration yielding in full coverage, a loading study was performed. Furthermore, the incubation time for liposomes to bind to the BSA-biotin MTP was determined.

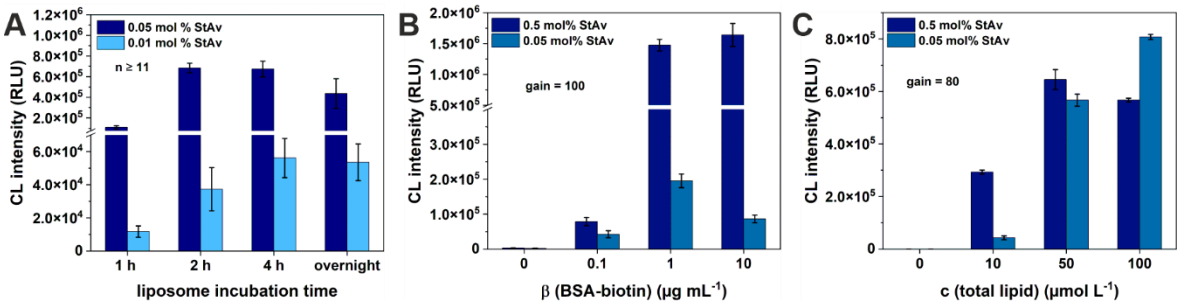

Figure 16 Loading study of streptavidin (StAv)-modified 30 mmol L^{-1} *m*-carboxy luminol liposomes with, A) variation of the liposome incubation time, B) variation of BSA-biotin loading concentration, C) variation in total lipid concentration. In A and B an approximately 10 µmol L^{-1} total lipid concentration was. Binding of the liposomes to the BSA-biotin MTP was performed in outer liposome buffer, chemiluminescence measurement was performed by adding 50 µL of 4 µmol L^{-1} hemin and 40 mmol L^{-1} H_2O_2 in 0.01 M CBS, pH 10.5, 2 s integration time, gain 100, RH 1 mm, n = 3

Initially, the required time for the liposomes to bind to the MTP was investigated. Here, a dependency on the amount of StAv on the surface was determined (**Figure 16 A**). With lower StAv amount on the surface, more time is required to reach saturation. Hence, an incubation time of 2 h for 0.05 mol% and 4 h for 0.01 mol% StAv was required to reach saturation. Incubation overnight, however, reaches in both cases full coverage. To obtain full coverage independent on the coupling equivalent, immobilization was thus standardly performed overnight. Furthermore, the obtained maximum CL signal with the 0.01 mol% StAv liposomes is by a factor of about 10 lower compared to 0.05 mol% StAv liposomes which corresponds to a lower number of immobilized liposomes. As a certain number of liposomes is required for the complement assay to maintain stability, the 0.01 mol% StAv liposomes were not further investigated due to their limited binding efficiency and inhomogeneous behavior in the complement assay (**Figure 18 A**). Following

the determination of the incubation time, the ideal loading concentration with varying BSA-biotin concentrations was tested with 0.05 mol% and 0.5 mol% StAv-modified liposome (**Figure 16 B**). With increasing BSA-biotin concentration, saturation of the plate was reached at 1 µg mL^{-1} BSA-biotin for 0.05 mol% and 0.5 mol% StAv-modified liposomes. Increasing the number of liposomes allowed to further increase the coverage of the plate with liposomes. Using 1 µg mL^{-1} BSA-biotin, saturation was reached at 50 µmol L^{-1} total lipid concentration for the 0.5 mol% StAv liposomes. For the 0.05 mol% StAv saturation was nearly reached with 50 µmol L^{-1} total lipid concentration (**Figure 16 C**). Thus, in the following experiments 50 µmol L^{-1} total lipid concentrations was applied.

5.3.4.2.2. Competitive biotin assay with StAv-modified liposomes

Besides various approaches exist to determine the StAv density on the liposomes surface[25], here, the inherent optical properties of the liposomes were used for quantification in a competitive biotin assay. The 0.5 mol% StAv-modified liposomes show a 10-times higher EC_{50} value, which correlates to the 10-times higher StAv coupling equivalent of these liposomes, compared to the 0.05 mol% StAv-modified liposomes (**Figure 17**). Here, a higher EC_{50} value correlates with the higher binding capacity of the StAv-modified liposomes towards free biotin. Thus, with the higher coupling equivalent more StAv was coupled to the surface which in turn is able to bind more biotin and hence, yields a higher EC_{50} value. This provides a relative measure for the assessment of StAv on the surface.

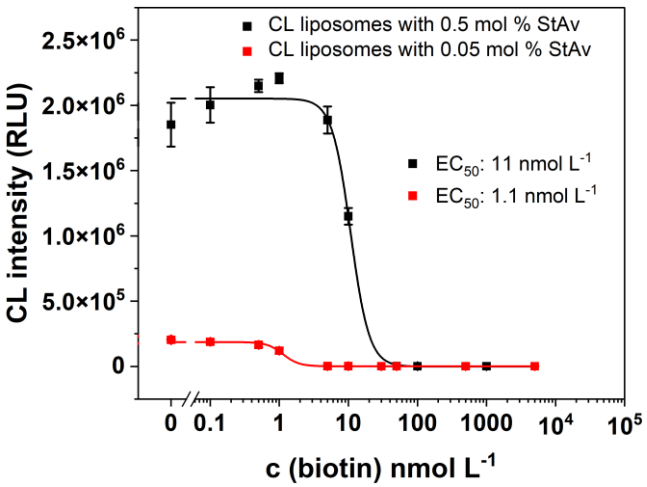

Figure 17 Competitive biotin assay with StAv-modified 30 mmol L^{-1} *m*-carboxy luminol liposomes. Chemiluminescence measurement was performed by adding 50 µL of 40 µmol L^{-1} hemin and 40 mmol L^{-1} H_2O_2 in 0.01 M CBS, pH 10.5, 2 s integration time, gain 100, RH 1 mm, n = 4

5.3.4.2.3. Complement assay with StAv-modified liposomes

Here, the liposomes can be successfully immobilized with equal efficiency as the biotinylated liposomes. The StAv-modified liposomes, however, show slight complement related lysis (**Figure 18**).

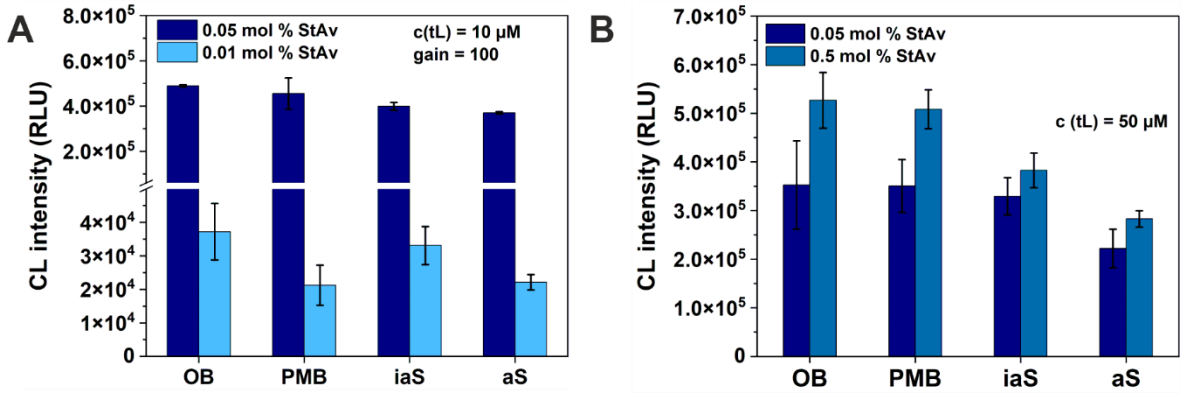

Figure 18 Heterogenous complement assay with modified CL liposomes. The complement assay was performed in A) with 0.01 mol% and 0.05 mol% StAv-modified liposomes and in B) with 0.05 mol% and 0.5 mol% StAv-modified liposomes. Liposomes were immobilized overnight on a BSA-biotin coated MTP (1 µg mL^{-1}) and incubated for 60 min at 37 °C in either outer liposome buffer, Paul Morgan buffer (PMB), inactive serum (iaS) and active serum (aS). Chemiluminescence measurement was performed by adding 50 µL of 4 µM hemin and 50 µL of 40 mM H_2O_2 in 0.01 M CBS, pH 10.5, 2 s integration time, gain 100 in A and gain 80 in B, RH 1 mm, T = 25 °C, n ≥ 2

Here, the liposomes already undergo lysis with 5 vol.-% human serum of about 30 % (**Table 16**). This needs further investigation to evaluate if this is a concentration dependent observation or if streptavidin indeed minorly triggers the complement system.

Table 16 Lysis values obtained in complement assay with StAv-modified liposomes

lipoosome modification	c(tL) for immobilization (µmol L^{-1})	I_{iaS}[a]	I_{aS}[b]	φ_{serum} (vol.-%)	% lysis[c]	% CL signal towards iaS[d]
0.01 mol% StAv	10	(0.33 ± 0.06)×10^5	(0.22 ± 0.02)×10^5	5	33 %	67 %
0.05 mol% StAv	10	(4.0 ± 0.2)×10^5	(3.70 ± 0.05)×10^5	5	7 %	93 %
0.05 mol% StAv	50	(3.3 ± 0.4)×10^5	(2.2 ± 0.4)×10^5	5	33 %	67 %
0.5 mol% StAv	50	(3.8 ± 0.4)×10^5	(2.8 ± 0.2)×10^5	5	26 %	74 %

[a] CL signal in inactivated serum, [b] CL signal in activated serum, [c]was determined according to (I_{iaS} - I_{aS})/ I_{iaS} × 100, [d] was determined according I_{aS}/ I_{iaS} × 100,

5.3.4.3. ACE2 coupling

The protein ACE2 is intended as recognition element in the final assay format. Therefore, a suitable coupling strategy is required. Two approaches were tested for efficient surface

modification. Covalent coupling often entails cross-coupling, especially when EDC/sNHS chemistry is used. This can interfere with the structural integrity of the protein and alter the binding side of the protein.[26] Furthermore, reactions at discrete sites of the protein are often not the only reactions that occur due to the presence of several primary amines and thus a variety of different binding sides.[26] Hence, a common strategy is side-specific enzymatic biotinylation of the intended protein allowing subsequently oriented binding.[27] Here, ACE2 with a terminal biotin group was used to immobilize ACE2 to the StAv-modified liposome surface. In the following, the covalent coupling and biotin-StAv approach were investigated with varying coupling equivalents. Successful coupling was verified by subsequent binding of the ACE2 liposomes to an RBD-modified MTP.

5.3.4.3.1. Coupling through molecular recognition of StAv and ACE2-biotin

Binding of ACE2-biotin through StAv onto the liposome surface was investigated with two coupling equivalents. After StAv coupling, the liposomes were measured with dynamic light scattering (DLS). The streptavidin liposomes were subsequently incubated overnight with ACE2-biotin at 4 °C in a 1:1 ratio towards the coupling equivalent of streptavidin and again measured with DLS. No subsequent dialysis was performed. The main characteristics of these liposomes are listed in **Table 17**.

Table 17 DLS results of *m*-carboxy luminol liposomes modified with streptavidin and ACE2-biotin

Liposome type	PdI[a]	Size[b] by Int (nm)	Zeta potential (mV)
Batch 14	0.090 ± 0.003	128 ± 41	-26.53 ± 0.05
Batch 14 – 0.05 mol% StAv	0.081 ± 0.006	129 ± 38	-24.4 ± 0.1
Batch 14 – 0.5 mol% StAv	0.139 ± 0.008	143 ± 51	-22.6 ± 0.2
Batch 14 – 0.05 mol% StAv – 0.05 mol% ACE2-biotin	0.133 ± 0.005	141 ± 51	-22 ± 1
Batch 14 – 0.5 mol% StAv – 0.5 mol% ACE2-biotin	0.27 ± 0.03	162 ± 75 2920 ± 1002	-22 ± 2

[a]PdI: Polydispersity index, [b]size refers to hydrodynamic diameter

The molecular dimension of streptavidin is known to be 4.5 × 4.5 × 5.0 nm^3.[28] With a molecular weight of approximately 86 kDa the minimum size of ACE2 was calculated according to (2) and (3) to be approximately 5.8 nm.[29]

$$R_{min} = \left(\frac{3\,V}{4\,\pi}\right)^{\frac{1}{3}} = 0.066\,M^{\frac{1}{3}} \quad (2)$$

with

V: Volume occupied by a protein in nm^3
M: molecular weight in Dalton (Da)
R_{min}: radius of protein with simplest shape

$$V = \left(\frac{\nu}{N_A}\right) \times M = \frac{0.73\,\frac{cm^3}{g} \times 10^{21} \frac{nm^3}{cm^3}}{6.023 \times 10^{23} \frac{Da}{g}} \times M = 1.212 \times 10^{-3}\,\frac{nm^3}{Da} \times M \quad (3)$$

with

V: Volume occupied by a protein in nm^3
M: molecular weight in Dalton (Da)
N_A : Avogadro number

Even though this is a rough method, a change of approximately 5 nm could indicates the presence of streptavidin on the surface of liposomes. For both StAv liposomes a change in the hydrodynamic diameter was obtained. However, with 0.05 mol% StAv no difference in the hydrodynamic diameter to the unmodified liposomes was obtained (**Figure 19**), whereas the liposomes with 0.5 mol% StAv show a change of 15 nm, similar to the liposomes with 0.05 mol% StAv and 0.05 mol% ACE2 with a change of 13 nm (**Table 17**). With 0.5 mol% StAv and 0.5 mol% ACE2 a change of 34 nm was determined (**Table 17**). Since proteins are typically not smooth spheres and possess an irregular surface, the average natural radius of a protein is larger than the calculated one.[29] Hence, considering the approximations within the calculation of the protein radius and the fact that with DLS the hydrodynamic diameter is determined, the obtained changes were within the magnitude of plausible dimensions and thus could indicate successful modification. The absence of a change in hydrodynamic diameter for the 0.05 mol% StAv liposomes is possibly due to the low number of StAv molecules bound to the liposome surface which may cannot be resolved by DLS.[30]

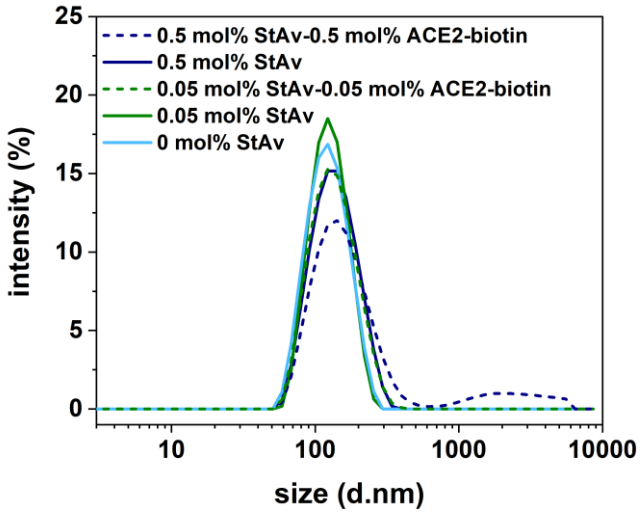

Figure 19 Dynamic light scattering results of streptavidin liposomes coupled to ACE2-biotin. Liposomes were diluted to 100 µmol L^{-1} total lipid concentration and measured in outer buffer with the following settings, refractive index (RI) of the material of 1.34, material absorbance of zero, RI of 1.342 of the dispersant, viscosity of 1.1185 mPa s were applied for DLS

Additionally, the zeta potential of 0.5 mol% StAv, 0.5 mol% StAv-0.5 mol% ACE2-biotin and 0.05 mol% StAv-0.05 mol% ACE2-biotin decreased to -23 mV and -22 mV, respectively, in contrast to the -27 mV of the unmodified liposomes which may indicate charge-vise coverage of the glutaryl groups on the surface with protein. However, for the 0.5 mol% coupling equivalent an additional peak is visible at > 1 µm which indicates aggregation of these particle.

5.3.4.3.2. Coupling through EDC and sNHS chemistry

Corresponding to the surface functionalization with StAv and ACE2-biotin, a coupling equivalent of 0.05 mol% and 0.5 mol% ACE2 was investigated with DLS for the covalent coupling approach. Here, a similar trend regarding the zeta potential and the hydrodynamic diameter was obtained (**Table 18**). However, the increase of the hydrodynamic diameter for both coupling conditions was significantly higher. Here, 0.05 mol% ACE2 yielded already in a 32 nm shift of the hydrodynamic diameter and 0.5 mol% ACE2 showed and 72 nm shift. This may indicate cross coupling of ACE2 yielding in a cluster of ACE2 protein that is coupled to the liposome surface and hence resulting in a larger size shift.

Table 18 DLS results of *m*-carboxy luminol liposomes modified with covalent coupling of ACE2

Liposome type	PdI[a]	Size[b] by Int (nm)	Zeta potential (mV)
Batch 14	0.090 ± 0.003	128 ± 41	-26.53 ± 0.05
Batch 14 – 0.05 mol% ACE2	0.16 ± 0.01	160 ± 68	-23.3 ± 0.1
Batch 14 – 0.5 mol% ACE2	0.26 ± 0.01	201 ± 103 4944 ± 641 35 ± 7	-22.48 ± 0.07

[a]PdI: Polydispersity index, [b]size refers to hydrodynamic diameter

Furthermore, with 0.5 mol% ACE2 coupling small and large aggregates were obtained. This may indicate a formation of clusters with a coupling equivalent of 0.5 mol% ACE2 (**Figure 20**, **Table 18**).

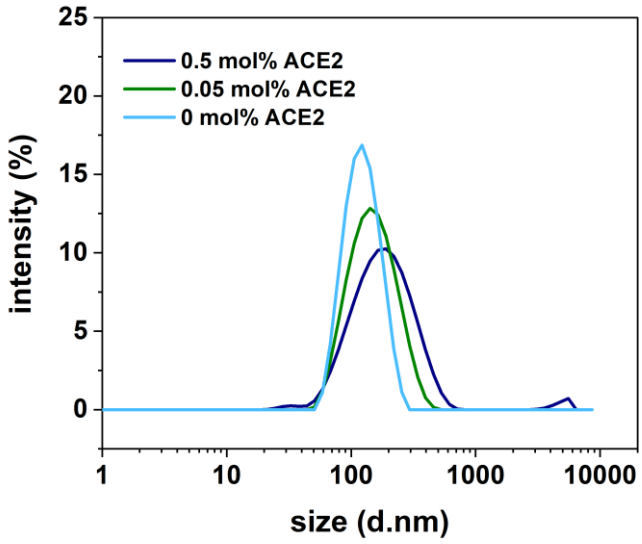

Figure 20 Dynamic light scattering results of streptavidin liposomes coupled in a 1:1 ratio to ACE2-biotin. Liposomes were diluted to 100 µmol L^{-1} total lipid concentration and measured in outer buffer with the following settings, refractive index (RI) of the material of 1.34, material absorbance of zero, RI of 1.342 of the dispersant, viscosity of 1.1185 mPa s were applied for DLS

5.3.4.3.3. Liposome immobilization test and ACE2 coupling proof

Investigation of successful immobilization of ACE2 to the liposome surface and evaluation of the integrity of ACE2 after the coupling was proven by binding the ACE2 liposomes to a RBD-coated MTP. With both coupling approaches, ACE2 was successfully immobilized on the liposome surface. Covalently coupled liposomes, however, show stronger CL signals in comparison to ACE2-biotin coupled liposomes (**Figure 21**).

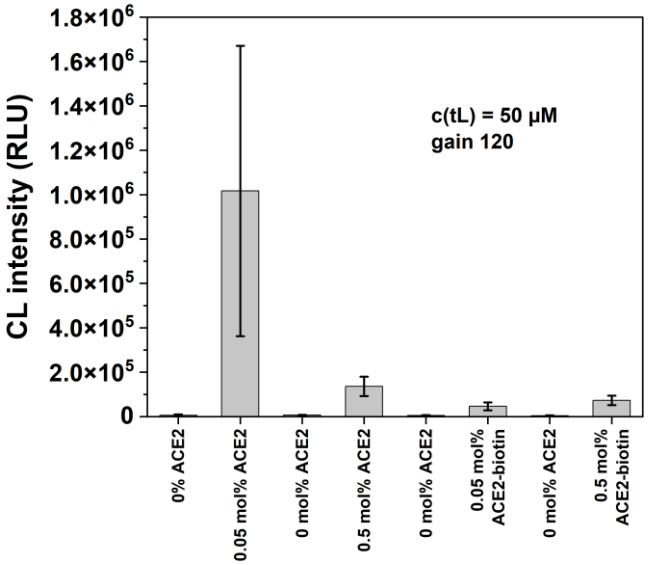

Figure 21 Liposome immobilization test with covalently coupled ACE2 liposomes in direct comparison to ACE2 coupling through biotin-streptavidin(StAv) interaction. 0 % ACE2 *equals* the negative control and correspond to the respective liposome type without ACE2. For the covalent approach, the bare liposome was used, for the biotin approach 0.5 mol% and 0.05 mol% StAv liposomes were used, respectively. Binding was achieved through an RBD (2 µg/mL) coated MTP. For each test a total lipid concentration of 50 µmol L^{-1} was applied. Chemiluminescence measurement was performed by adding 50 µL of 4 µmol L^{-1} hemin and 50 µL of 40 mmol L^{-1} H_2O_2 in 0.01 M CBS, pH 10.5, 2 s integration time, gain 120, RH 1 mm, T = 25 °C, n = 4

Consequently, the covalent coupling approach yielded in a higher density of ACE2 on the liposome surface compared to the StAv biotin approach. Furthermore, the recognition motif of ACE2 was maintained during coupling. Surprisingly, the 0.05 mol% covalently coupled ACE2 liposomes excel over the 0.5 mol% ACE2 liposomes. These results agree with the DLS data in **Figure 20** which indicates aggregate formation with the higher coupling equivalent. With a high degree of cross coupling structural changes in the recognition area of ACE2 can occur and thus binding to RBD can be negatively affected. With the ACE2-biotin approach 0.5 mol% equivalent indicates better binding to RBD. Here, no cross coupling of ACE2 can occur and streptavidin is probably less sensitive to structural changes with regard to its biotin binding ability. However, the biotin approach itself shows an overall weaker signal and is thus less favorable for modifying liposomes with ACE2. The respective negative control (labeled with 0 % ACE2 in **Figure 21**) correspond to the respective liposome type without ACE2. For the covalent approach the N-glutaryl liposome was used and for the biotin approach 0.5 mol% and 0.05 mol% StAv-liposomes were used, respectively.

Repeating the experiment with ACE2-biotin while including dialysis and varying ACE2-biotin equivalents showed that the binding performance was improved by a factor of 3 using a 1:2 (streptavidin:ACE2-biotin) ratio (**Figure 22**). Yet, the covalently coupled 0.05 mol% ACE2

liposomes still yield a 2-times higher CL signal compared to the optimized coupling approach through molecular recognition (**Figure 22**). With increasing the coupling ratios further to 1:5 and 1:10 the CL intensity actually decreased again suggesting that an excess of ACE2-biotin is not favorable for optimizing the immobilization. Overall, the covalent coupling approach with 0.05 mol% ACE2 was verified to show the best binding properties after coupling.

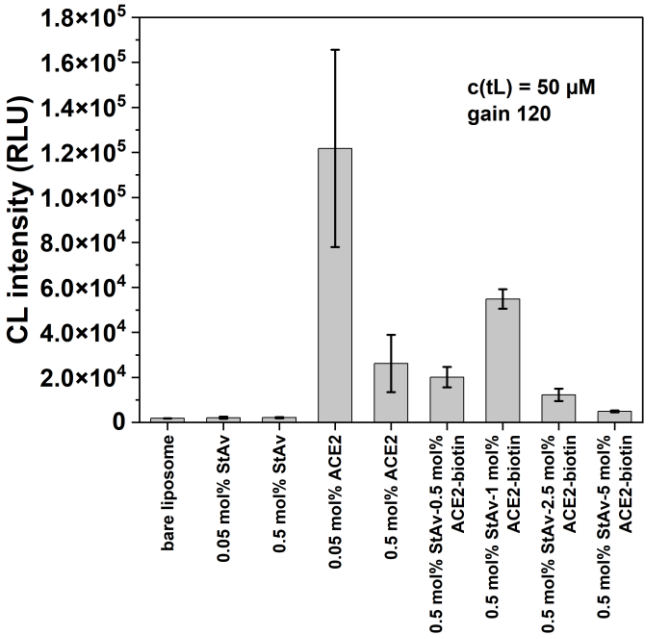

Figure 22 Liposome immobilization test with covalently coupled ACE2 liposomes in direct comparison to ACE2 coupling through biotin-streptavidin interaction. Binding was achieved through an RBD (2 µg/mL) coated MTP. For each test a total lipid concentration of 50 µmol L^{-1} was applied. Chemiluminescence measurement was performed by adding 50 µL of 4 µmol L^{-1} hemin and 50 µL of 40 mmol L^{-1} H_2O_2 in 0.01 M CBS, pH 10.5, 2 s integration time, gain 120, RH 1 mm, T = 25 °C, n = 4

Further investigation of the ACE2 coupling to the liposomes is required to study the stability of the protein and further increase the binding efficiency, so that these liposomes can be tested in a complement assay. This, however, will be addressed in a subsequent study and is not within the scope of this work.

5.4. Conclusion

This study represents the fundamental proof of the envisioned advanced neutralization assay concept combining liposomes and the human complement assay to detect neutralizing antibodies. For this, we studied various liposomes as reporter particles that can be specifically targeted for lysis through the human complement system in the presence of a trigger molecule. Throughout this study, biotinylated cationic, anionic, cationic pegylated

and anionic pegylated liposomes were investigated to identify a qualified reporter liposome for the final assay system. These liposomes were tested towards their stability in human serum in general and their receptivity to complement induced lysis in the presence of specific trigger molecules. Whereas anionic pegylated liposomes show complement induced lysis already in absence of a trigger molecule, the cationic, anionic and cationic pegylated formulation were stable in human serum and hence categorized as stealth liposomes. These liposomes were tested towards their susceptibility to lysis in the presence of a complement triggering anti-biotin antibody. Here, anionic liposomes were lysed to the highest degree (80%) followed by cationic liposomes (at maximum 65%). The pegylated liposomes show only minor lysis and similarly to the cationic liposomes, they showed rather inconsistent lysis values preventing adequate interpretation and thus were neglected for further studies. Additionally to the external trigger, a positive control with an internal trigger was developed by integrating lipopolysaccharide (LPS) into the lipid bilayer membrane of anionic liposomes. These liposomes were again successfully lysed by the complement system validating the initial concept of targeted complement induced liposome lysis in presence of a trigger molecule. To identify the effect of the complement system on neighboring liposomes without a trigger molecule after activation, a bystander assay was performed. This bystander assay revealed that complement induced lysis is a localized event and bystander liposomes are not affected by the lysis process of the targeted liposome. This is an essential prerequisite for the final assay to work.

Finally, various surface modifications of the liposomes were tested either to investigate the trigger potential of antibodies when used with liposomes or to develop liposomes with a suitable recognition element. Modification of liposomes with ARMS was successful and binding of the antibodies in a competitive assay was confirmed. Yet, due to the significantly reduced immobilization of these liposomes in contrast to the streptavidin-biotin mediated immobilization of the biotinylated liposomes, no complement assay could be successfully performed to investigate the anti-ARMS antibodies as trigger molecule. Modification of the liposomes with ACE2 was possible through side-directed and covalent attachment. Yet, the side-directed immobilization through streptavidin biotin interaction was significantly less efficient compared to the covalent coupling approach. Here, on the contrary, cross coupling and hence aggregate formation especially with high coupling equivalents was observed. In both scenarios, optimization and further investigations are required to elucidate the ideal conditions and should be subject to subsequent studies. Even though, we are at the very beginning of this multifaceted project, the initial results are promising towards the final assay

concept. We could show that localized and targeted lysis of liposomes is possible. Furthermore, a pool of potent trigger molecules was identified and validated within a liposome-based complement assay. Successful functionalization of liposomes with the ACE2 receptor was established together with stealth liposomes which are, despite their overall stability in human serum, still possible to be lysed through the complement system.

A true benefit of the targeted complement-initiated lysis is the possibility to do a one-step homogenous assay. Here, fluorescent liposomes are better suited as continuous measurements can easily be conducted and compatibility of the dye with the inevitable serum matrix is given. However, within this study, mainly chemiluminescence liposomes were investigated in a heterogenous assay format to take advantage of the accompanied higher sensitivity. Yet, the incompatibility of the chemiluminescence reaction with human serum, due to the radical scavengers counteracting the radical reaction mechanism of the CL reaction, constrained this line of research to a heterogenous assay. This circumvents the negative effect of the serum matrix on the CL signal but is at the expense of a single-step assay. Still, considering a standard neutralization assay, already the heterogenous complement assay diminishes the complexity and time requirements a neutralization assay demands, as it can be performed like a typical enzyme-linked immunosorbent assay (ELISA). Thinking one step further, alteration of the current assay towards a pseudo homogenous assay, where CL liposomes freely interact with the human serum and are subsequently captured on a nitrocellulose membrane, would yield in an elegant point-of-care test to identify neutralizing antibodies in a simple rapid test. Here, chemiluminescence detection can add extra sensitivity, which fluorescence cannot offer.

5.5. References

[1] F. Krammer, V. Simon, *Science (New York, N.Y.)* **2020**, *368*, 1060.

[2] Y. Lu, J. Wang, Q. Li, H. Hu, J. Lu, Z. Chen, *Scand J Immunol* **2021**, *94*.

[3] P. Prabakaran, X. Xiao, D. S. Dimitrov, *Biochemical and biophysical research communications* **2004**, *314*, 235.

[4] K. L. S. Cleary, H. T. C. Chan, S. James, M. J. Glennie, M. S. Cragg, *Journal of immunology (Baltimore, Md. : 1950)* **2017**, *198*, 3999.

[5] S. K. Sahu, D. H. Kulkarni, A. N. Ozanturk, L. Ma, H. S. Kulkarni, *Trends in microbiology* **2022**, *30*, 390.

[6] J. R. Dunkelberger, W.-C. Song, *Cell research* **2010**, *20*, 34.

[7] S. M. Moghimi, I. Hamad, *Journal of liposome research* **2008**, *18*, 195.

[8] A. Menny, M. Serna, C. M. Boyd, S. Gardner, A. P. Joseph, B. P. Morgan, M. Topf, N. J. Brooks, D. Bubeck, *Nature communications* **2018**, *9*, 5316.

[9] a) S. C. Semple, A. Chonn, P. R. Cullis, *Advanced Drug Delivery Reviews* **1998**, *32*, 3; b) J. Szebeni, S. M. Moghimi, *Journal of liposome research* **2009**, *19*, 85.

[10] H.A.H. Rongen, A. Bult, W.P. van Bennekom, *Journal of Immunological Methods* **1997**, *204*, 105.

[11] Y. Ishimori, K. Rokugawa, *Clinical Chemistry* **1993**, *39*, 1439.

[12] M. Mayer, S. Takegami, M. Neumeier, S. Rink, A. Jacobi von Wangelin, S. Schulte, M. Vollmer, A. G. Griesbeck, A. Duerkop, A. J. Baeumner, *Angew. Chem.* **2018**, *130*, 414.

[13] D. Peterhoff, V. Glück, M. Vogel, P. Schuster, A. Schütz, P. Neubert, V. Albert, S. Frisch, M. Kiessling, P. Pervan et al., *Infection* **2021**, *49*, 75.

[14] P. Nakhaei, R. Margiana, D. O. Bokov, W. K. Abdelbasset, M. A. Jadidi Kouhbanani, R. S. Varma, F. Marofi, M. Jarahian, N. Beheshtkhoo, *Frontiers in bioengineering and biotechnology* **2021**, *9*, 705886.

[15] N. Niyonzima, B. Halvorsen, B. Sporsheim, P. Garred, P. Aukrust, T. E. Mollnes, T. Espevik, *Molecular immunology* **2017**, *84*, 43.

[16] A. Chonn, P. R. Cullis, D. V. Devine, *Journal of immunology (Baltimore, Md. : 1950)* **1991**, *146*, 4234.

[17] S. Sivasankar, S. Subramaniam, D. Leckband, *Proceedings of the National Academy of Sciences of the United States of America* **1998**, *95*, 12961.

[18] S. W. Vukajlovich, J. Hoffman, D. C. Morrison, *Molecular immunology* **1987**, *24*, 319.

[19] B. Bertani, N. Ruiz, *EcoSal Plus* **2018**, *8*.

[20] P. G. Adams, L. Lamoureux, K. L. Swingle, H. Mukundan, G. A. Montaño, *Biophysical journal* **2014**, *106*, 2395.

[21] F. Dati, G. Schumann, L. Thomas, F. Aguzzi, S. Baudner, J. Bienvenu, O. Blaabjerg, S. Blirup-Jensen, A. Carlström, P. Hyltoft-Petersen et al., *Clinical Chemistry and Laboratory Medicine* **1996**, *34*.

[22] N. A. Daha, N. K. Banda, A. Roos, F. J. Beurskens, J. M. Bakker, M. R. Daha, L. A. Trouw, *Molecular immunology* **2011**, *48*, 1656.

[23] G. M. Hänsch, *Immunopharmacology* **1992**, *24*, 107.

[24] J. Yang, S. J. L. Petitjean, M. Koehler, Q. Zhang, A. C. Dumitru, W. Chen, S. Derclaye, S. P. Vincent, P. Soumillion, D. Alsteens, *Nature communications* **2020**, *11*, 4541.

[25] P. D. Quevedo, T. Behnke, U. Resch-Genger, *Analytical and bioanalytical chemistry* **2016**, *408*, 4133.

[26] G. T. Hermanson, *Bioconjugate techniques*, Elsevier Academic Press, Amsterdam, **2008**.

[27] M. Fairhead, M. Howarth, *Methods in molecular biology (Clifton, N.J.)* **2015**, *1266*, 171.

[28] R. Reiter, H. Motschmann, W. Knoll, *Langmuir* **1993**, *9*, 2430.

[29] H. P. Erickson, *Biological procedures online* **2009**, *11*, 32.

[30] S. Bhattacharjee, *Journal of controlled release : official journal of the Controlled Release Society* **2016**, *235*, 337.

6. Conclusion and Perspective

Progressing standard (bio)analytical systems to simple, fully stand-alone platforms that can be operated by everyone and everywhere providing rapid responses at similar sensitivities to laboratory standards, is one of the major driving forces in analytical research. Although this point-of-care testing (POCT) concept is by itself growing since over 30 years, only a handful of suitable systems managed the successful transfer from research to the diagnostic market as true POCT. This is often associated with limited sensitivities or specificity and their merely semi-quantitative nature.[1] Among these ideas, paper-based microfluidics are one of the most promising platforms that gained special attention in society not least due to the COVID-19 pandemic and the accompanied urge for rapid analysis solutions.[2] However, they are also known to struggle with sensitivity issues, accuracy and reliability as delicately confirmed during the exhaustive endurance test in the last two years of the ongoing COVID-19 pandemic.[3]

In order to address these challenges, this thesis aimed to improve current POCT system by integrating chemiluminescence as more sensitive detection technique into existing paper-based POCT systems such as paper-based microfluidics (µPADs) and lateral flow assays (LFA). Furthermore, the merit of label enrichment and signal amplification to the bioanalysis field with focus on medical diagnostics was investigated. In a separate line of research, the optimized labels were assessed in a novel neutralization assay approach to profit from the enhanced signal that these labels inherently possess.

Chemiluminescence (CL) has been known for decades as elegant detection technique that provides highly sensitive optical signals needless of external excitation sources. In contrast to other optical detection methods, it stands out with high signal-to-noise ratios, simple instrumentation and broad dynamic ranges that is also demonstrated within this work. It is standardly used in research, clinical diagnostic, environmental analysis, forensics and many more fields to solve demanding analytical questions.[4] For a long time and despite its excellent features for POCT, CL has been limited to advanced laboratory use only, due to the naturally low quantum yields of typical CL probes, its transient signal, and the lack of sensitive low-cost detection devices. Although chemiluminescence detection manages sensing with as little as an optical transducer, the overall low quantum yields require sophisticated detectors such as photomultiplier tubes (PMT) or cooled charge coupled device (CCD) cameras to sufficiently resolve the generated signals.[5] Until recently, the integration of such optical sensors into POCT concepts, has been mainly restricted by their large dimensions, high costs and electrical demand.[5] Progress in the optical sensor field

with regard to miniaturization, connectivity and chip development finally cleared the path on the instrumental side to benefit from chemiluminescence's great properties with new miniaturized low light sensor chips. This renewed the interest in CL for straightforward quantitative POCT. From the chemistry side, refinement of existing luminophores to enhance the emission assists to expand the area of application of CL analysis in the same direction. Simple alteration of an additional carboxy group to the benzoic ring of luminol amplified its electrochemiluminescence (ECL) and CL outcome and simultaneously increased its water solubility.[6,7] This is always beneficial for bioanalytical applications to ensure the compatibility of the applied reagent. Several alterations of the basic luminol have been synthesized and evaluated[8] and although the complete underlying process is until now not fully elucidated, some trends have been identified to increase the CL intensity by structural modification.[7] However, these alterations were typically at the expense of the water solubility and thus less suited for bioanalytical applications.[8] *m*-Carboxy luminol on the other hand stands out as it combines improved light emission and bioanalytical compatibility with the possibility to be detected either with ECL or CL. The herein evaluated CL performance of *m*-carboxy luminol furthermore demonstrated the merit of stronger emitting CL probes with regard to sensitivity improvement in typical bioanalytical applications. Both methods comply with typical POCT requirements, yet paper-based analysis systems benefit from the simplicity that is accompanied by CL detection due to the independency of electrodes and an external power supply to initiate the reaction. The CL-based µPAD that originated within this work combined the advances in optical sensors and the improved CL probe to establish a simple but sensitive solution to detect biomarkers such as lactate. Here, the higher quantum yield and stronger CL emission permits the use of less sensitive optical sensors such as simple smartphone cameras which are within the budget of POCT and allow to approach sensitivity levels of laboratory capturing devices. Yet, to fully harness on the advantages of this easy image taking evaluation, automated algorithms for the detection software is needed to ensure user independent signal evaluation and adequate interpretation of the results. In this context it should be noted, that despite *m*-carboxy luminol's excellent performance within the presented work this CL-probe has so far only been benchmarked to its parent luminol. The competitiveness to established CL probes, such as acridinium esters, dioxetanes or peroxyoxalic derivatives is yet to be proven and should be subject to subsequent studies.

In a second line of research signal amplification through label enrichment was investigated. Here, liposomes were studied in different analytical setups with a variety of different dyes, by different detection techniques and surface modifications. Liposomes belong to the most

explored nanocontainers that are used in targeted drug delivery.[9] Their excellent loading capacity, stability, biodegradability, flexible surface chemistry and inherent biocompatibility as well as their low immunogenicity render these particles ideal not only for drug delivery purposes. Liposomes can ameliorate assay performance in bioanalysis simply by label enrichment to overcome detection limitation by low-level signals. They showed their great potential as highly suitable label and signal amplification moiety especially with focus towards point-of-care analysis already in several applications.[10] Particularly, highly visible dye-encapsulating liposomes raised attractiveness for improvement of paper-based POCT as demonstrated by Edwards *et al.*[11]. Contrary, to previously reported applications of liposomes in lateral flow assays (LFA)[12], this work concentrated on making liposomes ready for commercialization by establishing a suited dehydration process, refining the liposome to obtain maximal signal output and optimizing the bioconjugation to produce stable and functional reporter particles.[13] The system was benchmarked to commercial gold nanoparticles with an over 10-times lower limit of detection that allowed quantitative detection of IL-6, a low concentration biomarker for inflammatory processes, in the clinical relevant range and matrix. Switching from purely colorimetric and fluorescent liposomes to chemiluminescence liposomes allows for a significant improvement of the signal-to-noise ratios which once more highlights the benefit of chemiluminescence over other optical detection techniques and demonstrates the broad spectrum of liposomal labels.

However, within this work some limitations to the application of liposomes in their current state can be pointed out. It is important, that liposomes are prepared under controlled conditions, thoroughly characterized, and tested under real assay conditions to prove their usefulness to the developed system. Further challenges need to be addressed in the future to facilitate the long overdue transfer as label to industrial applications. For example, as for nanoparticles in general it is still difficult to control size, shape, stability and size distribution of nanoparticles throughout the synthesis.[14] Especially relevant for industrial use is the reproducible mass production of such particles. However, the upscaling of particle synthesis is in general not a simple task.[9] Here, microfluidic can assist in reproducible synthesis of liposomes for industrial applications.[9] Furthermore, despite the flexible surface modification of liposomes by as easy as mixing the respectively modified lipid to the standard lipid composition, there are numerous lipids available and finding the perfect lipid compositions that produces liposomes which contain the required features can be tedious and elaborate.

Within this study we showed that liposomes as reporter particle can be used in POCT setups such as lateral flow assays purely by naked eye readout but also advanced detection through photometry, fluorescence and chemiluminescence is easily possible. Furthermore,

combining the CL-based LFA with a portable CL-reader allows comparable detection to a modified benchtop detection approach. The CL-reader uses photodiodes, which perfectly align with the POCT requirements regarding costs and dimensions but are also known to perform rather poorly in their native state for low light signals detection compared to other optical sensors. The benchtop device on the other hand uses the gold standard for low light detection, a photomultiplier tube. Considering the different light sensor types, the obtained results demonstrated that optimized sensor architecture and readout electronics allow photodiodes to approach sensitivities of highly sensitive light sensors that often do not fit the budget of POCT. This alternative optical setup will further strengthen the upward trend of CL in POCT for future applications due to affordable detection systems.

However, especially the more sensitive readout strategies such as fluorescence and chemiluminescence can struggle with the excess dye load that is introduced to the system through the liposomes, as non-specific binding will become a more pronounced issue. Furthermore, access to the reporter molecules which are encapsulated in the liposomes can be challenging and typically introduces additional steps to the assay procedure. This is especially for POCT applications an unwanted side procedure and has to be justified by significantly increased sensitivities. Besides the obvious fast lysis through organic solvents or surfactants that has been widely used, more advanced strategies such as the human complement system[15] and physical destruction through heat can be employed. The latter offer the possibility to direct the lysis in case of the complement system or to integrate lysis into a detection device to circumvent additional procedural steps by the user. Both strategies are fit for lysing liposomes in a directed manner. For autonomous procedures, however, optimization is still needed and will be subject to future investigations.

This work further shows that CL liposomes can be implemented in an advanced neutralization assay, that function as high throughput assays for laboratory testing with great sensitivities. In the course of this work, the fluorescence approach proved to be more useful with regard to bioanalytically relevant sample matrices and assay procedure. Despite chemiluminescence's many advantages, it can be strongly affected by matrices that contain radical scavengers such as human serum or milk. They can hamper the chemiluminescence detection, due to its underlying radical based mechanism and caused a significant decline in the signal intensity. In order to still profit from CL's advantages in bioanalysis clever assay setups and strategies are required that separate radical scavengers from the ongoing CL reaction *e.g.,* by washing steps or masking agent for the radical scavengers.

Overall, this thesis provides a multifold toolbox that offers solutions for a variety of bioanalytical challenges. Liposomes are once more demonstrated to be a superior label with not only signal enhancement possibilities, but also high flexibility with regard to their surface properties. Easy functionalization and great stability make them particularly interesting not only as drug delivery system but render liposomes as an intriguing class of labels with their easy adaptability to different detection and assay principles.

6.1. References

[1] J. D. Bishop, H. V. Hsieh, D. J. Gasperino, B. H. Weigl, *Lab on a chip* **2019**, *19*, 2486.

[2] M. Naseri, Z. M. Ziora, G. P. Simon, W. Batchelor, *Reviews in Medical Virology* **2022**, *32*.

[3] A. Nilghaz, L. Guan, W. Tan, W. Shen, *ACS Sens.* **2016**, *1*, 1382.

[4] L. Gámiz-Gracia, A. M. García-Campaña, J. F. Huertas-Pérez, F. J. Lara, *Anal. Chim. Acta* **2009**, *640*, 7.

[5] A. Roda, M. Mirasoli, E. Michelini, M. Di Fusco, M. Zangheri, L. Cevenini, B. Roda, P. Simoni, *Biosens. Bioelectron.* **2016**, *76*, 164.

[6] M. Mayer, S. Takegami, M. Neumeier, S. Rink, A. Jacobi von Wangelin, S. Schulte, M. Vollmer, A. G. Griesbeck, A. Duerkop, A. J. Baeumner, *Angew. Chem., Int. Ed. Engl.* **2018**, *57*, 408.

[7] S. Rink, A. Duerkop, A. Jacobi von Wangelin, M. Seidel, A. J. Baeumner, *Anal. Chim. Acta* **2021**, *1188*, 339161.

[8] A. G. Griesbeck, Y. Díaz-Miara, R. Fichtler, A. Jacobi von Wangelin, R. Pérez-Ruiz, D. Sampedro, *Chem. - Eur. J.* **2015**, *21*, 9975.

[9] H. Nsairat, D. Khater, U. Sayed, F. Odeh, A. Al Bawab, W. Alshaer, *Heliyon* **2022**, *8*, e09394.

[10] a) K. A. Edwards, A. J. Baeumner, *Talanta* **2006**, *68*, 1421; b) K. A. Edwards, O. R. Bolduc, A. J. Baeumner, *Curr. Opin. Chem. Biol.* **2012**, *16*, 444; c) M. Mayer, S. Takegami, M. Neumeier, S. Rink, A. Jacobi von Wangelin, S. Schulte, M. Vollmer, A. G. Griesbeck, A. Duerkop, A. J. Baeumner, *Angew. Chem., Int. Ed.* **2018**, *57*, 408.

[11] K. A. Edwards, R. Korff, A. J. Baeumner, *Methods in molecular biology (Clifton, N.J.)* **2017**, *1571*, 407.

[12] a) H.-W. Wen, W. Borejsza-Wysocki, T. R. DeCory, A. J. Baeumner, R. A. Durst, *Eur. Food Res. Technol.* **2005**, *221*, 564; b) D. Martorell, S. T. Siebert, R. A. Durst, *Anal. Biochem.* **1999**, *271*, 177.

[13] S. Rink, B. Kaiser, M.-S. Steiner, A. Duerkop, A. J. Baeumner, *Analytical and bioanalytical chemistry* **2022**, *414*, 3231.

[14] Y. Herdiana, N. Wathoni, S. Shamsuddin, M. Muchtaridi, *OpenNano* **2022**, *7*, 100048.

[15] J. Szebeni, S. M. Moghimi, *Journal of liposome research* **2009**, *19*, 85.

Curriculum Vitae

Simone Rink
simone.rink@ur.de

Hochschulausbildung:

12/2018 – 04/2022	**Promotionsstudium Chemie,** Universität Regensburg *„Investigating and optimizing strategies for quantitative point of care diagnostics through chemiluminescence probes and liposomes"* Institut für Analytische Chemie, Chemo- und Biosensorik (Prof. Dr. Antje J. Bäumner)
10/2016 – 10/2018	**Masterstudiengang Chemie,** Universität Regensburg *„Development and Characterization of a New Chemiluminescent Probe for Bioanalytical Application"* Institut für Analytische Chemie, Chemo- und Biosensorik (Prof. Dr. Antje .J. Bäumner)
09/2014 – 07/2015	**Bachelorstudiengang Forensic and Analytical Science,** Robert Gordon University *„Synthesis of Molecular Probes for the Investigation of Alzheimer´s Pathology"* School of Pharmacy and Life Science (Dr. Kai Jakoby, Dr. Alberto Di Salvo)
09/2012 – 09/2015	**Bachelorstudienganges Naturwissenschaftliche Forensik**, Hochschule Bonn-Rhein-Sieg

Berufserfahrung:

seit 05/2022	**Scientist**, Roche Diagnostic GmbH, Penzberg
09/2009 - 09/2012	**CTA**, Institut für klinische Neurobiologie, Würzburg
09/2007 - 07/2009	**CTA Ausbildung,** Institut Dr. Flad, Stuttgart

Stipendien:

11/2019	Stipendium im Rahmen des finanzielles Anreizsystem zur Förderung der Gleichstellung der Universität Regensburg
10/2014 - 12/2014	Stipendium des DAAD-Programms PROMOS 2014 zur Steigerung der Mobilität von Studierenden an deutschen Hochschulen

Publications

[8] **Rink, S.**, Duerkop, A., Baeumner, A. J. Enhanced Chemiluminescence of a Superior Luminol derivative Provides Sensitive Smartphone-based Point-of-Care Testing with Enzymatic µPADs. *Analysis Sensing,* accepted (2022).

[7] **Rink, S.**, Baeumner, A. J. Progression of Paper-Based Point-of-Care Testing toward Being an Indispensable Diagnostic Tool in Future Healthcare. *Anal. Chem*., accepted (2022).

[6] Wang, Y., **Rink, S.**, Baeumner, A. J., Seidel, M. Microfluidic flow-injection aptamer-based chemiluminescence platform for sulfadimethoxine detection. *Microchim Acta 189*, 117 (2022).

[5] **Rink, S.**, Kaiser, B., Steiner, M. S., Duerkop, A., Baeumner, A. J. Highly sensitive interleukin 6 detection by employing commercially ready liposomes in an LFA format. *Anal. Bioanal. Chem. 414***,** 3231–3241 (2022).

[4] **Rink, S.**, Duerkop, A., Jacobi von Wangelin, A., Seidel, M., Baeumner, A. J. Next generation luminol derivative as powerful benchmark probe for chemiluminescence assays. *Anal. Chim. Acta*. *1188*, 339161 (2021).

[3] Yagati, A. K., Behrent, A., Beck, S., **Rink, S.**, Goepferich, A. M., Min, J., Lee, M. H., Baeumner, A. J. Laser-induced graphene interdigitated electrodes for label-free or nanolabel-enhanced highly sensitive capacitive aptamer-based biosensors. *Biosens. bioelectron. 164*, 112272 (2020).

[2] Mayer, M., Hahn, M., Gerstl, F., Köwer, T., **Rink, S.**, Kunz, W., Duerkop, A., Baeumner, A. J. Shedding Light on the Diversity of Surfactant Interactions with Luminol Electrochemiluminescence for Bioanalysis. *Anal. Chem. 91*(20), 13080–13087 (2019).

[1] Mayer, M., Takegami, S., Neumeier, M., **Rink, S.**, Jacobi von Wangelin, A., Schulte, S., Vollmer, M., Griesbeck, A. G., Duerkop, A., Baeumner, A. J. Electrochemiluminescence Bioassays with a Water-Soluble Luminol Derivative Can Outperform Fluorescence Assays. *Angew. Chem. Int. Ed.*, *57*(2), 408–411 (2018).

Presentations

Oral Presentations

03/2021 **Pittcon 2021**: „Paper-based Point-of-Care Detection of L-lactate Shines by Employing a Stronger Emitting Luminol"

03/2019 **ANAKON 2019**: „Development and Characterization of a New Chemiluminescent Probe for Bioanalytical Applications"

Poster Presentations

10/2020 **Sensors in Medicine 2020**: „A New Luminol Probe Excels in Chemiluminescent Bioanalytical Strategies"

Eidesstattliche Erklärung

Ich erkläre hiermit an Eides statt, dass ich die vorliegende Arbeit ohne unzulässige Hilfe Dritter und ohne Benutzung anderer als der angegebenen Hilfsmittel angefertigt habe; die aus anderen Quellen direkt oder indirekt übernommenen Daten und Konzepte sind unter Angabe des Literaturzitats gekennzeichnet.

Weitere Personen waren an der inhaltlich-materiellen Herstellung der vorliegenden Arbeit nicht beteiligt. Insbesondere habe ich hierfür nicht die entgeltliche Hilfe eines Promotionsberaters oder anderer Personen in Anspruch genommen. Niemand hat von mir weder unmittelbar noch mittelbar geldwerte Leistungen für Arbeiten erhalten, die im Zusammenhang mit dem Inhalt der vorgelegten Dissertation stehen.

Die Arbeit wurde bisher weder im In- noch im Ausland in gleicher oder ähnlicher Form einer anderen Prüfungsbehörde vorgelegt.

Regensburg, den 21. Dezember 2022

Simone Rink (Author)